

Treatment of Water-borne Nutrients,
Pathogens, and Pharmaceutical
Compounds using Basic Oxygen Furnace
Slag

by

Syed Ismail Hussain

A thesis
presented to the University of Waterloo
in fulfillment of the
thesis requirement for the degree of
Doctor of Philosophy
in
Earth Sciences

Waterloo, Ontario, Canada, 2013

©Syed Ismail Hussain 2013

AUTHOR'S DECLARATION

I hereby declare that I am the sole author of this thesis. This is a true copy of the thesis, including any required final revisions, as accepted by my examiners.

I understand that my thesis may be made electronically available to the public.

Abstract

Phosphorus (P) is one of the essential nutrients for living organisms; however, excess P in aquatic systems often causes environmental and ecological problems including eutrophication. Removal of P from domestic wastewater, industrial wastewater, and agricultural organic-waste systems is required to minimize loading of P to receiving water bodies. A variety of sorbents or filter materials have previously been evaluated for P removal, including natural materials, industrial byproducts, and synthetic products. Among these materials industrial byproducts were reported as most effective. However, only a few of these studies were based on field experiments. Pharmaceutically active compounds (PhACs) and acesulfame-K (an artificial sweetener) are emerging contaminants observed in wastewater. The removal of PhACs in conventional wastewater treatment systems has been studied; however, few studies on alternative treatment systems are available. Studies related to the removal of acesulfame-K are even more limited. This thesis was focused on evaluation of basic oxygen furnace slag (BOFS), a byproduct from the steel manufacturing industry, as a potential reactive media for P removal from surface water and wastewater. The removal of PhACs and acesulfame-K in wastewater treatment systems containing BOFS as a treatment component was also evaluated.

The effectiveness of BOFS for removing P from lake water was evaluated in a three year pilot-scale hypolimnetic withdrawal P treatment system at Lake Wilcox, Richmond Hill, Ontario. Phosphate concentrations of the hypolimnion water ranged from 0.3 to 0.5 mg L⁻¹. About 83-100% P was removed during the experiment. The reactive mixtures were changed each year to improve the performance of the treatment system. Elevated pH (9-12) at the effluent of the

treatment system was adjusted by sparging $\text{CO}_{2(g)}$ to near neutral pH. Elevated Al was removed through this pH adjustment. Elevated concentrations of V were removed in a column containing 5 wt% zero valent iron (ZVI) mixed with sand (0.5 m^3) at the end of the BOFS based column. Removal of P in the BOFS based media is attributed to adsorption and co-precipitation at the outer layer of BOFS. Geochemical modeling results showed supersaturation with respect to hydroxyapatite, β -tricalciumphosphate, aragonite, and calcite. Solid phase analyzes of the BOFS based reactive media collected after completion of the year 2 experiment (spent media) through combination of scanning electron microscopy (SEM) and energy dispersive X-ray spectroscopy (EDX), X-ray photoelectron spectroscopy (XPS), Fourier transform infrared spectroscopy (FTIR), and X-ray absorption near edge structure spectroscopy (XANES) support the presence of calcium phosphate minerals on the outer layer of the spent media.

A multistep wastewater treatment experiment was carried out in an indoor facility at the Center for Alternative Wastewater Treatment, Fleming College, Lindsay, Ontario, Canada. This experiment evaluated the removal of P, ammonia, cBOD_5 , COD, *E. coli*, total coliform, and trace metals in a series of treatment cells including a mixing cell, a vertical subsurface flow aerobic cell, a vertical subsurface flow P treatment cell containing BOFS, and a horizontal subsurface flow anaerobic cell. About 97-99% removal of P, NH_3 , cBOD_5 , *E. coli*, and total coliform; and ~72% removal of COD were achieved in the treatment system. The mixing cell and the aerated cell reduced the concentrations of P, ammonia, cBOD_5 , *E. coli*, and total coliform significantly and the P treatment cell provided additional treatment. However, the primary objective of the P treatment cell was to reduce P concentrations to the acceptable range according to the water quality guidelines. The P treatment cell had successfully fulfilled this

objective. Elevated concentration of Al and V were also observed in the P treatment cell effluent. The concentration of Al decreased to below the guideline value of 0.075 mg L^{-1} after introducing a pH adjustment unit between the P treatment cell and the anaerobic cell. The concentration of V was decreased in the anaerobic cell effluent. However, the effluent concentration of V was much higher than the guideline value. Geochemical speciation modeling results showed supersaturation with respect to hydroxyapatite, β -tricalciumphosphate, aragonite and calcite along the flow path. Accumulation of P on the outer layer of the spent BOFS media was identified by energy dispersive X-ray spectroscopy (EDX). Although X-ray photoelectron spectroscopy (XPS) can provide information to a depth of 5-7 nm from the outer layer of the spent media, both Ca and P were positively identified in some of the samples. Accumulation of P at the edge of the grains of the spent media was clearly identified on the element map of polished cross-sections and corresponding FTIR spectra. The phosphate and carbonate functional groups were identified by the distribution of different vibrational frequencies through FTIR spectroscopy. The presence of calcite and hydroxyapatite were inferred based on the wave numbers assigned for these minerals in the literature. Finally, X-ray absorption near edge structure spectroscopy (XANES) on the outer layer samples from the spent BOFS media and corresponding linear combination fitting analysis indicated the presence of β -tricalciumphosphate, hydroxyapatite, and calcium phosphate dibasic.

Based on the observations from the indoor wastewater treatment experiment, a multistep demonstration-scale outdoor wastewater treatment experiment was conducted to investigate the applicability of the integration of the P treatment technology and engineered wetland technology at a relatively large scale prior to a full-scale field installation. The anaerobic treatment cell was

not included in this outdoor system because this unit did not efficiently remove ammonia and metals (e.g. V) from the Cell 4 effluent in the indoor system. A 10 cm layer of zero valent iron was placed at the bottom part of the down flowing P treatment cell to address the elevated V in the P treatment cell effluent observed in the indoor system and also to treat PhACs in the effluent. More than 99% removal of P, *E. coli*, and total coliform; >82, >98, and >76% removal of ammonia, cBOD₅, and COD were achieved in this treatment system. The effluent pH (10.88±1.47) was neutralized and the concentration of V remained < 0.006 mg L⁻¹. The Al concentration was adjusted to <0.075 mg L⁻¹ with the neutralization of pH. Geochemical speciation modeling results showed the supersaturation of hydroxyapatite, β-tricalciumphosphate, octacalciumphosphate, aragonite, and calcite. The FTIR and XANES spectra showed the presence of calcium phosphate minerals on the outer layer of the spent media.

Removal of the PhACs, including caffeine, ibuprofen, carbamazepine, naproxen, and sulfamethoxazole, and acesulfame-K was monitored in the demonstration-scale outdoor wastewater treatment system, which consisted of five different treatment cells including a horizontal subsurface flow constructed wetland, a vertical subsurface flow aerated cell, a vertical subsurface flow BOFS cell, and a pH neutralization unit. Significant removal of caffeine (>75%) and ibuprofen (50-75%), and moderate removal of sulfamethoxazole and naproxen (25-50%) were observed. The removal of carbamazepine was less effective with <25% removal observed. Acesulfame-K was also persistent along the flow path with <25% removal.

This study demonstrated that removal of P from lake water and wastewater in excess of 95% could be achieved using BOFS as a reactive media. Integration of this media into an engineered

wetland system enhances its performance in removing nutrients and other wastewater contaminants.

Acknowledgements

I would like to take advantage to recognize the support from the people around me during the completion of this research. First of all, I am indebted to my (co) supervisors, Dr. David Blowes and Dr. Carol Ptacek for their insight, guidance, patience, and unwavering support throughout this process. I thank Dr. David Rudolph, Dr. Will Robertson, and Dr. Wayne Parker for their constructive comments and critical observations that ensure the quality of my research.

Thank you to Dr. Brent Wootton for your unswerving support in the major part of this research. I thank Dr. Gordon Balch for his immense support in construction and monitoring of the indoor and outdoor engineered wetland wastewater treatment systems. I also thank Daniel Olding for his cordial support in the field including construction and monitoring of the treatment columns.

Thank you David Smyth for introducing me in the field activities related to my research, which included construction of the PRB and aqueous and solid phase sampling from the treatment system. Thank you to Jeff Bain for your continuous logistic support in laboratory and field experiments, reviewing manuscripts, sharing research related issues, and amiable exposition on various topics. Thank you to Laura Groza for your cordial cooperation in analyzing metals in the aqueous phase samples, in analyzing pharmaceutical compounds, in synthesizing calcium phosphate minerals, and in building laboratory columns. Thank you to Dr. Matt Lindsay for valuable suggestions regarding my laboratory and field experiments, introducing me to SEM and EDX, and monitoring field columns in my absence due to some of my family emergencies.

The XANES experiments were performed at the Canadian Light Source, which is supported by NSERC, NRC, CIHR, and the University of Saskatchewan on the 06B1-1 (SXRMB) beamline as part of proposal # 16-4419. I also thank Yongfeng Hu for assistance with operating the beamline. Thank you Julia Jamieson-Hanes for your help in analyzing solid phase samples using XANES. I also thank to Dr. Blair Gibson for his valuable tips in processing XANES data.

I want to thank Dr. Kam Tong Leung, Dr. Nina Heinig, Dr. Jake Fisher, Dr. Howard Siu, Mary Jane Walzak, and Mark Biesinger for helping me with solid phase sample analysis. I also want to thank Joy Hu, Stephanie Collins, Heather Broadbend, Ann Solomon, and Jing Ma for helping me with aqueous phase sample analysis.

Thank you to all graduate students, coop students, and friends who helped me out in the field and laboratory. This includes Ying Ying Liu, Peng Liu, Eric Michell, Ashley Stanton, Hector Ruiz, Jeff Sparks, Ou Wang, Corina McDonald, Michelle Sabourin, Lingyi Kong, Adnan Al-Wahid, Dr. Enayetur Rahim, Dr. Shahed Alam, Dr. Rajesh Palit, Dr. Abdullah-Al Mamun, Dr. Ilias Mahmud, Abdus Sabur, Ghulam Hussain, and Jeffrey Leon for helping me out with field and laboratory experiments.

This research was supported by the Idea to Innovation (I2I) program of the Natural Sciences and Engineering Research Council (NSERC) of Canada, the Ontario Ministry of Research and Innovation Research Excellence Fund, the Lake Simcoe Region Conservation Authority, the Lake Simcoe Clean-up Fund of Environment Canada, the Ontario Ministry of the Environment, the Natural Sciences and Engineering Research Council of Canada, the Ontario Ministry of

Research and Innovation Research Excellence Fund, the Town of Richmond Hill, Ontario, Canada, and Stantec Consulting Ltd.

I offer my sincere thanks to my parents, siblings, parents-in-law, and friends for their moral support in my study period. I am very grateful to my elder sister, Syeda Ferdous Mahal, who is my childhood icon due to her academic achievements that inspire me to pursue higher education. I am also very thankful to my elder brother, Syed Zakir Hussain, who provided me financial supports during my undergraduate and encouraged me every possible ways.

Finally, I am sincerely grateful to my wife Farzana Sultana for her support, patience and understanding. You sacrificed your time, showed great tolerance, and encouraged me throughout this endeavor. I am also thankful to my son, Safwan Syed Hussain, who made my life enjoyable and inspired me.

Dedication

This thesis is dedicated to my parents, Late Syed Fazle Hussain and Mrs. Rezia Khatun, for their unparalleled sacrifice, love, support, and patience over the years.

Table of Contents

AUTHOR'S DECLARATION.....	ii
Abstract.....	iii
Acknowledgements.....	viii
Dedication.....	xi
Table of Contents.....	xii
List of Figures.....	xvi
List of Tables.....	xxiii
List of Abbreviations.....	xxv
Chapter 1 <i>Introduction</i>	1
1.1 Background.....	1
1.1.1 Geochemistry of the contaminants.....	1
1.2 Research Objectives.....	10
1.2.1 Main objective.....	10
1.2.2 Specific objectives.....	10
1.3 Thesis Organization.....	11
Chapter 2 <i>Evaluation of Basic Oxygen Furnace Slag for Removal of Phosphorus from Lake Water</i>	14
2.1 Executive Summary.....	14
2.2 Introduction.....	15
2.3 Materials and Methods.....	18
2.3.1 Reactive material.....	18
2.3.2 System configuration.....	18
2.3.3 Sample collection and analysis.....	19
2.3.4 Characterization of reactive material.....	20
2.3.5 Geochemical modeling.....	22
2.4 Results and Discussion.....	23
2.4.1 Characteristics of the reactive materials.....	23
2.4.2 pH, Eh, alkalinity, and temperature.....	23
2.4.3 Major ion chemistry.....	25
2.4.4 Phosphorus removal.....	25
2.4.5 Geochemical modeling.....	32
2.4.6 Trace metals.....	34

2.4.7 Accumulation of precipitates in columns	36
2.5 Conclusions	36
<i>Chapter 3 Removal of Nutrients and Pathogens in an Advanced Pilot-scale Engineered Wetland</i>	
<i>Wastewater Treatment System</i>	62
3.1 Executive Summary	62
3.2 Introduction	63
3.3 Materials and Methods	66
3.3.1 System configuration.....	66
3.3.2 Reactive material characterization.....	68
3.3.3 Water sample collection and analysis.....	69
3.3.4 Solid-phase sample collection and analysis.....	70
3.3.5 Geochemical modeling.....	73
3.4 Results and Discussion.....	73
3.4.1 Characteristics of the reactive materials.....	73
3.4.2 Influent chemistry.....	74
3.4.3 pH and alkalinity	74
3.4.4 Major ion chemistry	75
3.4.5 Phosphorus	76
3.4.6 Ammonia and nitrate	86
3.4.7 Carbonaceous biochemical oxygen demand (cBOD ₅) and chemical oxygen demand (COD)..	87
3.4.8 Geochemical modeling.....	88
3.4.9 Trace metals	89
3.4.10 Removal of bacterial indicators (<i>E. coli</i> and total coliforms).....	89
3.4.11 Hydraulic performance.....	90
3.5 Conclusions	91
<i>Chapter 4 Advanced Phosphorus Removal in a Demonstration-scale Engineered Wetland Wastewater</i>	
<i>Treatment System</i>	125
4.1 Executive Summary	125
4.2 Introduction	126
4.3 Materials and Methods	128
4.3.1 System configuration.....	128
4.3.2 Characterization of the reactive material and reaction products	130

4.3.3 Sample collection and analysis	132
4.3.4 Geochemical modeling	132
4.4 Results and Discussion	133
4.4.1 Characteristics of the reactive materials	133
4.4.2 Flow characteristics.....	133
4.4.3 pH and alkalinity.....	134
4.4.4 Phosphorus removal.....	135
4.4.5 Ammonia and nitrate.....	141
4.4.6 Carbonaceous biochemical oxygen demand (cBOD ₅) and chemical oxygen demand (COD)	142
4.4.7 Major ion chemistry	143
4.4.8 Trace metals	144
4.4.9 Removal of bacterial indicators (total coliforms and <i>E. coli</i>)	146
4.5 Conclusions.....	146
Chapter 5 <i>Transport and Attenuation of Pharmaceutical Compounds and Acesulfame-K in a</i>	
<i>Demonstration-scale Wastewater Treatment System</i>	168
5.1 Executive Summary	168
5.2 Introduction.....	169
5.3 Materials and Methods.....	172
5.3.1 Chemicals/ chemical standards	172
5.3.2 Field methods.....	173
5.3.3 Analytical methods	175
5.4 Results and Discussion	178
5.4.1 Characteristics of wastewater.....	179
5.4.2 Carbonaceous biochemical oxygen demand (cBOD ₅).....	180
5.4.3 Pharmaceutical compounds (PhACs).....	181
5.4.4 Artificial sweetener	186
5.4.5 Removal mechanisms	186
5.5 Conclusions.....	191
Chapter 6 <i>Conclusions</i>	210
6.1 Summary of Findings.....	210
6.2 Scientific Contributions	213
6.3 Recommendations and Future Work.....	214

References	216
Appendix A Summary of Data Presented in Chapter 2.....	236
Appendix B Summary of Data Presented in Chapter 3.....	257
Appendix C Summary of Data Presented in Chapter 4.....	279
Appendix D Summary of Data Presented in Chapter 5.....	316

List of Figures

Figure 1.1 Phosphorus release mechanisms at the sediment-water interface modified from Hupfer and Lewandowski (2008). a) Oxidized sediment surface with high P retention capacity; b) Reduced sediment surface, where redox cycle controls P availability in the hypolimnion; c) Reduced sediment surface, where high sulfate concentration consume Fe and enhance the P release.	12
Figure 1.2 Potential point and non-point sources of PhACs to surface water, groundwater, and drinking water (After Ternes, 1998 and Heberer, 2002a).....	13
Figure 2.1 Schematic diagram of the field columns at Lake Wilcox, Richmond Hill, Ontario. Influent waters were collected from the hypolimnion of the lake and made available periodically for continuous flow by gravity feed into the treatment system.....	38
Figure 2.2 pH values, alkalinity and PO ₄ -P concentrations versus vertical distance along the treatment flow path in years 1, 2, and 3 of the hypolimnetic withdrawal P treatment experiment, respectively. C1, C2, C3, and CO ₂ at the top represent Columns 1 to 3 and the neutralization tank, respectively. The dashed lines represent the relevant Ontario Provincial Water Quality Objectives (PWQO).....	39
Figure 2.3 Eh values measures along the flow path in years 1, 2, and 3	40
Figure 2.4 Ca, Na, Mg, Mn, and SO ₄ concentrations versus distance along the treatment flow path in three successive years of the hypolimnetic withdrawal P treatment experiment. C1, C2, C3, and CO ₂ at the top represent Columns 1 to 3 and the neutralization tank, respectively.	41
Figure 2.5 pH values and PO ₄ -P, Ca, Na, Mg, and SO ₄ concentrations versus distance along the treatment flow path in year 3 of the hypolimnetic withdrawal P treatment experiment. C1, C2, C3, and CO ₂ at the top represent Columns 1 to 3 and the neutralization tank, respectively. The dashed lines represent the relevant water quality guidelines for Ontario.	42
Figure 2.6 Flow rate, PO ₄ -P concentrations in the influent and effluent, and P load in the treatment system during years 1, 2, and 3.....	43
Figure 2.7 SEM images of fresh BOFS (sample 1) and precipitates that formed on the spent reactive media along the flow path (sample 2-9) in year 2. The direction of flow is indicated by the arrows. Unless indicated with small circles, the EDX data were	

obtained from the entire image area. The phosphorus contents obtained from the EDX data are shown on the images.	44
Figure 2.8 a) Dissolved P and solid phase P versus distance, and b) pH and solid phase P versus distance along the treatment flow path in year 2 of the hypolimnetic withdrawal P treatment experiment. C1, C2, and C3 at the top represent Columns 1, 2, and 3.	45
Figure 2.9 FTIR spectrum of sample C2-S10 and major phosphate vibrational bands of a) HAP-S, and b) β -TCP; and major carbonate bands of c) calcite, and d) aragonite are compared. Vertical dotted lines in “a” and “b” represent phosphate vibrational bands, while vertical dotted lines in “c” and “d” represent carbonate vibrational bands.	46
Figure 2.10 XANES spectra for reference materials, PO_4 sorbed on CaCO_3 (PSC), and samples C2-S10 and C3-S1. Vertical lines represent various spectral features: a) pre edge feature for FeP; b) absorption edge (white line) for CaP species; c) shoulder (sharpness dependent on the degree of crystallinity); d) spectral feature common in HAP; e) oxygen oscillation.	47
Figure 2.11 Linear combination fit results for spent BOFS samples C2-S10 and C3-S1.	48
Figure 2.12 Saturation indices for calcium phosphate and other related phases calculated using PHREEQCI versus distance from influent to final effluent in year 3. Saturation index of hydroxyapatite (indicated by *) was plotted using a modified $\log K_{sp}$ value (Baker et al., 1998).	49
Figure 2.13 a) Concentrations of V and Al versus distance along the treatment flow path for three successive years of the trial. Five representative sampling events were selected for each year. b) Concentrations of V and Al in the BOFS effluent for all three years and for ZVI in year 3. C1, C2, C3, and CO_2 at the top represent Columns 1 to 3 and the neutralization tank, respectively. The dashed lines represent the relevant water quality guidelines for Ontario.	50
Figure 2.14 Optical microscopy images for a sample of reactive media collected 15 cm below the top surface of Column 1. The magnified images (40X) on the right hand side correspond to the boxed areas from the left hand side.	51
Figure 3.1 Schematic diagram of the cells in the pilot-scale treatment system. Wastewater continuously flows through the system by combination of gravity feed and pumping.	93
Figure 3.2 Cross-section of the Mixing cell (Cell 2) showing the thickness and vertical distribution of different components of the cell.	94

Figure 3.3 Cross-section of the Aerated EW cell (Cell 3) showing the thickness and vertical distribution of different components of the cell.....	95
Figure 3.4 Cross-section of the BOFS cell (Cell 4) showing the thickness and vertical distribution of different components of the cell.....	96
Figure 3.5 Cross-section of the Anaerobic polishing cell (Cell 5) showing the thickness and vertical distribution of different components of the cell.....	97
Figure 3.6 Locations of solid phase spent media collected from the BOFS cell, where P represents locations of profile samples and S represents locations of samples within individual profiles.....	98
Figure 3.7 Box plots of pH, alkalinity, Eh and PO ₄ -P versus distance (Cells 1-5) along the treatment flow path. Dotted lines represent the Ontario Provincial Water Quality Objective (PWQO). pH and alkalinity of the total study period, before and after pH adjustment are presented in rows 1 and 2, Eh of the total study period, alkalinity before and after pH adjustment are presented in row 3, and PO ₄ -P of the total study period, phases 1 and 2 are presented in row 4. Horizontal solid lines and broken lines on the boxes represent median and mean concentrations. Top and bottom most dots represent maximum observation above upper fence and minimum observation below lower fence.....	99
Figure 3.8 Concentrations of Ca, Na, Mg and SO ₄ versus distance (Cells 1-5) along the treatment flow path. The 4 and 4* represent BOFS cell and pH adjustment cell.....	100
Figure 3.9 Flow rate, PO ₄ -P concentrations in the influent and effluent, and P load in the treatment system.....	101
Figure 3.10 Solid phase P versus depth from the surface of Cell 4. Phosphorus content in fresh BOFS is plotted at a depth of 0 cm.....	102
Figure 3.11 Saturation indices for calcium phosphate and other related phases calculated using PHREEQCI versus distance (Cells 2-5) along the reaction flow path. Saturation indices of HAP were plotted twice using an inferred K _{sp} value from Baker et al. (1998) (indicated by * in the plot) and a K _{sp} value for HAP obtained from the WATEQ4F database.....	103
Figure 3.12 High magnification BSE image, X-ray intensity element maps, and EDX spectra for a phosphorus-rich area and an area with no phosphorus accumulation.....	104

Figure 3.13 FTIR-ATR spectrum from the phosphorus rich zone on particle surface indicated by a white square.....	105
Figure 3.14 FTIR spectrum of sample S-20 (with highest mass) and major phosphate vibrational bands of a) HAP-S, and b) β -TCP; and major carbonate bands of c) calcite, and d) aragonite are compared. Vertical dotted lines in subplots a) and b) represent phosphate vibrational bands while vertical dotted lines in c) and d) represent carbonate vibrational bands.	106
Figure 3.15 High-resolution XPS spectra showing O (1s), Ca (2p), C (1s), and P (2p) peaks.	107
Figure 3.16 XANES spectra for reference materials and sample S 20. Vertical lines represent various spectral features: (a) pre edge feature for FeP, (b) absorption edge (white line) for CaP species, (c) shoulder (sharpness dependent on the degree of crystallinity, (d) spectral feature common in HAP, and (e) oxygen oscillation.....	108
Figure 3.17 XANES spectra for PO_4 sorbed on CaCO_3 (PSC), LC fit for sample S 20 with the combination of β -TCP, HAP-S, and CPD; and samples S 20, S 21, S 16, and S 11. Vertical dotted lines represent (a) absorption edge (white line); (b) shoulder (sharpness dependent on the degree of crystallinity); (c) spectral feature common in HAP; and (d) oxygen oscillation.	109
Figure 3.18 Linear combination fit of XANES spectra for spent BOFS samples S 20, S 21, S 16 and S 11.....	110
Figure 3.19 Box plots of $\text{NH}_4\text{-N}$ and $\text{NO}_3\text{-N}$ concentrations versus distance (Cells 1-5) along the flow path. Columns 1, 2, and 3 of this figure represent total treatment period, Phase 1, and Phase 2. Horizontal solid lines and broken lines on the boxes represent median and mean concentrations. Top and bottom most dots represent maximum observation above upper fence and minimum observation below lower fence.	111
Figure 3.20 Box plots of DO, cBOD_5 , and COD concentrations versus distance (Cells 1-5) along the treatment flow path. Columns 1, 2, and 3 of this figure represent total treatment period, Phase 1, and Phase 2, respectively. Horizontal solid lines and broken lines on the boxes represent median and mean concentrations. Top and bottom most dots represent maximum observation above upper fence and minimum observation below lower fence.	112

Figure 3.21 Box plots of V, Al, Cu, Zn, Fe, Ni, Mn, Cr, and Pb concentrations versus distance (Cells 1-5) along the treatment flow path. Dotted lines represent the Ontario Provincial Water Quality Objective (PWQO).	113
Figure 3.22 Concentrations of V and Al in the treatment cells effluent versus time. Concentrations of Al decreased abruptly in the anaerobic cell effluent as the pH was adjusted to near neutral, reflecting the amphoteric nature of this element.	114
Figure 3.23 Box plots of <i>E.coli</i> and total coliform concentrations versus distance (Cells 1-5) along the treatment flow path. Horizontal solid lines and broken lines on the boxes represent median and mean concentrations. Top and bottom most dots represent maximum observation above upper fence and minimum observation below lower fence.	115
Figure 3.24 SEM images of precipitates that formed on the spent reactive media collected from location 1, 18, 20, and 21 (Figure 3.6) indicated by a, b, c, and d. Unless indicated with circles, the EDX data were obtained from the entire image area. The phosphorus contents obtained from the EDX data are shown on the images. Well-defined crystal faces were observed in “b” (sample S-18). Formation of crystal faces were also noted in “d” (sample S-21).	116
Figure 4.1 Schematic diagram of the EW-BOFS demonstration-scale treatment system. The treatment system comprises 4 outdoor cells (Cells 1-4) and an indoor cell (Cell 5). Wastewater continuously flushes through the system by a combination of gravity feed and pumping. In this diagram HSSF EW represents horizontal subsurface flow engineered wetland, VSSF aerated EW represents vertical subsurface flow aerated engineered wetland, BOFS represents basic oxygen furnace slag, and CLK represents City of lake Kawartha.	148
Figure 4.2 Cross-section of the Aerated EW cell (Cell 3) showing the thickness and vertical distribution of different components of the cell.	149
Figure 4.3 Cross-section of the BOFS cell (Cell 4) showing the thickness and vertical distribution of different components of the cell.	150
Figure 4.4 Locations of solid phase spent media collected from the BOFS cell.	151
Figure 4.5 Flow rate, PO ₄ -P concentrations in the influent and effluent, and P load in BOFS Cell.	152
Figure 4.6 Box plots of pH values, Eh, conductivity, alkalinity, PO ₄ -P, DO, cBOD ₅ , COD, Cl, SO ₄ , NH ₃ -N, NO ₃ -N, NO ₂ -N, NH ₃ -N/N _T , NO ₃ -N/N _T versus distance (Cells 1-4) along	

the treatment flow path. Dotted lines represent the Ontario Provincial Water Quality Objective (PWQO). Horizontal solid lines and broken lines on the boxes represent median and mean concentrations. Top and bottom most dots represent maximum observation above upper fence and minimum observation below lower fence..... 153

Figure 4.7 pH values, Ca, Al, and PO₄-P concentrations versus distance (Cells 1-5) along the flow path..... 154

Figure 4.8 Saturation indices for calcium phosphate and other related phases (calculated using PHREEQCI) along the treatment cells during 3 sampling events. Saturation index of hydroxyapatite (indicated by *) was plotted using a modified log K_{sp} value (Baker et al., 1998)..... 155

Figure 4.9 FTIR spectrum of sample with highest mass and reference materials and sample P2-S1, with phosphate vibrational bands for a) HAP-S, b) β-TCP, c) calcite, d) aragonite. Vertical dotted lines in “a” and “b” represent phosphate vibrational bands, while vertical dotted lines in “c” and “d” represent carbonate vibrational bands. 156

Figure 4.10 XANES spectra for reference materials, PO₄ sorbed on CaCO₃ (PSC; Peak et al., 2002), and samples P2-S1, P2-S2, P8-S1. Vertical lines represent various spectral features: a) pre edge feature for FeP; b) absorption edge (white line) for CaP species; c) shoulder (sharpness dependent on the degree of crystallinity; d) spectral feature common in HAP; e) oxygen oscillation. 157

Figure 4.11 Linear combination fit results for spent BOFS samples P2-S1, P2-S2, and P8-S1. 158

Figure 4.12 Box plots of Ca, Na, Mg, K, SO₄, and Cl concentrations versus distance (Cells 1-4) along the flow path. Horizontal solid lines and broken lines on the boxes represent median and mean concentrations. Top and bottom most dots represent maximum observation above upper fence and minimum observation below lower fence..... 159

Figure 4.13 Box plots of V, Al, Cu, Zn, Fe, Ni, Mn, Cr, and Pb concentrations versus distance (Cells 1-4) along the flow path. Dotted lines represent the Ontario Provincial Water Quality Objective (PWQO). Horizontal solid lines and broken lines on the boxes represent median and mean concentrations. Top and bottom most dots represent maximum observation above upper fence and minimum observation below lower fence.. 160

Figure 4.14 Concentrations of *E. coli*, total coliform (in the left Y-axis), DO, pH (in the right Y-axis) versus cells (1-4) along the flow path..... 161

Figure 5.1 Schematic diagram of the outdoor cells of the EW-BOFS pilot-scale treatment system. Cell 2 represents a horizontal subsurface flow constructed wetland, Cell 3 represents a vertical subsurface flow aerated engineered wetland, and Cell 4 contains a mixture of BOFS and ZVI. Wastewater was continuously flushed through the system by a combination of gravity feed and pumping (from Chapter 4). In this diagram HSSF EW represents horizontal subsurface flow engineered wetland, VSSF aerated EW represents vertical subsurface flow aerated engineered wetland, BOFS represents basic oxygen furnace slag, and CLK represents City of lake Kawartha.	192
Figure 5.2 Box plots of pH, alkalinity, Eh, cBOD ₅ , DO, Cl, NH ₃ -N, NO ₃ -N, NH ₃ -N/NO ₃ -N, Fe, Mn, and SO ₄ versus distance (Cells 1-4) along the treatment flow path. Horizontal solid lines and broken lines on the boxes represent median and mean concentrations.	193
Figure 5.3 pH versus distance (Cells 1-5) along the treatment flow path.	194
Figure 5.4 Selected pharmaceutical compounds, caffeine (CAF), carbamazepine (CBZ), sulfamethoxazole (SMX), ibuprofen (IBU), naproxen (NAP), and an artificial sweetener, acesulfame-K (ACE), along the treatment flow path.	195
Figure 5.5 Box plots of selected pharmaceutical compounds, caffeine (CAF), carbamazepine (CBZ), sulfamethoxazole (SMX), ibuprofen (IBU), naproxen (NAP), and an artificial sweetener, acesulfame-K (ACE), along the treatment flow path. Horizontal solid lines and broken lines on the boxes represent median and mean concentrations.	196
Figure 5.6 Selected pharmaceutical compounds, caffeine (CAF), carbamazepine (CBZ), sulfamethoxazole (SMX), ibuprofen (IBU), naproxen (NAP), and an artificial sweetener, acesulfame-K (ACE), along the treatment flow path. a) Contribution of each cell to the total removal efficiency, b) total removal efficiency.	197
Figure 5.7 pKa of each pharmaceutical of interest plotted on the pH scale with dotted lines and the pH range of the treatment cells (Cells 1-4) shown with vertical bars.	198
Figure 5.8 Calculated values of log D _{ow} versus pH in the influent (Cell 1 effluent) and three other treatment cells (Cells 2, 3, and 4).	199

List of Tables

Table 2.1 Components of the reactive media and mass distribution during the study period.	52
Table 2.2 Physical and chemical properties of the BOFS materials used in the experiments.	53
Table 2.3 Mean values and range of pH, alkalinity, and PO ₄ -P of the input and BOFS column effluent in years 1, 2, and 3.	54
Table 2.4 P mass loading in the treatment system during years 1, 2, and 3.	55
Table 2.5 EDX data showing the composition of the selected samples.	55
Table 2.6 Vibrational bands of calcium carbonate minerals.	56
Table 2.7 Vibrational bands of phosphate in the reference materials.	57
Table 2.8 Vibrational bands of calcium phosphate minerals.	58
Table 2.9 Ca/C, Ca/P and O/Ca ratios of the samples analyzed.	59
Table 2.10 Linear combination fitting results of spent BOFS samples.	60
Table 3.1 Chemical composition of BOFS used in this study analyzed by XRF and analysis from previous studies.	117
Table 3.2 Physical properties and mineralogical composition of the.	118
Table 3.3 Semiquantitative EDX measurements showing the composition of the selected samples.	119
Table 3.4 Vibrational bands of phosphate in the reference materials.	120
Table 3.5 Ca/P and O/Ca ratios of the samples analyzed.	121
Table 3.6 Linear combination fitting results of spent BOFS samples.	122
Table 3.7 Values of pH, alkalinity and concentration ranges of other target parameters including PO ₄ -P, NH ₃ -N, NO ₃ -N, Al, V in the effluents of Cell 1, 2, 3, 4, 4*, and 5.	123
Table 3.8 Concentration ranges of DO, cBOD ₅ , COD, <i>E. coli</i> , and total coliform in the effluents of Cell 1, 2, 3, 4, 4*, and 5.	124
Table 4.1 K _{sp} values of the calcium phosphate minerals added to the PHREQCI database.	162
Table 4.2 Physical and chemical properties of the BOFS materials used in the experiments.	163
Table 4.3 Mean concentrations and concentration ranges (expressed as average of maximum and minimum values) of pH, alkalinity, conductivity, and other target parameters including PO ₄ , NH ₃ -N, NO ₃ -N, NO ₂ -N, Cl, and SO ₄ in the effluents of Cells 1, 2, 3, and 4.	164
Table 4.4 Vibrational bands of carbonate and phosphate and the corresponding wavenumbers in the FTIR spectra of the surface materials.	165

Table 4.5 Linear combination fitting results of spent BOFS samples.....	166
Table 4.6 Mean concentrations and concentration ranges (expressed as average of maximum and minimum values) of DO, cBOD ₅ , COD, total coliform, and <i>E. coli</i> in the effluents of Cells 1, 2, 3, and 4.	167
Table 5.1 Chemical properties and structures of pharmaceutically active compounds (Trenholm et al., 2006) and artificial sweetener, along with their molecular weights. Molecular weights of the internal standards are also provided.....	200
Table 5.2 Quality control samples and preparation blanks, continuing calibration verification and continuing calibration blanks.....	201
Table 5.3 Internal standard recoveries of laboratory blanks, trip blanks, field blanks, continuous calibration blk (CCB), and continuous calibration verification (CCV) of each analysis during the study period.	202
Table 5.4 Values of pH, Eh, alkalinity and the concentration range of the pharmaceuticals and acesulfame-K in the influent and the treatment cells.....	208
Table 5.5 P-values obtained from t-Test, two-sample assuming unequal variances, for Cells 1-2, 2-3, 3-4, 1-3, 1-4, and 2-4 for the selected chemicals	209

List of Abbreviations

BSE	Backscatter electron
BOFS	Basic oxygen furnace slag
BOFO	Basic oxygen furnace oxide
cBOD ₅	Carbonaceous biochemical oxygen demand
COD	Chemical oxygen demand
CPD	Calcium phosphate dibasic
CPDD	Calcium phosphate dibasic dihydrate
CW	Constructed wetland
<i>E. Coli</i>	Escherichia coli
EDX	Energy dispersive X-ray
EW	Engineered wetland
FE-SEM	Field emission-scanning electron microscopy
FTIR	Fourier transform infrared spectroscopy
HAP	Hydroxyapatite
IC	Ion chromatography
ICP-MS	Inductively coupled plasma-mass spectrometry
ICP-OES	Inductively coupled plasma-optical emission spectroscopy
PHREEQCI	pH (pH), RE (redox), EQ (equilibrium), C (program written in C), interactive
PSC	Phosphate sorbed on calcite
SI	Saturation index
TCP	Tricalcium phosphate
XANES	X-ray absorption near edge structure
XPS	X-ray photoelectron spectroscopy
XRD	X-ray diffraction
ZVI	Zero-valent iron

Chapter 1

Introduction

1.1 Background

1.1.1 Geochemistry of the contaminants

The release of phosphorus (P) to any surface water body has environmental significance because P is an essential component of cells in living organisms, and the limiting nutrient in many aquatic ecosystems (Schindler 1974, 1977). Excess P in surface water can cause eutrophication, which is a process that leads to excessive growth of aquatic plant life and depletion of dissolved oxygen (Parry 1998). Phosphorus concentrations in wastewater are typically 5 to 15 mg L⁻¹ PO₄-P (Snoeyink and Jenkins, 1980). The P attenuation capacity of natural sediments is limited, thus, excess inputs of P can result in the unattenuated movement of this contaminant in groundwater flow systems. The discharge of domestic wastewater or agricultural organic-waste systems in close proximity to surface waters is a particular concern due to P mobility, and potential impacts on surface water bodies. Groundwater discharge or surface runoff can contribute P loading to the receiving surface water bodies. The internal cycling of P in lake sediments is an important cause of eutrophication (Nürnberg, 1988; Bostrom et al., 1988; Søndergaard et al., 2003). The concentration ranges of total phosphorus for ultra-oligotrophic, oligotrophic, mesotrophic, meso-eutrophic, eutrophic, and hyper-eutrophic lakes described in CWQG (2005) are <0.004, 0.004-0.01, 0.01-0.02, 0.02-0.035, 0.035-0.1, and >0.1 mg L⁻¹. To prevent eutrophication, phosphate concentrations should be below 0.025 mg L⁻¹ within a lake and below 0.05 mg L⁻¹ when streams

discharge into lakes (U. S. EPA 1986). Thus, loading of very small concentrations of P (0.001 to 0.01 mg L⁻¹) in lakes can boost algal growth (Tomson and Vignona, 1984).

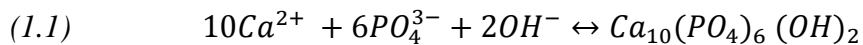
Factors that control the P exchange between sediments of lakes and the overlying water column are primarily biological, chemical, and physical. The biological factors include bacterial activities, biomineralization processes, and bioturbation; chemical factors include redox conditions, pH, Fe:P ratio, nitrate availability; and physical factors include resuspension and sediment mixing (Boström and Petterson, 1982; Søndergaard et al., 2003). Phosphorus release from lake sediments is related to thermal stratification and anoxia in the hypolimnion, which is the dense, bottom layer of water in a thermally-stratified lake (Nürnberg, 1984).

Anoxic conditions in the sediment-water interface favour P release from the lake sediment to the overlying water column (Bostrom et al., 1988). Under anoxic conditions, P and Fe are released from the lake sediment through reductive dissolution of iron oxy-hydroxide -phosphate complexes. Sulfate in the sediment (if present) can be reduced to sulfide under anoxic conditions and combines with Fe released from sediment to form FeS and ultimately increases the concentrations of P in the water column (Caraco et al., 1993; Figure 1.1). Søndergaard et al. (2003) also described the redox-dependent release of FeOOH-bound P and microbial processes as major P release mechanisms from lake sediments. In addition to release of P under anaerobic conditions, P also can be released from sediments under aerobic conditions through desorption, mineral dissolution and organic matter oxidation reactions (Reed et al., 2011).

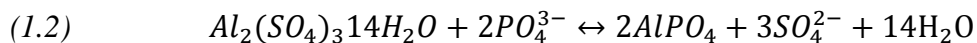
About 90% of the anaerobically released P is derived from the sediment Fe-P fraction and both the amount of aerobically released P and the maximum growth yield of algae is proportional to the sediment Fe-P fraction (Hosomi et al., 1982).

Phosphorus removal from wastewater is an important challenge in the development of wastewater treatment technologies. Existing technologies for control of P can be classified into several broad categories, such as chemical precipitation, biological P removal, crystallization technologies, advanced chemical precipitation and nutrient removal, and sludge-based processes Morse et al. (1998).

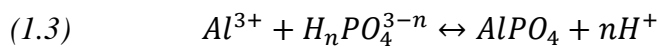
Chemical precipitation is one of the most important mechanisms for inorganic P removal. Precipitation of calcium-, aluminum-, and iron-phosphates are three commonly applied methods of chemical precipitation (Yeoman et al., 1988). Calcium ion (Ca^{2+}) derived from lime or any other sources can be combined with aqueous phase phosphate ion (PO_4^{3-}) to produce hydroxyapatite, or other calcium-phosphate minerals, under the pH range 8.0 to 11.0, through reactions of the following form (Yeoman et al., 1988):



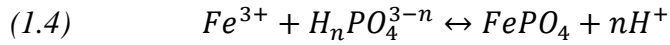
Precipitation of aluminum phosphate using aluminum sulfate (Shannon, 1980):



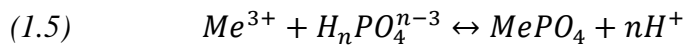
Precipitation of aluminum phosphate from trivalent aluminum salts (Metcalf and Eddy, 2003; Arvin, 1983):



Precipitation of ferric phosphate from trivalent iron salts (Stumm & Morgan, 1981; Metcalf and Eddy, 2003):



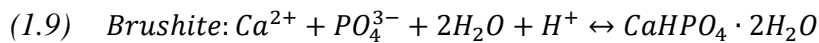
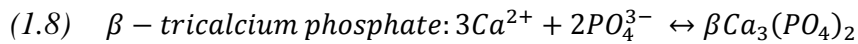
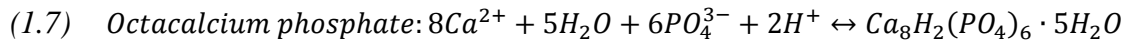
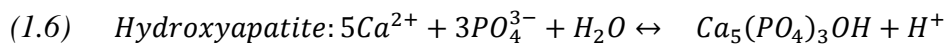
Thus, the basic reaction associated with phosphate removal by trivalent metals (Aguilar et al., 2002):



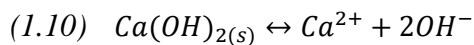
A number of low-cost reactive materials to remove phosphate from wastewater have been identified. Of these, the low-cost reactive materials that showed significant capacity in removing phosphate can be classified as natural materials (natural soils, limestone, opoka, clay minerals, zeolite, sand, manganese nodules), modified natural materials (granular activated carbon and bone char), and waste materials (water treatment plant residuals, blast furnace slag, red mud, steel furnace slag, fly ash, and activated red mud) (Mortula et al., 2007). Phosphate removal capacities (performance) of the commonly used filter media to remove phosphate from wastewater have been reviewed by Vohla et al. (2011). In this review, 39 articles on natural materials, 25 articles on industrial byproducts, and 10 articles on man-made products were summarized. The industrial byproducts, including some furnace slags, showed the highest phosphate removal capacities of about 420 g P kg⁻¹. The natural materials and the man-made filter media demonstrated maximum removal capacities of about 40 g P kg⁻¹ and 12 g P kg⁻¹ respectively.

Baker et al. (1998) observed >90% P removal over four years in a laboratory column containing basic oxygen furnace (BOF) oxide combined with crushed limestone and silica sand

and >99% P removal over two years in another laboratory column containing activated alumina combined with crushed limestone and silica sand. Baker et al. (1998) suggested two potential phosphate removal mechanisms based on mineralogical investigations, which include phosphate adsorption on the surfaces of metal oxides, and precipitation of insoluble calcium phosphate. Thus, the governing reactions would be related to one of the following calcium phosphate mineral forming reactions:



Basic oxygen furnace slag contains a high percentage of lime (CaO) and portlandite Ca(OH)₂. Dissolution of these components significantly increases the pH (to pH~12) and the concentration of Ca in solution (Baker et al. 1998).



At these high pH values, hydroxyapatite may precipitate and retain phosphate on the solid phase in the BOFS based reactive media.

There are challenges in the identification of an effective media and a suitable methodology for sustained phosphate removal from a large volume of wastewater and phosphate contaminated surface water. The phosphate retention capacity, low cost, and availability of BOF slag and BOF oxide suggest that these materials may be appropriate media to restrict phosphate release to

surface-water flow systems. Several of the previous studies, however, have identified concerns that may limit the widespread application of this approach. These concerns include the release of high pH effluent, which may have a negative impact on aquatic receptors; the release of elevated concentrations of Al and V; and the formation of secondary minerals, notably calcium carbonate, which may limit water flow through the reactive material.

Pharmaceutically active compounds (PhACs) have been identified as potential surface water and groundwater contaminants over the last two decades. PhACs can be introduced to surface water and groundwater through sewage-treatment plant effluent, surface runoff from agricultural applications of manure and sewage sludge, waste-disposal sites, septic systems, and pharmaceutical production plants (Figure 1.2; Heberer, 2002a; Daughton, 2003; Khetan and Collins, 2007; Sabourin et al., 2009). The individual concentrations of these contaminants are usually very low (ng L^{-1} to $\mu\text{g L}^{-1}$) in surface water and groundwater (Ternes, 1998, Halling-Sørensen et al., 1998; Daughton and Ternes, 1999; Sacher et al., 2001; Kolpin et al., 2002; Ternes et al., 2007; Carrara et al., 2008; Fram and Belitz 2011; Sanderson, 2011). However, the combined effect of multiple PhACs has potential to develop significant environmental concern.

Immense attention has focused on these compounds, due to their wide distribution in the aquatic ecosystem, and due to their unknown individual or collective impact on living organisms including humans and fish. Efforts are underway to explore effective remediation options to prevent the release of PhACs to groundwater and surface water flow systems.

Environmental exposures of PhACs are well documented in literature. Most articles published in last two decades focused on the occurrence of PhACs at various points of entry to the

environment and transport pathways (Halling-Sørensen et al., 1998; Ternes, 1998; Dughton and Ternes, 1999; Kolpin et al., 2002; Heberer, 2002a; Nikolaou et al., 2007; Khetan and Collins, 2007), and some articles discussed the potential for their removal (Heberer, 2002a; Ternes, 1998; Matamoros et al., 2005; Castiglioni et al., 2006; Carballa et al., 2007; Suarez et al., 2008; Benotti et al., 2009; Matamoros et al., 2009).

Caffeine is one of the most studied compounds detected in the aquatic environment and often is considered as a potential wastewater tracer (Heberer et al., 2002). Conventional wastewater treatment plants usually remove caffeine with high efficiency (up to >99%) through aeration and clarification processes (Ternes et al., 2001; Heberer et al., 2002; Bendz et al., 2005; Conkle et al., 2008). In the US surface streams, the frequency of detection for caffeine is reported as 62% with a maximum concentration of $6.0 \mu\text{g L}^{-1}$ (Kolpin et al., 2002). This compound is also detected in groundwater at concentrations between 0.02 and $0.29 \mu\text{g L}^{-1}$ (Rabiet et al., 2006; Barnes et al., 2008; Fram and Belitz, 2011), and in drinking water sources (Focazio et al., 2008).

Ibuprofen is another frequently detected PhAC in STPs effluent and surface water. Although some municipal STPs remove up to 95% ibuprofen (Lishman et al., 2006; Suarez et al., 2010), STPs are not always effective (<25% removal) in removing this compound (Metcalf et al., 2003). Ibuprofen can be removed both in aerobic and anaerobic conditions as this compound is recognized as one of the most biodegradable PhACs in the aquatic environment (Dordio et al., 2010). However, aerobic conditions (91-99% removal) are more efficient than anaerobic conditions (11-63% removal) (Suarez et al., 2010). Ibuprofen is also detected in surface water (Kolpin et al., 2002; Rabiet et al., 2006), groundwater (Carrara et al., 2008; Barnes et al., 2008), and drinking water sources (Webb et al., 2003; Focazio et al., 2008).

Carbamazepine is frequently detected in STP effluents and surface water (Ternes, 1998; Heberer, 2002a; Miao and Metcalfe, 2003) and often detected in groundwater (Sacher et al., 2001). Carbamazepine is not significantly removed in many STPs due to its low biodegradability and its neutral form ($pK_a=13.9$) under the pH conditions prevalent in most wastewaters (Ternes et al., 2007). In many STPs, the effluent concentrations of carbamazepine are higher than the influent concentrations (Metcalf et al., 2003; Vieno et al., 2006, Spongberg and Witter, 2008). In surface water bodies, concentrations of carbamazepine range from 0.06 to 1.10 $\mu\text{g L}^{-1}$ (Kolpin et al., 2002; Rabiet et al., 2006; Vieno et al., 2006). Carbamazepine is also detected in groundwater at concentrations from 0.03 to 0.42 $\mu\text{g L}^{-1}$ (Webb et al., 2003; Fram and Belitz, 2011), and untreated drinking water at concentrations from <0.05 to 0.19 $\mu\text{g L}^{-1}$ (Webb et al., 2003; Focazio et al., 2008). The recalcitrant nature of carbamazepine in the aquatic environment has been reported in previous studies (Andreozzi et al., 2002; Heberer, 2002a; Matamoros et al., 2005). Although conventional STPs show low to negative removal of carbamazepine, significant removal (20 to 48%) of this compound in different types of constructed wetlands has been reported (Hijosa-Valsero et al., 2010; Matamoros et al., 2007; Matamoros et al., 2008; Zhang et al., 2011). Dordio et al. (2010) reported extremely high (86-99%) removal of carbamazepine in microcosm constructed wetland systems filled with light expanded clay aggregates and planted with *Typha* spp.

Naproxen is a widely used PhAC and frequently detected in STP effluents and surface water. Over 90% removal of this PhAC in STPs is reported in previous studies (Ternes, 1998; Metcalfe et al., 2003; Bendz et al., 2005; Lishman et al., 2006, Carrara et al., 2008). Occurrence of naproxen in surface water is also reported in some studies (Ternes, 1998; Stumpf et al., 1999;

Verenitch et al., 2006; Khetan and Collins, 2007). Photodegradation is an important process involving transformation of naproxen to its photoproducts (Khetan and Collins, 2007).

Sulfamethoxazole has been detected in aquatic environments including STP effluent, surface water and groundwater. Although some STPs remove sulfamethoxazole with more than 34-78% efficiency (Stumpf et al, 1999; Hendricks and Pool, 2012), some other STPs show negative removal of this compound (Spongberg and Witter, 2008, Bendz et al., 2005). Sulfamethoxazole also is detected in surface water (Kolpin, 2002) and groundwater (Sacher et al., 2001; Barnes et al., 2008). Poor attenuation while passing through aquifer materials and resistance to biodegradation makes this compound persistent in groundwater and surface water (Sacher et al., 2001; Snyder et al., 2004; Suarez et al., 2010; Benotti and Brownawell, 2009).

Acesulfame-K is one of the widely used artificial sweeteners that is detected in the aquatic environment. Acesulfame-K is detected in wastewater treatment plant effluents and often the effluent concentrations exceed the influent concentrations (Buerge et al., 2009). Acesulfame-K also is detected in groundwater samples (Buerge et al., 2009, van Stempvoort et al., 2011a,b; Robertson et al., 2013), and surface water (Buerge et al., 2009; Scheurer et al., 2009; van Stempvoort et al., 2011a,b). Acesulfame-K is identified as one of the potential tracers for anthropogenic contamination due to its wide spread distribution in the aquatic environment including wastewater treatment effluents, surface water, groundwater, and even in drinking water (Scheurer et al., 2009; Buerge et al., 2009; Robertson et al., 2013; van Stempvoort et al., 2011a).

The current study focuses on the use of BOF slag for P removal, attempts to address potential concerns associated with this material, and investigates the P removal mechanism(s). This study

also investigates the attenuation and persistence of a number of frequently detected PhACs and an artificial sweetener in a wastewater treatment system incorporating a BOF slag component.

1.2 Research Objectives

1.2.1 Main objective

The goals of the proposed research project are to evaluate the P retention capacity of BOF slag, to determine the mechanisms of P removal, to assess the applicability of the use of BOF slag as a reactive media at various levels and scales of P contamination, and to assess the removal efficiencies in multistep wastewater treatment systems for nutrients (P and N), pathogens, and PhACs.

1.2.2 Specific objectives

The specific objectives of this research are to:

- Evaluate the effectiveness of BOF slag for removal of P in field settings.
- Investigate field scale columns to better understand P removal mechanisms through evaluating aqueous geochemistry and solid-phase analyzes of the precipitates on spent reactive media.
- Evaluate CO₂ addition as a method to neutralize the high pH of the effluent from a BOF slag filter.
- Assess the mechanisms of V removal from the effluent of reactive media (mixture of BOF slag, gravel, and sand) filter.

- Evaluate mechanisms and the effectiveness of pH adjustment and sand filtration to remove Al from the effluent of a reactive media (mixture of BOF slag, gravel, and sand) filter.
- Evaluate the effectiveness of the integration of a P treatment cell (BOFS cell with a layer of ZVI) into an engineered wetland wastewater treatment system for the removal of nutrients, pathogens, PhACs, and an artificial sweetener.
- Evaluate the removal of PhACs within aerated cells and a BOFS cell with a layer of ZVI in an integrated wastewater treatment system.

1.3 Thesis Organization

This thesis consists of six chapters including an introduction, four research chapters and a conclusion. Chapter 2, the first research chapter, describes a three year field-scale column experiment conducted to evaluate the potential for BOF slag to remove P from lake water, and to investigate the P-removal mechanisms. This chapter also addresses the potential issues related to elevated pH and metal release from BOFS reactive media. Chapters 3 and 4 describe the pilot-scale indoor and demonstration-scale outdoor experiments where the integration of a P treatment cell into an engineered wetland wastewater treatment system for removing nutrients and pathogens was evaluated. Detailed solid-phase analyzes of the precipitates from the outer layer of the spent reactive media were performed at the end of the experiments are described in Chapters 2, 3, and 4. Chapter 5 describes the effectiveness of the demonstration-scale outdoor system in removing five PhACs and an artificial sweetener.

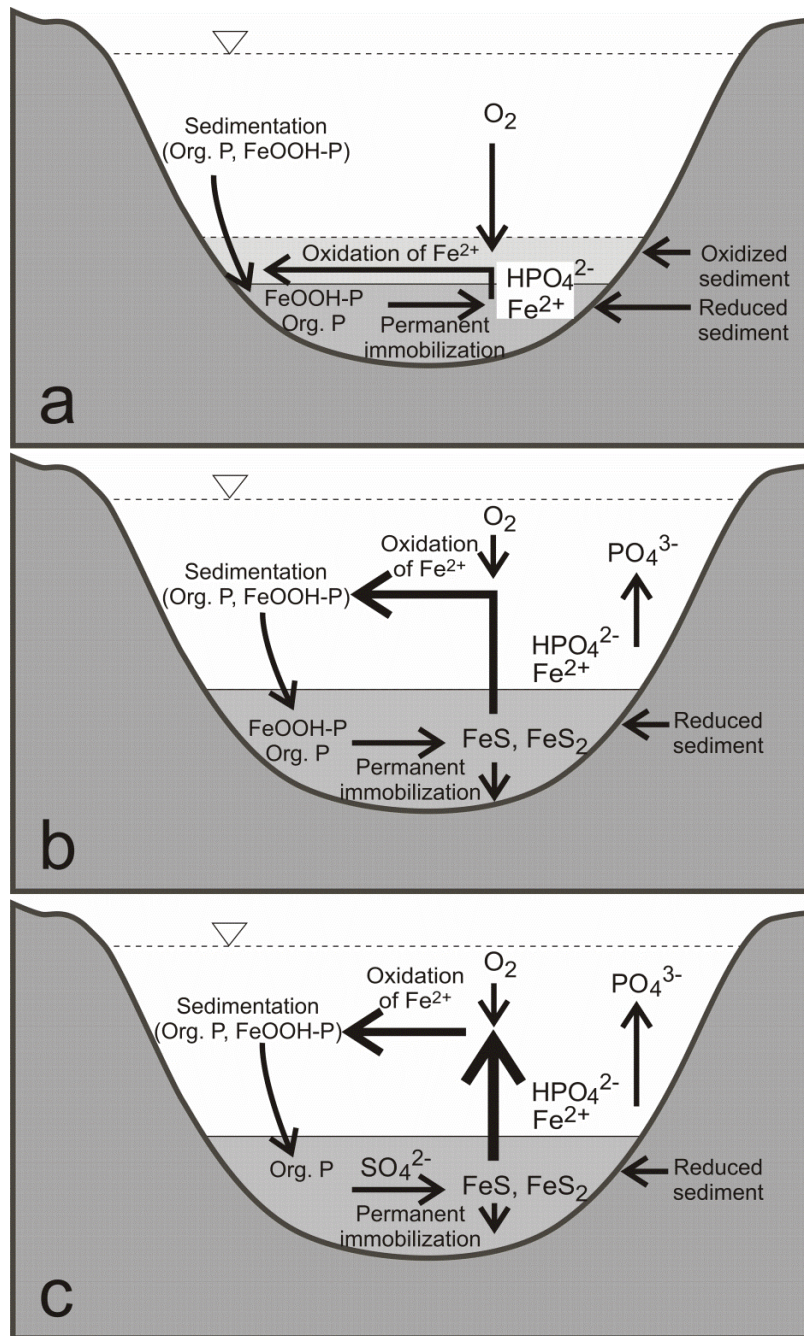


Figure 1.1 Phosphorus release mechanisms at the sediment-water interface modified from Hupfer and Lewandowski (2008). a) Oxidized sediment surface with high P retention capacity; b) Reduced sediment surface, where redox cycle controls P availability in the hypolimnion; c) Reduced sediment surface, where high sulfate concentration consume Fe and enhance the P release.

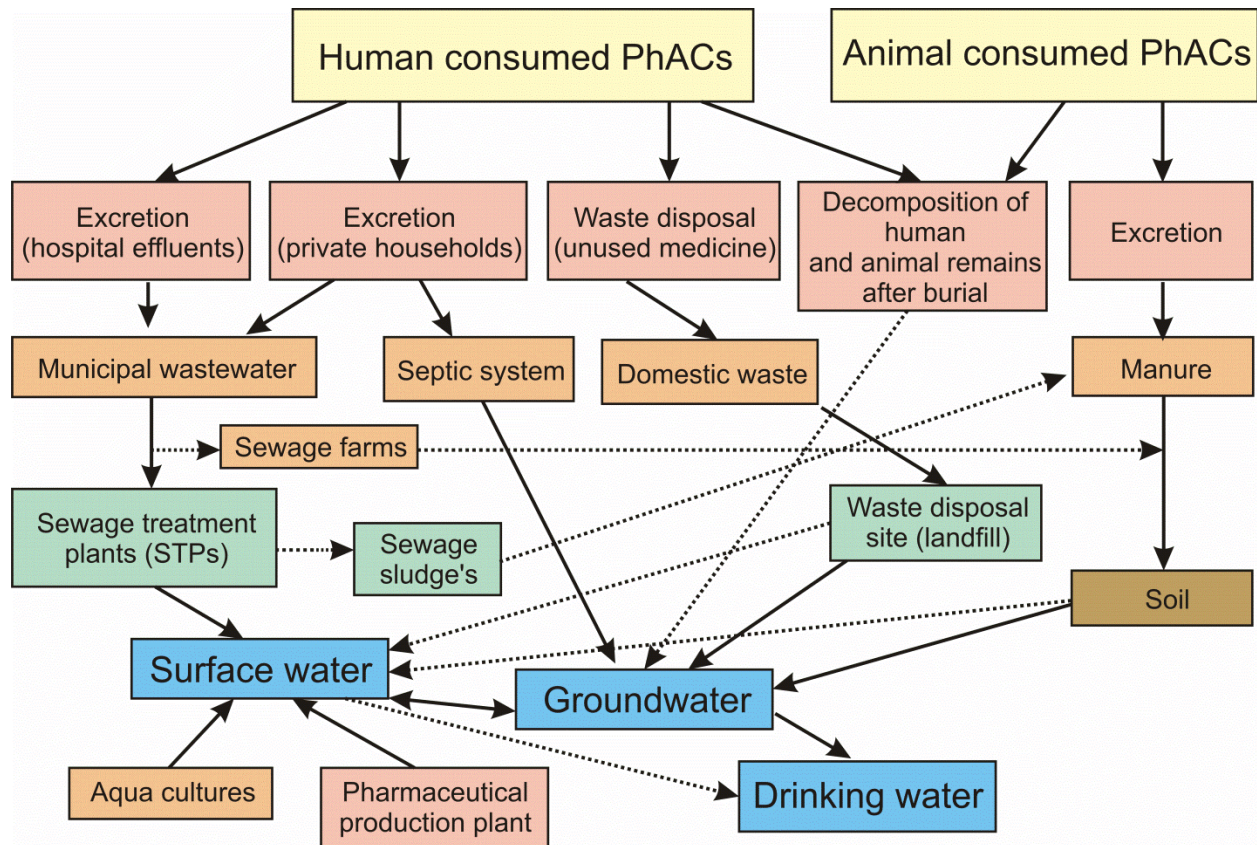


Figure 1.2 Potential point and non-point sources of PhACs to surface water, groundwater, and drinking water (After Ternes, 1998 and Heberer, 2002a).

Chapter 2

Evaluation of Basic Oxygen Furnace Slag for Removal of Phosphorus from Lake Water

2.1 Executive Summary

The effectiveness of basic oxygen furnace slag (BOFS) for removing dissolved phosphorus (P) was evaluated in a hypolimnetic withdrawal experiment. Lake water gravity fed through a small scale (pore volume, $\sim 0.87 \text{ m}^3$) field treatment system consisting of three BOFS columns arranged in series and operated over three successive summers. Phosphate ($\text{PO}_4\text{-P}$) influent concentrations ranged from 0.3 to 0.5 mg L^{-1} , of which 82.9-94.8%, 96.1-98.1%, and 97.4-99.9% was removed in years 1, 2, and 3, respectively. The PO_4 removal rate was positively dependent on pH and hydraulic retention time. The hydraulic retention times in years 1, 2, and 3 were 0.73 to 0.98 days, 0.26 to 0.58 days, and 0.33 to 0.42 days. Column effluent pH was 8.69 ± 0.43 , 11.37 ± 0.17 , and 11.96 ± 0.17 in years 1, 2, and 3, respectively, with the increase attributed to dissolution of calcium oxide and calcium hydroxide from the BOFS. The effluent was neutralized by addition of $\text{CO}_2(\text{g})$ before discharging to the environment. Vanadium and Al derived from the BOFS were likely removed within a 5 wt. % granular zero valent iron mixture with sand and by neutralizing pH. Diminished hydraulic performance in year 2 was attributed to calcium carbonate accumulating on the spent media. The solid phase analyzes of the outer layer materials of the spent media through FESEM-EDX, XPS, FTIR, and XANES spectroscopy confirmed the presence of calcium carbonate and calcium phosphate minerals. Restricting ingress of atmospheric CO_2 into the system minimized calcium carbonate accumulation on the

treatment media and ultimately led to improved hydraulic characteristics in year 3. The results show potential for effective removal of P.

2.2 Introduction

Release of phosphorus (P) to surface water bodies is of environmental significance. Phosphorus is an essential, often limiting nutrient for plants and microorganisms, especially in aquatic ecosystems impacted by anthropogenic activities (Schindler, 1977). Phosphorus can be introduced to aquatic ecosystems through both groundwater and surface waters impacted by urban and agricultural activities (Sharpley, 1994). Excess P in surface waters may cause eutrophication (Parry, 1998), which can lead to toxic algal blooms; loss of oxygen; fish kills; loss of biodiversity, including loss of species important for commerce and recreation; loss of aquatic plants and coral reefs; and other problems (Carpenter et al., 1998). Eutrophication can result in the development of anoxic, P-rich lake bottom sediments, which, in turn, release P that accumulates in anoxic hypolimnia (Nürnberg and Peters, 1984). Hypolimnetic withdrawal is a restoration method whereby water is withdrawn from an anoxic hypolimnion to enhance the removal of limiting nutrients and to reduce anoxic conditions at the sediment surface interface (Kortmann et al., 1983). In many systems, the withdrawn water is discharged to water bodies downstream (Nürnberg et al., 1987). In this study, however, the objective was to remove P and return the treated water to the lake. Specifically, this study was conducted to evaluate P removal from the hypolimnion of Lake Wilcox, Richmond Hill, Ontario, Canada, a mesotrophic, hard water lake that strongly stratifies in the summer and quickly develops anoxia within the entire hypolimnion (Nürnberg et al., 2003).

Phosphorus can be removed from water in several ways, including chemical removal, advanced biological treatment, or a combination of both. Typically, chemical treatment is specifically aimed at the removal of P from wastewaters. Several studies have evaluated P removal through surface adsorption and combined adsorption and precipitation (Morse et al., 1998; Vohla et al., 2011). Natural materials including limestone (Drizo et al. 1999), opoka (Johansson and Gustafsson, 2000), and zeolite (Sakadevan and Bravor, 1998), modified natural materials including granular activated carbon and bone char (Mortula et al., 2007), and industrial by-products including basic oxygen furnace slag (BOFS) (Baker et al., 1998; Smyth et al., 2002a; Kim et al., 2006), basic oxygen furnace oxide (BOF Oxide) (Baker et al., 1998), blast furnace slag (BFS) (Mann and Bavor, 1993; Yamada et al., 1996; Baker et al., 1998; Johansson and Gustafsson, 2000), and electric arc furnace slag (EAFS) (Drizo et al., 2006) are capable of removing P from water. Steel slag removes dissolved inorganic PO_4 through adsorption, with higher rates of adsorption observed for materials with greater porosity (Yamada et al., 1996). Basic oxygen furnace slag (BOFS) is one of the major waste by-products of the steel-making process (Mikhail et al., 1994; Bowden et al., 2009). The major phases (>10 wt. %) of BOFS are di-calcium silicate (Ca_2SiO_4), tri-calcium silicate (Ca_3SiO_5), ferrous oxide (FeO), and Ca-Mg-Mn-Zn-ferrite ($(\text{Ca},\text{Mg},\text{Mn},\text{Zn})\text{Fe}_2\text{O}_4$) (Mikhail et al., 1994). The mean percentage of the major constituents of 17 BOFS samples are Ca (28.01%), Fe (18.43%), Si (5.97%), Mg (5.53%), Mn (3.29%), and Al (2.38%); significant minor constituents are P (0.32%), C (0.26%), Cr-total (0.13%), S (0.11%), and V (0.10%) (Proctor et al., 2000). Major oxides that comprise 70-80% of BOFS include CaO, Fe_2O_3 , and SiO_2 , with lesser contributions from MgO, MnO, Al_2O_3 , P_2O_5 , TiO_2 , K_2O , Na_2O , and Cr_2O_3 (Kim et al., 2006; Bowden et al., 2009).

Due to the dissolution of lime (CaO) and portlandite (Ca(OH)₂), the concentration of dissolved Ca and the pH of water in contact with BOFS can significantly increase (Baker et al., 1998). At these high pH values (e.g., ~12), hydroxyapatite (Ca₅(PO₄)₃(OH)) may precipitate and retain PO₄ on the solid phase in the reactive media (Yeoman et al., 1988; Baker et al., 1998). Removal of phosphorus by BOF Oxide has been observed over a prolonged period of flow, with the removal attributed to adsorption and precipitation (Baker et al., 1998). Due to microbial inactivation at high pH, BOFS media also effectively removes coliforms, such as *E. coli*, from wastewater (Smyth et al., 2002b). Potentially toxic trace elements V and Cr may leach from BOFS (Proctor et al., 2000), but can be removed from water using granular zero valent iron (ZVI) filings (Blowes et al., 2000; Morrison et al., 2002).

This chapter describes experiments focused on P removal in a hypolimnetic withdrawal system using BOFS from two different sources as the reactive media. The study evaluated the extent of P removal under recirculating conditions and determined the mechanisms of P removal. An additional ZVI layer, incorporated at the effluent end of the system and intended to remove V from the BOFS effluent, was evaluated in year 3. The outer layer of the spent reactive media of year 2 were investigated in this study in order to characterize the phases contributing to P removal.

2.3 Materials and Methods

2.3.1 Reactive material

Basic oxygen furnace slag (BOFS) was obtained from the Levy Corporation (Detroit, MI, USA) for the initial trial (BOFS-A) and from the US Steel Stelco Hilton Works facility (Hamilton, ON, Canada) for the two subsequent years (BOFS-B and BOFS-C). The particle density of the BOFS was determined using a pycnometer (Air Comparison Beckman, Model 930). Surface area was determined with a surface area analyzer (Micromeritics Gemini[®], VII 2390 Series). The composition of the BOFS was determined by X-ray fluorescence (XRF; MiniPal4, PANanalytical). The constituent phases of the BOFS were determined using X-ray diffractometry (XRD) (Rigaku D/MAX 2500 rotating anode powder diffractometer) with monochromatic CuK α radiation at 50 kV and 260 mA.

2.3.2 System configuration

The hypolimnetic withdrawal treatment system was constructed adjacent to Lake Wilcox. The system consisted of three fiberglass columns with a total volume of 2.09 m³ (Figure 2.1). The columns were filled with a mixture of BOFS-A (screened coarser than 149 μ m; 100 mesh) and aggregate (19 mm, $\frac{3}{4}$ in) during year 1. In year 2, the BOFS-A mixture was replaced with an aggregate mixture containing BOFS-B, and in year 3 an aggregate mixture containing BOFS-C.

In Column 1, the reactive material filled the entire column, extending from the base to the top (Table 2.1). The influent water samples temperature were between 8.7 and 24.2⁰C in year 1, between 7.0 and 24.5⁰C in year 2, and between 8.0 and 24.8⁰C in year 3. Columns 2 and 3, which

were longer than Column 1, had 30 cm of head space above the material. In year 3, 5 wt. % ZVI, mixed with sand, was added to the upper half of Column 3. Total pore volume of the BOFS reactive materials was 0.87 m^3 , 0.87 m^3 , and 0.78 m^3 in years 1, 2, and 3, respectively. The three columns were placed in series and connected with a piping network (Figure 2.1). Each column included lateral ports (designated as Px in Figure 2.1) to collect samples at various distances along the flow path. An influent tank was placed above the maximum height of the treatment columns to maintain flow due to gravity. The influent tank was filled with water from the hypolimnion withdrawal system (to maintain constant head) and was introduced to the series of columns by gravity flow. The flow was adjusted manually using a metering valve. A $\text{CO}_{2(g)}$ tank was installed following the treatment columns to lower the pH of the column effluent via sparging. Carbon dioxide was added occasionally in year 1, and more consistently in years 2 and 3. A sand filter, graded from coarse gravel to coarse sand, was installed after the CO_2 addition tank to remove CaCO_3 precipitates and excess aluminum hydroxide precipitates. Finally, an effluent tank was installed after the filtration tank before discharging to a municipal sanitary sewer system.

2.3.3 Sample collection and analysis

The pilot treatment system was monitored weekly. Samples were collected from 13 different locations along the treatment system, including the influent and effluent tanks. The pH was measured in the field on unfiltered samples. Samples for determination of PO_4 , anion, cation, and trace metal concentrations were passed through $0.45 \mu\text{m}$ syringe filters into polyethylene bottles, chilled to less than 4°C during transport to the laboratory, and refrigerated until analysis. Cation

samples were acidified in the field with HNO_3 to a pH of less than 2, and PO_4 samples were acidified in the field with H_2SO_4 to a pH of less than 2. Alkalinity was measured in the field on filtered (0.45 μm) samples with standardized H_2SO_4 using a Hach™ digital titrator, where phenolphthalein and bromocresol green-methyl red pH indicators were used to distinguish hydroxide alkalinity from total alkalinity. The concentration of S^{2-} was measured in the field using the methylene-blue method (APHA, 2005), and ortho-phosphate was analyzed using the ascorbic acid method (APHA, 2005) within 7 days of collection. Major cations were analyzed by inductively coupled plasma optical emission spectroscopy (ICP-OES) and trace elements were analyzed by ICP-mass spectrometry (ICP-MS).

2.3.4 Characterization of reactive material

In year 2, the hydraulic performance of the treatment system declined after 144 days of operation and Column 2 and Column 3 were bypassed at this time. The reactive media were sampled at the end of year 2. Solid-phase samples were collected at 15-20 cm intervals from all three columns and examined using a Leo 1530 field emission scanning electron microscope (FE-SEM) with energy dispersive X-ray (EDX) analysis. The materials of the spent BOFS outer layer were analyzed by Fourier transform infrared spectroscopy (FTIR). Transparent 1 cm diameter KBr disks/pellets were prepared using a 13 mm pellet die by pressing (with 5 to 6 tonnes pressure for 1 min) a mixture of the ground samples and KBr (sample to KBr ratio were approximately 1:100). A Bruker Tensor 27 infrared spectrometer was used to examine the KBr pellets. The data acquisition parameters for these analyzes included 4 cm^{-1} resolution, sixteen scans, and wave numbers between 4000 and 400 cm^{-1} . Spectra for blank KBr samples were subtracted from each

sample spectrum to minimize the influence of the KBr. Reference materials were purchased from Sigma Aldrich, Canada. These included iron (III) phosphate (FeP), β -tricalcium phosphate (β -TCP), α -tricalcium phosphate (α -TCP), hydroxyapatite (HAP-S), calcium phosphate dibasic (CPD), and calcium phosphate dibasic dihydrate (CPDD). In addition, hydroxyapatite was synthesized in the laboratory following a liquid mix technique described in Pena and Vallet-Regi (2003) and included as an additional reference material (labeled hydroxyapatite-wet method; HAP-WM). Phosphate sorbed on calcite (PSC) was synthesized by adding 5 g calcite powder to 1 L of a 250 mg L⁻¹ PO₄-P solution and shaking for 48 hours. The white precipitates were collected on a Whatman grade no.4 filter paper and freeze dried before characterization by FTIR and SEM-EDX. The percent of phosphate in the PSC was estimated from the initial and the final concentrations of P in the solution.

X-ray photoelectron spectroscopic (XPS) analyzes were performed using a Kratos Axis Ultra spectrometer. This instrument used a monochromatic Al K(α) source (15mA, 14kV). XPS can provide information from the uppermost 5-7 nm of the surface and can detect all elements but hydrogen and helium with detection limits varying from 0.1 to 0.5 atomic percent depending on the element. The work function of the instrument was calibrated to a binding energy (BE) of 83.96 eV based on Au 4f_{7/2} line for metallic gold and the dispersion of the spectrometer was adjusted to a BE of 932.62 eV based on Cu 2p_{3/2} line of metallic copper. The Kratos charge neutralizer system was used for all samples. The acquired spectra were corrected for charge to the main line of the carbon 1s spectrum and set to 284.8 eV. The XPS data processing software CasaXPS (version 2.3.14) was used to analyze the spectra.

XANES analysis was conducted at the Canadian Light Source, Saskatoon, Canada. The energy of the storage ring in this facility is 2.9 GeV. Soft X-ray Micro-characterization Beam line (SXRMB; 06B1-1) covering the energy region of 1700-10000 eV with photon resolution of 0.2eV and a beam spot size of 300 μm x 300 μm was used to record XANES data for phosphorus. XANES data were collected in Total Electron Yield (TEY) and Fluorescent Yield (FY) mode. A monochromator with Si (111) crystals and a flux of $>1 \times 10^{11}$ photons s^{-1} was used to collect experimental and standard data. To improve signal-to-noise ratios the spectral data were averaged over 2–3 scans. The reference materials used for the FTIR analysis, also were used for the XANES experiments. The XANES spectra of the unknown samples were compared with reference materials through linear combination fitting using Athena software package, version 0.8.56 (Ravel and Newville, 2005).

2.3.5 Geochemical modeling

The geochemical modeling code PHREEQC Interactive (Parkhurst and Appelo, 1999) was used to calculate the saturation indices (SI) for calcium phosphate and other mineral phases relevant to the treatment system. The WATEQ4F database was used for these calculations. Solubility product values for brushite, monetite, octacalciumphosphate, β -tricalciumphosphate, and variscite were added to the WATEQ4F database using previously published thermodynamic data (Baker et al., 1998; Stumm and Morgan, 1981). Calculations were conducted with data from five sampling events at all 13 sampling locations during the final year of the experiment.

2.4 Results and Discussion

2.4.1 Characteristics of the reactive materials

The surface area of all three BOFS samples was dominated by the finest fraction (Table 2.2). The particle densities of BOFS-A, BOFS-B, and BOFS-C were 3.30, 3.67, and 3.53 g cm⁻³, respectively, demonstrating the consistency of the BOFS materials. All BOFS samples contained between 33 and 40 wt. % CaO. BOFS-C contained a lower percentage of Fe₂O₃ and a higher proportion of SiO₂ than BOFS-A and BOFS-B (Table 2.2). The main mineral phases obtained from the XRPD analysis were srebrodolskite (Ca₂Fe₂O₅), larnite (Ca₂SiO₄), periclase (MgO), wuestite (Fe_{0.942}O), magnetite-ulvöspinel (Fe₃O₄-Fe₂TiO₄), lime (CaO), hatrurite (Ca₃(SiO₄)O), and anhydrite (CaSO₄) in BOFS-A; wuestite (Fe_{0.925}O), larnite (Ca₂SiO₄), brownmillerite (Ca₂((Fe_{1.885}Al_{0.115})O₅), lime (CaO), anhydrite (CaSO₄) and quartz (SiO₂) in BOFS-B; larnite (Ca₂SiO₄), wuestite (Fe_{0.9}O), hatrurite (Ca₃(SiO₄)O), lime (CaO), anhydrite (CaSO₄) in BOFS-C. Beside these minerals phases portlandite (Ca(OH)₂; peak at 4.92Å, 18.00 2-theta) was a probable mineral phase in all of these BOFS samples.

2.4.2 pH, Eh, alkalinity, and temperature

The pH of the influent water, collected from the hypolimnion of Lake Wilcox, was consistently near neutral (7.28±0.08 in year 1, 7.32±0.07 in year 2, and 7.26 ±0.11 in year 3; Figure 2.2). In year 1, a gradual increase in pH was observed as the water flowed through the reactive columns. A maximum pH of 9.6 was observed during year 1 of the study; during year 2 and year 3, the pH increased rapidly in Column 1 and then remained relatively constant through the rest of the

columns, reaching a maximum of 11.53 in year 2 and 12.13 in year 3 (Figure 2.2). The alkalinity of the effluent in years 1, 2, and 3 was 129 ± 51 , 183 ± 75 , and 698 ± 448 mg L⁻¹ as CaCO₃, respectively (Figure 2.2). The total alkalinity did not change abruptly along the column profile during years 1 and 2. However, the total alkalinity increased rapidly in the initial stage (maximum 1214 mg L⁻¹ as CaCO₃) of year 3 and gradually decreased with time as the system was continuously flushed and as free lime (CaO) and portlandite (Ca(OH)₂) were leached from the outer layer of the BOFS. A decrease in the caustic alkalinity, compared to the total alkalinity, was observed in year 3. The release of high pH effluent from the treatment system was addressed through the addition of a neutralization component in year 1, 2 and 3. The pH adjustment involved addition of CO₂ following the treatment columns. The amount of CO₂ required to neutralize the high effluent pH was determined on the basis of the difference between the OH⁻ concentration measured in the effluent from Column 3 and the desired OH⁻ concentration (typically 10⁻² moles of CO₂ per litre of effluent were required to reduce the pH from 12 to 7.5). The pH of the treatment column effluent typically varied between 6.5 and 8.5; however, there were a few exceptions when an insufficient amount of CO₂ was delivered to the system (Figure 2.2).

The Eh of the influent varied between -24 and 154 mV in year 1, between -25 and 186 mV in year 2, and between -8 and 73 mV in year 3 (Figure 2.3). The Eh of the treatment system effluent varied between 283 and 341 mV in year 1, and between 286 and 403 mV in year 2 and between 226 and 428 in year 3 (Figure 2.3). The temperature of the treatment system effluents varied between 5.9 and 26⁰ C.

2.4.3 Major ion chemistry

During year 1, Ca concentrations gradually increased along Columns 1 and 2 and then decreased along Column 3 (Figure 2.4). In year 2, Ca concentrations initially increased along Columns 1 and 2, and then decreased later in the year. However, clogging was observed during year 2, and Ca concentrations did not follow a discernable pattern later in the year (Figure 2.4). In the early stages of year 3, sharp increases in Ca concentrations accompanied increases in pH and caustic (OH⁻ based) alkalinity observed in Column 1 (Figure 2.4, Figure 2.5). The dissolution of calcium hydroxide, calcium oxides and calcium hydroxosilicates probably were the principal sources of Ca to the water.

In year 1, Mg concentrations progressively increased along the flow path through the treatment materials. In contrast, Mg concentrations declined sharply along the flowpath during both year 2 and year 3. In year 3, for example, Mg concentrations decreased sharply in Column 1 and remained low in the remainder of the columns (Figure 2.5).

Influent SO₄ concentrations were 10.9±1.4, 11.7±0.9, and 11.9±1.8 mg L⁻¹ in years 1, 2, and 3 and remained relatively uniform throughout the study (Figure 2.5). Each year a decline in SO₄ concentrations along the length of the treatment system was observed. In year 3, this removal resulted in an 80% decline in the SO₄ concentration at the beginning of the year and a 40% decline at the end of the year (Figure 2.5).

2.4.4 Phosphorus removal

Mean influent PO₄-P concentrations were 0.362, 0.345 and 0.339 mg L⁻¹ in years 1, 2 and 3, respectively; the corresponding mean effluent concentrations were 0.034, 0.011, and 0.005 mg L⁻¹

¹ (Figure 2.2, Table 2.3). These mean effluent concentrations were in the range observed for meso-eutrophic, mesotrophic, and oligotrophic conditions for years 1, 2, and 3, respectively (CCME, 2004). In year 1, between 82.9 and 94.8% removal of PO₄ was observed when the flow rate was adjusted between 1.2 and 0.89 m³ day⁻¹ (hydraulic retention time 0.73 to 0.98 days) by a valve at the system inlet tank. In year 2, the flow rate was adjusted several times, between 3.31 and 1.51 m³ day⁻¹ (hydraulic retention time 0.26 to 0.58 days), corresponding to 96.1 to 98.1% removal of PO₄. Finally, in year 3, the flow rate was adjusted to between 2.35 and 1.86 m³ day⁻¹ (hydraulic retention time 0.33 to 0.42 days), corresponding to a PO₄ removal of 97.4 to 99.9%. At the end of year 1, the extent of PO₄ removal decreased. There was no significant decrease in the extent of PO₄ removal during years 2 and 3. The total P-masses that entered in the treatment system were 36, 50, and 55 g in years 1, 2, and 3; while the total P-masses that exited from the system were 6, 1, and 1 g in years 1, 2, and 3 (Figure 2.6, Table 2.4). Thus the total masses retained by the system were 86, 98, and 98% in years 1, 2, and 3.

At pH values over 9, adsorption of the dominant phosphate species (HPO₄²⁻ and PO₄³⁻) onto iron oxyhydroxides is not expected (Stumm and Morgan, 1981). However, certain oxides (MgO and Al₂O₃) may favour limited adsorption due to the high pH of the zero point of charge (pH_{ZPC}) of these phases. The presence of 8-9% MgO (pH_{ZPC} = 12.4; Parks, 1965) and 4-6% Al₂O₃ (pH_{ZPC} = 9.1; Parks, 1965) in the BOFS materials used in this study suggests that adsorption was one of the potential PO₄ removal mechanisms. Precipitation of calcium phosphate phases (dependent on the Ca concentration) including hydroxyapatite (HAP) is another potentially important PO₄ removal mechanism in BOFS-based treatment systems (Baker et al., 1998; Bowden et al., 2009). However, Mg in the pore water may replace the Ca in hydroxyapatite and inhibit the formation

of crystalline hydroxyapatite (Kim et al., 2006). Thus, both adsorption and precipitation were probable mechanisms involved in removing PO_4 in this treatment system. At the end of year 1, the rate of PO_4 removal decreased (Figure 2.2). However, there was no significant decrease in the rate of PO_4 removal during years 2 and 3.

The FE-SEM images and EDX data were collected from samples of the fresh BOFS material and from the spent media along the flow path from the year 2 material, to investigate changes in composition on the outer layers of these materials (Figure 2.7, Table 2.5). The phosphorus content of the fresh BOFS was ~ 0.08 wt% and the mass of P on the spent media increased with increasing distance along the flow path (Figure 2.7, 2.8). The phosphorus content was negatively correlated ($r=-0.96$) with the dissolved PO_4 concentration and positively correlated ($r=0.88$) with the aqueous pH in Columns 1 and 2 (Figure 2.8). The P mass in the upper part of Column 2 was slightly less than in the middle zone of Column 2 (Figure 2.7, Sample 8-9), which suggests extensive removal of aqueous PO_4 in the middle zone of Column 2. In Column 3, which was beyond the P-removal front, the solid mass of P remained low (Table 2.5).

In year 1, BOFS-A was used in the reactive mixture. The PO_4 removal efficiency of this slag was not as high as observed in previous laboratory experiments (Figure 2.2; Baker et al., 1998). Low effluent pH (as low as 8.75 after two months of operation) and less efficient PO_4 removal (83%) were observed. BOF slag is an industrial byproduct, which is stored in stockpiles out of doors. The low PO_4 -removal efficiency observed for BOFS-A suggests that this material likely underwent prolonged exposure to atmospheric CO_2 before it was acquired for this experiment. BOFS-B was used during year 2. Moderately high effluent pH and low PO_4 concentrations were observed (Figure 2.2). The reactive material was replaced in year 3 with BOFS-C. High effluent

pH, very low effluent PO₄ concentrations immediately after Column 1 and high alkalinity values suggest that this BOFS-C was less weathered than the BOFS-A or BOFS-B (Figure 2.2).

2.4.4.1 FTIR

The FTIR spectra of the outer layer materials of the spent media from different parts of Columns 1, 2, and 3 from year 2 were analyzed. Carbonate vibrational bands including ν_4 at 712-713 cm⁻¹, ν_3 at 1424-1428 cm⁻¹, ν_2 at 874-875 cm⁻¹, and carbonate overtones or combination bands $\nu_1 + \nu_4$ at 1796-1799 cm⁻¹, $\nu_1 + \nu_3$ or $2\nu_2 + \nu_4$; at 2513-2517 cm⁻¹, and $2\nu_3$ at 2871-2876 cm⁻¹ and 2979-2986 cm⁻¹ (Gillet et al., 1996; Vongsavat et al., 2006; Tatzber et al., 2007; Gunasekaran and Anbalagan, 2008) were observed in the FTIR spectra in the samples. Presence of these carbonate bands, particularly the range obtained for ν_4 and ν_2 were comparable to the ranges reported for calcite (Vagenas et al., 2003; Vongsavat et al., 2006; Ni and Ratner, 2008; Kurap et al., 2010), which suggested that calcite is the principal carbonate mineral in the precipitates collected from the outer layer of the spent BOFS (Table 2.6). However, the presence of a shoulder of carbonate ν_2 band at 858 cm⁻¹ (an unique feature of aragonite; Vongsavat et al., 2006), in sample C2-S10 in addition to the sharp ν_2 band at 875 cm⁻¹ and ν_4 band at 712 cm⁻¹ suggested that the sample may contain a small percentage of aragonite as well.

The phosphate vibrational bands for the reference materials were determined. Vibrational bands for the hydroxyapatite (Sigma) were at 475 cm⁻¹ (ν_2), 568 cm⁻¹ (ν_4), 603 cm⁻¹ (ν_4), and 633 cm⁻¹ (ν_4), 962 cm⁻¹ (ν_1), 1045 cm⁻¹ (ν_3), and 1092 cm⁻¹ (ν_3). For the laboratory-synthesized hydroxyapatite, vibrational bands were at 474 cm⁻¹ (ν_2), 571 cm⁻¹ (ν_4), 602 cm⁻¹ (ν_4), and 633 cm⁻¹ (ν_4), 962 cm⁻¹ (ν_1), 1042 cm⁻¹ (ν_3) and 1090 cm⁻¹ (ν_3); and for β -TCP, vibrational bands were at

474 cm^{-1} (ν_2), 564 cm^{-1} (ν_4), 603 cm^{-1} (ν_4), and 634 cm^{-1} (ν_4), 962 cm^{-1} (ν_1), 1033 cm^{-1} (ν_3) and 1098 cm^{-1} (ν_3) (Table 2.7). These values were consistent with the vibrational bands observed in other studies (Table 2.8; Rehman and Bonfield, 1997; Pena and Vallet-Regi, 2003).

Phosphate ν_3 bands were observed in all of the samples at 1009-1041 cm^{-1} and 1078-1082 cm^{-1} . Weak peaks from phosphate ν_4 bands were mainly observed at 581-586 cm^{-1} . However, in some samples it was possible to identify very weak phosphate ν_4 bands at 600-608 cm^{-1} , 588-595 cm^{-1} , and 562-578 cm^{-1} . Weak phosphate ν_2 bands were observed in most of the samples at 444-473 cm^{-1} . Phosphate ν_1 bands were observed in samples C2-S10 (at 979 cm^{-1}) and C2-S3 (at 977 cm^{-1}) as very weak shoulders. Among the samples analyzed, C2-S10 and C2-S3 showed more distinct and complete vibrational bands for carbonate and phosphate (Figure 2.9). Due to the weak phosphate vibrational bands (corresponding to low phosphorus concentrations 0.65 -1.29 wt. %) it was very difficult to confirm the occurrence of hydroxyapatite or β -TCP. However, the location of the peaks indicated the possibility of formation of similar Ca-PO_4 phases. The unused BOFS showed similar carbonate vibrational bands observed in the samples, however, the phosphate vibrational bands were not as distinct compared to the samples.

2.4.4.2 XPS

The XPS survey spectra of samples C1-S2, C1-S3, C1-S4, C2-S4, C2-S9, S2-S10, and C2-S1 were obtained. Most of the samples showed peaks for O, Ca, Mg, C, P, Si and Al in the survey XPS spectra. High resolution spectra of samples with the highest P concentrations, C1-S2 (0.4% P) and C1-S3 (0.3% P), were collected. A calcium carbonate reference material showed a peak of Ca 2p_{3/2} at binding energies of 346.7 to 347.0 eV, and a calcium phosphate reference material

showed peak of Ca 2p_{3/2} at a binding energy of 347.3 eV and P 2p_{3/2} peak at 133.0 eV. The binding energies of Ca 2p_{3/2}, Ca p_{1/2}, and carbonate peaks of samples C1-S2 and C1-S3 were at 346.88, 350.43, and 289.38 eV and 347.07, 350.62, and 289.54 eV (Table 2.9), which are consistent with the values for calcite and vaterite reported in Ni and Ratner (2008). The surface atomic ratios of Ca/C in samples C1-S2 (0.32) and C1-S3 (0.29) were much lower than the ratio reported for calcite or vaterite reported in Ni and Ratner (2008). Whereas the surface atomic ratio of O/Ca in sample C1-S2 was ~88% higher than that of calcite and in sample C1-S3 the O/Ca ratio was ~25% higher expected for vaterite reported in Ni and Ratner (2008). The binding energies of P 2p_{3/2} and P 2p_{1/2} were at 132.57 and 133.41 eV for C1-S2 and 132.77 and 133.61 eV for C1-S3 (Table 2.9). The binding energies of Ca 2p_{3/2} and P 2p_{3/2} in the samples and the reference materials were within the same range. However, due to low concentrations of P in the samples the intensity of the P 2p_{3/2} peaks was not high enough to interpret the type of calcium phosphate in the samples.

2.4.4.3 XANES

Phosphorus K-edges or white lines (energy required to eject electrons from the K shell of P atoms; Güngör et al., 2007) for phosphate reference materials were observed at 2151.6 ± 0.1 eV. Similar peak positions for phosphate species are reported in previous studies (Shober et al., 2006; Brandes et al., 2007). Depending on the charge, electronegativity, and interatomic distance of the coordinating cation, the position of white lines for phosphate phases may vary between ± 0.5 eV (Franke and Hormes, 1995). XANES spectra of the reference materials showed pre- and post-edge features between -3 and ~18 eV (Figure 2.10), which were within the range (from -50 to

+200 eV with respect to the edge energy) described by Kelly et al. (2008). The FeP reference material showed white line at 2152 eV and a pre-edge feature at ~2148.5 eV (-2.5 eV with respect to the white line), which is consistent (between -2 and -5 eV) with previous studies (Hesterberg et al., 1999; Khare et al., 2007; Ajiboye et al., 2008; Shober et al., 2006, Sato et al., 2005, Eveborn et al., 2009; and Beauchemin et al., 2003). Despite the fact that the primary peak positions of the phosphate-bearing (oxidation state +5) phases are similar, the characteristics of the secondary spectral features, including size, shape, and position, are diagnostic for different compounds and minerals (Brandes et al., 2007). Phosphorus K-edge XANES spectra with all spectral features for Ca-, Al-, and Fe-phosphates were characterized in previous studies to adapt the finger printing approach in interpreting unknown samples (Hesterberg et al., 1999; Ajiboye et al., 2008; Shober et al., 2006; Sato et al., 2005; Eveborn et al., 2009; Beauchemin et al., 2003).

The presence of a shoulder at ~2154.7 eV (Figure 2.10 c), peaks at ~2162.5 eV and ~2169 eV (Figure 2.10 d, e) were important spectral features observed in all calcium phosphate reference materials. The post-edge features have been attributed to the presence of Ca-PO₄ species and the oxygen oscillation. The relative positions of these features with respect to P K-edge were consistent features observed in other studies (Peak et al., 2002; Sato et al., 2005).

Comparison of the XANES spectra of reference materials and the samples (Figure 2.10) indicates the presence of spectral features similar to the reference materials particularly CaP within the samples. The white lines of the samples and the CaP reference materials fell within the same range of 2151.6 ± 0.1 eV. The post-edge features in the samples spectra were located in the same energy range as observed in the reference materials. However, none of the samples

showed post-edge features as distinct as observed for the crystalline CaP reference materials including HAP and β -TCP. Linear combination (LC) fitting analysis of a series of binary and ternary combinations of spectra from the reference materials showed that mixtures of β -TCP, α -TCP, and CPDD provided the best-fitting spectra for samples C3-S1 and C2-S10 with lower χ^2 values of 2.13 and 2.30 (Figure 2.11, Table 2.10). The LC fitting results indicated that FeP does not constitute a significant component of the samples, due to the absence of the distinct pre-edge feature, which was not present in any of the samples. LC fitting for the other samples including C2-S9, C1-S2, C2-S11, and C2-S4 showed comparatively higher χ^2 values of 3.21, 3.29, 4.42, and 5.48 (Table 2.10) lesser goodness of fit to these spectra. The combination of α -TCP, β -TCP, and CPDD provided the best combination for all of these samples.

2.4.5 Geochemical modeling

The influent water during year 3 was undersaturated with respect to brushite, monetite, octacalcium phosphate, β -tricalcium phosphate, vivianite, and, variscite (Figure 2.12). This water also was undersaturated with respect to calcite and aragonite and supersaturated with respect to hydroxyapatite, MnHPO_4 , strengite, gibbsite, goethite, and ferrihydrite. The influent water was supersaturated with respect to hydroxyapatite according to the WATEQ4F database, but undersaturated with respect to hydroxyapatite using $\log K_{sp}$ value derived from a laboratory experiment using BOF oxide at pH values similar to those in this study (Baker et al., 1998). Using both K_{sp} values, the water passing through the columns became supersaturated with respect to hydroxyapatite, β -tricalcium phosphate, brucite, calcite, and aragonite. Although the

water remained supersaturated with respect to gibbsite, ferrihydrite, MnHPO_4 , and strengite in the first 1m of the flow path, it was undersaturated with respect to these mineral phases for the remainder of the flow path. The water remained undersaturated with respect to brushite, monetite, and octacalcium phosphate along the flow path. Hydroxyapatite is considered one of the major P-bearing phases in Ca- and P-rich environments (Stumm and Morgan, 1981; Baker et al., 1998; Bowden et al., 2009), and the supersaturation with respect to hydroxyapatite observed in the pore water of all three columns. The very low concentrations of phosphate in the column effluent and indications of the presence of Ca- PO_4 phases in FTIR and XANES spectra, suggest that precipitation of Ca- PO_4 phases is a mechanism through which P is retained by the reactive media. The PHREEQCI model results showed that the pore water was supersaturated with respect to calcite and aragonite along the flow path, which is consistent with the high carbonate alkalinity measurements and the identification of calcite in the column materials during the mineralogical study. These observations suggest that the dissolved Ca concentrations are probably limited by the precipitation of CaCO_3 and Ca- PO_4 phases.

A zone of Mg removal progressively migrated along the length of the system over the course of year 3 (Figure 2.5). The migration of the Mg reaction front coincides with the migration of the decline in pH and the $\text{PO}_4\text{-P}$ removal zone, suggesting that both reaction fronts may be associated with the depletion of Ca oxides and hydroxides. The geochemical modeling results suggest that at high (>9.2) pH values, the formation of $\text{MgCO}_{3(s)}$ is favoured; however, no MgCO_3 precipitates were observed during the mineralogical examination of the treatment materials. The decrease in Mg concentrations may also be due to co-precipitation of Mg with CaCO_3 or Ca- PO_4 precipitates. The substitution of Mg for Ca in hydroxyapatite (Kim et al.,

2006) is a possible mechanism contributing to Mg removal. An elevated abundance of Mg (~13%), associated with Ca in precipitates, was observed in some of the EDX data. In addition, the pore water was supersaturated with respect to brucite when the hydroxide alkalinity contributed to the total alkalinity.

PHREEQCI speciation calculations indicated that the pore water throughout the columns was undersaturated with respect to gypsum and other SO_4 minerals, indicating that the decrease in SO_4 concentrations observed along the columns was probably not due to precipitation of SO_4 -bearing phases. Sulfate also may be removed from the water by SO_4 reduction and metal sulfide precipitation. Measurements made in year 3 indicate that dissolved S^{2-} concentrations in the influent were above detection (0.005 to 0.8 mg L^{-1}). Later, in year 3, dissolved S^{2-} concentrations gradually decreased to very low concentrations, and were often below the detection limit.

PHREEQCI results indicated saturation with respect to amorphous FeS was attained occasionally.

2.4.6 Trace metals

Dissolved trace metals, including Cd, Co, Cr, Cu, Fe, Mo, Ni, Pb, Ti, and Zn, were present in the treatment system effluent at very low concentrations that remained low, below water quality guidelines for Ontario (MOEE, 1994). However, Al and V concentrations were up to 0.85 mg L^{-1} and 0.13 mg L^{-1} respectively, exceeding guideline values of 0.075 mg L^{-1} and 0.006 mg L^{-1} .

Vanadium concentrations in the influent during all three years of the trial were close to or below the detection limit (0.000025 mg L^{-1}). In the BOFS column effluent, mean V concentrations

increased to 0.008, 0.098, and 0.039 mg L⁻¹ in years 1, 2, and 3, respectively (Figure 2.13). The configuration of the treatment system was modified in year 3 when 5 wt. % ZVI, mixed with sand, was added to the upper half of Column 3. Following this modification, the mean effluent V concentrations derived from the ZVI layer was 0.027 mg L⁻¹. Vanadium was removed from the system to below the water quality guidelines (0.006 mg L⁻¹) for 50 days after introducing the ZVI layer. The removal decreased after this period, suggesting that 5 wt. % ZVI (2.05 vol. %) is insufficient to sustain prolonged V removal and an increase in the ZVI content would be required for full-scale implementation.

Mean Al concentrations in the influent water were 0.002, 0.002, and 0.010 mg L⁻¹ in years 1, 2, and 3, respectively; the corresponding mean effluent Al concentrations were 0.022, 0.294, and 0.426 mg L⁻¹ (Figure 2.13). The influent water and pore water in Column 1 were supersaturated with respect to gibbsite but, as the pH increased, the water became undersaturated with respect to gibbsite and Al concentrations increased. The solubility of Al reaches a minimum at near neutral pH values (Stumm and Morgan, 1981). Therefore, the pH was adjusted through CO₂ addition to decrease the dissolved Al concentration in the final effluent and a sand filter was added to remove the particulate Al that formed. After these system modifications, Al concentrations decreased to below 0.075 mg L⁻¹, the water quality guidelines for Ontario (MOEE, 1994). Geochemical calculations indicate that the column effluent became supersaturated with respect to gibbsite following the pH adjustment and suggest that the Al concentrations declined due to precipitation of an Al hydroxide phase, with subsequent removal of this phase in the sand filter.

2.4.7 Accumulation of precipitates in columns

No noticeable impedance in flow of lake water through the treatment system was observed during year 1. However, during year 2 there was a noticeable decline in flow. Extensive precipitation was observed near the top of Column 1 at the end of year 2 and was presumed responsible for the observed decline in flow. Samples of the precipitate reacted with HCl vigorously, indicating the presence of carbonate minerals. Binocular microscopic examination of the precipitate from the top of the Column 1 showed the presence of abundant acicular crystals (Figure 2.14). Crystals with well-developed faces and elevated concentrations of Ca (9%), C (45%), and O (25%) were observed in the FE-SEM images and EDX data (Figure 2.5, Sample 5a). All of these observations suggest that the precipitates were CaCO_3 , which formed due to the ingress of atmospheric $\text{CO}_{2(g)}$ into the BOFS columns, and reaction with Ca derived from the BOFS. Hydraulic performance was greatly improved in year 3 by sealing the reactive columns to restrict the ingress of atmospheric $\text{CO}_{2(g)}$ and prevent the formation of excessive CaCO_3 .

2.5 Conclusions

Basic oxygen furnace slag (BOFS), a waste by-product of the steel-making process, was used in a hypolimnetic withdrawal phosphorus treatment system. The BOFS removed phosphorus (P) (up to >99% removal) to concentrations of $< 0.005 \text{ mg L}^{-1}$. Precipitation of P-bearing solids was the principal P removal mechanism. The BOFS treatment material generated a high pH effluent (ranging from pH 8 to 12), attributed to dissolution of CaO and Ca(OH)_2 . This effluent was neutralized by sparging with $\text{CO}_{2(g)}$ prior to discharge to the environment. Elevated V and Al concentrations also were derived from the BOFS. Vanadium in the effluent was removed likely

by reduction with 5 wt. % granular zero valent iron mixed with sand. Aluminum was removed by a sand filter following pH neutralization. Utilization of less weathered BOFS in years 2 and 3 led to improved P removal. In year 3, further isolating the BOFS from atmospheric CO₂ by tightly sealing the treatment columns lessened the extent of CaCO₃ accumulation on the treatment media, which in turn improved the hydraulic performance of the system. A trend of increasing P content along the flow path in first two columns indicates that the location of maximum P accumulation coincided with the location of a sharp increase the pH and a sharp decrease in the PO₄ aqueous concentration. Surface techniques including BSE imaging with EDX spectra, XPS, FTIR, and XANES spectra and corresponding LC fitting suggest that phosphorus accumulated on the outer layer of the spent BOFS media as β-tricalciumphosphate and α-tricalciumphosphate. The results of this study suggest that the BOFS based reactive material can be used for extended periods with little maintenance, potentially providing a sustainable option for the removal of P from small lakes.

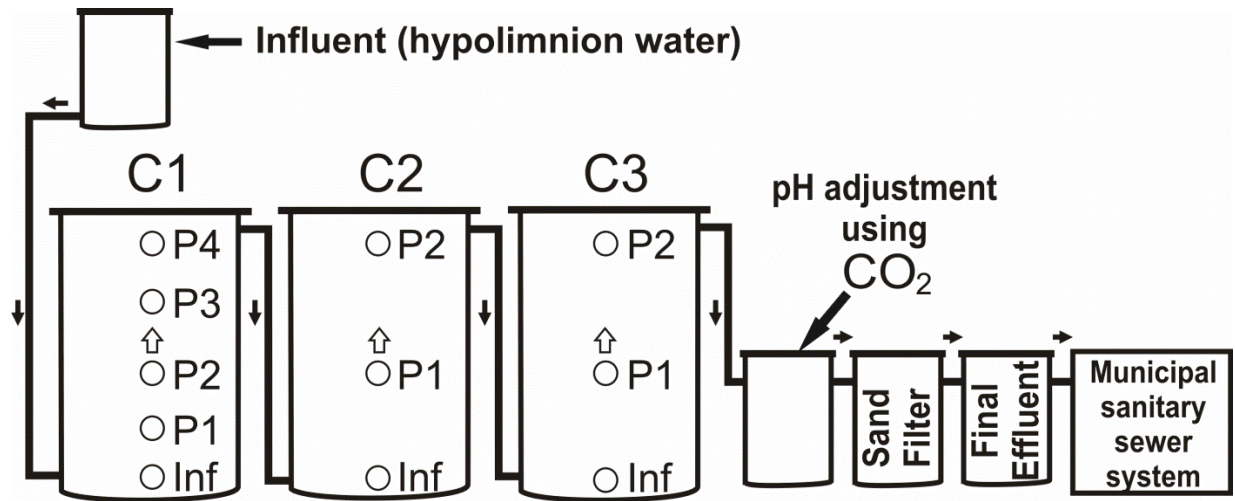


Figure 2.1 Schematic diagram of the field columns at Lake Wilcox, Richmond Hill, Ontario. Influent waters were collected from the hypolimnion of the lake and made available periodically for continuous flow by gravity feed into the treatment system.

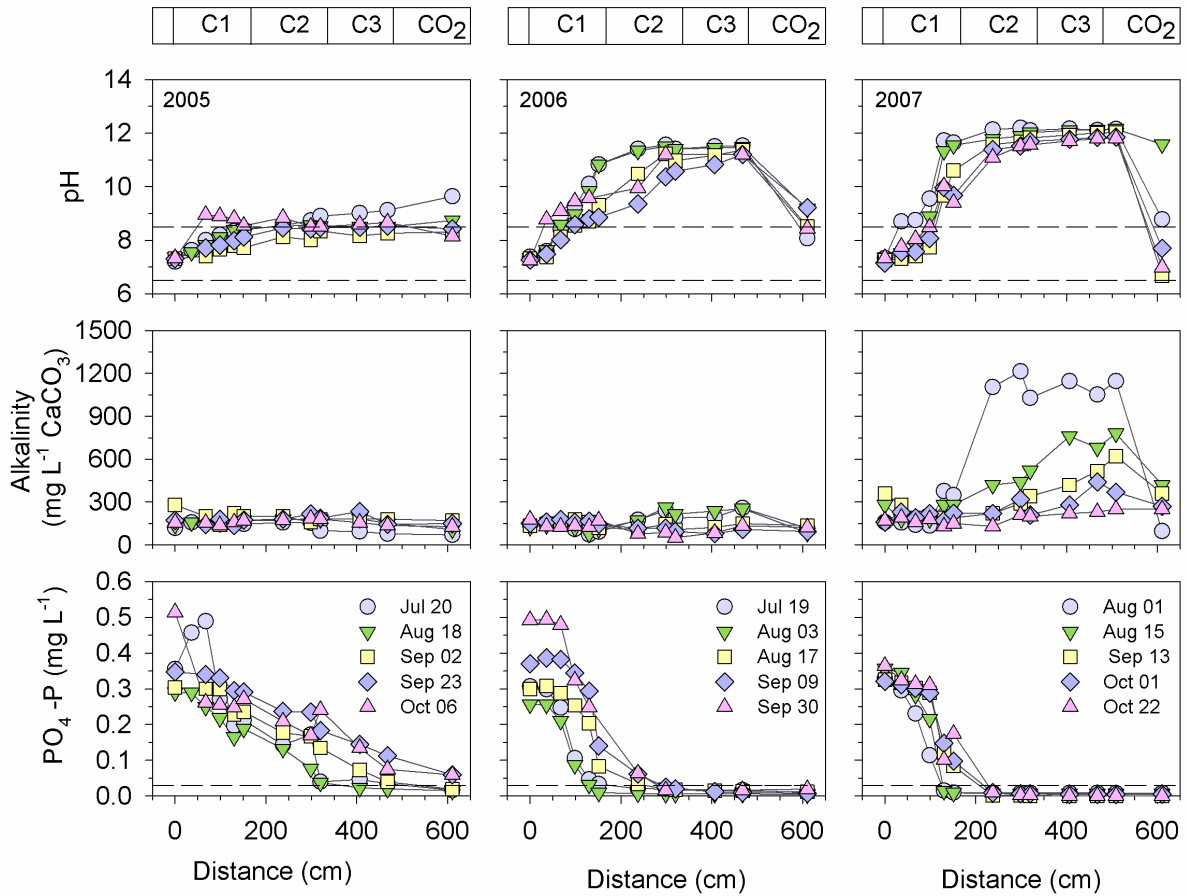


Figure 2.2 pH values, alkalinity and PO₄-P concentrations versus vertical distance along the treatment flow path in years 1, 2, and 3 of the hypolimnetic withdrawal P treatment experiment, respectively. C1, C2, C3, and CO₂ at the top represent Columns 1 to 3 and the neutralization tank, respectively. The dashed lines represent the relevant Ontario Provincial Water Quality Objectives (PWQO).

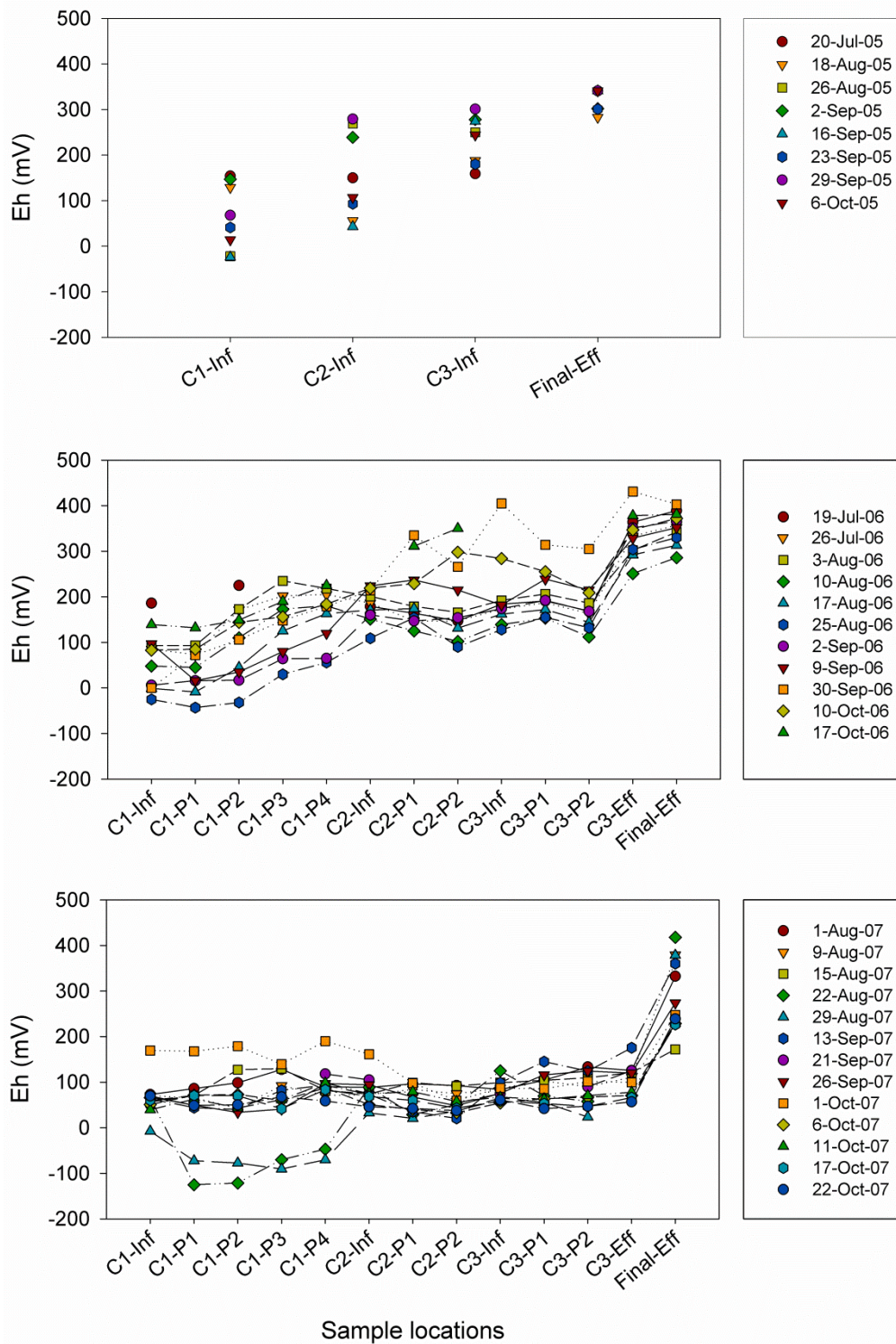


Figure 2.3 Eh values measures along the flow path in years 1, 2, and 3

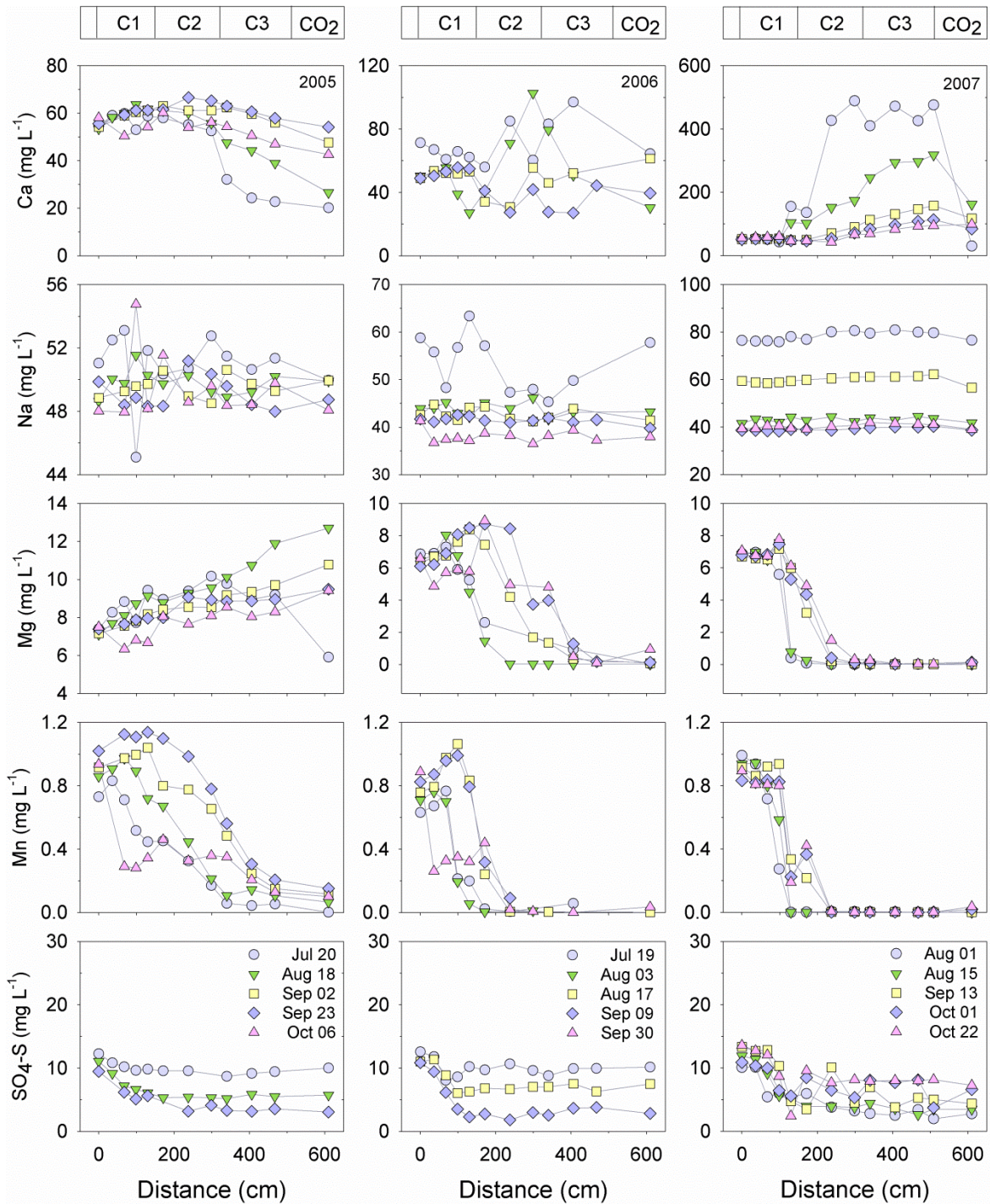


Figure 2.4 Ca, Na, Mg, Mn, and SO₄ concentrations versus distance along the treatment flow path in three successive years of the hypolimnetic withdrawal P treatment experiment. C1, C2, C3, and CO₂ at the top represent Columns 1 to 3 and the neutralization tank, respectively.

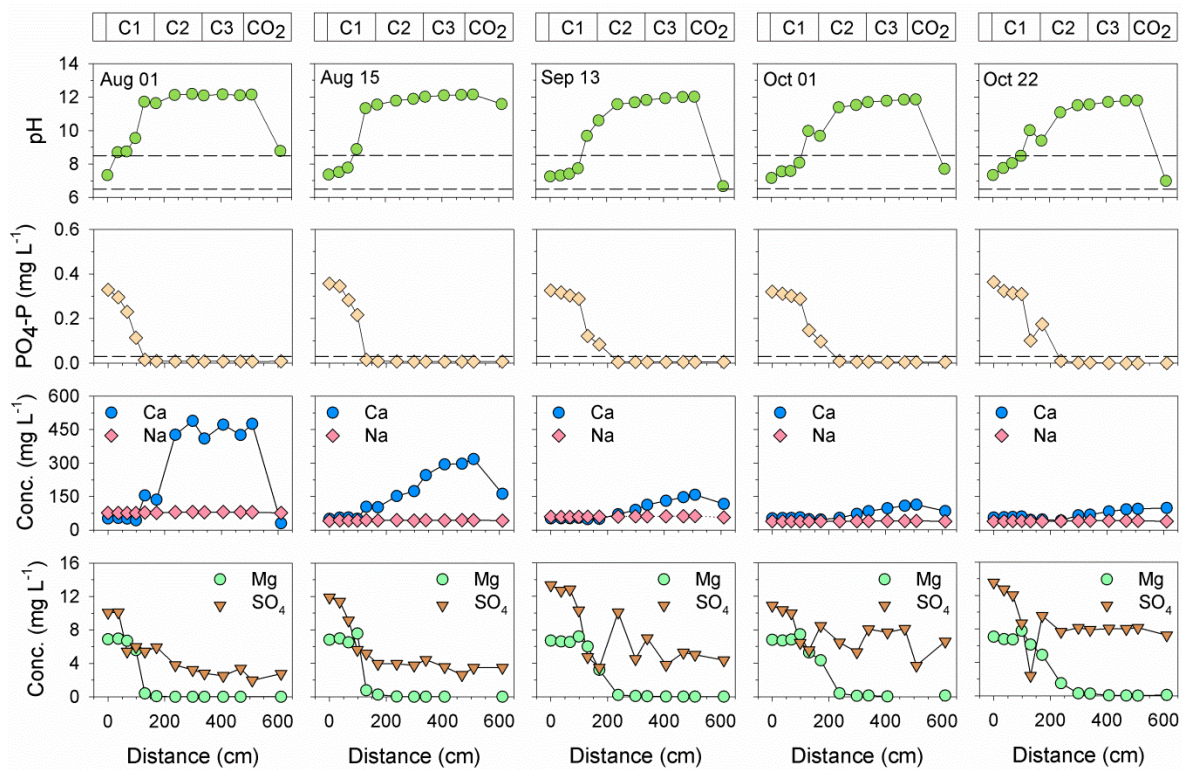


Figure 2.5 pH values and PO₄-P, Ca, Na, Mg, and SO₄ concentrations versus distance along the treatment flow path in year 3 of the hypolimnetic withdrawal P treatment experiment. C1, C2, C3, and CO₂ at the top represent Columns 1 to 3 and the neutralization tank, respectively. The dashed lines represent the relevant water quality guidelines for Ontario.

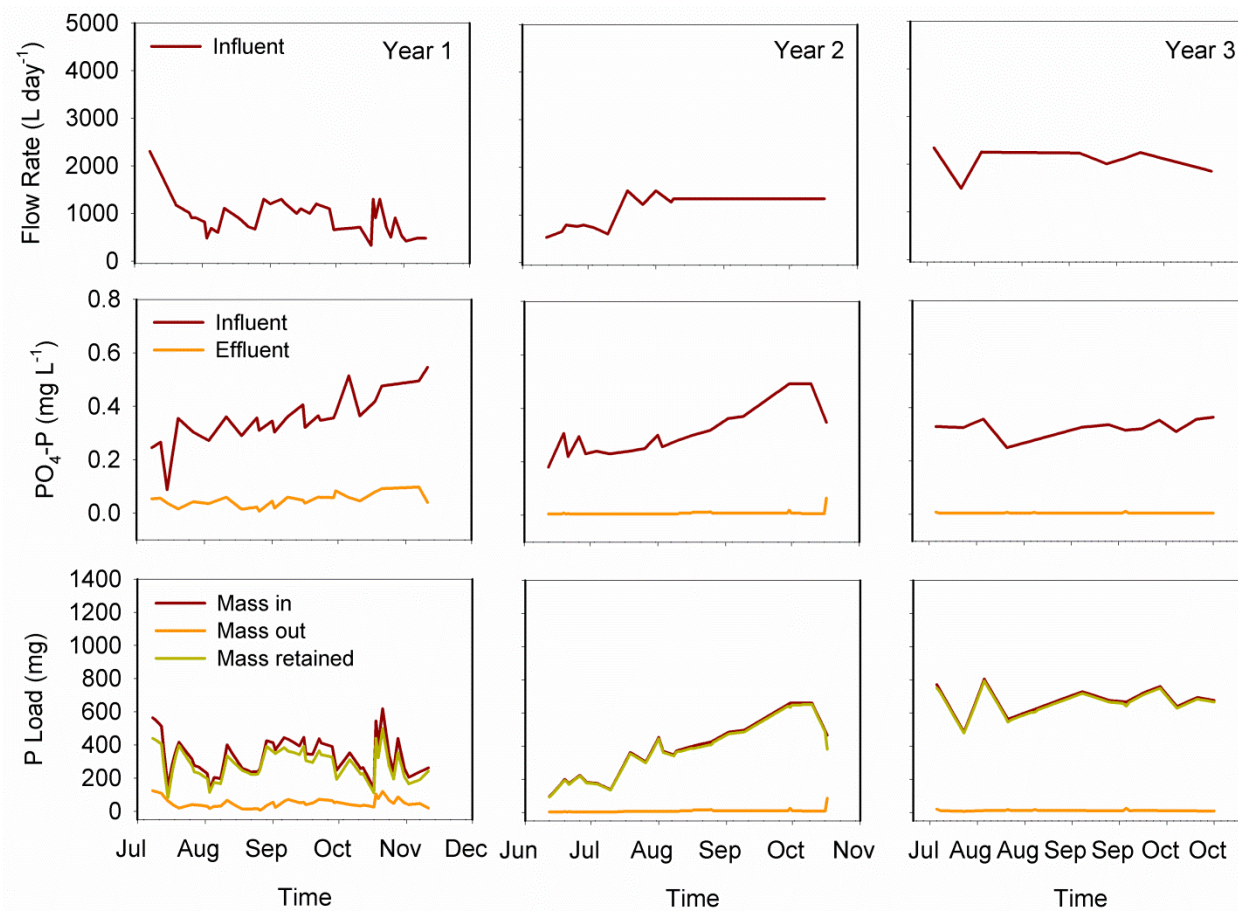


Figure 2.6 Flow rate, PO₄-P concentrations in the influent and effluent, and P load in the treatment system during years 1, 2, and 3.

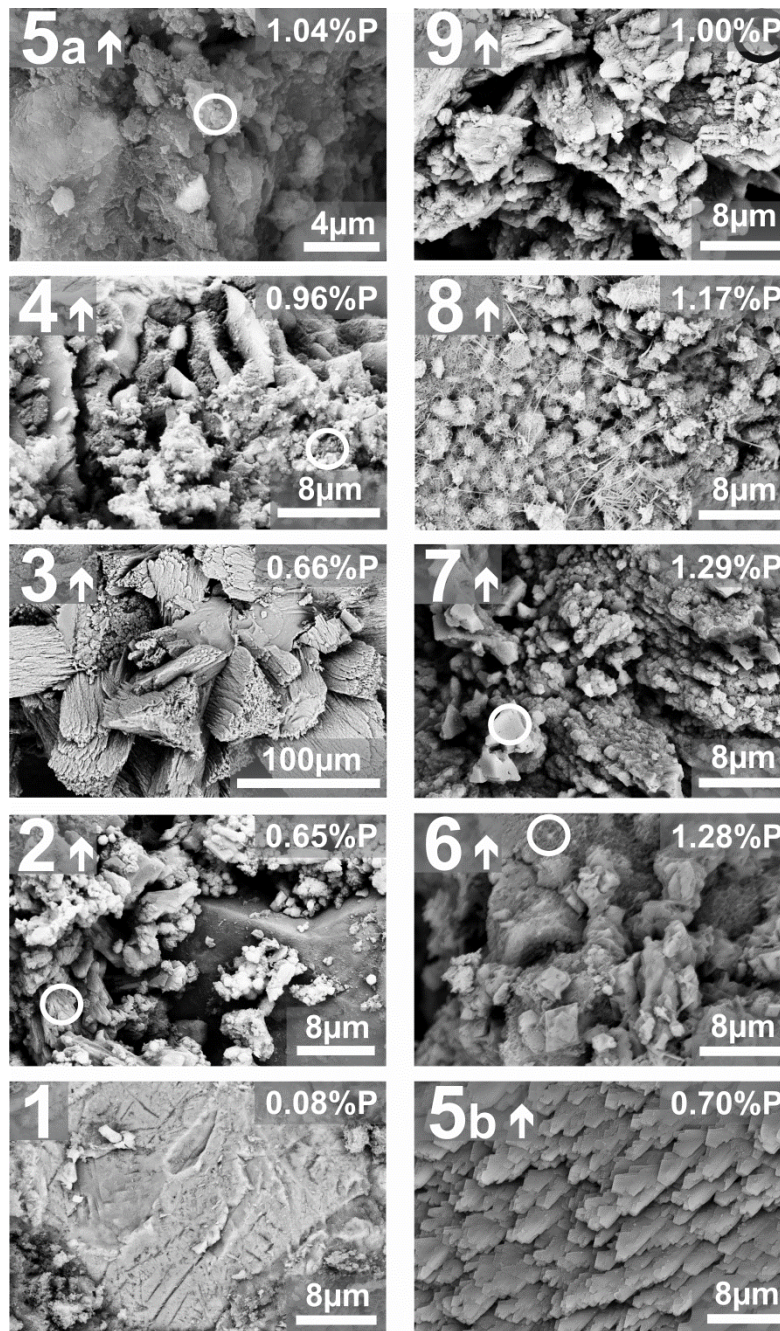


Figure 2.7 SEM images of fresh BOFS (sample 1) and precipitates that formed on the spent reactive media along the flow path (sample 2-9) in year 2. The direction of flow is indicated by the arrows. Unless indicated with small circles, the EDX data were obtained from the entire image area. The phosphorus contents obtained from the EDX data are shown on the images.

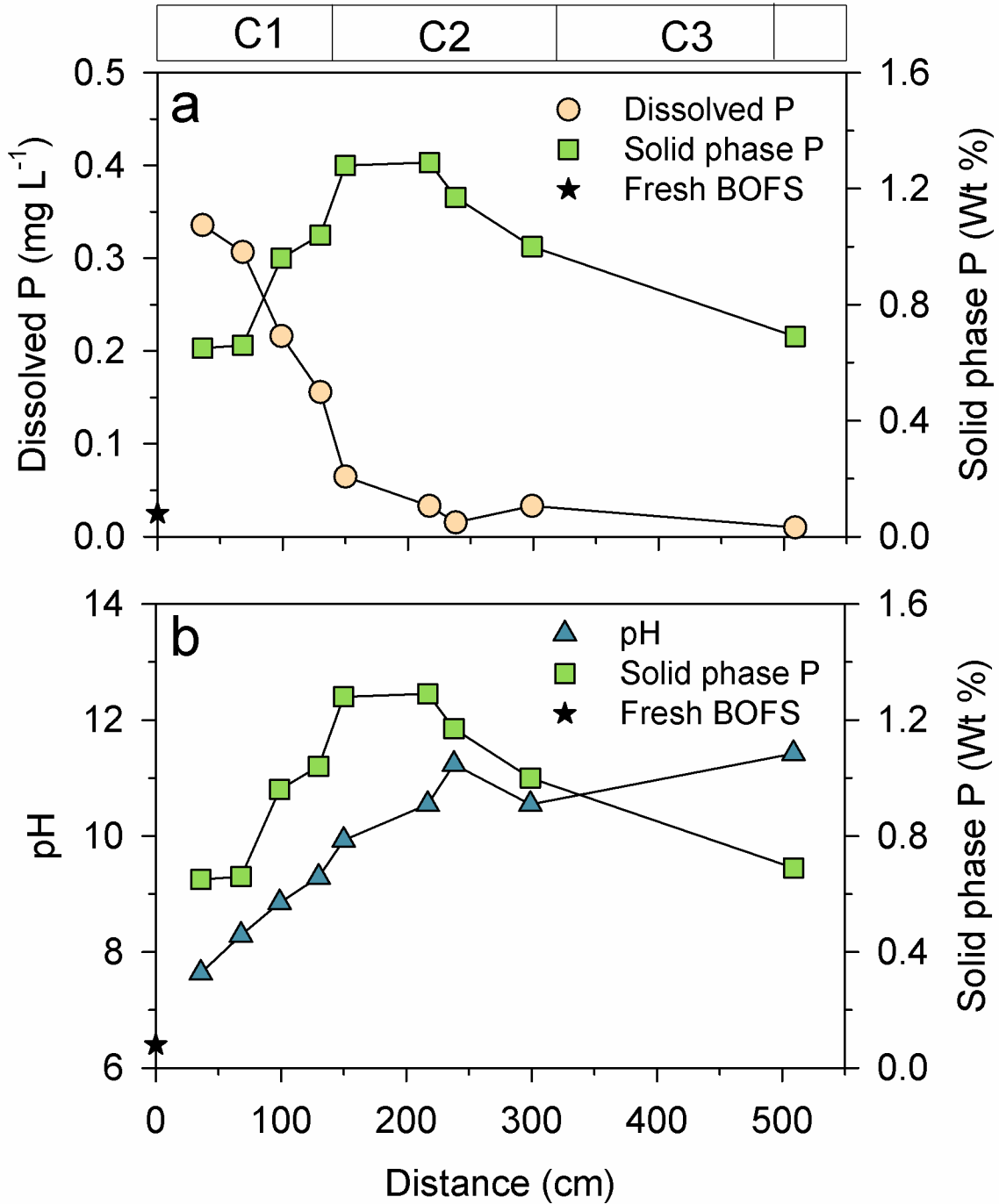


Figure 2.8 a) Dissolved P and solid phase P versus distance, and b) pH and solid phase P versus distance along the treatment flow path in year 2 of the hypolimnetic withdrawal P treatment experiment. C1, C2, and C3 at the top represent Columns 1, 2, and 3.

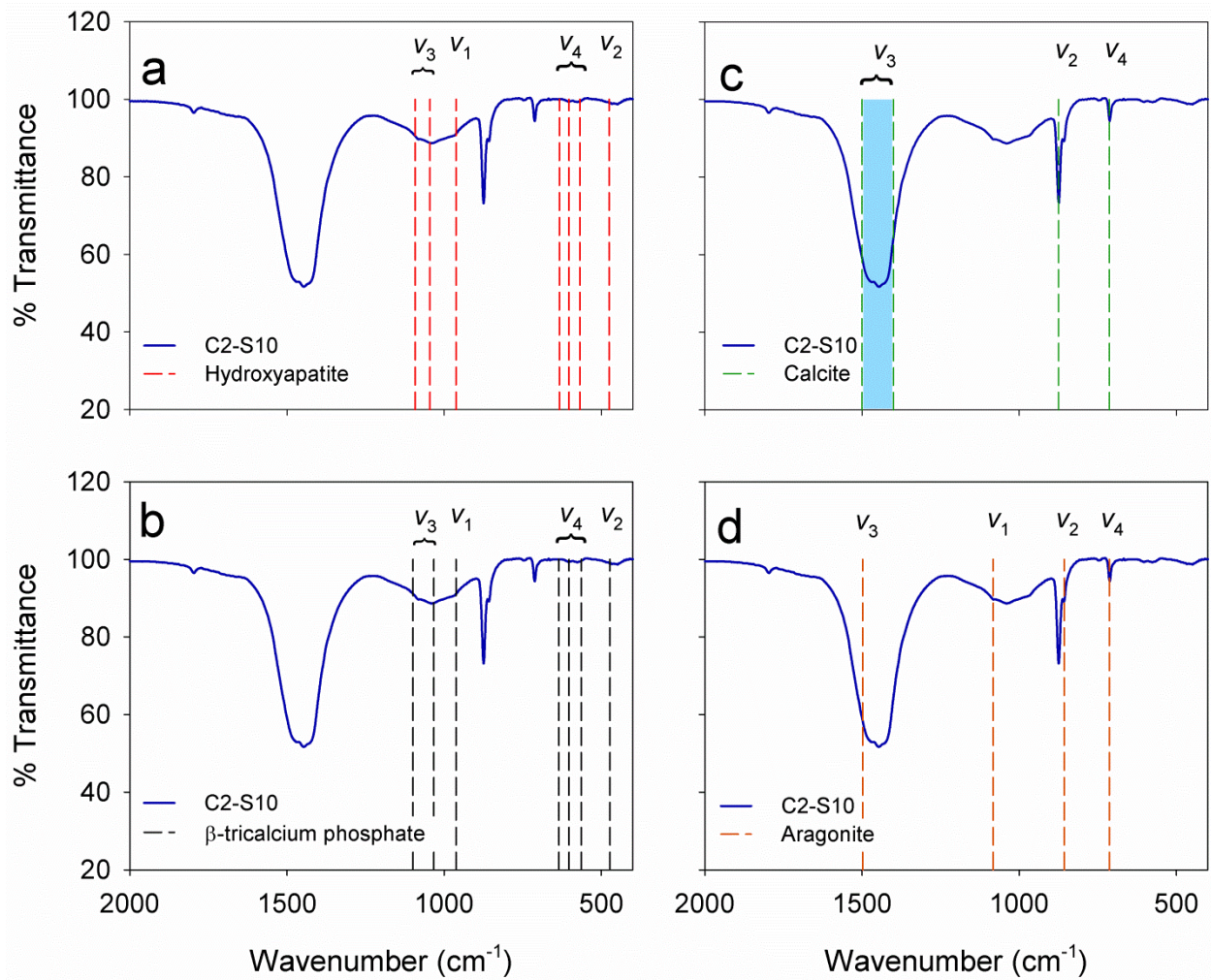


Figure 2.9 FTIR spectrum of sample C2-S10 and major phosphate vibrational bands of a) HAP-S, and b) β -TCP; and major carbonate bands of c) calcite, and d) aragonite are compared. Vertical dotted lines in “a” and “b” represent phosphate vibrational bands, while vertical dotted lines in “c” and “d” represent carbonate vibrational bands.

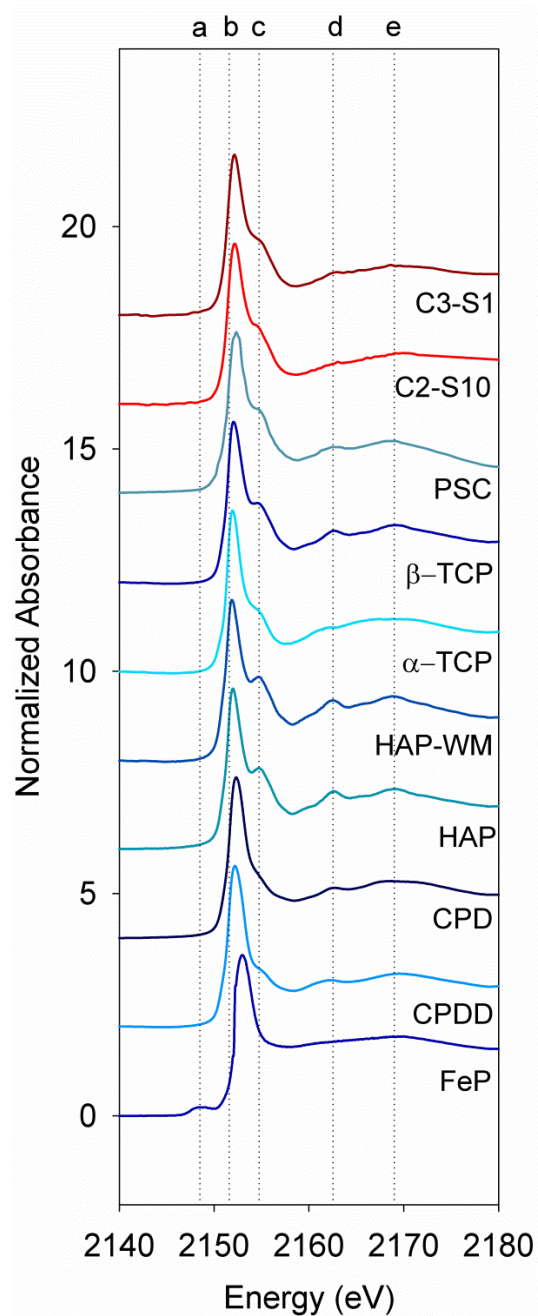


Figure 2.10 XANES spectra for reference materials, PO_4 sorbed on CaCO_3 (PSC), and samples C2-S10 and C3-S1. Vertical lines represent various spectral features: a) pre edge feature for FeP; b) absorption edge (white line) for CaP species; c) shoulder (sharpness dependent on the degree of crystallinity); d) spectral feature common in HAP; e) oxygen oscillation.

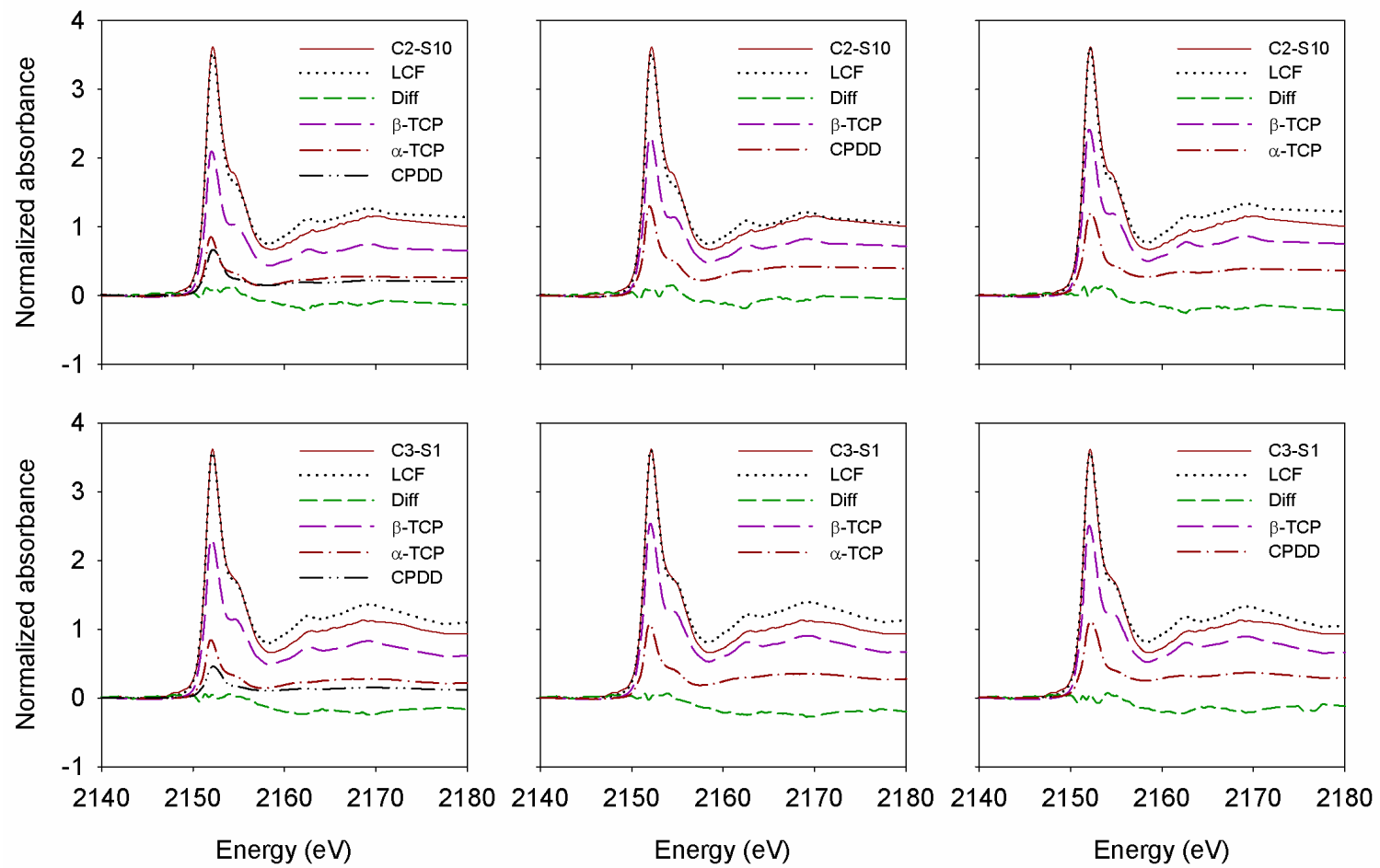


Figure 2.11 Linear combination fit results for spent BOFS samples C2-S10 and C3-S1.

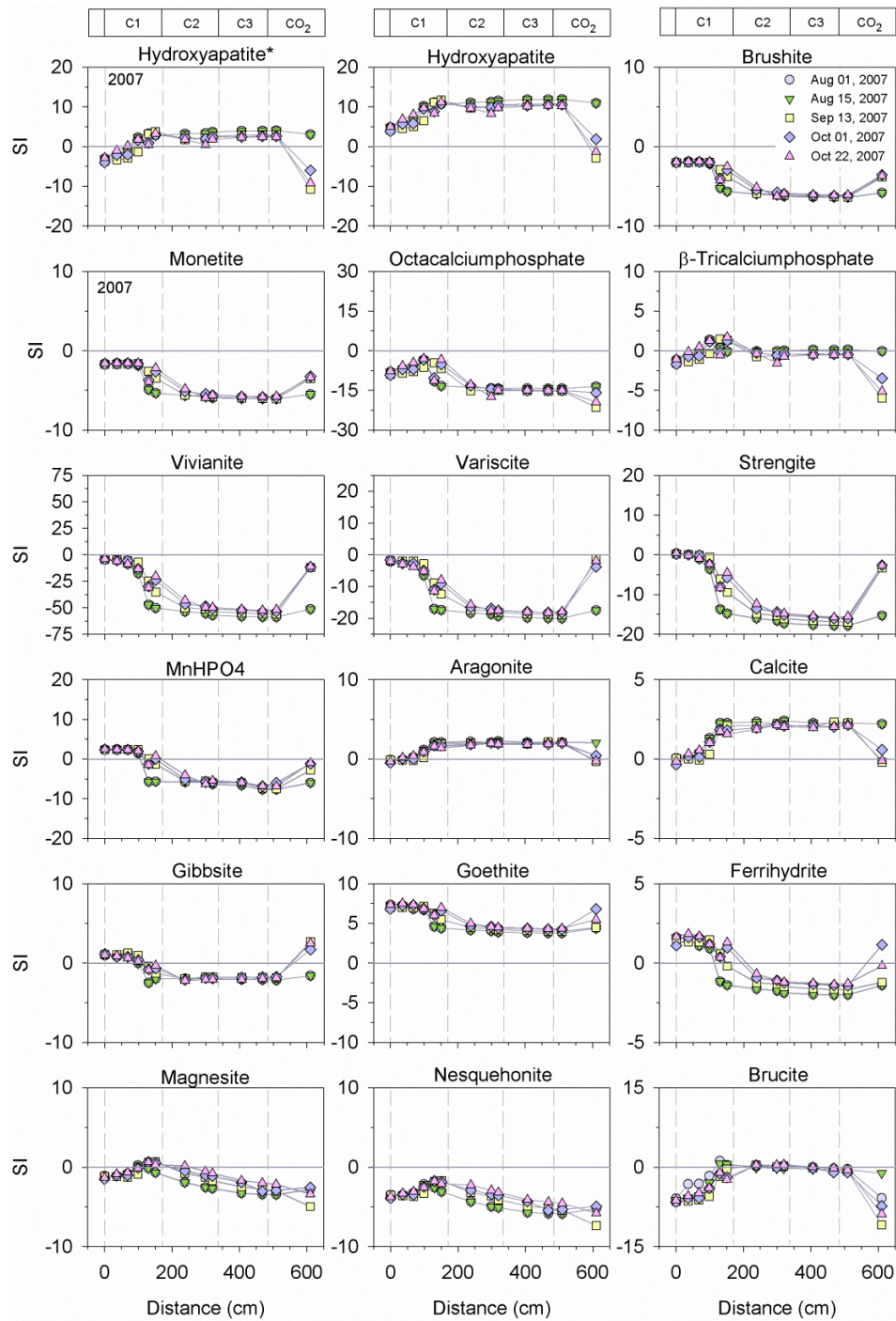


Figure 2.12 Saturation indices for calcium phosphate and other related phases calculated using PHREEQCI versus distance from influent to final effluent in year 3. Saturation index of hydroxyapatite (indicated by *) was plotted using a modified $\log K_{sp}$ value (Baker et al., 1998).

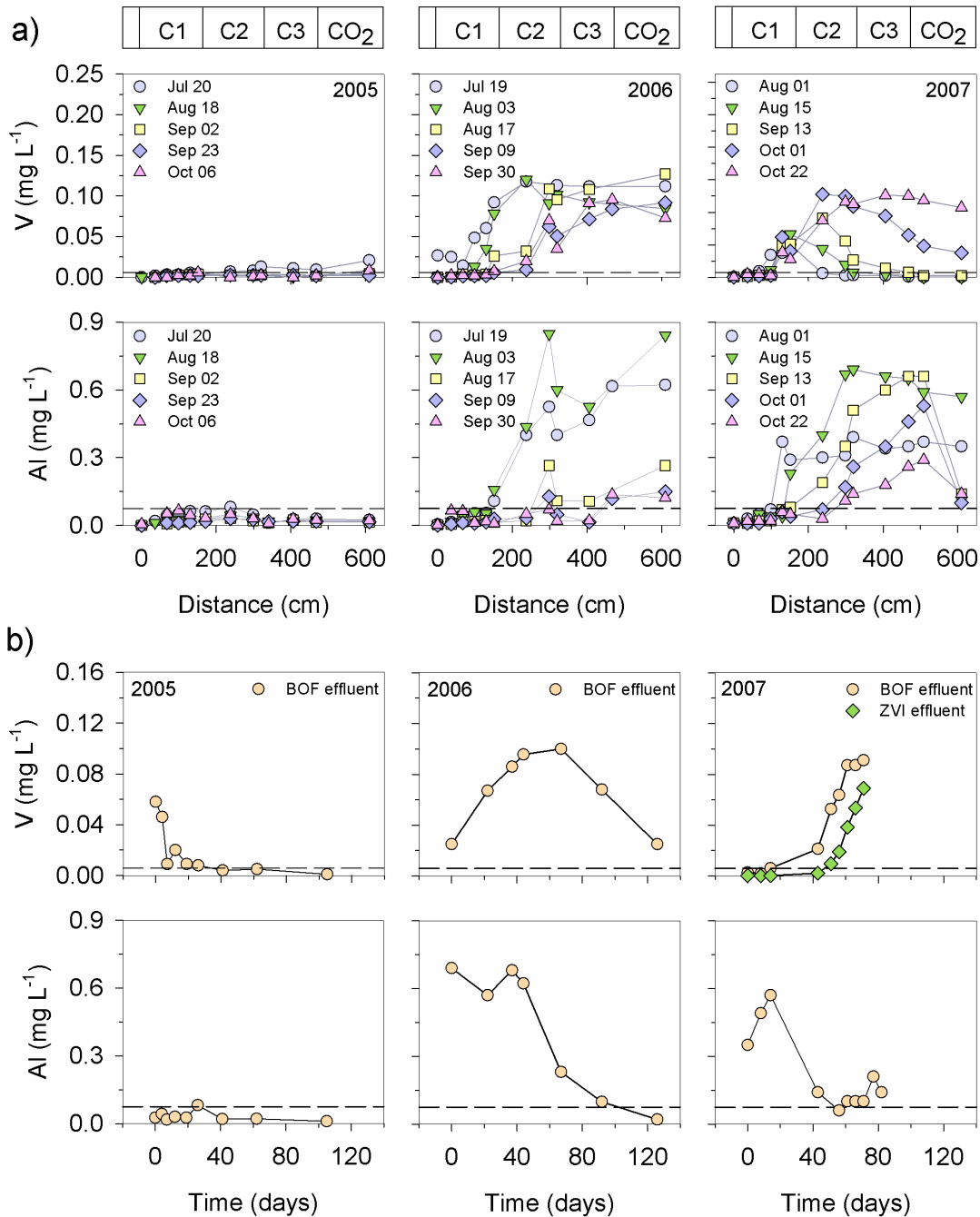


Figure 2.13 a) Concentrations of V and Al versus distance along the treatment flow path for three successive years of the trial. Five representative sampling events were selected for each year. b) Concentrations of V and Al in the BOFS effluent for all three years and for ZVI in year 3. C1, C2, C3, and CO₂ at the top represent Columns 1 to 3 and the neutralization tank, respectively. The dashed lines represent the relevant water quality guidelines for Ontario.

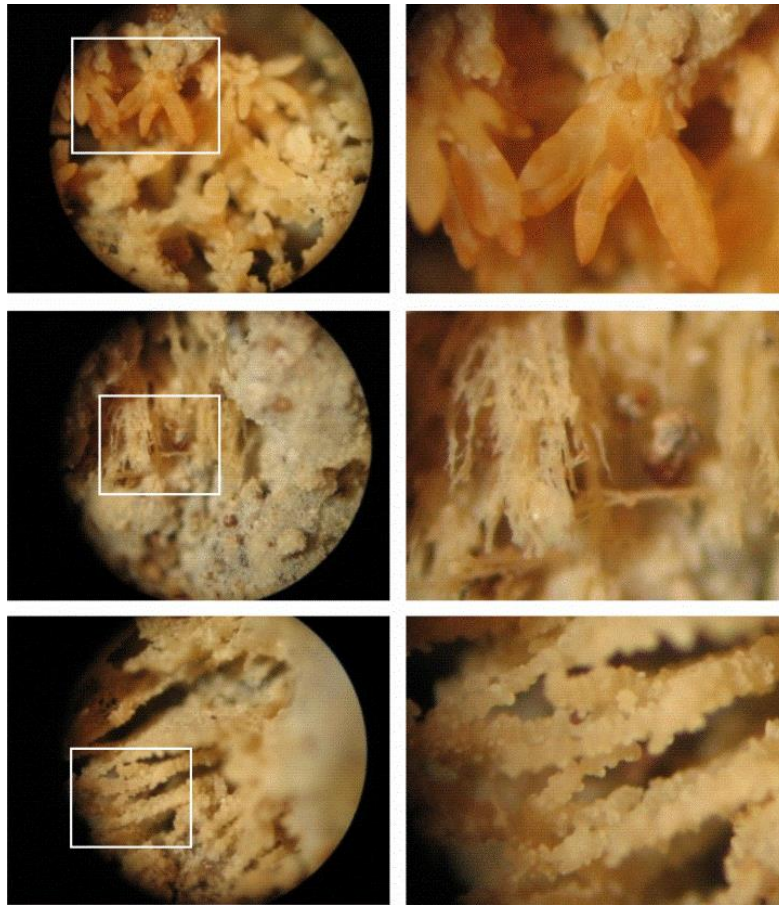


Figure 2.14 Optical microscopy images for a sample of reactive media collected 15 cm below the top surface of Column 1. The magnified images (40X) on the right hand side correspond to the boxed areas from the left hand side.

Table 2.1 Components of the reactive media and mass distribution during the study period.

		Year 1		Year 2		Year 3			
	Slag Source	Levy, Detroit		Stelco, Hamilton		Stelco, Hamilton			
Column 1	Total Vol. (m ³)	0.695		0.695		0.695			
	Media components	BOFS	Gravel	BOFS	Gravel	BOFS		Gravel	
	Vol. ratio	0.5	0.5	0.5	0.5	0.5		0.5	
	Mass* (kg)	677	534	752	534	724		534	
Column 2	Total Vol. (m ³)	0.695		0.695		0.695			
	Media components	BOFS	Gravel	BOFS	Gravel	BOFS		Gravel	
	Vol. ratio	0.5	0.5	0.5	0.5	0.5		0.5	
	Mass* (kg)	677	534	752	534	724		534	
Column 3	Total Vol. (m ³)	0.695		0.695		0.347 (Lower part)		0.347 (Upper part)	
	Media components	BOFS	Gravel	BOFS	Gravel	BOFS	Gravel	ZVI	Sand
	Vol. ratio	0.5	0.5	0.5	0.5	0.5	0.5	0.02	0.98
	Mass* (kg)	677	534	752	534	362	267	12	298

* Media component masses were calculated using particle densities (Table 2.2) and measured porosity values (0.41, 0.42, 0.50, and 0.34 for the BOFS, gravel, ZVI, and sand, respectively).

Table 2.2 Physical and chemical properties of the BOFS materials used in the experiments.

BOFS type		BOFS-A	BOFS-B	BOFS-C	
BOFS source		Levy, Detroit	Stelco, Hamilton	Stelco, Hamilton	
Physical properties	Particle size (mm)	Surface area (m ² g ⁻¹)			
	4-2	2.66	4.62	3.22	
	2-1	4.29	5.05	4.67	
	1-0.5	6.11	7.33	6.82	
	<0.5	7.33	9.00	9.60	
	Particle size (mm)	Mass weighted surface area (m ² g ⁻¹)			
	4-2	73.0	121	82.8	
	2-1	76.7	94.5	71.2	
	1-0.5	70.3	87.9	77.9	
	<0.5	317	388	442	
Density (g cm ⁻³)		3.30	3.67	3.53	
Chemical properties	Chemical composition (wt. %)	CaO	36.3	33.1	40.0
		Fe ₂ O ₃	24.7	33.8	18.1
		SiO ₂	9.21	11.8	15.3
		MgO	9.41	7.95	9.08
		MnO	3.39	5.43	4.04
		Al ₂ O ₃	5.84	3.96	5.05
		P ₂ O ₅	0.66	-	-
		TiO ₂	0.45	0.38	1.13
		K ₂ O	<0.01	0.02	0.03
		Na ₂ O	<0.10	0.10	0.09
		Cr ₂ O ₃	0.11	-	-
Loss on ignition	5.78	3.49	7.12		

Table 2.3 Mean values and range of pH, alkalinity, and PO₄-P of the input and BOFS column effluent in years 1, 2, and 3.

		Year 1			Year 2			Year 3		
		Input	BOFS Column Eff.	Final Eff.	Input	BOFS Column Eff.	Final Eff.	Input	BOFS Column Eff.	Final Eff.
pH	Mean	7.40	8.49	8.47	7.30	10.94	8.84	7.73	11.95	8.13
	Range	7.20-7.85	8.09-9.12	7.72-9.64	7.18-7.58	9.36-11.63	8.07-9.64	7.15-10.94	11.78-12.17	6.18-12.17
Alk (mg L ⁻¹ CaCO ₃)	Mean	169	183	157	155	111	111	225	493	344
	Range	118-280	78-362	70-240	124-262	60-176	78-134	160-360	130-1146	96-1020
PO ₄ -P (mg L ⁻¹)	Mean	0.37	0.07	0.03	0.32	0.03	0.02	0.34	<0.005	0.005
	Range	0.29- 0.55	0.02-0.12	0.01-0.06	0.02- 0.49	0.01-0.15	<0.005-0.06	0.31-0.38	<0.005-0.008	<0.005-0.012

Table 2.4 P mass loading in the treatment system during years 1, 2, and 3.

Year	Total P mass in (g)	Total P mass out (g)	Total P mass removed (g)	Total mass retained
1	42	6	36	86%
2	51	1	50	98%
3	56	1	55	98%

Table 2.5 EDX data showing the composition of the selected samples.

Media	Sample	wt. % of important elements					
		C	O	Mg	Si	P	Ca
Fresh BOFS	1	10.8	24.3	2.47	2.15	0.08	14.0
Spent media from Column 1	2	5.87	8.86	0.25	0.78	0.65	67.2
	3	17.7	31.4	2.38	2.07	0.66	31.7
	4a	14.0	29.5	1.56	1.45	0.96	37.5
	5a	5.95	11.8	1.74	4.16	1.04	36.0
	5b	45.5	25.0	2.30	1.60	0.70	8.90
	5c	14.2	40.9	13.4	7.31	0.35	10.1
Spent media from Column 2	6	23.5	30.5	8.08	9.93	1.28	7.53
	7	15.2	26.1	1.17	1.01	1.29	37.1
	8	11.8	24.0	1.56	3.84	1.17	25.1
	9	21.4	36.3	5.93	7.63	1.00	14.0
Spent media from Column 3	10	18.2	36.3	1.80	4.29	0.69	19.8

Table 2.6 Vibrational bands of calcium carbonate minerals.

Reference materials	Carbonate vibrational bands				Reference
	ν_1	ν_2	ν_3	ν_4	
Calcite	-	874		713	Ni and Ratner (2008)
		875	1440	713	Vongsavat et al. (2006)
		877	1420	713	Andersen and Brecevic (1991)
		872			Amarie et al. (2012)
Aragonite		858		713, 700	Ni and Ratner (2008)
	1083	854	1488, 1440	713, 700	Andersen and Brecevic (1991)
	1083	857	1498	713	Vongsavat et al. (2006)
Vaterite		874		744	Ni and Ratner (2008)
	1089	877, 873	1487, 1445	746, 738	Andersen and Brecevic (1991)
Amorphous CaCO_3	1067	864	1490, 1425	725, 690	Andersen and Brecevic (1991)

Table 2.7 Vibrational bands of phosphate in the reference materials.

Reference materials	Phosphate vibrational bands			
	ν_3	ν_1	ν_4	ν_2
HAP-S	1092	962	568	475
	1045		603	
			633	
HAP-WM	1090	962	571	474
	1042		602	
			633	
β -TCP	1098	962	564	471
	1033		603	
			634	

Table 2.8 Vibrational bands of calcium phosphate minerals.

Reference	Phosphate vibrational bands				OH	Comments	Reference
	ν_1	ν_2	ν_3	ν_4			
HAP			1046	569	3443		Kim et al. (2006)
	966		1037		3576		Balan et al. (2011)
	962	472	1090, 1042	632, 602, 566	3570	Merck	Rehman and Bonfield (1997)
	961	471	1096, 1031	604, 566	3744, 3440	nano particle	Panda et al. (2003)
	963	477	1094, 1024	606, 574	3574		Matković et al. (2012)
	962		1087, 1040	601, 571			Pena and Vallet-Regi (2003)
	960	475	1092, 1044, 1036	573			De Oliveira Ugarte et al. (2005)
			1020-1025			Non-stoichiome	Petra et al. (2005)
	962	477, 437	1089-1053	603, 569	3571		Sargin et al. (1997)
	963		1090, 1052	602, 573	3571		Rapacz-Kmita et al. (2005)
			1092, 1060, 1029			Sigma	Antonakos et al. (2007)
	970		1026	598, 555	3571		Jalota et al. (2005)
	962		1030		3570		Nishikawa (2001)
	963	473		602, 571	3452		Ribeiro et al. (2006)
Dicalcium phosphate	962		1090, 1020	632, 601, 570	3571		Fernandez et al. (2012)
β -Tricalcium phosphate	967		1126, 1024	614, 549			Matković et al. (2012)
	972, 945		1120, 1042, 1025	606, 594, 552			Pena and Vallet-Regi (2003)
	971, 948		1120, 1042	604			De Oliveira Ugarte et al. (2005)
α -Tricalcium phosphate	948, 954		1055, 1025	613, 597, 585, 563, 551			Pena and Vallet-Regi (2003)

Table 2.9 Ca/C, Ca/P and O/Ca ratios of the samples analyzed.

Sample ID	Ca P3/2	Ca P1/2	Carbonate	P 2p3/2	P 2p1/2	Ca/C	O/Ca	Ca/P
C1-S2	346.88	350.43	289.38	132.57	133.41	0.32	5.3	24
C1-S3	347.07	350.62	289.54	132.77	133.61	0.29	4.8	33

Table 2.10 Linear combination fitting results of spent BOFS samples.

Linear combination fits to C2-S10 as norm(E)					
Combination	R-factor	χ^2	β -TCP (weight)	α -TCP (weight)	CPDD (weight)
β -TCP, α -TCP, CPDD	5.71E-3	2.30	0.581	0.236	0.184
β -TCP, CPDD	6.27E-3	2.52	0.64	0	0.36
β -TCP, α -TCP	6.30E-3	2.53	0.67	0.33	0
α -TCP, CPDD	9.80E-3	3.94	0	0.413	0.587
Linear combination fits to C1-S2 as norm(E)					
Combinations	R-factor	χ^2	α -TCP (weight)	β -TCP (weight)	CPDD (weight)
α -TCP, β -TCP, CPDD	8.47E-03	3.29	0.495	0.441	0.064
α -TCP, β -TCP	8.52E-03	3.31	0.523	0.477	0
α -TCP, CPDD	1.09E-02	4.24	0.639	0	0.361
β -TCP, CPDD	1.11E-02	4.30	0	0.561	0.439
Linear combination fits to C2-S4 as norm(E)					
Combinations	R-factor	χ^2	α -TCP (weight)	β -TCP (weight)	CPDD (weight)
α -TCP, β -TCP, CPDD	1.48E-02	5.48	0.494	0.401	0.104
α -TCP, β -TCP	1.53E-02	5.67	0.552	0.448	0
α -TCP, CPDD	1.69E-02	6.27	0.618	0	0.382
β -TCP, CPDD	1.74E-02	6.46	0	0.518	0.482
Linear combination fits to C2-S9 as norm(E)					
Combinations	R-factor	χ^2	α -TCP (weight)	β -TCP (weight)	CPDD (weight)
α -TCP, β -TCP, CPDD	8.97E-03	3.21	0.676	0.255	0.069
α -TCP, β -TCP	9.27E-03	3.32	0.725	0.275	0
α -TCP, CPDD	9.97E-03	3.57	0.812	0	0.188
β -TCP, CPDD	1.47E-02	5.28	0	0.471	0.529
Linear combination fits to C2-S11 as norm(E)					
Combinations	R-factor	χ^2	α -TCP (weight)	β -TCP (weight)	CPDD (weight)
α -TCP, β -TCP, CPDD	1.16E-02	4.42	0.607	0.366	0.027
α -TCP, β -TCP	1.18E-02	4.47	0.621	0.379	0
α -TCP, CPDD	1.38E-02	5.24	0.875	0	0.125
β -TCP, CPDD	1.68E-02	6.38	0	0.635	0.365

Table 2.10 Continued Linear combination fitting results of spent BOFS samples.

Linear combination fits to C3-S1 as norm(E)					
Combinations	R-factor	χ^2	β -TCP (weight)	α -TCP (weight)	CPDD (weight)
β -TCP, α -TCP, CPDD	5.25E-03	2.13	0.641	0.233	0.126
β -TCP, α -TCP	5.57E-03	2.26	0.703	0.297	0
β -TCP, CPDD	5.78E-03	2.34	0.694	0	0.306
α -TCP, CPDD	1.01E-02	4.10	0	0.415	0.585

Chapter 3

Removal of Nutrients and Pathogens in an Advanced Pilot-scale Engineered Wetland Wastewater Treatment System

3.1 Executive Summary

A pilot-scale, multi-step Engineered Wetland (EW) wastewater treatment system with a phosphorus removal component was evaluated to assess the potential for removal of phosphorus (P), ammonia, cBOD₅, COD, *E. coli*, total coliform, and trace metals. Septic system effluent passed through the treatment system, composed of four cells including a mixing cell, a vertical subsurface flow (VSSF) aerobic cell based on Forced Bed Aeration™, a VSSF phosphorus treatment cell based on the use of basic oxygen furnace (BOF) slag as a treatment material, and a horizontal subsurface flow (HSSF) anaerobic cell. The system was operated for 9 months with an average flow rate of 0.068 m³ d⁻¹. The mean influent concentrations of P, ammonia, cBOD₅, and COD were 7, 25, 27, and 60 mg L⁻¹, respectively, and the mean influent levels of *E. coli* and total coliform were 2.2x10⁴ and 8.9x10⁴ CFU 100 mL⁻¹. Effluent from the system had 97-99% lower concentrations of P, NH₃, cBOD₅, *E. coli*, and total coliform, and a 72% lower concentration of COD, compared to influent values. The pH of the BOF slag cell was elevated (pH, 11.66±0.70), and was neutralized by sparging CO_{2(g)} prior to discharge to the subsequent anaerobic cell. Vanadium and Al were leached from the BOF slag at levels that exceeded guideline values. There was no significant decline in hydraulic performance observed during the study. Backscatter scanning electron (BSE) images and energy dispersion X-ray (EDX) spectra

and X-ray intensity element maps along with Fourier transform infrared (FTIR) spectra confirm the presence of phosphorus on the outer layer of the spent reactive material. The FTIR spectra also indicate the occurrence of calcium carbonate and phosphate minerals. The X-ray absorption near edge structure (XANES) spectra provides information on the speciation of solid-phase calcium phosphates accumulated on the spent reactive media.

3.2 Introduction

Phosphorus (P) in the discharge of wastewater treatment facilities is an important environmental concern. The release of an excessive amount of this nutrient can cause eutrophication and deterioration of water bodies (Sedlak, 1991; Parry, 1998). Thus, increasingly more conservative discharge criteria have been imposed. During the last decade, constructed wetland (CW) designs have been developed to achieve better overall treatment performance, and to provide compound-specific treatment (Vymazal, 2011). Recent studies have focused on the use of treatment media with a high efficiency for phosphorus removal, identifying bacteria which promote treatment processes, and development of models to optimize pollution removal (Vymazal, 2011).

Conventional CWs effectively treat a broad range of wastewater effluents. However, these CWs are relatively ineffective at removing phosphorus (Kadlec and Knight, 1996; Kadlec et al., 2000). Although high initial rates of P removal have been observed in CWs, up to 42% (Kadlec and Knight, 1996; Knight et al., 2000) and 45.7% (Vymazal, 2004), P removal has been observed to decline over time. Development of multistep systems and integration of more complete phosphorus removal with a conventional CW could provide superior P treatment efficiency.

A number of studies have focused on the role of substrate materials used in CWs to improve the P treatment capacity (Johansson, 1999; Drizo et al., 1999; Drizo et al., 2002; Jenssen and Krogstad, 2003). Materials with high sorption capacity and/or the ability to precipitate phosphate phases are considered as candidate substrates for CWs to remove P from wastewater. The most promising substrates are industrial by-products including blast furnace (BF) slag (Grüneberg and Kern, 2001; Cameron et al., 2003; Korkusuz et al., 2005; Gustafsson et al., 2008), basic oxygen furnace (BOF) slag (Mann and Bavor, 1993; Drizo et al., 1999; Cha et al., 2006), electric arc furnace (EAF) slag (Drizo et al., 2002; Drizo et al., 2006), shale (Drizo et al., 1999), and lightweight aggregates (Jenssen and Krogstad, 2003). BOF slag is among the treatment materials that can be used to remove phosphorus from the effluent of the CWs. BOFS is a waste by-product generated during the steelmaking process (Mikhail et al., 1994; Shi, 2004; Bowden et al., 2009). The major phases (>10 wt. %) of BOFS are di-calcium silicate (Ca_2SiO_4), tri-calcium silicate (Ca_3SiO_5), ferrous oxide (FeO), and Ca-Mg-Mn-Zn-ferrite ($(\text{Ca},\text{Mg},\text{Mn},\text{Zn})\text{Fe}_2\text{O}_4$) (Mikhail et al., 1994). Calcium oxides, Fe_2O_3 , and SiO_2 are the main chemical components that comprise approximately 70-85 wt. % of BOFS, and MgO, MnO, Al_2O_3 , P_2O_5 , TiO_2 , K_2O , Na_2O , and Cr_2O_3 comprise the remaining portion of the material (Table 3.1; Cha et al., 2006; Xue et al., 2009; Mahieux et al., 2009; Yildirim and Prezzi, 2011; Belhadj et al., 2012). The average percentage of the major constituents of BOFS are Ca (28.01%), Fe (18.43%), Si (5.97%), Mg (5.53%), Mn (3.29%), and Al (2.38%); minor constituents are P (0.32%), C (0.26%), Cr-total (0.13%), S (0.11%), and V (0.10%) (Proctor et al., 2000).

BOFS has been recognized as a potential material for removing phosphorus, arsenic, and waterborne pathogens from groundwater and wastewater (Blowes et al., 1996; Bowden et al.,

2009; Xue et al., 2009). Laboratory and field applications have demonstrated very high levels of removal (often >99%) of arsenic, phosphate, and pathogen indicators (e.g. *E-coli*) in simulated wastewater and wastewater (Baker et al., 1997, 1998; McRae et al., 1999; Blowes et al., 2000; Smyth et al., 2002b; Stimson et al., 2010). The extent of removal depends on the contact time between the BOFS and wastewater, with contact times of up to 24 hours required to ensure maximum removal of phosphorus (Baker et al., 1998). Exceedingly alkaline effluent and the potential for metal leaching from BOFS are two of the potential drawbacks that need to be reasonably eliminated prior to widespread application of BOFS as a wastewater treatment material.

Aerated sand filters are effective in removing cBOD₅ (>90%) from wastewater (Johnson and Mara, 2005). Enzymes related to processes in the *E. coli* bacterium are often pH-sensitive. Faecal coliform die-off quickly at pH > 9 and nutrient-poor conditions (Pearson et al., 1987), and the bacterial indicators are also removed through aeration stages (Johnson and Mara, 2005). Highly aerobic conditions induced by aeration enhance die-off of *E. coli* (Seaman et al., 2009).

This paper describes the incorporation of a BOFS cell into an engineered wetland (EW) system in a pilot-scale indoor facility with an average flow rate of 68 liters per day. The study investigated the capacity of the treatment system to remove P, NH₃, pathogens, dissolved metals, and the leaching behaviour of BOFS. A carbon dioxide injection system was used for the neutralization of the high pH effluent from the BOFS cell. Changes in the hydraulic conductivity of the BOFS cell were evaluated by monitoring the flow rate in this cell. Solid-phase analyses on outer layer material of the spent BOFS were used to determine the PO₄ removal mechanism.

3.3 Materials and Methods

3.3.1 System configuration

A pilot-scale indoor wastewater treatment system (Figure 3.1) with a capacity of 50 -100 L day⁻¹, was constructed in the Center for Alternative Wastewater Treatment, Fleming College, Lindsay, Ontario, in the spring of 2009. The system consisted of a feed tank, a mixing cell to provide more uniform input chemistry (120 cm long, 100 cm wide, and 116 cm deep), a saturated top-dosed aerated engineered vegetated wetland (EW) cell (Cell 3), a sealed and unvegetated BOFS cell (Cell 4), a pH adjustment cell (Cell 4*), and a vertical subsurface flow (VSSF) EW cell, which was anaerobic at the base and vegetated at the top (Cell 5). A distribution manifold and collection manifold, both comprised of three parallel perforated polyvinyl chloride (PVC) pipes, were installed within each cell to evenly distribute the influent and to capture the effluent from all portions of the cell.

Wastewater (sewage feed collected from the septic tank of the college) was stored in the feed tank (Cell 1, 1.0 m³) and introduced to the mixing cell (Cell 2) as required, and then transmitted through the treatment cells by gravity. The mixing cell had a 5 cm layer of sand placed at its base to cushion a water collection manifold. The collection manifold was covered with a 10 cm layer of washed gravel (Figure 3.2). The HRT of this cell was about 14 days. The mixing cell contained a heavy duty drum/barrel mixer, which was driven by a 1/4 horse power, single-phase, 60 Hz motor (Cole Parmer Leeson).

Cell 3 was a saturated top-dosed aerated engineered wetland (EW) cell, constructed according to the Forced Bed Aeration™ technology. A 5 cm thick sand layer was placed at the bottom of

the cell to hold the distribution manifold. The distribution manifold was then covered with 10 cm thick layer of washed gravel layer and a specially-constructed aerator was installed on top of it. The aerator consisted of a 1.9 cm ($\frac{3}{4}$ in) PVC pipe connected to three 0.95 cm ($\frac{3}{8}$ in) plastic tubes, which were perforated with 0.32 cm ($\frac{1}{8}$ in) holes at regular intervals. A small air blower (HAILEA Model: ACO-009D), driven by a 135W, 110V/60 Hz motor, was used to provide 125 L min⁻¹ of air at a pressure of >0.004 Mpa. The aerator was overlain by a 98 cm thick layer of washed limestone gravel with a porosity of about 0.35 (Figure 3.3). The nominal hydraulic retention time of wastewater passing through the Aerated Cell was 7 days, at an influent flow rate of 68 L day⁻¹. A distribution manifold (with perforations on the top) was placed on the surface of the upper gravel layer. Finally, this cell was vegetated with cattails, *Typha spp.*

Cell 4 contained a substrate of 50 vol. % screened BOFS and 50 vol. % washed limestone gravel with a median grain size of 1.9 cm ($\frac{3}{4}$ inch). The cell was designed to be sealed and airtight. The vertical distribution of reactive materials within Cell 4 included a 10 cm basal layer of sand, which supported the outlet collection grid, a 57 cm thick layer of the BOFS-gravel mixture in the central portion of the cell, and a 10 cm layer of 1.9 cm diameter ($\frac{3}{4}$ inch) crushed limestone was placed on top. The top gravel layer supported the distribution manifold at the top of the cell (Figure 3.4). The BOFS was screened and washed prior to use in the cell. The mean hydraulic retention time was 6.3 days with an average influent wastewater flow rate of 68 L day⁻¹. Cell 4* was an open-topped vessel into which effluent from Cell 4 flowed. Carbon dioxide gas was bubbled from the bottom of the vessel using large gas spargers. This CO₂ addition cell was introduced between Cell 4 and Cell 5 after 15 weeks of operation.

The design of Cell 5 was similar to Cell 3 but without aeration. The base of the cell was filled with a 5 cm thick sand layer. A collection manifold was placed on top of the sand layer and the manifold was covered with a 10 cm gravel layer. The gravel layer was overlain by a 50 cm thick layer of substrate (a mixture of 7 parts pulp and paper biosolids to provide a source of organic carbon, 5 parts gravel, and 2 parts sand). This layer was overlain by another 25 cm thick layer of substrate (a mixture of 7 parts pulp and paper biosolids, 12 parts gravel, and 2 parts sand). Finally, there was a 25 cm thick unwashed gravel layer placed at the top. The perforated distribution manifold was placed on top of the final gravel layer and leveled (Figure 3.5). This cell was also vegetated with transplanted cattails, *Typha spp.* The mean hydraulic retention time was 6.5 days. The treatment cells were placed in series and connected with a piping network. Sample collection ports (plastic valves) were located between cells.

3.3.2 Reactive material characterization

This study used BOFS from the US Steel Stelco Hilton Works facility (Hamilton, ON, Canada). The particle density of the BOFS was determined using a pycnometer (Air Comparison Beckman Model 930). Surface area was determined with a surface area analyzer (Micromeritics Gemini[®] VII 2390 Series). The composition of BOFS was determined by X-ray fluorescence (XRF, MiniPal4, PANanalytical). The constituent phases of BOFS were obtained using a Rigaku D/MAX 2500 rotating anode powder diffractometer using monochromatic CuK α radiation at 50 kV and 260 mA. The measurements were conducted with 2 θ angular range from 5-70⁰, where the step size and scan speed were 0.02⁰ and 1⁰/min. The phase identification was performed by using JADE version 9.3 coupled with the ICSD and ICDD diffraction databases.

3.3.3 Water sample collection and analysis

The treatment system was monitored over an 8 month period at indoor temperatures (~23 °C) from July 2009 to February 2010. Influent, effluent from each cell, and overall system effluent samples were collected weekly. Sampling valves were purged at least three times before sample collection. The pH and Eh were measured on unfiltered samples immediately after collection using combination electrodes (Thermo Scientific Orion ROSS pH electrode and Thermo Scientific Orion Eh electrode). Alkalinity was measured on filtered (0.45 µm filter size) samples using a Hach™ digital titrator and standardized sulfuric acid and with phenolphthalein and bromocresol green-methyl red pH indicators. Samples were filtered through 0.45 µm dedicated syringe filters and collected into polyethylene bottles for analysis of anions (not acidified), cations and trace metals (acidified to pH 2 with concentrated HNO₃), PO₄ and ammonia (acidified to pH 2 with 18 N H₂SO₄). Field blanks consisted of MilliQ water collected using the same collection and preservation methods like other samples in the field to evaluate whether contamination occurred during the filtering process or transport. The trip blanks were unfiltered MilliQ water (brought to the field) samples collected directly from a plastic container in the field and preserved in the same manner as the other samples to determine whether any contamination occurred in from the bottles and during the transport. All samples and blanks were stored on ice packs in a cooler at ~4°C during transport to the laboratory and refrigerated until analysis.

Samples were analyzed for ortho-phosphate and total phosphate using a UV-spectrophotometer (HACH, DR-2800) within 7 days of collection. The ascorbic acid method (HACH Method 8048 based on SM 4500 P E) was used for ortho-phosphate analysis and an ascorbic acid with acid persulfate digestion method (HACH method 8190 based on S M 4500 P

E) for total phosphate analysis (APHA, 1998). Samples were analyzed for major cations using inductively coupled plasma optical emission spectroscopy (ICP-OES; Thermo Instruments iCAP 6500 Duo), for trace elements using inductively coupled plasma mass spectrometry (ICP-MS; Thermo Instruments XSeries 2), and for anions using ion chromatography (Dionex Ion Chromatograph model DX120, anion AS50 analytical column). The $cBOD_5$ was measured using a HACH BOD meter (HQ40D) and probe (LBOD101) following standard method “SM 5210 B” (APHA, 1998). Samples were analyzed for COD using a UV-spectrophotometer (HACH, DR-2800) following standard method “SM 8000” (APHA, 1998). Dissolved oxygen was measured using a YSI 5100 Dissolved Oxygen Meter following the method described in the manufacturer’s operations manual. Conductivity of the samples was measured using a YSI 3100 Conductivity meter (equipped with a temperature sensor and a platinum electrode) based on the method SM 2510 B (APHA, 1998). Samples were analyzed for NH_3-N using a UV-spectrophotometer (HACH, DR-2800) following Salicylate (colorimetric) Method (HACH Method 10031). Coliform and *Escherichia coli* (*E.coli*) most probable number counts were determined using a 96 well titer plate method (Coliplate™). All samples were analyzed in CAWT Laboratory, Fleming College and the Environmental Geochemistry Laboratory, University of Waterloo. A subset of samples was analyzed for cations and trace metals at SGS Lakefield Research Limited, Lakefield, Ontario for QA/QC purposes.

3.3.4 Solid-phase sample collection and analysis

At the conclusion of the experiment, the formation of a white precipitate on the reactive media in Cell 4 was noted; therefore, the cell was excavated to collect samples for mineralogical analysis.

Samples were collected in 10-15 cm intervals from the top down to the base, in five vertical profiles (Figure 3.6). These samples were analyzed to determine the composition of the precipitate. Solid-phase samples were examined using scanning electron microscopy (Leo 1530 field emission scanning electron microscopy (FE-SEM)) with energy dispersive X-ray (EDX) analysis.

These samples also were studied by Fourier transform infrared spectroscopy (FTIR) (Tensor 27, Bruker). Samples of the scale accumulated on the particle surfaces (adsorbed or precipitated material) were mixed with KBr with a ratio of approximately 1:100, ground in a mortar, and pressed into 1 cm diameter transparent disks/pellets (with 5 to 6 tonnes pressure for 1 min). Additional FTIR analyzes were performed with a second infrared spectrometer (IFS 55, Bruker) using a diamond compression cell in combination with a microscope equipped with micro-ATR (attenuated total reflectance). FTIR spectra were collected over a range of 4000-400 wave numbers (cm^{-1}). A total of 16 scans were collection at a scan resolution of 4 cm^{-1} . Background noise was minimized by subtracting a blank KBr data from each spectrum. In addition to the KBr pellets, mounted sections of selected samples were prepared and polished. These samples were examined by optical microscopy. Reference materials including iron (III) phosphate (FeP), β -tricalcium phosphate (β -TCP), α -tricalcium phosphate (α -TCP), hydroxyapatite (HAP-S), calcium phosphate dibasic (CPD), and calcium phosphate dibasic dehydrate (CPDD) were obtained from Sigma Aldrich, Canada. Additional reference material, hydroxyapatite (HAP-WM), was synthesized in the laboratory following a liquid mix technique described in Pena and Vallet-Regi (2003). These reference materials were also used in X-ray absorption near edge structure (XANES) analysis. The polished sections were also examined by scanning electron

microscopy coupled with energy dispersive X-ray spectroscopy (SEM/EDX) using a backscattered electron detector and EDX X-ray intensity elemental mapping. The phosphorus-rich areas were chosen for FTIR analysis using the micro ATR crystal (germanium) through the EDX X-ray intensity elemental maps constructed from analyzes 80-100 μm in diameter to a depth of 1-2 μm .

X-ray photoelectron spectroscopic (XPS) analyzes were performed using a Kratos Axis Ultra spectrometer. A monochromatic Al K (α) source (15mA, 14kV) was used in this spectrometer. XPS can investigate the surface (penetration depth 5-7 nm) and detect all elements except hydrogen and helium. Depending on the element, the detection limits varied from 0.1 to 0.5 atomic percent. The work function of the instrument was calibrated with respect to Au 4f_{7/2} line for metallic gold to a binding energy (BE) of 83.96 eV. The dispersion of the spectrometer was adjusted with respect to the Cu 2p_{3/2} line of metallic copper to a BE of 932.62 eV. For all specimens, the Kratos charge neutralizer system was used. The analysis area and pass energy of the survey scan analyzes were 300 x 700 microns and 160 eV, while the analysis area and the pass energy of high resolution analyzes were 300 x 700 μm and 20 eV. The spectra obtained were corrected for charge to the main line of the carbon 1s spectrum (adventitious carbon) set to 284.8 eV. The CasaXPS software (version 2.3.14) was used to analyze the spectra.

XANES experiments were conducted at the Canadian Light Source, Saskatoon, Canada using the 2.9 GeV storage ring. Phosphorus K absorption edge data was recorded using Soft X-ray Micro-characterization Beam line (SXRMB; 06B1-1) covering the region of 1700-10000 eV with photon resolution of 0.2eV and a beam spot size of 300 μm x 300 μm . XANES spectra were acquired in Total Electron Yield (TEY) and Fluorescent Yield (FY) modes. Experimental and

standard data were collected using a monochromator with Si (111) crystals and a flux of $>1 \times 10^{11}$ photons s^{-1} . Spectral data were averaged over 2–3 scans to improve signal-to-noise ratios. The XANES spectra of the unknown samples (spent BOFS) were compared with reference materials through linear combination fitting using data processing software, Athena, version 0.8.56 (Ravel and Newville, 2005).

3.3.5 Geochemical modeling

The saturation indices (SI) for calcium phosphate phases including hydroxyapatite and other mineral phases relevant to the treatment system were calculated using the geochemical modeling code PHREEQC Interactive (Parkhurst and Appelo, 1999). The WATEQ4F database was used for these calculations and solubility product values for brushite, monetite, octacalciumphosphate, β -tricalciumphosphate, and variscite were added to this database using published data (Baker et al., 1998; Stumm and Morgan, 1981).

3.4 Results and Discussion

3.4.1 Characteristics of the reactive materials

The coarsest fraction of the BOFS had the highest mass weighted surface area (Table 3.2) as the material was screened and washed before use. The particle density of the BOFS was 3.49 g cm^{-3} . The BOFS sample contained 39 wt.% CaO, 24 wt.% Fe_2O_3 , 12 wt.% SiO_2 , 11 wt.% MgO, 3.8 wt.% MnO, and 3.4 wt.% Al_2O_3 (Table 3.1). The XRD patterns indicated the presence of Wuestite (FeO), Lime (CaO), Larnite ($\text{Ca}(\text{SiO}_4)$), Srebrodolskite ($\text{Ca}_2\text{Fe}_2\text{O}_5$), Anhydrite (CaSO_4) and possibly Portlandite ($\text{Ca}(\text{OH})_2$) in BOFS (Table 3.2).

3.4.2 Influent chemistry

There were distinct differences in influent chemistry observed during the study period, reflecting changes in the student population at the college. During the first 157 days of the experiment influent concentrations of alkalinity, phosphate, ammonia, cBOD₅, and COD were much lower than during the following 91 days. A low student population in the college during the first 157 days of the experiment is one of the reasons for lower concentrations of these dissolved constituents. The mixing process was discontinued during the last 91 days, which largely reduced the influence of Cell 2 in this period and contributed to changes in the influent water composition. Based on the differences in the influent concentrations, the results are discussed in two phases (Phase 1 includes the first 157 days and Phase 2 includes the final 91 days).

3.4.3 pH and alkalinity

The pH of Cell 1 effluent (treatment system influent) was 7.44 ± 0.53 . Small pH increases were observed in the effluent of Cell 2 (7.98 ± 0.56) and Cell 3 (8.12 ± 0.54) due to the presence of carbonate minerals in the gravel and the influence of atmospheric CO₂ which was introduced to the cells during mixing and aeration (Figure 3.7). In the Cell 4 effluent, pH abruptly increased and remained very high (between 10.96 and 12.36) throughout the trial. A sudden drop in pH from 11.20 ± 0.98 to 7.36 ± 0.56 was observed in the Cell 5 effluent following the pH-adjustment unit (Figure 3.7). Mean alkalinity in Cells 1, 2, 3, and 4 effluents during Phase 1 were 298, 249, 233, and 634 mg L⁻¹ as CaCO₃; during Phase 2 these values were 575, 523, 198, and 243 mg L⁻¹ as CaCO₃ (Figure 3.7). Mean alkalinity values in the Cell 5 effluent were 433 and 239 mg L⁻¹ as CaCO₃ before and after CO₂ sparging as the dissolved Ca in Cell 4 effluent reacted with CO₂ to

form particulate calcium carbonate and precipitate in the sparging cell (Figure 3.7). Cell 4 effluent initially released very high alkalinity water (total alkalinity $>1500 \text{ mg L}^{-1}$ as CaCO_3) and pH (>12), probably due to the dissolution of free lime and portlandite from the BOFS (Figure 3.7). However, the alkalinity gradually decreased to below 200 mg L^{-1} as CaCO_3 , and the pH gradually decreased to 10.96 at the end of the trial. Precipitates of CaCO_3 were observed in the pH adjustment unit (Cell 4a) as CO_2 was introduced to lower the pH. Based on the difference between the initial OH^- concentration measured in Cell 4 effluent and the final OH^- concentration, typically 10^{-2} moles of CO_2 were required to reduce the pH from 12 to 7.5 per liter of effluent.

3.4.4 Major ion chemistry

The mean Ca concentration in the system influent was 108 mg L^{-1} , and decreased slightly in Cell 2 effluent (104 mg L^{-1}) and Cell 3 effluent (98 mg L^{-1}). The substrate (washed limestone gravel) used in Cell 3 did not contribute any additional Ca. At the beginning of the trial, the Ca concentrations increased sharply ($\sim 294 \text{ mg L}^{-1}$) in the Cell 4 effluent, probably due to the dissolution of CaO and Ca(OH)_2 in the BOFS. Over time the concentration gradually decreased to 123 mg L^{-1} as the cell was continuously flushed (Figure 3.8). Calcium concentrations decreased significantly in Cell 4* as Ca reacted with CO_2 resulting in the formation of CaCO_3 (Figure 3.8). This CaCO_3 accumulated at the bottom of the standing water in the cell. Higher Ca concentrations in the Cell 5 effluent compared to the Cell 4* effluent suggest that Ca may be derived from the pulp & paper mill bio-solids (a substrate used in Cell 5), which contained leachable amounts of Ca (Vance, 2000a). The mean Na concentrations in Cells 1, 2, 3, 4, and 5

effluents were 112 mg L⁻¹, 110 mg L⁻¹, 109 mg L⁻¹, 106 mg L⁻¹ and 108 mg L⁻¹ (Figure 3.8). The Na concentrations were more or less steady among the cells, although the influent concentrations gradually increased throughout the trial. Mean Mg concentrations in Cells 1, 2, 3, 4, and 5 effluents were 12.22, 12.13, 12.05, 0.09, and 0.35 mg L⁻¹. There were small variations in Mg concentrations observed in the effluent of Cells 1, 2, and 3. However, Mg concentrations decreased sharply to less than 0.01 mg L⁻¹ in the Cell 4 effluent, probably due to the incorporation of Mg in CaCO₃ precipitates. A slight increase of the Mg concentrations (0.35 mg L⁻¹) was observed in Cell 5 effluent (Figure 3.8).

The mean SO₄²⁻ concentrations in the effluent of Cells 1, 2, 3, 4, and 5 were 43.39, 43.02, 45.09, 33.10, and 40.45 mg L⁻¹. About 16-66% less SO₄²⁻ was observed in the Cell 5 effluent compared to Cell 3 effluent (Figure 3.8). Dissolved S²⁻ concentrations in Cell 1 effluents were lower than the detection limit (0.005 mg L⁻¹), and increased in Cell 3 effluents (0.007 mg L⁻¹). Both SO₄²⁻ and S²⁻ concentrations decreased in the Cell 4 effluent; the dissolved S²⁻ concentration decreased to below detection, compared to the upstream treatment cells. However, the dissolved S²⁻ concentration increased significantly in Cell 5 (average 0.311 mg L⁻¹) to concentrations that were higher than the SO₄²⁻ concentrations. Eh measurements also suggest that reducing conditions prevailed in both Cells 4 and 5 (Figure 3.7).

3.4.5 Phosphorus

Mean PO₄-P concentrations in Cells 1, 2, 3, 4, and 5 effluents were 6.97, 4.69, 3.01, 0.02, and 0.35 mg L⁻¹ (Figure 3.7). Between 40% and 60% of the PO₄-P entering Cell 2 was removed during the initial stage of the experiment. However, the extent of PO₄-P removal decreased

substantially after ~73 days of operation and remained between 3 and 33% with few exceptions (Figure 3.7). The removal efficiency of $\text{PO}_4\text{-P}$ in Cell 3 was $32\pm 31\%$ (average 36%), which is close to the values (40-60%) found in previous studies of constructed wetland cells (Kadlec and Knight, 1996; Knight et al., 2000, and Vymazal, 2004). The removal efficiency of PO_4 in Cell 4 with respect to the concentration in Cell 3 effluent was 97.4-99.9%. Higher PO_4 concentrations were observed in Cell 5 effluent compared to Cell 4 effluent, which indicates that the biosolids added to Cell 5 released a small amount of PO_4 . The total P-masses in, masses out and masses retained in the BOFS Cell were 47.7, 0.30, and 47.4 g. Thus about 99.4% P-masses were retained by the BOFS Cell (Figure 3.9).

Inorganic PO_4 can be adsorbed on hydrous oxides of Fe and Al under acidic conditions, and can combine with Ca to form calcium phosphate in alkaline environments (Qualls and Richardson, 1995). Inadequate concentrations of Ca, Fe, and Al (the most common metals present in P-bearing phases; Vymazal, 2004) in the filtration medium of Cell 3 (crushed stone) explains the limited P removal capacity. The BOFS, used in the reactive mixture of Cell 4, contains significant amounts of Ca, Fe, Al, and Mg oxides (Table 3.1), thus favored greater removal of P. Precipitation of calcium phosphate phases (dependent on the Ca concentration) including hydroxyapatite (HAP) is another potentially important PO_4 removal mechanism in BOFS based treatment systems (Baker et al., 1998; Bowden et al., 2009). However, the formation of crystalline hydroxyapatite can be inhibited by the substitution of Mg into the Ca position in the hydroxyapatite structure (Kim et al., 2006). Moreover, Fe, Al, and Mg-phosphate phases may also form under certain pH conditions in BOFS-based treatment systems. When wastewater was introduced to Cell 4, the reactive media, which contained a high percentage of

CaO, developed a highly alkaline condition ($\text{pH} > 9$). Adsorption is less favoured under the conditions prevalent in Cell 4 because HPO_4^{2-} and PO_4^{3-} become the dominant phosphate species at $\text{pH} > 9$. These species are attracted to positively charged surfaces, which tend to be less prevalent under high pH conditions (Stumm and Morgan, 1981). However, BOFS does contain metal oxides with elevated pH of zero point of charge (pH_{ZPC}) values, including MgO (with pH_{ZPC} of 12.4; Parks, 1965), Al_2O_3 (with pH_{ZPC} of 9.1; Parks, 1965), and Fe_2O_3 (with pH_{ZPC} of 8.5; Davis and Kent, 1990), therefore limited PO_4 adsorption in the BOFS cell is possible. Significant quantities of Fe_2O_3 (24.3%), MgO (11.2 %), and Al_2O_3 (3.4 %) were present in the BOFS materials used in this study (Table 3.1) suggesting that adsorption may be a possible PO_4 removal mechanism. There was no substantial decrease in the rate of PO_4 removal during the study.

Although precipitation of Al-phosphate and Fe-phosphate is favoured under near neutral to acidic conditions (Stumm and Morgan, 1981), the Cell 4 effluent remained strongly basic, suggesting that formation of Al- and Fe-phosphate minerals is unlikely to result in significant PO_4 retention. The substrate, pulp and paper mill biosolids, present in Cell 5 contained a significant amount of PO_4 (Vance, 2000a, Vance, 2000b). As a result, an elevated PO_4 concentration was observed in Cell 5 effluent. However, the PO_4 concentration in Cell 5 effluent were much lower (~70%) than the untreated wastewater (Figure 3.7).

FES-EM images and EDX data were collected from samples of the fresh BOFS material and from the spent media to investigate changes in composition near the surfaces of these materials. The phosphorus content of the fresh BOFS was ~0.38 wt. %. Samples of the spent media from Cell 4 were collected in 10-15 cm intervals in five vertical profiles (Figure 3.6, Table 3.3). The

mass of P on the spent media was greatest (up to 8.55 wt. %) in the samples obtained from within close proximity to the distribution manifold and gradually decreased with depth at all locations sampled in Cell 4.

The solid-phase phosphorus contents in Profiles 1 and 2 were lower than Profiles 3, 4, and 5. Profile 5, located in the effluent side of Cell 4 opposite to the inlet piping, showed the highest P contents at depths 40 cm, 55 cm, and 70 cm from the surface of the Cell (Figure 3.10). The high P content in Profile 5 and the accumulation of precipitates on the distribution matrix in close proximity of this profile (coordinate: 0, 80, 0), and cementation along the profile suggest that this part of Cell 4 received the majority of the input, possibly due to uneven distribution or preferential flow paths. At all depth levels, a gradual decrease in P content from Profiles 5 to 3 was observed (Figure 3.10). The bottom-most part of Profile 3, close to the outlet port, had a P content of 0.41 wt. %, which is similar to the fresh BOFS (0.38 wt. %). This low P content in the reactive media in close proximity of the outlet port and very low mean PO_4 concentration (0.02 mg L^{-1}) in the Cell 4 effluent indicates that the aqueous PO_4 in the Cell 4 influent (3.01 mg L^{-1}) was attenuated in the upper part of Cell 4 and the bottom part of Profile 3 was beyond the P-removal front (Figure 3.7, 3.10).

The influent water was undersaturated with respect to brushite, monetite, vivianite, and variscite (Figure 3.11) in both sampling events, undersaturated with respect to strengite and gibbsite in the first sampling event, and supersaturated with respect to strengite and gibbsite in the second sampling event. The influent water was also supersaturated with respect to octacalciumphosphate, β -tricalciumphosphate, strengite, MnHPO_4 , calcite, aragonite, goethite, ferrihydrite, hydroxyapatite, and an inferred hydroxyapatite phase (Baker et al., 1998). The pore

water was supersaturated with respect to calcium phosphate phases including hydroxyapatite, a common phosphate bearing phase in calcium and phosphorus rich environments (Yamada et al., 1986; Bowden et al., 2009; Stumm and Morgan, 1981). Very low phosphate concentrations in Cell 4 effluent suggest that precipitation of hydroxyapatite or another calcium phosphate phase is a possible mechanism for P retention in the BOFS media.

3.4.5.1 FTIR

Elemental maps of polished cross-sections of samples S-20 and S-21 collected from Cell 4 (Figure 3.6) indicate accumulation of phosphorus on the boundary of the grains. The EDX spectra collected from two locations observed in the elemental maps suggested the occurrence of phosphorus at the boundary of the grains (Figure 3.12). FTIR-ATR spectra from phosphorus rich boundaries showed vibrational frequencies of carbonate and phosphate bands (Figure 3.13). The vibrational frequencies at 712 cm^{-1} (carbonate ν_4), 872 cm^{-1} (carbonate ν_2), and 1408 cm^{-1} (carbonate ν_3) indicate the occurrence of calcite, whereas the vibrational frequencies at 1027 cm^{-1} (phosphate ν_3), a very weak shoulder at 960 cm^{-1} (phosphate ν_3), and at 602 cm^{-1} (phosphate ν_4) along with the OH^- stretch at 3277 cm^{-1} indicated the occurrence of hydroxyapatite (Rehman and Bonfield, 1997; Panda et al., 2003; Pena and Vallet, 2003; and De Oliveira Ugarte et al., 2005; Ribeiro et al., 2006; Kim et al., 2006; Singh and Purohit, 2011, Matković et al., 2012).

The FTIR spectra of the samples were compared with the major vibrational bands of phosphate and carbonate phases. An example of these comparisons is shown in Figure 3.14. The spectra of the solid-phase samples collected from Cell 4 showed a sharp carbonate ν_4 band at 712 and 713 cm^{-1} , well-defined and broad carbonate ν_3 band at 1424 - 1428 cm^{-1} , sharp carbonate ν_2 band at

873-875 cm^{-1} , and carbonate overtones or combination of the carbonate bands at 1796-1799 cm^{-1} ($\nu_1 + \nu_4$; Gillet et al., 1996; Vongsavat et al., 2006; Tatzber et al., 2007; Gunasekaran and Anbalagan, 2008), at 2513-2514 cm^{-1} ($\nu_1 + \nu_3$; Vongsavat et al., 2006; $2\nu_2 + \nu_4$; Gunasekaran and Anbalagan, 2008). Weak carbonate overtones or a combination of the carbonate bands at 2872-2876 cm^{-1} and 2980-2984 cm^{-1} were also observed ($2\nu_3$; Gunasekaran and Anbalagan, 2008). The vibrational frequencies 712-713 cm^{-1} (carbonate ν_4) and 873-875 cm^{-1} (carbonate ν_2), along with other vibrational frequencies of different carbonate bands and overtones indicated that calcite was the main carbonate mineral accumulated on the spent reactive materials (Vagenas et al., 2003; Vongsavat et al., 2006; Ni and Ratner, 2008; Kurap et al., 2010).

The vibrational bands of phosphate for reference materials are provided in Table 3.4. Phosphate ν_3 , ν_4 , and ν_2 bands were obtained in most of the samples collected from Cell 4. However, comparatively sharp peaks of ν_3 and ν_4 bands were observed in the spectrum of sample S-20 at 1045 cm^{-1} (phosphate ν_3) and a doublet at 604 and 572 cm^{-1} (phosphate ν_4). A very weak shoulder of phosphate ν_1 at 963 cm^{-1} and weak peaks of phosphate ν_2 at 446 and 454 cm^{-1} were also observed in the spectrum of sample 20. Phosphate ν_3 at 1048 cm^{-1} , phosphate ν_4 doublet at 604 and 571 cm^{-1} , phosphate ν_2 at 456 and 468 cm^{-1} , and very weak phosphate ν_1 peak at 959 cm^{-1} were also observed in the spectrum of sample S-21, however, phosphate ν_3 , ν_4 , and ν_2 peaks were not as prominent as observed in the spectrum for sample S-20. The vibrational frequencies 1048 cm^{-1} (phosphate ν_3), 604 and 572 cm^{-1} (phosphate ν_4), 446 and 454 cm^{-1} (phosphate ν_2), and a very weak shoulder at 963 cm^{-1} (phosphate ν_1) were observed, which were similar to the reference HAP-S, HAP-WM, and β -TCP, and also consistent with previous studies (Rehman and Bonfield, 1997; Ribeiro et al., 2006; Panda et al., 2003; Singh and Purohit, 2011, Matkovic

et al., 2012; Kim et al., 2006; Pena and Vallet, 2003; and De Oliveira Ugarte et al., 2005). These similarities in vibrational bands indicated the possible occurrence of hydroxyapatite or β -TCP in samples S-20 and S-21.

3.4.5.2 XPS

The XPS survey spectra and high resolution spectra of sample S-20, S-21, S-16, S-11, and S-1 powder were studied. Oxygen, Ca, Mg, C, P, Si and Al peaks were observed in the survey XPS spectra of most samples. The surface atomic ratio of Ca/P and O/Ca were two to three times higher than the typical hydroxyapatite (Table 3.5; Lu et al., 2000). Calcium 2p_{3/2} binding energies for all samples range from 346.8 and 347.3 eV. Phosphorus 2p_{3/2} binding energies range from 132.6 to 133.1 eV. The Ca 2p_{3/2} peak from a reference sample of calcium carbonate has a binding energy of 346.7 to 347.0 eV. The Ca 2p_{3/2} binding energy for a calcium phosphate reference sample was at 347.3 eV with the P 2p_{3/2} peak at 133.0 eV. The binding energies of Ca 2p_{3/2} and P 2p_{3/2} obtained in the samples were within the same range of the binding energies of calcium phosphate and calcium carbonate, which is consistent with the presence of both calcium phosphate and calcium carbonate. An example high resolution spectra is given in Figure 3.15.

3.4.5.3 XANES

XANES refers to the portion of the X-ray absorption spectra near an absorption edge, extending approximately from -50 to +200 eV with respect to the edge energy (Kelly et al., 2008). The primary fluorescence peak positions of the phosphate-bearing (PO₄ tetrahedra with oxidation state +5) phases are very similar. However, the characteristics of the secondary spectral features, including size, shape, and position, are diagnostic for different compounds and minerals

(Brandes et al., 2007). The primary peak positions for phosphate species are around 2151 eV, which represent strong peaks or absorption edges or white lines in XANES spectra (Brandes et al., 2007). The white line of P represents the energy required to eject electrons from the K shell of P atoms (Güngör et al., 2007). The white line for phosphate may vary between ± 0.5 eV depending on the charge, electronegativity, and interatomic distance of the coordinating cation (Franke and Hormes, 1995). P K-edge XANES also has been reported at 2150 eV (Shober et al., 2006). Spectral characteristics of phosphorus K-edge XANES spectra for Ca-, Al-, and Fe-phosphates are reviewed comprehensively in previous studies (Hesterberg et al., 1999; Ajiboye et al., 2008; Shober et al., 2006; Sato et al., 2005; Eveborn et al., 2009; Beauchemin et al., 2003).

In this study, the XANES spectra of the reference materials displayed a number of pre- and post-edge spectral features (Figure 3.16). The white lines of reference materials ranged between 2151.5 and 2151.7 eV except for FeP (2152.2 eV). Iron (III) phosphate showed a unique pre-edge feature at 2148.5 eV (-3.7 eV with respect to the white line), which is consistent (between -2 and -5 eV) with previous studies (Hesterberg et al., 1999; Khare et al., 2007; Ajiboye et al., 2008; Shober et al., 2006; Sato et al., 2005; Eveborn et al., 2009; and Beauchemin et al., 2003). The presence of a shoulder at ~ 2154.7 eV was one of the important spectral features observed in all calcium phosphate reference materials (Figure 3.16 c). However, the sharpness of this feature increased with an increase in crystallinity. Similar spectral features are reported by Peak et al. (2002). Two other dominant spectral features were observed at ~ 2162.5 eV and ~ 2169 eV in all calcium phosphate samples and reference materials (Figure 3.16 d, e). The relative positions of these features with respect to P K-edge were similar to the features observed at around ~ 2170 eV

and ~2175 eV (Peak et al., 2002) and ~2159 eV and 2166 eV (Sato et al., 2005), and were identified as a signature of calcium phosphate species and oxygen oscillation.

XANES spectra of the spent BOFS samples displayed a number of post edge spectral features similar to the reference materials, however, no pre-edge spectral features were observed in these samples (Figure 3.16). The white lines of the samples ranged between 2151.4 and 2151.6 eV, which was similar to the range obtained for the reference materials. Although the locations of the post-edge features of the samples and the reference materials appeared in the similar energy range, the sharpness of the features varied substantially from one spectrum to another. After careful visual inspection it was evident that the spectra from sample S-20 resembled the crystalline calcium phosphate reference materials more closely than that of samples S-21, S-16, and S-11. This observation is not unexpected because S-20 contained a higher mass of PO₄ than the other samples. A PO₄ sorbed on CaCO₃ standard was also included as the reference materials. This spectrum exhibited similar post-edge spectral features to sample S-20 (Figure 3.16, 3.17). The spectral similarities of PO₄ sorbed on CaCO₃ with sample S-20 suggest that sorbed PO₄ could be present in the reacted BOFS. The FTIR spectra of each spent BOFS samples indicated the presence of calcite.

Linear combination fitting was conducted to determine the similarity between the spectra for the spent BOFS samples and the spectra for the reference materials. XANES spectra of FeP was excluded from the LC fitting analysis because the distinctive pre-edge feature at around 2148.5 eV (a, Figure 3.16), which is characteristic of Fe-PO₄ phases, was not observed in the spectra of spent BOFS samples. A series of binary and ternary combination fittings of the reference materials were conducted for the spent BOFS samples. The proportion of the contributing

phosphate species were predicted with χ^2 goodness of fit criteria. All of the best-fit combinations included β -TCP as a significant component. Beta-tricalcium phosphate, HAP-S, and CPD provided the best combination ($\chi^2 = 1.03$) for sample S-20, whereas β -TCP and CPD were the best combination for sample S-21 ($\chi^2 = 0.79$), and β -TCP, α -TCP, and CPDD provided the optimum LC fitting for samples S-16 ($\chi^2 = 1.26$) and S-11 ($\chi^2 = 2.91$). Although the χ^2 value was slightly lower with respect to β -TCP, CPD, and HAP-S combination fit for sample S-21, the total weight of the contributing reference materials was overestimated (1.006) and contribution from HAP-S was zero. Thus this combination was not considered. Sample S-11 showed poor fitting with high χ^2 values for different combinations, which is probably due to the lower phosphate accumulation on the BOFS in this sample location. FTIR and EDX analyzes also showed strong indications of the presence of a more soluble phosphate phase in this sampling location (Figure 3.12, 3.13, 3.14). Among the calcium phosphate reference materials considered in this study, β -TCP was identified as the most abundant component (contributing between 50 and 100% to the LC fitting) in all of the spent BOFS samples (Figure 3.18, Table 3.6). A significant contribution from HAP-S (~22 %) was observed in sample S-20, however HAP-S provided little to no contribution in the S-21 LC fit and no contribution in the other samples. These results were consistent with the FTIR results (Figure 3.16). A small contribution from CPD (~9%) was also indicated in LC fits for samples S-20 and S-21, however no contribution was observed in the other samples (Figure 3.18, Table 3.6). There were significant contributions from α -TCP (between 36 and 40%) observed in samples S-16 and S-11. The predicted contributions of CPDD in samples S-16 and S-11 were between 4 and 9%.

3.4.6 Ammonia and nitrate

The concentration ranges, mean concentrations, and removal efficiencies of $\text{NH}_3\text{-N}$ and $\text{NO}_3\text{-N}$ along the flow path in Phases 1 and 2 are summarized in Table 3.7. There was a sharp difference in influent $\text{NH}_3\text{-N}$ concentrations between Phase 1 ($7.70 \pm 7.60 \text{ mg L}^{-1}$) and 2 ($51.0 \pm 26.1 \text{ mg L}^{-1}$, Figure 3.19). The overall removal efficiency of $\text{NH}_3\text{-N}$ in Cells 2, 3, and 4 was 97%. However, the average $\text{NH}_3\text{-N}$ concentrations increased in Cell 4 effluents by >5 times compared to the Cell 3 effluent. Cell 5 played a negative role on the overall NH_3 removal (51% removal) to the system. Small increases in $\text{NH}_3\text{-N}$ concentrations were observed in Cell 5 effluents with respect to the Cell 4 effluent. There was an increasing trend observed in $\text{NO}_3\text{-N}$ concentrations from Cells 1 to 3 in both phases (Figure 3.19). These trends were attributed to oxidation of ammonia to nitrate in Cells 2 and 3. Ammonia oxidation was enhanced by the mixing and aeration systems, which resulted in high DO concentrations in Cells 1 and 2 (Figure 3.15, 3.19; Table 3.8). The $\text{NO}_3\text{-N}$ concentrations decreased slightly in Cell 3 effluent (~4%) in Phase 1 from the preceding cell (Cell 2), probably due to mixing and oxidation in Cell 2. However, a sharp increase in $\text{NO}_3\text{-N}$ concentration was observed in Phase 2, when the mixing was eventually suspended. In both phases $\text{NO}_3\text{-N}$ concentrations gradually decreased in Cell 4, and the Cell 5 effluent was similar to the Cell 3 effluent (Figure 3.19). There was a negative correlation observed between $\text{NH}_3\text{-N}$ and $\text{NO}_3\text{-N}$ concentrations (Figure 3.19). Thus, in both phases NH_3 oxidized to NO_3 in the presence of $\text{O}_{2(g)}$, which is consistent with results observed in previous studies (Davies and Hart, 1990). Relatively more reducing conditions, which prevailed in Cell 5, resulted in lower NO_3 concentrations, and increased concentrations of NH_3 in both phases of the study.

3.4.7 Carbonaceous biochemical oxygen demand (cBOD₅) and chemical oxygen demand (COD)

The concentration ranges, mean concentrations, and removal efficiencies of cBOD₅ and COD along the flow path in Phases 1 and 2 are summarized in Figure 3.20 and Table 3.8. The removal efficiencies of cBOD₅ in Cells 2, 3, 4, 4*, 5, and 6 were calculated with respect to the Cell 1 effluent in both phases. Although a decrease in the removal efficiency of cBOD₅ was observed in both phases, this was not as significant in Phase 2. The concentrations of cBOD₅ decreased gradually in Cells 2, 3, and 4. However, concentrations increased by approximately 7 times (in Phase 1) and 10 times (in Phase 2) in the Cell 5 effluent compared to the Cell 4 effluent. The removal of cBOD₅ in aerated EW cell (Cell 3) was 87% with respect to Cell 1 effluent, which was similar to previously reported values (90%; Johnson and Mara, 2005). The removal of cBOD₅ in the treatment cells in both phases indicate that both aeration cells (Cells 2 and 3) and highly alkaline conditions (in Cell 4) played an important role in degrading labile organic carbon. Low cBOD₅ concentrations (below the detection limit of 1 mg L⁻¹) in the Cell 4 effluent throughout the experiment suggest that the BOFS present in Cell 4 has the potential to remove cBOD₅ (Figure 3.20). The mechanism contributing to cBOD₅ removal, however, is unclear. Although the cBOD₅ concentration increased in the Cell 5 effluent, the cumulative removal efficiencies of cBOD₅ in phases 1 and 2 were 79 and 90%. The elevated cBOD₅ in Cell 5 effluent probably was derived from the breakdown of the biosolids included in the substrate.

Although the COD concentration did not change significantly in Cells 2 and 3 during Phase 1, much lower concentrations were observed in the Cell 4 effluent during Phase 1 (Table 3.8, Figure 3.20). In Cell 5 effluent, COD concentrations increased by ~4 times from Cell 4 effluent.

A negative removal efficiency of COD in Cell 5 (-40%) with respect to Cell 1 effluents suggests that the substrate (boisolds) in Cell 5 added to the excess concentration. The concentrations of COD gradually decreased in Cells 2-4 with maximum 87% removal in the Cell 4 effluent compared to the Cell 1 effluent. However, COD concentrations increased again in Cell 5 effluents by ~25%. Due to high removal efficiencies of cBOD₅ and COD in Cells 2-4, the concentrations of these two parameters decreased to low levels (Figure 3.20).

3.4.8 Geochemical modeling

The influent water was undersaturated with respect to brushite, monetite, vivianite, and variscite (Figure 3.11) in both sampling events, undersaturated with respect to strengite and gibbsite in the first sampling event, and supersaturated with respect to strengite and gibbsite in the second sampling event. The influent water was also supersaturated with respect to octacalciumphosphate, β -tricalciumphosphate, strengite, MnHPO₄, calcite, aragonite, goethite, ferrihydrite, hydroxyapatite, and an inferred hydroxyapatite phase (Baker et al., 1998). Supersaturation of the pore water with respect to calcium phosphate phases including hydroxyapatite, one of the common P-bearing phases in Ca- and P-rich environments (Yamada et al., 1986; Bowden et al., 2009; Stumm and Morgan, 1981), and the very low phosphate concentrations in Cell 4 effluent suggest that precipitation of hydroxyapatite or another calcium phosphate phase are possible mechanisms for P retention in the BOFS media.

3.4.9 Trace metals

The concentrations of dissolved trace metals, including Zn, Fe, Mn, Cr, Ni, and Pb, in the treatment system effluent remained below the Provincial Water Quality Objectives (PWQO) for Ontario (Figure 3.21, MOEE, 1994). Mean Al concentrations in Cells 1, 2, 3, 4, and 5 were 6.16, 5.71, 7.44, 683, and 401 $\mu\text{g L}^{-1}$. Initially (for 108 days), Cell 5 received high pH water from Cell 4 effluent until the pH adjustment cell was introduced. Mean Al concentrations in Cell 5 effluent before and after installing the pH adjustment cell were 1290 $\mu\text{g L}^{-1}$, and 20 $\mu\text{g L}^{-1}$, which is consistent with the predicted pH dependent solubility of Al (Figure 3.22; Stumm & Morgan, 1981). A sharp increase in Al concentrations was observed in Cell 4 effluent, which initially increased from 670 $\mu\text{g L}^{-1}$ to a maximum concentration of 1185 $\mu\text{g L}^{-1}$, then gradually decreased to 186 $\mu\text{g L}^{-1}$ (Figure 3.21, 3.22). Mean V concentrations in Cells 1, 2, 3, 4, and effluent were 0.42, 0.64, 1.33, 27, and 12 $\mu\text{g L}^{-1}$ (Figure 3.21). The BOFS in Cell 4 released V (>PWQO value of 6 $\mu\text{g L}^{-1}$) after continuous flushing of wastewater for 72 days. This was the initiation of the rising limb of the V concentration curve (Figure 3.22). The concentrations of V increased to as high as 48.6 $\mu\text{g L}^{-1}$. The influent Cu concentrations exceeded the PWQO value of 1 $\mu\text{g L}^{-1}$ and were mostly higher than the treatment cell effluents, which suggest that the BOFS did not release Cu, but rather removed Cu to some extent (Figure 3.21).

3.4.10 Removal of bacterial indicators (*E. coli* and total coliforms)

Mean influent concentrations of *E. coli* and total Coliform were 2.2×10^4 and 8.9×10^4 CFU per 100 mL, which sharply decreased (>99%) while passing through Cell 3 by aeration and the

bacterial indicators were completely (~100%) attenuated in Cell 4 due to its highly alkaline condition (Figure 3.23). Thus no additional disinfection was required downstream of Cell 4.

3.4.11 Hydraulic performance

Mean flow rate was 68 L day⁻¹. The extent of carbonate-mineral precipitation and cementation in the spent media was investigated to evaluate the longevity of the treatment system in terms of hydraulic performance. Cell 4 was uncovered and excavated after completion of the study.

Growth of green algae was noted on the top part of the cell; development of white precipitates on the outlet side of the distribution manifold and coatings of yellowish brown precipitates on reactive materials were observed. While excavating the cell, cemented media was encountered along the outlet side of the cell. These precipitates including scale, coatings, and cements reacted vigorously with HCl and produced effervescence. The FE-SEM images and EDX data of the precipitates or adsorbents scraped from the outer layer of the spent reactive material collected from the top of the cell at the effluent end indicated a composition consistent with a carbonate phase rich in calcium and phosphorus and from the bottom part of the effluent side indicated a composition predominantly calcium carbonate (Figure 3.24). Despite sealing the Cell 4 container to restrict air ingress, the dissolved CO₂ was sufficient to result in precipitation of carbonate minerals. It is likely that the effluent from Cell 3 (influent for Cell 4) contained an elevated HCO₃⁻ concentration, which reacted with Ca on the outer layer of the BOFS grains, and released from the BOFS, to form calcium carbonate. Approximately 15% (by volume) of the media had been cemented by carbonate precipitates. However, although the pore spaces were partially clogged, the media was not impermeable. Moreover, the degree of cementation observed around

the outlet piping network was not sufficient to impede the expected flow. Thus, a similar system configuration can be anticipated to operate without a significant decline in hydraulic performance. However, provisions for removing precipitates from the piping network could be incorporated in future designs.

3.5 Conclusions

A multi-step wastewater treatment system, was installed and operated in an indoor facility. Removal efficiencies for cBOD₅, COD, PO₄, NH₃, *E. coli*, and total in Cells 3 and 4 were often >99% with respect to the system influent. High pH and elevated concentrations of V and Al derived from the BOFS materials used in the system were of potential concern. The pH of the system was neutralized by sparging with CO_{2(g)} prior to discharge to the environment. Aluminum concentrations declined following pH neutralization. There was no significant change in hydraulic performance of the treatment system. Sealing of Cell 4 (BOFS cell) limited the ingress of CO_{2(g)}. Phosphorus on the outer layer of the spent reactive material was characterized using combination techniques including BSE imaging and EDX spectra analysis, and examination of X-ray intensity element maps, and FTIR spectra. Some samples showed the probable occurrence of carbonated hydroxyapatite or β-TCP. XANES analysis and LC fit results confirmed the probable occurrence of β-TCP. In addition to phosphate removal, the system disinfected the wastewater and, with the exception of V, resulted in declines in trace metal(loid) concentrations. The final horizontal subsurface flow anaerobic constructed wetland cell did not enhance the treatment efficiency of the system. Thus this system enhancement is not likely required in future studies. The results of these experiments suggest that this integrated treatment system can be

used to provide removal of multiple contaminants from wastewater including P using a relatively passive design.

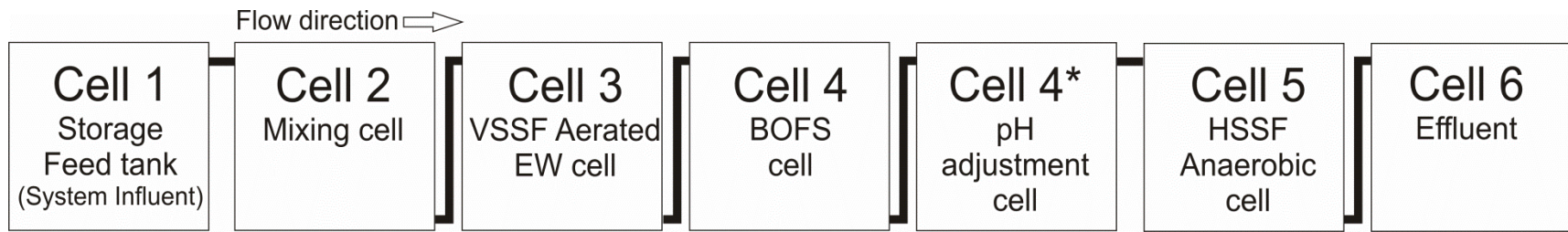


Figure 3.1 Schematic diagram of the cells in the pilot-scale treatment system. Wastewater continuously flows through the system by combination of gravity feed and pumping.

Cell 2 (Mixing Cell)

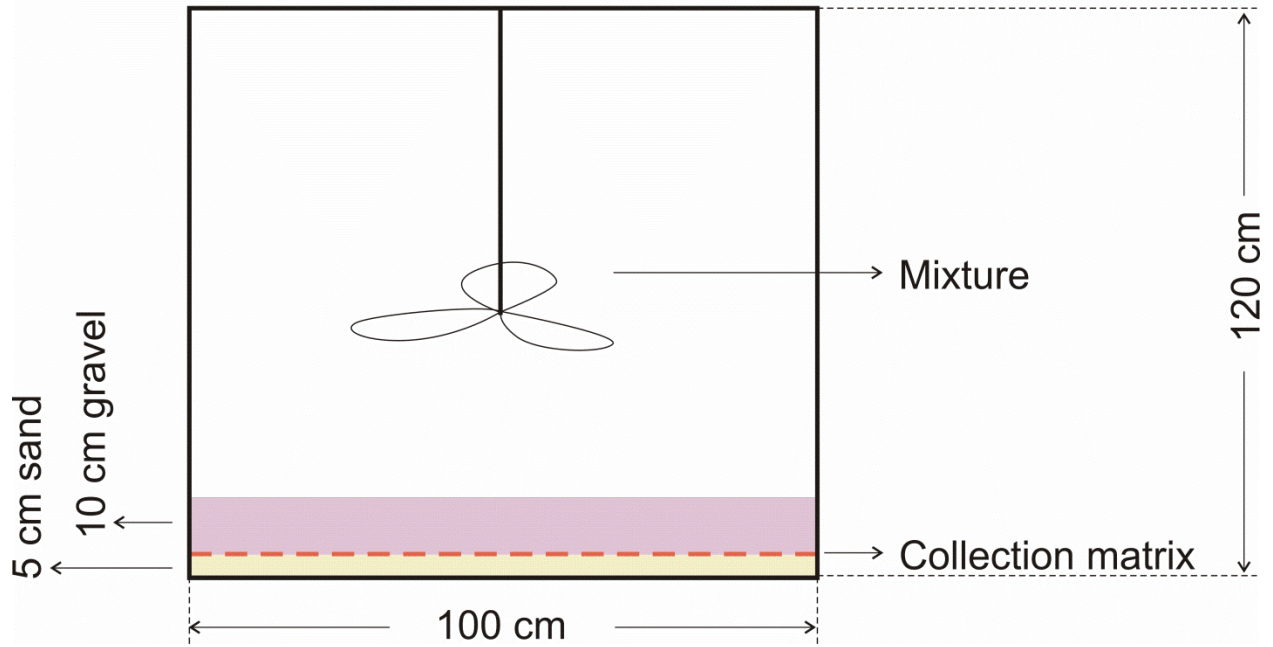


Figure 3.2 Cross-section of the Mixing cell (Cell 2) showing the thickness and vertical distribution of different components of the cell.

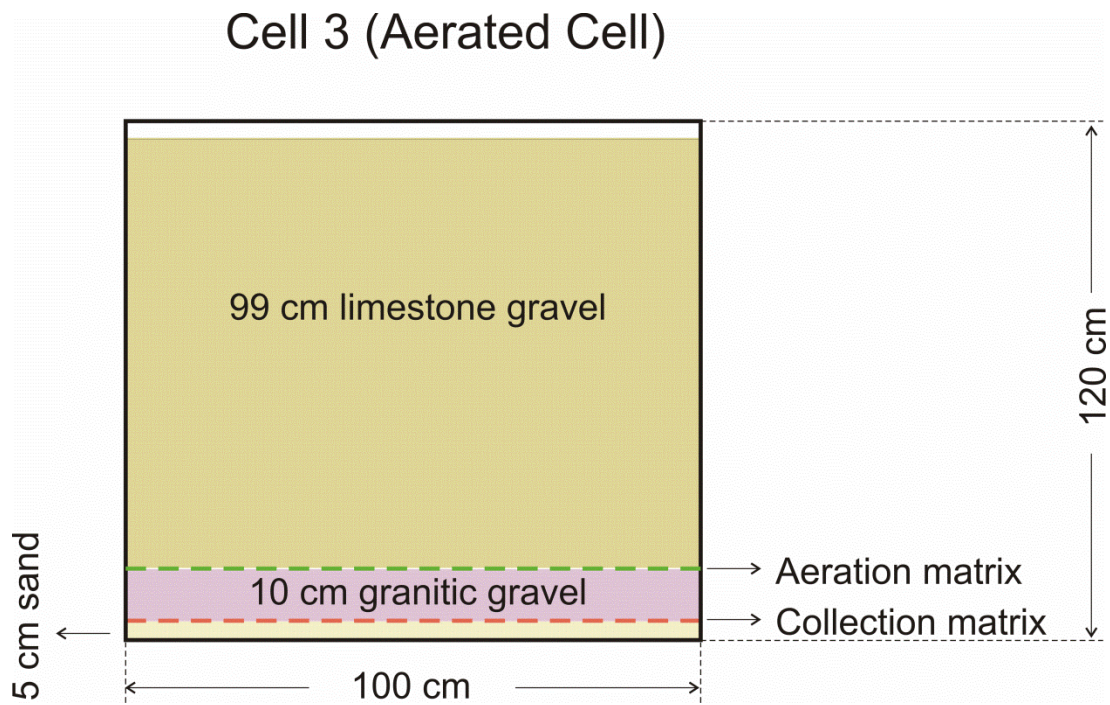


Figure 3.3 Cross-section of the Aerated EW cell (Cell 3) showing the thickness and vertical distribution of different components of the cell.

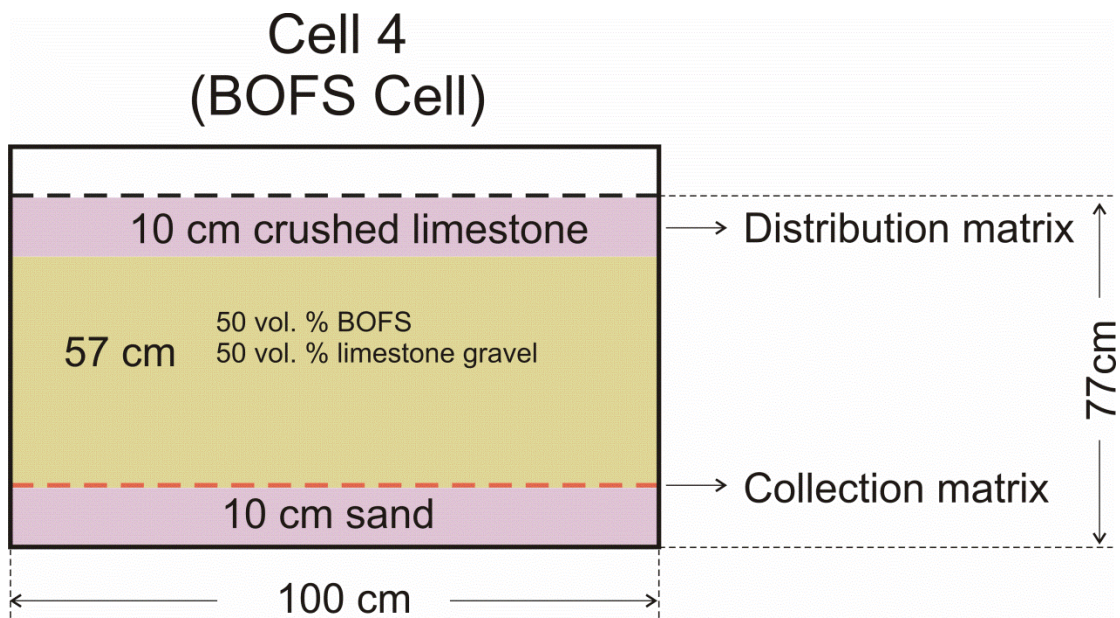


Figure 3.4 Cross-section of the BOFS cell (Cell 4) showing the thickness and vertical distribution of different components of the cell.

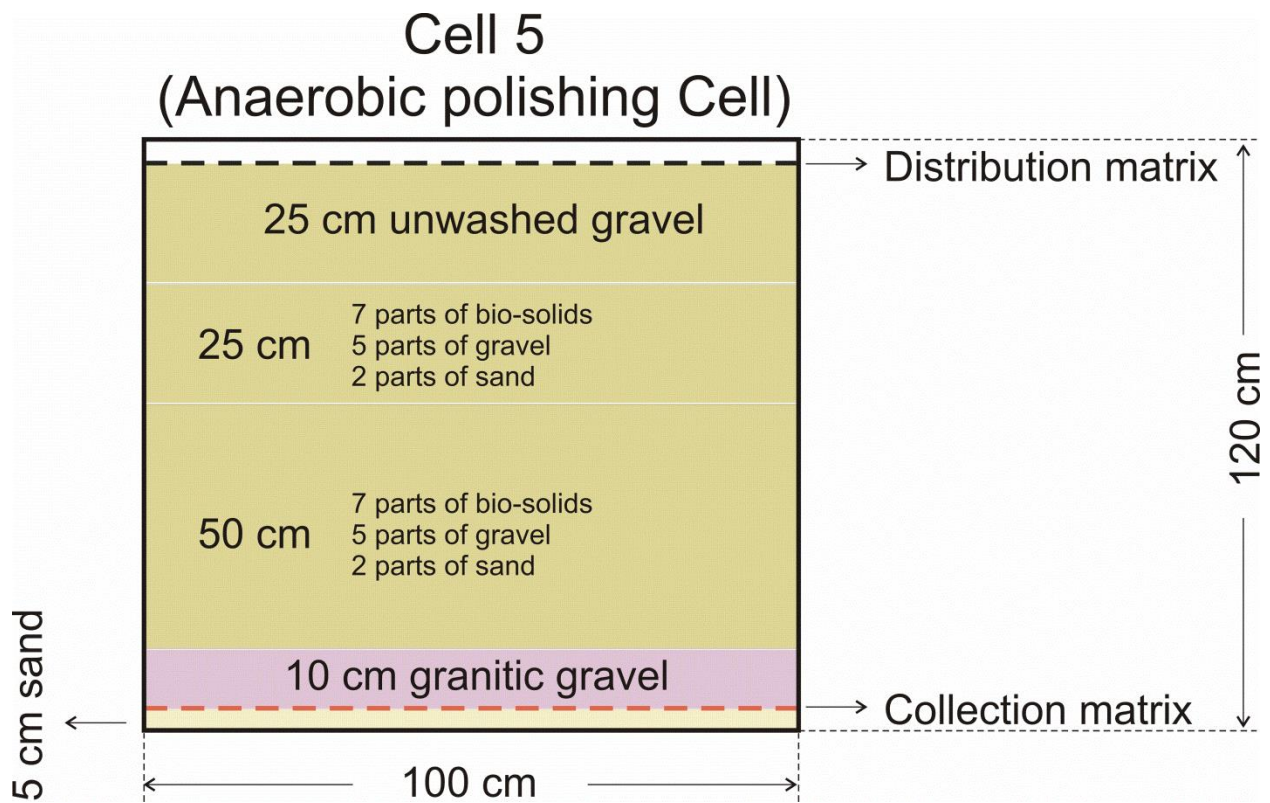


Figure 3.5 Cross-section of the Anaerobic polishing cell (Cell 5) showing the thickness and vertical distribution of different components of the cell.

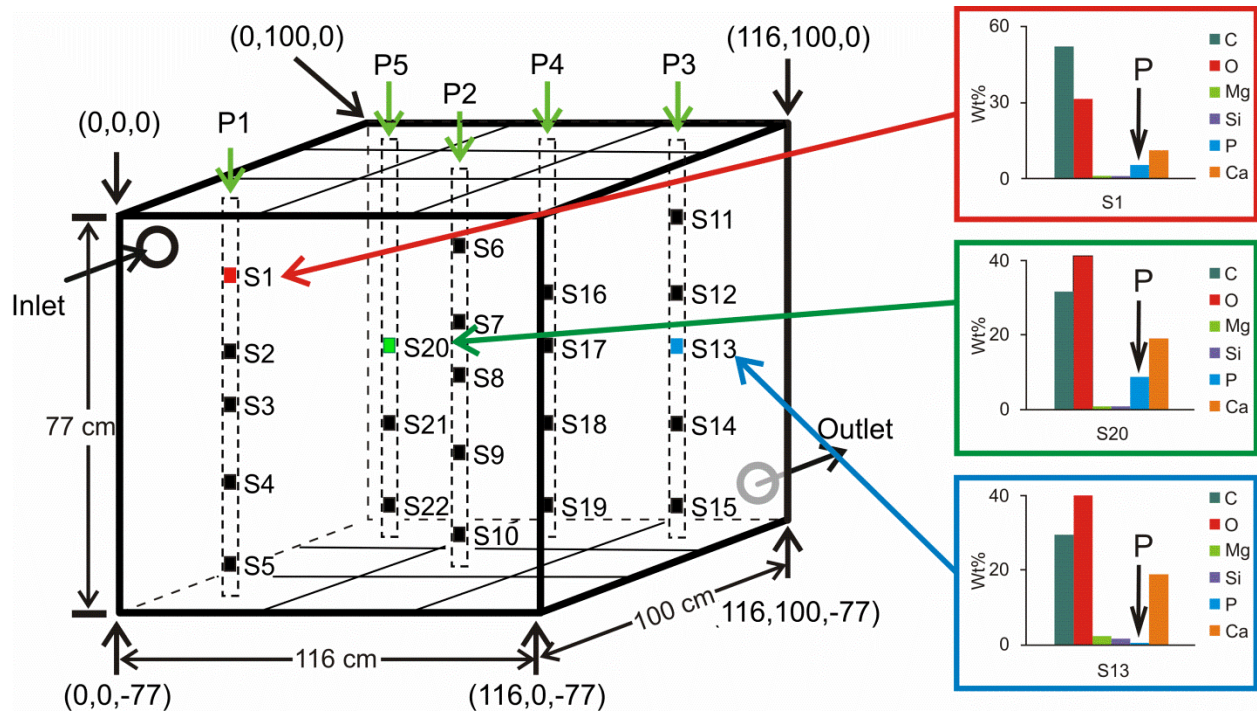


Figure 3.6 Locations of solid phase spent media collected from the BOFS cell, where P represents locations of profile samples and S represents locations of samples within individual profiles.

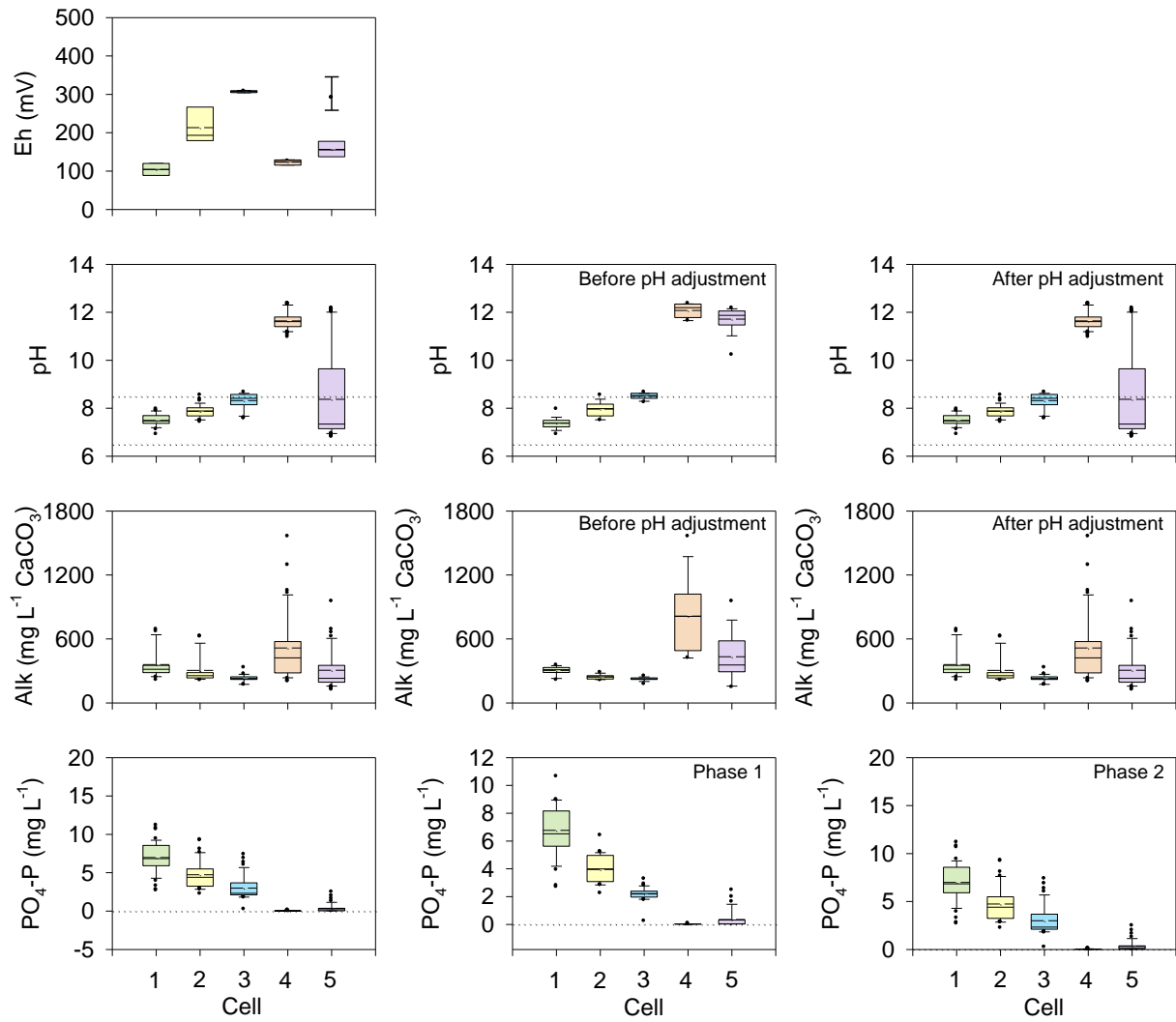


Figure 3.7 Box plots of pH, alkalinity, Eh and $\text{PO}_4\text{-P}$ versus distance (Cells 1-5) along the treatment flow path. Dotted lines represent the Ontario Provincial Water Quality Objective (PWQO). pH and alkalinity of the total study period, before and after pH adjustment are presented in rows 1 and 2, Eh of the total study period, alkalinity before and after pH adjustment are presented in row 3, and $\text{PO}_4\text{-P}$ of the total study period, phases 1 and 2 are presented in row 4. Horizontal solid lines and broken lines on the boxes represent median and mean concentrations. Top and bottom most dots represent maximum observation above upper fence and minimum observation below lower fence.

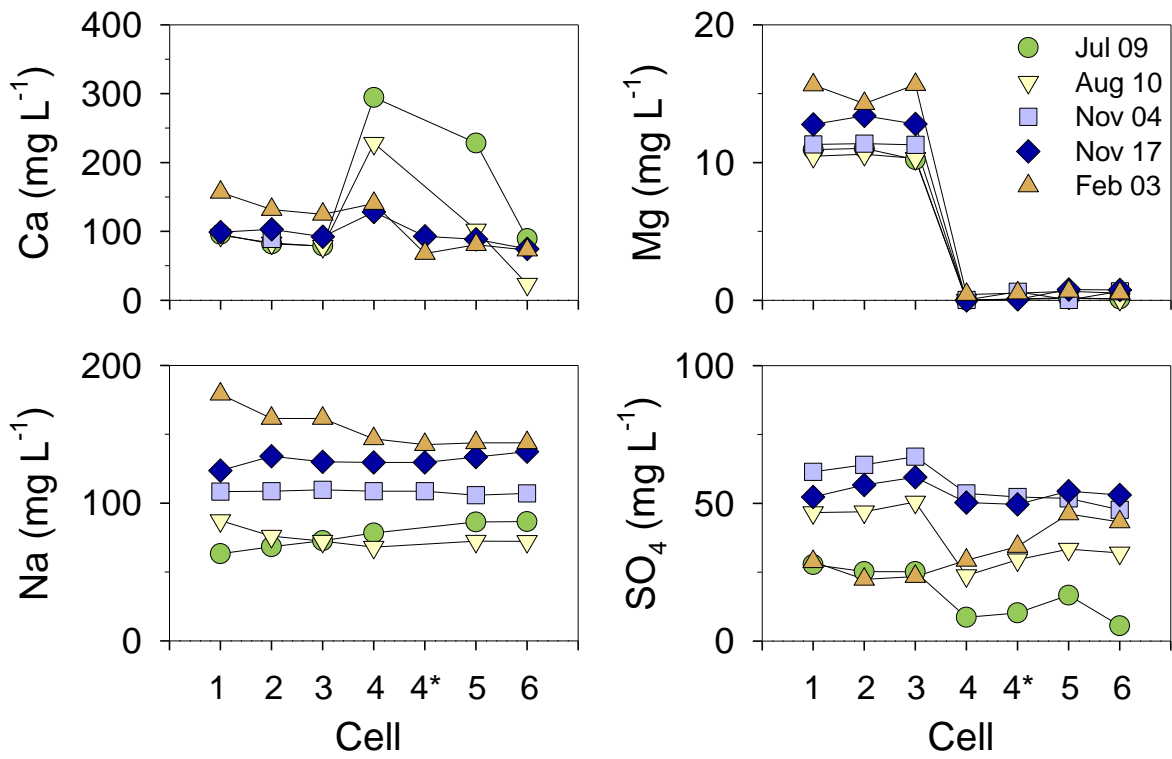


Figure 3.8 Concentrations of Ca, Na, Mg and SO₄ versus distance (Cells 1-5) along the treatment flow path. The 4 and 4* represent BOFS cell and pH adjustment cell.

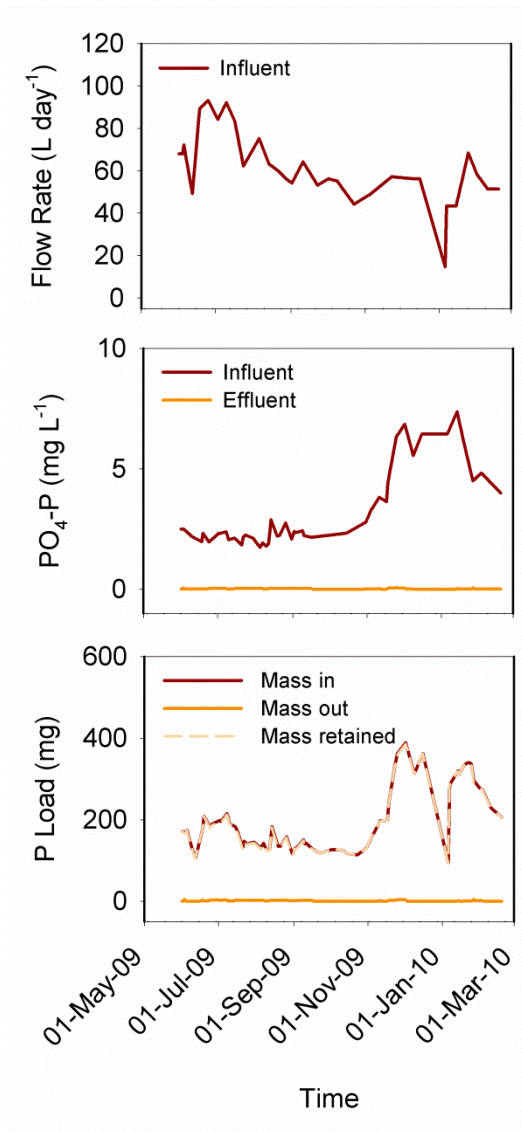


Figure 3.9 Flow rate, PO₄-P concentrations in the influent and effluent, and P load in the treatment system.

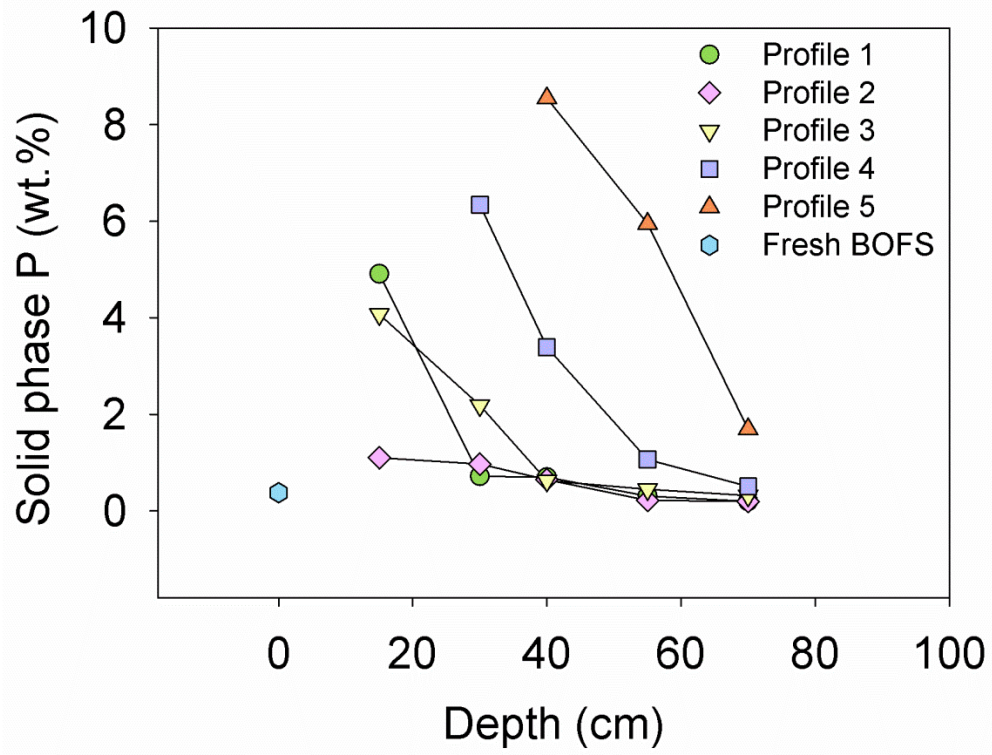


Figure 3.10 Solid phase P versus depth from the surface of Cell 4. Phosphorus content in fresh BOFS is plotted at a depth of 0 cm.

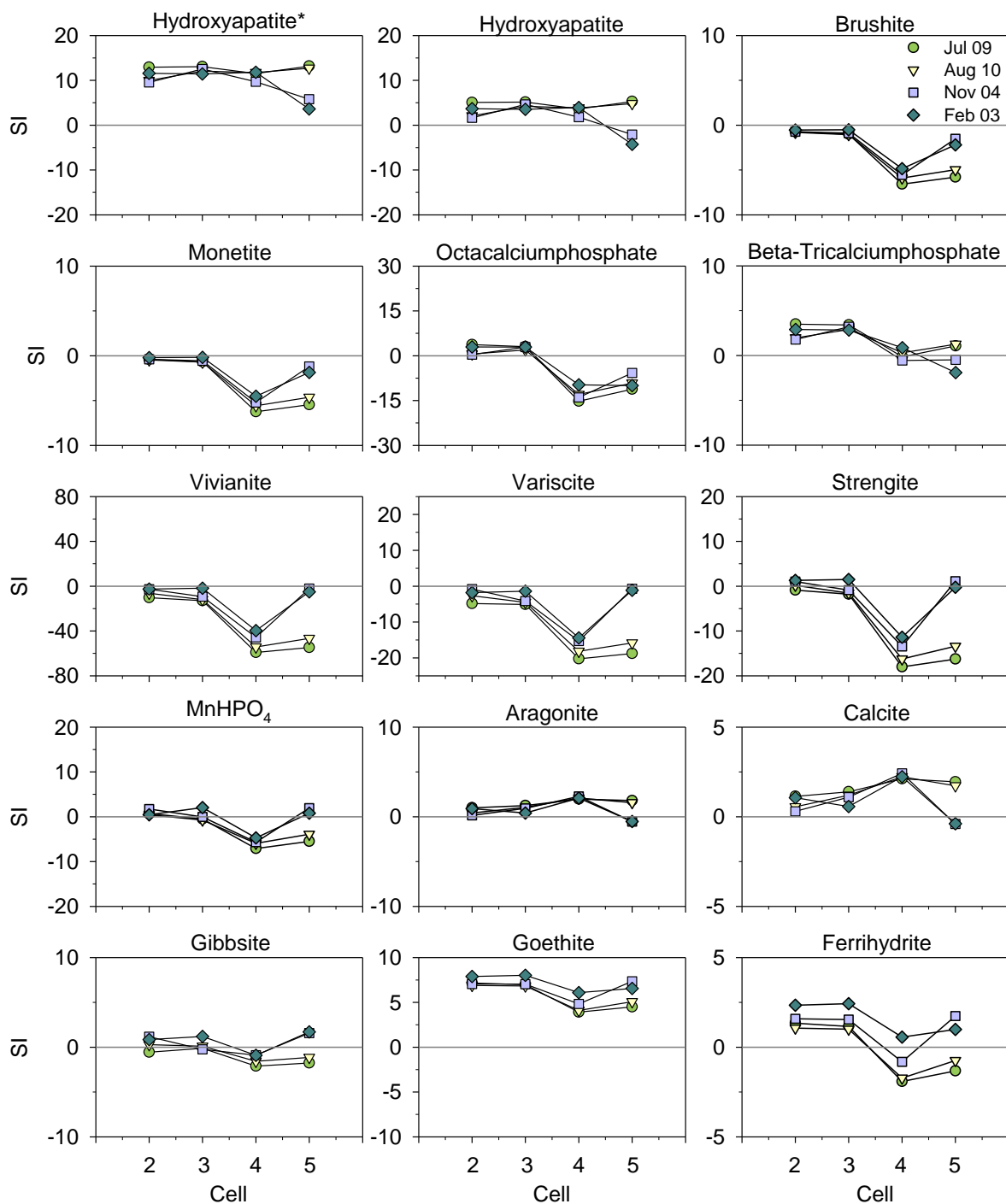


Figure 3.11 Saturation indices for calcium phosphate and other related phases calculated using PHREEQCI versus distance (Cells 2-5) along the reaction flow path. Saturation indices of HAP were plotted twice using an inferred K_{sp} value from Baker et al. (1998) (indicated by * in the plot) and a K_{sp} value for HAP obtained from the WATEQ4F database.

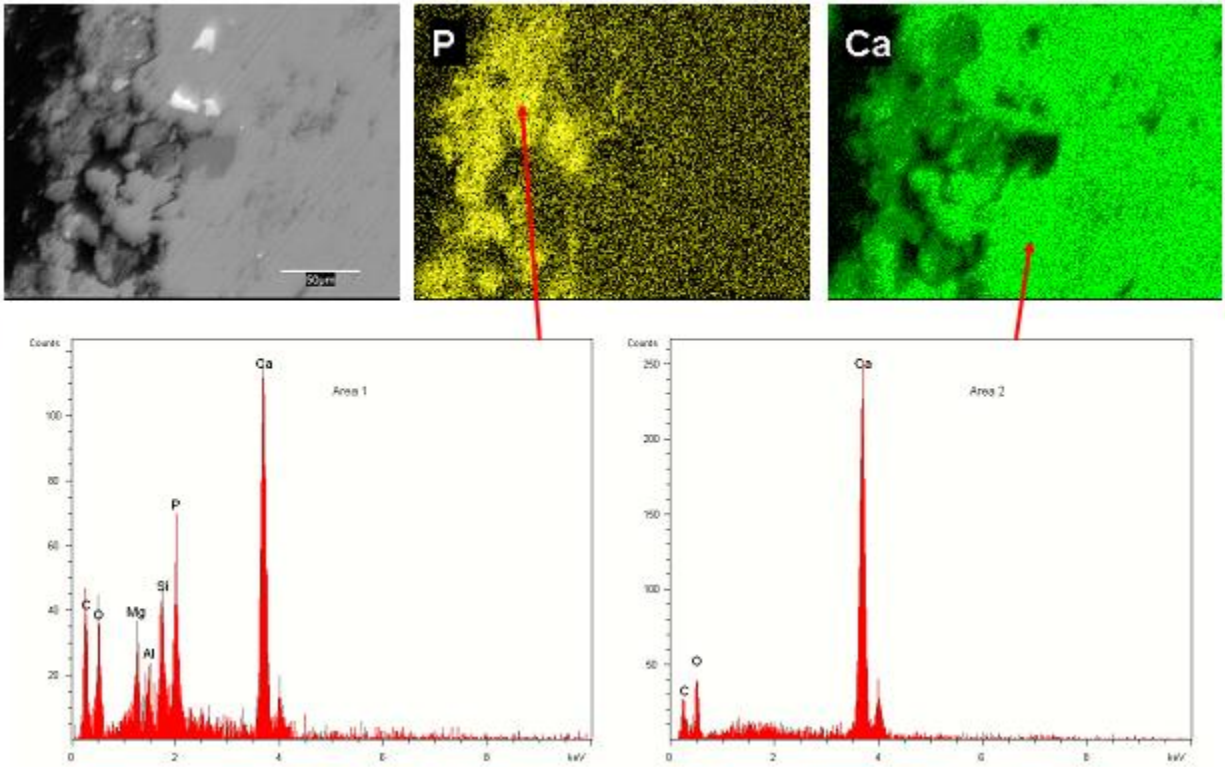


Figure 3.12 High magnification BSE image, X-ray intensity element maps, and EDX spectra for a phosphorus-rich area and an area with no phosphorus accumulation.

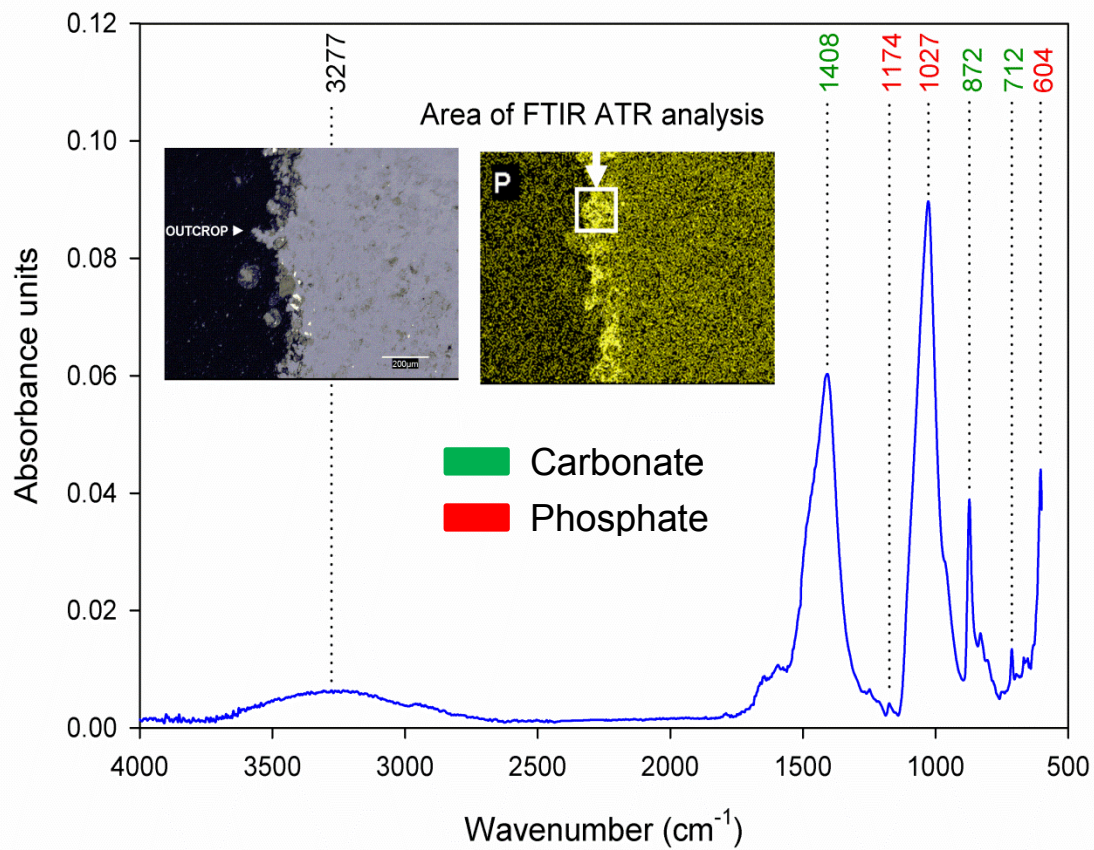


Figure 3.13 FTIR-ATR spectrum from the phosphorus rich zone on particle surface indicated by a white square.

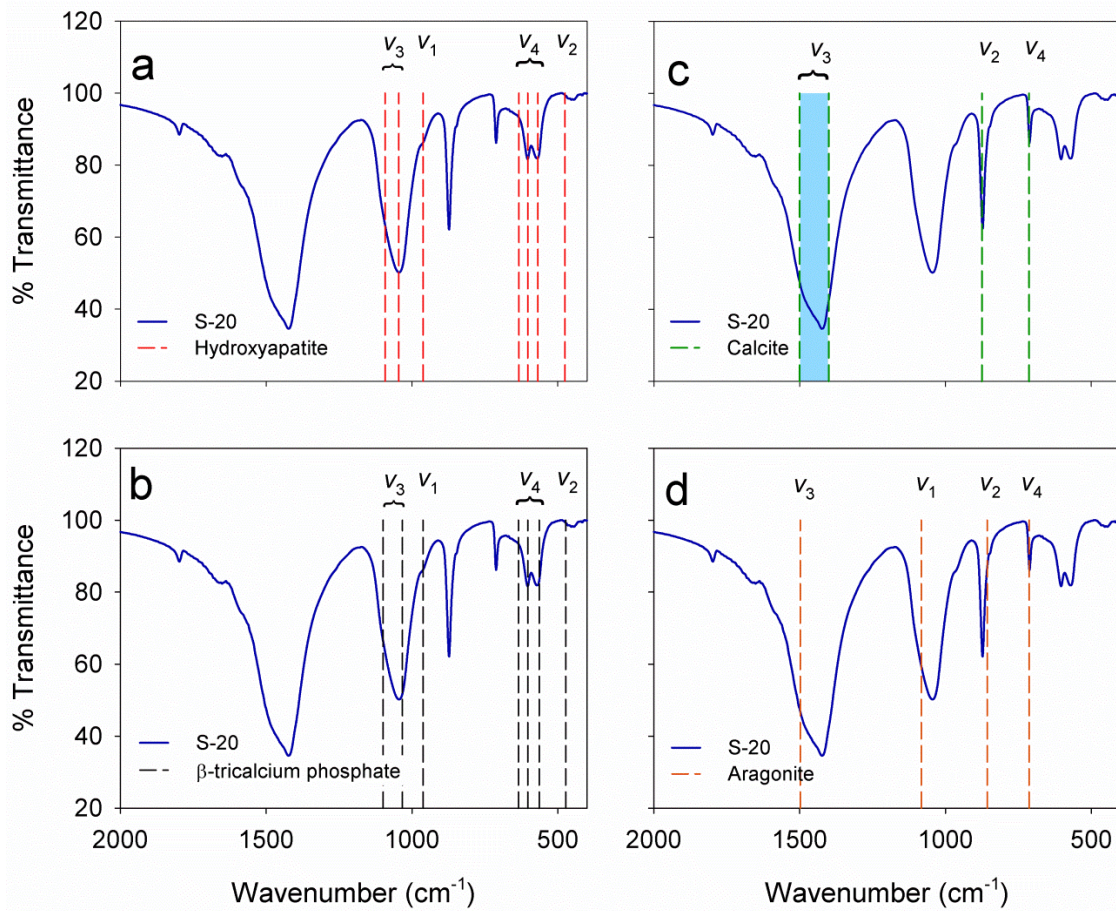


Figure 3.14 FTIR spectrum of sample S-20 (with highest mass) and major phosphate vibrational bands of a) HAP-S, and b) β -TCP; and major carbonate bands of c) calcite, and d) aragonite are compared. Vertical dotted lines in subplots a) and b) represent phosphate vibrational bands while vertical dotted lines in c) and d) represent carbonate vibrational bands.

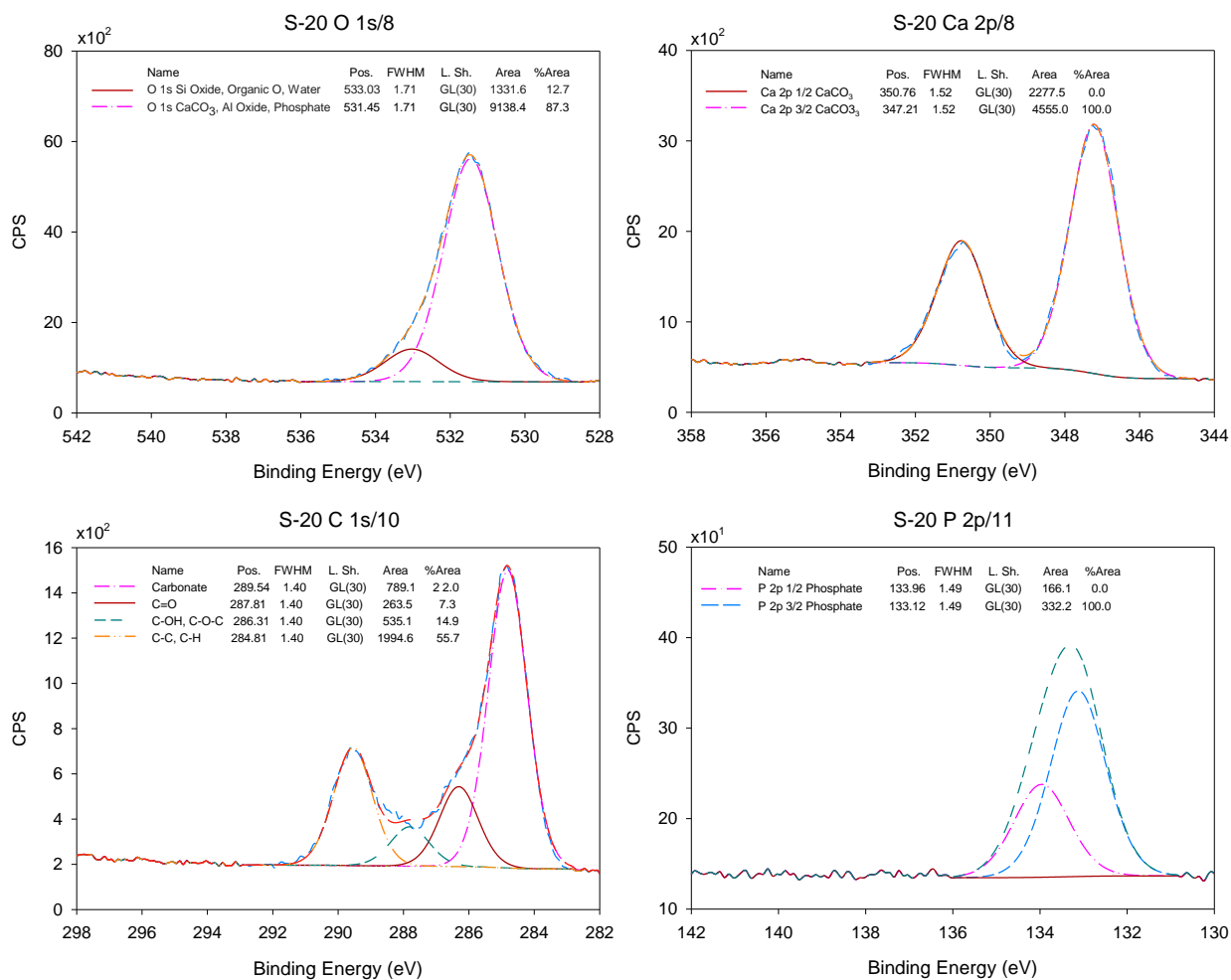


Figure 3.15 High-resolution XPS spectra showing O (1s), Ca (2p), C (1s), and P (2p) peaks.

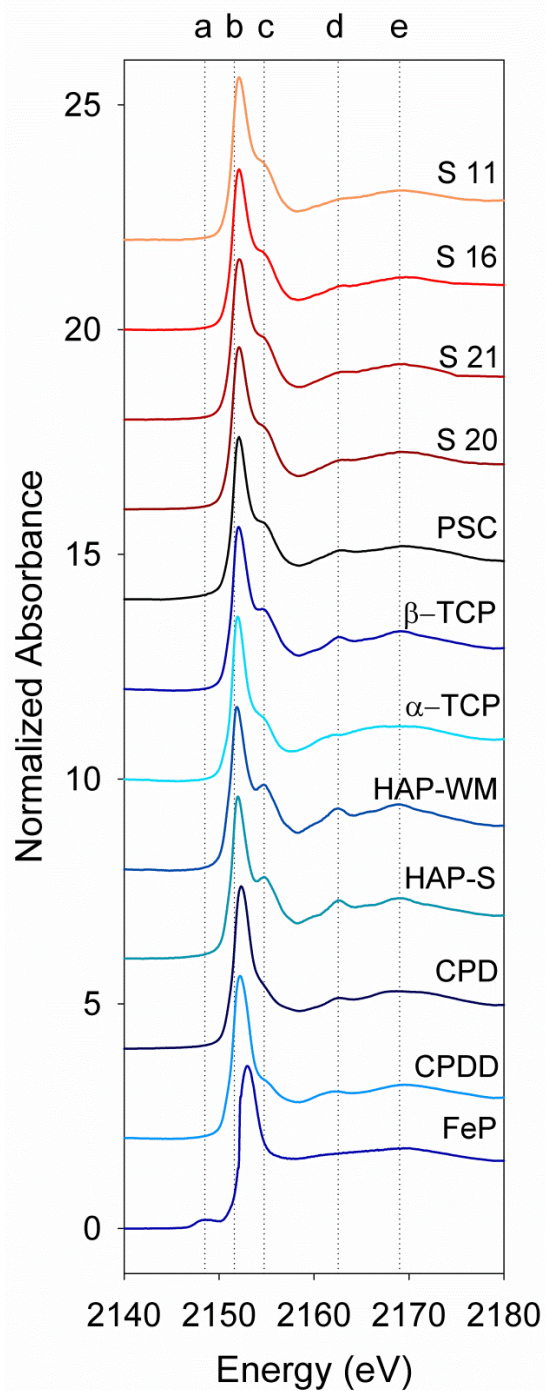


Figure 3.16 XANES spectra for reference materials and sample S 20. Vertical lines represent various spectral features: (a) pre edge feature for FeP, (b) absorption edge (white line) for CaP species, (c) shoulder (sharpness dependent on the degree of crystallinity), (d) spectral feature common in HAP, and (e) oxygen oscillation.

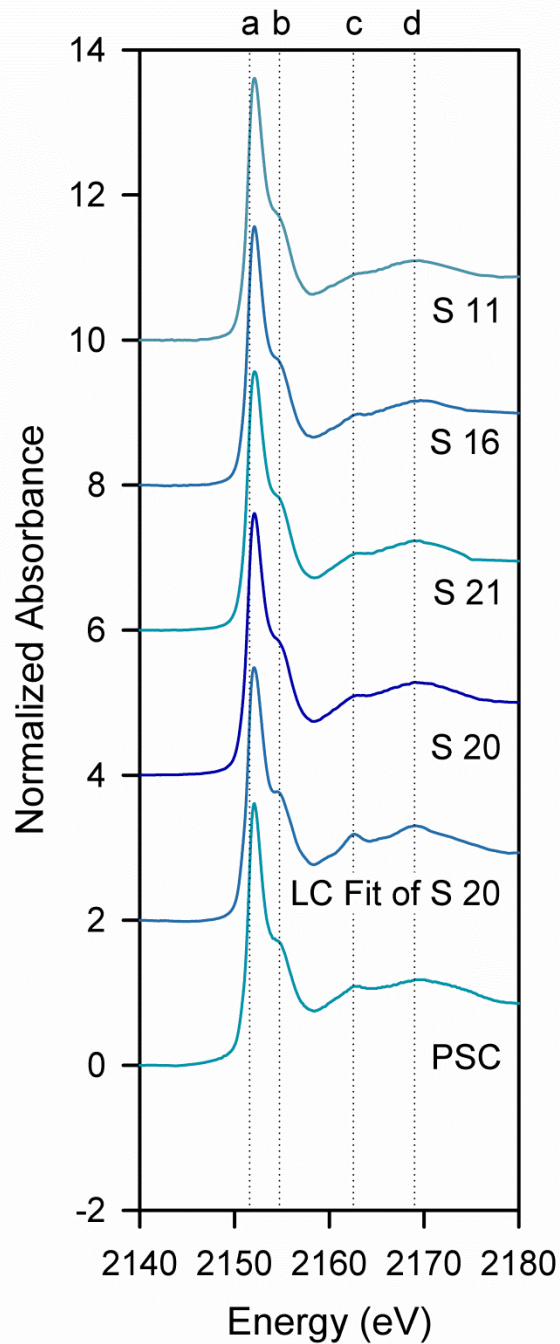


Figure 3.17 XANES spectra for PO₄ sorbed on CaCO₃ (PSC), LC fit for sample S 20 with the combination of β -TCP, HAP-S, and CPD; and samples S 20, S 21, S 16, and S 11. Vertical dotted lines represent (a) absorption edge (white line); (b) shoulder (sharpness dependent on the degree of crystallinity); (c) spectral feature common in HAP; and (d) oxygen oscillation.

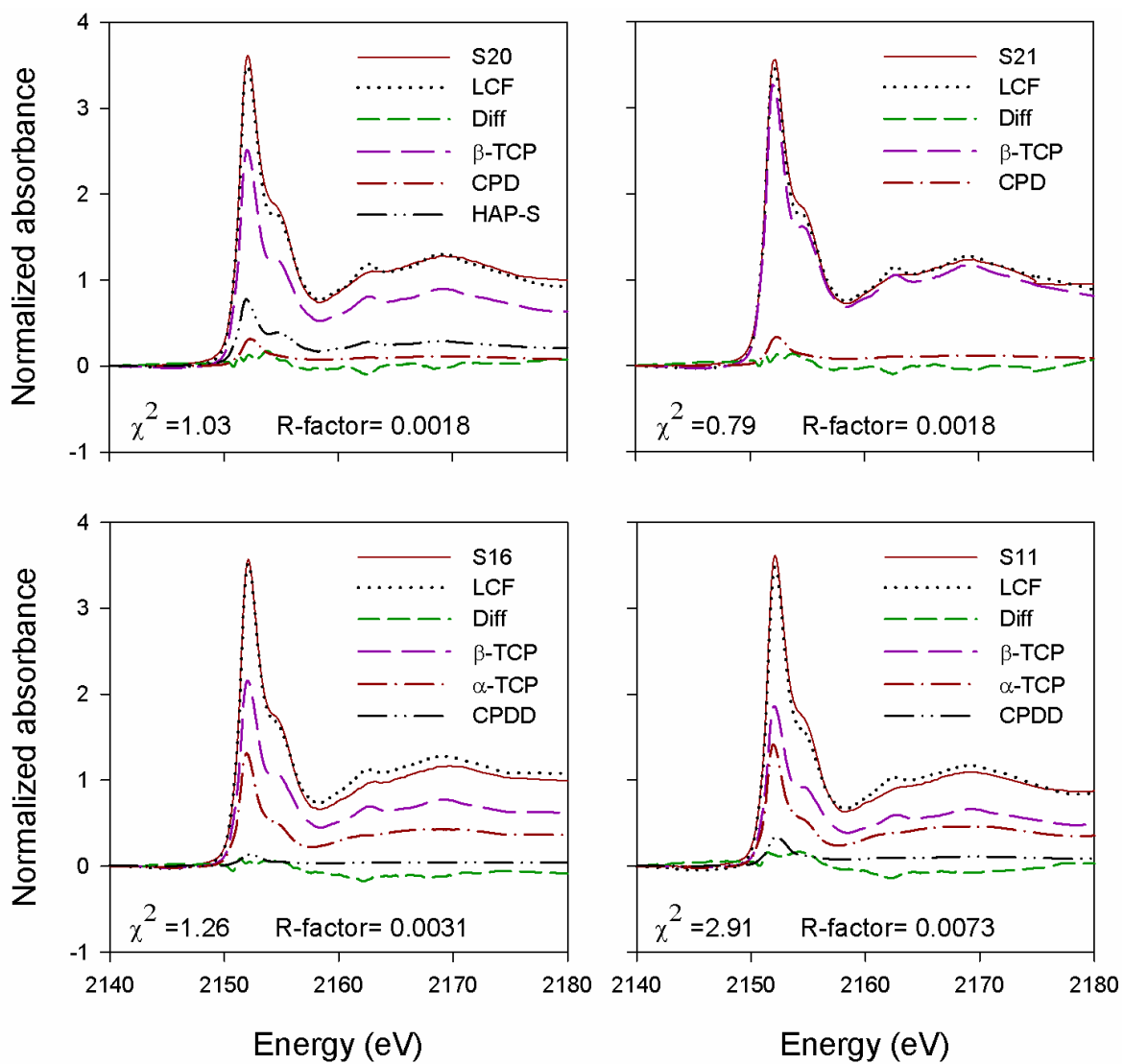


Figure 3.18 Linear combination fit of XANES spectra for spent BOFS samples S 20, S 21, S 16 and S 11.

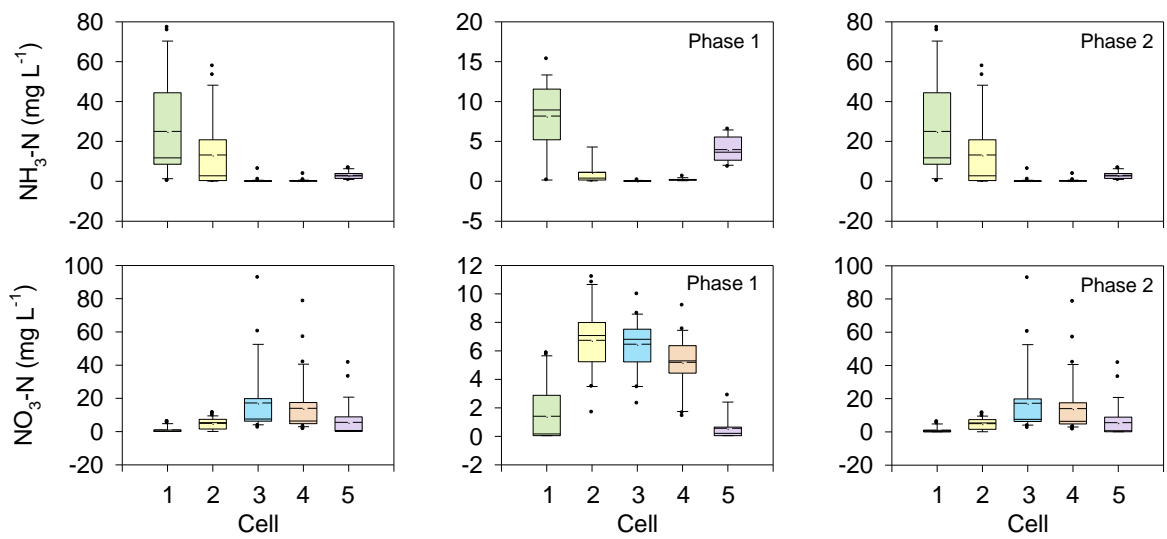


Figure 3.19 Box plots of $\text{NH}_4\text{-N}$ and $\text{NO}_3\text{-N}$ concentrations versus distance (Cells 1-5) along the flow path. Columns 1, 2, and 3 of this figure represent total treatment period, Phase 1, and Phase 2. Horizontal solid lines and broken lines on the boxes represent median and mean concentrations. Top and bottom most dots represent maximum observation above upper fence and minimum observation below lower fence.

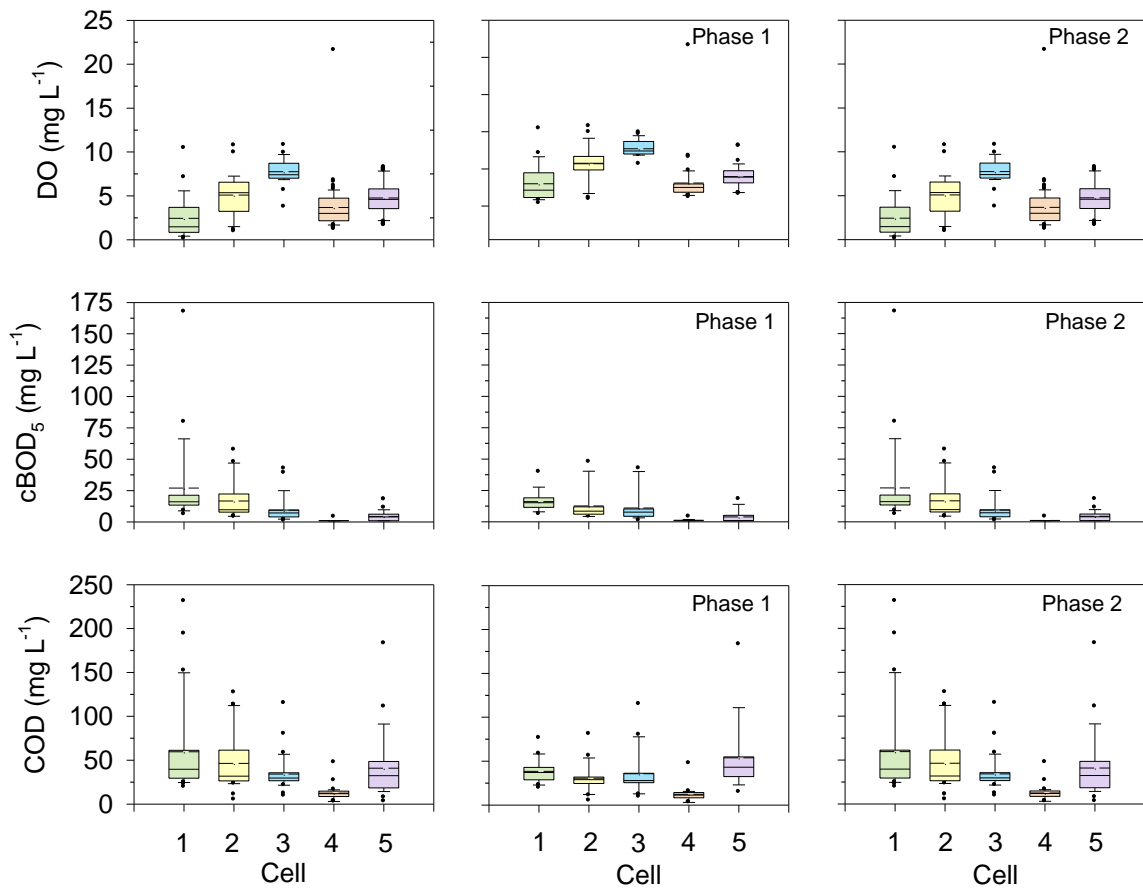


Figure 3.20 Box plots of DO, cBOD₅, and COD concentrations versus distance (Cells 1-5) along the treatment flow path. Columns 1, 2, and 3 of this figure represent total treatment period, Phase 1, and Phase 2, respectively. Horizontal solid lines and broken lines on the boxes represent median and mean concentrations. Top and bottom most dots represent maximum observation above upper fence and minimum observation below lower fence.

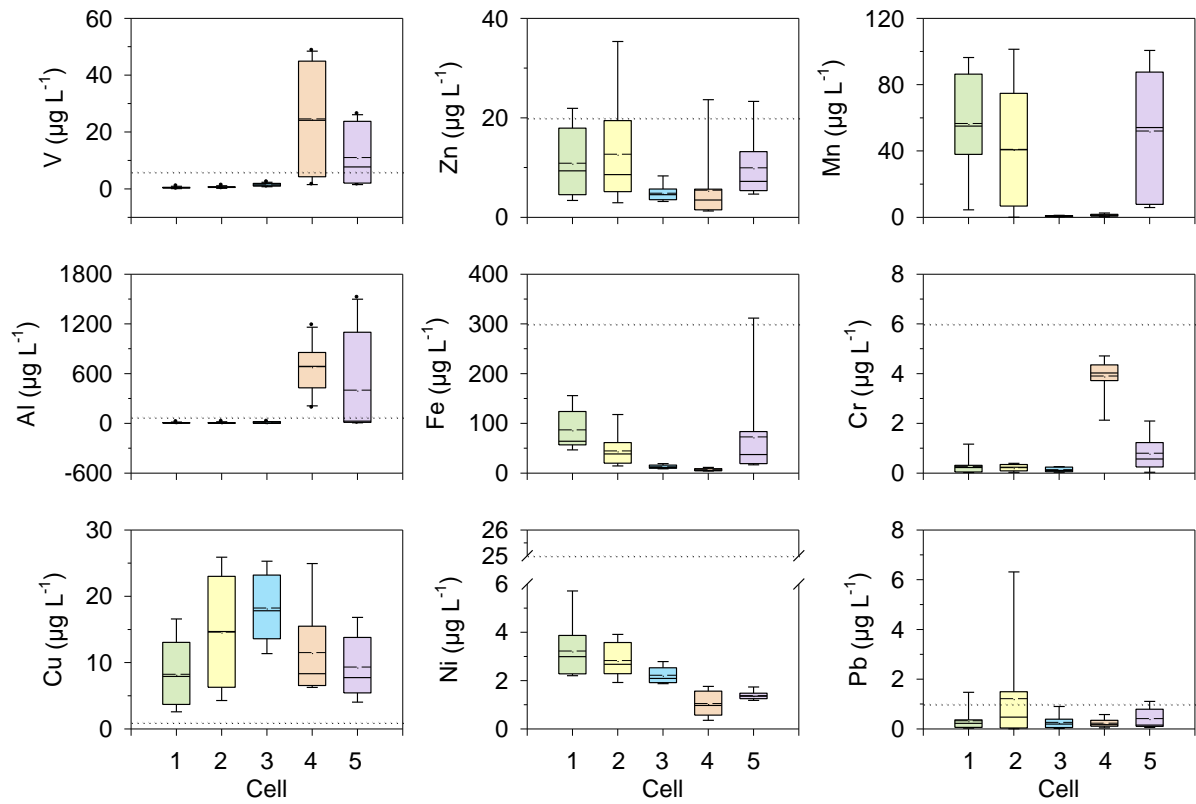


Figure 3.21 Box plots of V, Al, Cu, Zn, Fe, Ni, Mn, Cr, and Pb concentrations versus distance (Cells 1-5) along the treatment flow path. Dotted lines represent the Ontario Provincial Water Quality Objective (PWQO).

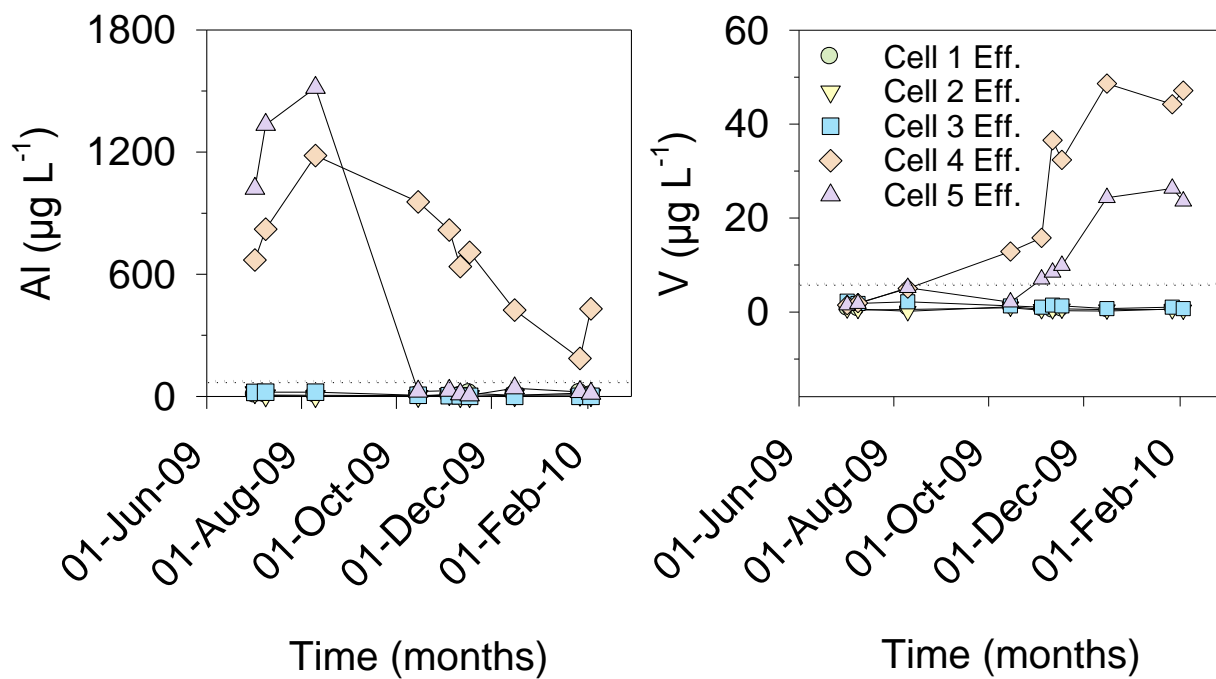


Figure 3.22 Concentrations of V and Al in the treatment cells effluent versus time. Concentrations of Al decreased abruptly in the anaerobic cell effluent as the pH was adjusted to near neutral, reflecting the amphoteric nature of this element.

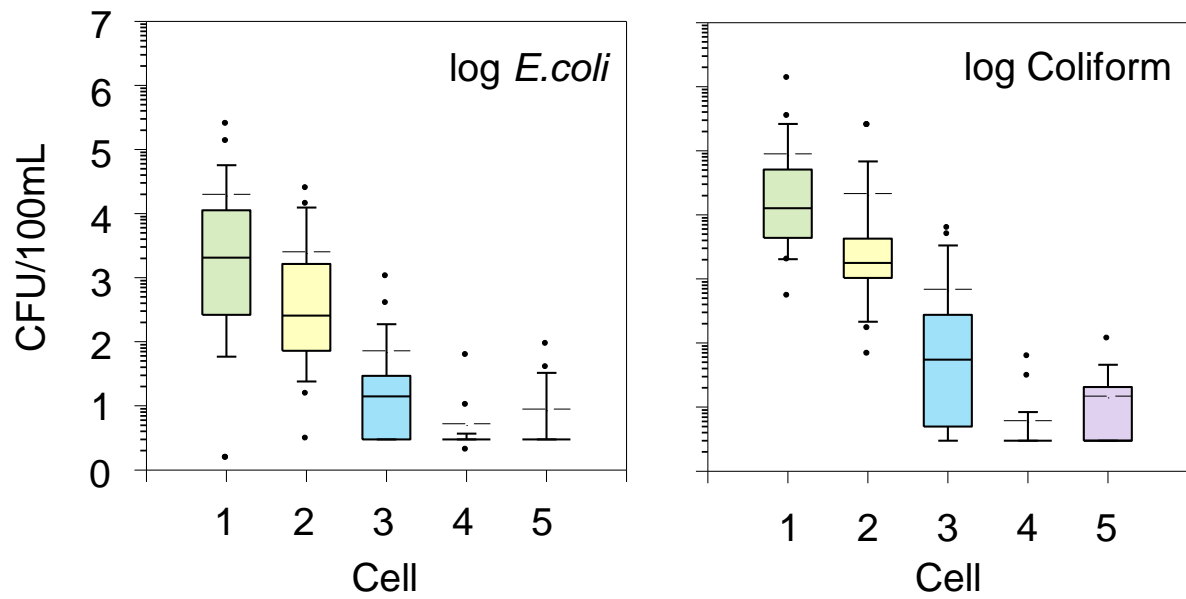


Figure 3.23 Box plots of *E.coli* and total coliform concentrations versus distance (Cells 1-5) along the treatment flow path. Horizontal solid lines and broken lines on the boxes represent median and mean concentrations. Top and bottom most dots represent maximum observation above upper fence and minimum observation below lower fence.

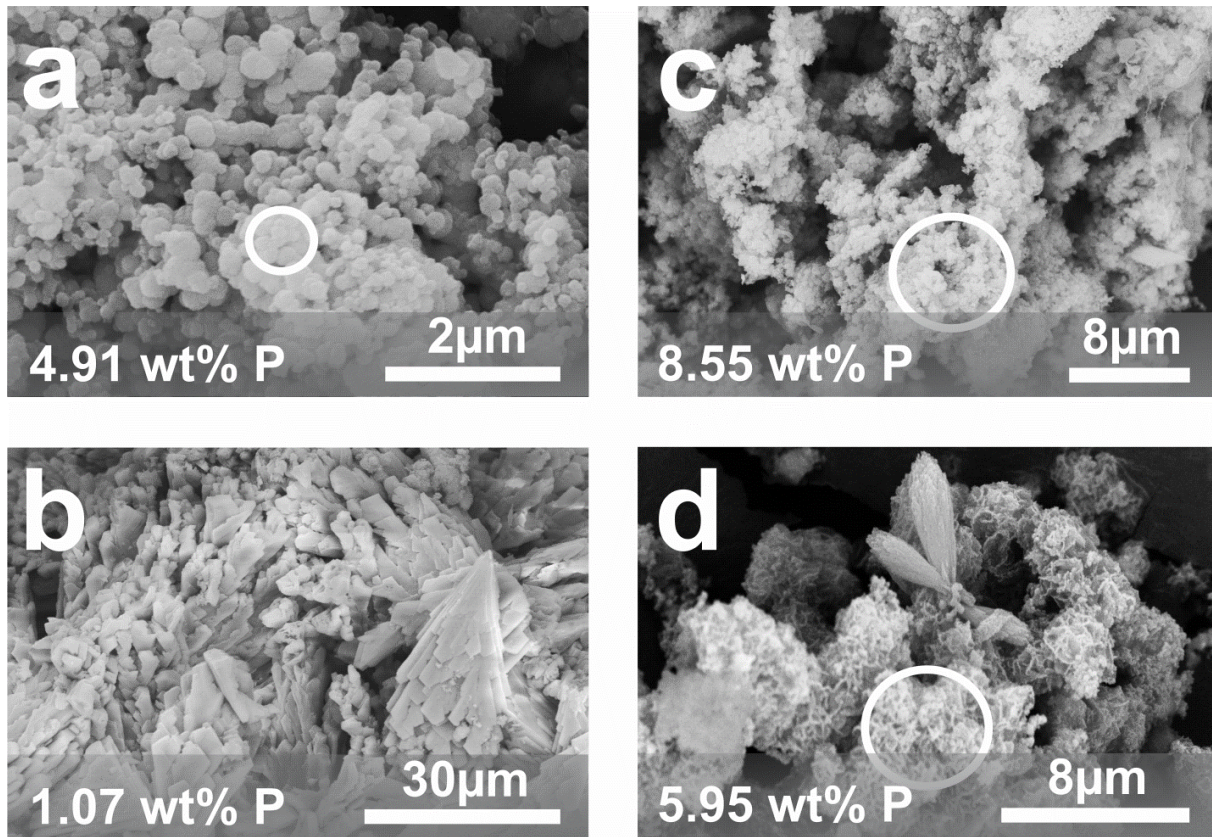


Figure 3.24 SEM images of precipitates that formed on the spent reactive media collected from location 1, 18, 20, and 21 (Figure 3.6) indicated by a, b, c, and d. Unless indicated with circles, the EDX data were obtained from the entire image area. The phosphorus contents obtained from the EDX data are shown on the images. Well-defined crystal faces were observed in “b” (sample S-18). Formation of crystal faces were also noted in “d” (sample S-21).

Table 3.1 Chemical composition of BOFS used in this study analyzed by XRF and analysis from previous studies.

wt. %	CaO	SiO ₂	Al ₂ O ₃	MgO	FeO	Fe ₂ O ₃	Fe total	SO ₃	MnO	TiO ₂	P ₂ O ₅	Free CaO	K ₂ O	Na ₂ O	Cr ₂ O ₃	Cl	Loss on ignition
This study	38.8	11.5	3.40	11.2		24.3			3.81	0.30	-		<0.0	<0.1	-		6.75
A	45.0	10.8	1.90	4.50		32		0.40	2.60	0.50	1.40						1.10
B	39.4	12.0	2.16	9.69	30.2			0.12	2.74	0.40	1.00		0.05	0.25	0.20	0.01	1.80
C	47.7	13.3	3.00	6.40	-	24.4	-	-	2.60	0.70	1.50	9.20					
D	45.4	13.7	6.80	7.30	-	-	17.8	-	-	-	-	-	-	-	-	-	-
E	47.5	11.8	2.00	6.30	-	22.6	-	-	1.90	0.50	2.70	-					
F	39.3	7.80	0.98	8.56	-	38.1	-	-	4.20	0.90	-	-					
G	52.2	10.8	1.30	5.04	17.2	10.1	-	-	2.50	0.60	1.30	10.2					
H	32.1	19.6	3.16	2.53	-	17.9	-	-	2.02	0.46	0.73	-	0.06	0.25	-	-	0.80
I	30.0	8.00	1.00	5.00	10.0			0.05	2.00	0.40	0.20				0.10		
	-	-	-	-	-			-	-	-	-				-		
	55.0	20.0	6.00	15.0	35.0			0.15	8.00	2.00	2.00				0.50		

^aBelhadj et al., 2012; ^bYildirim and Prezzi, 2011; ^cWaligora et al., 2010; ^dXue et al., 2009; ^eMahieux et al., 2009; ^fShen et al., 2009; ^gPoh et al., 2006; ^hCha et al., 2006; ⁱShi, 2004.

Table 3.2 Physical properties and mineralogical composition of the BOFS material used in the experiments

Slag type: BOFS		
BOFS source: Stelco, Hamilton		
Physical properties	Particle size (mm)	Surface area (m²g⁻¹)
	4-2	7.14
	2-1	9.35
	1-0.5	14.65
	<0.5	15.31
	Particle size (mm)	Mass weighted surface area (m²g⁻¹)
	4-2	515.04
	2-1	124.1
1-0.5	88.58	
<0.5	130.83	
	Density (g cm ⁻³)	3.49
Mineralogical composition of BOFS	This study	Yildirim and Prezzi (2011)
	Wuestite (FeO) Lime (CaO) Larnite (Ca(SiO ₄)) Srebrodolskite (Ca ₂ Fe ₂ O ₅) Anhydrite (CaSO ₄) and Probable Portlandite (Ca(OH) ₂)	Portlandite (Ca(OH) ₂) Srebrodolskite (Ca ₂ Fe ₂ O ₅) Merwinite (Ca ₃ Mg(SiO ₄) ₂) Larnite (Ca ₂ SiO ₄) Calcite (manganoan) ((Ca, Mn)CO ₃) Lime (CaO) Dolomite (CaMg(CO ₃) ₂) Probable Wollastonite (CaSiO ₃) Periclase (MgO) Pentahydrate (MgSO ₄ ·5H ₂ O) Monticellite (CaMgSiO ₄) Hematite (Fe ₂ O ₃) Magnesite (MgCO ₃)

Table 3.3 Semiquantitative EDX measurements showing the composition of the selected samples

ID	Elements (wt. %)					
	C	O	Mg	Si	P	Ca
S1	51.6	30.91	0.5	0.65	4.91	10.63
S2	12.13	38.23	1.32	13.51	0.72	23.55
S3	19.77	22.64	0.49	1.13	0.7	52.42
S4	18.09	45.73	1.07	1.31	0.31	31.72
S5	12.4	35.07	4.22	8.69	0.2	21.96
S6	25.05	36.48	11.59	8.03	1.1	4.24
S7	22.4	40.37	1.73	1.23	0.97	31.15
S8	18.1	38.79	7.49	7.21	0.65	20.37
S9	7.93	33.86	11.32	8.83	0.22	18.89
S10	15.14	34.01	2.3	1.81	0.2	21.24
S11	52.19	30.8	0.73	0.47	4.07	11.73
S12	20.9	36.07	8.03	4.73	2.19	16.44
S13	26.97	39.57	3.75	3.31	0.63	16
S14	19.11	34.92	1.07	0.77	0.45	38.51
S15	19.34	32.37	1.13	5.86	0.32	26.7
S16	44.93	27.52	1.21	1.45	6.34	18.54
S17	18.93	37.78	0.95	1.1	3.39	29.16
S18	20.38	48.18	0.43	0.38	1.07	29.56
S19	7.64	26.22	0.73	7.59	0.51	45.92
S20	30.99	40.07	0.76	0.81	8.55	18.7
S21	25.63	27.1	4.74	2	5.95	18.71
S22	29.67	37.31	4.62	2.73	1.7	19.96
Mineral phase	C	O	Mg	Si	P	Ca
Calcite, CaCO ₃	12	47.96				40.04
Aragonite, CaCO ₃	12	47.96				40.04
Hydroxyapatite,	-	41.41			18.5	39.89
Carbonate Hydroxyapatite,	1.24	41.25			15.97	41.33
References: http://webmineral.com/						

Table 3.4 Vibrational bands of phosphate in the reference materials.

Reference materials	Phosphate vibrational bands			
	ν_3	ν_1	ν_4	ν_2
HAP-S	1092	962	568	475
	1045		603	
			633	
HAP-WM	1090	962	571	474
	1042		602	
			633	
β -TCP	1098	962	564	471
	1033		603	
			634	

Table 3.5 Ca/P and O/Ca ratios of the samples analyzed.

	S-20	S-21	S-16	S-11	S-1 powder
Ca/P	4.34	3.02	3.68	3.61	3.24
O/Ca	3.59	3.13	3.58	4.01	4.38

Table 3.6 Linear combination fitting results of spent BOFS samples.

Sample ID	Combination	R-factor	χ^2	β -TCP (weight)	HAP-S (weight)	CPD (weight)
S 20 norm(E)	β -TCP, HAP-S, CPD	1.79E-03	1.03	0.697	0.215	0.087
	β -TCP, HAP-S	1.89E-03	1.09	0.772	0.228	0
	β -TCP, CPD	1.94E-03	1.12	0.911	0	0.089
	HAP-S, CPD	3.02E-03	1.74	0	0.753	0.247
Sample ID	Combination	R-factor	χ^2	β -TCP (weight)	CPD (weight)	HAP-S (weight)
S 21 norm(E)	β -TCP, CPD, HAP-S	1.82E-03	0.79	0.908	0.098	0
	β -TCP, CPD	1.86E-03	0.80	0.908	0.092	0
	β -TCP, HAP-S	2.15E-03	0.93	1	0	0
	CPD, HAP-S	5.54E-03	2.39	0	0.356	0.644
Sample ID	Combination	R-factor	χ^2	β -TCP (weight)	α -TCP (weight)	CPDD (weight)
S 16 norm(E)	β -TCP, α -TCP, CPDD	3.13E-03	1.26	0.599	0.363	0.038
	β -TCP, α -TCP	3.36E-03	1.36	0.625	0.375	0
	β -TCP, CPDD	4.60E-03	1.85	0.719	0	0.281
	α -TCP, CPDD	7.74E-03	3.11	0	0.581	0.419
Sample ID	Combination	R-factor	χ^2	β -TCP (weight)	α -TCP (weight)	CPDD (weight)
S 11 norm(E)	β -TCP, α -TCP, CPDD	7.27E-03	2.91	0.515	0.392	0.093
	β -TCP, α -TCP	7.40E-03	2.96	0.566	0.434	0
	β -TCP, CPDD	8.85E-03	3.54	0.62	0	0.38
	α -TCP, CPDD	1.06E-02	4.22	0	0.557	0.443

Table 3.7 Values of pH, alkalinity and concentration ranges of other target parameters including PO₄-P, NH₃-N, NO₃-N, Al, V in the effluents of Cell 1, 2, 3, 4, 4*, and 5.

		Unit	Cell 1	Cell 2	Cell 3	Cell 4	Cell 4*	Cell 5	Cell 6	
pH	Total treat. period		6.91-7.97	7.42-8.54	7.58-8.66	10.96-12.36	5.20-10.68			
	Before CO2 addition						-	10.22-12.17		
	After CO2 addition						5.20-10.68	6.80-7.92		
Alk	Total treat. period	mg L ⁻¹	214-688	212-626	168-270	200-1560	42-338	122-952		
	Phase 1		214-352	212-284	175-271	340-1560				
	Phase 2		432-688	397-625	168-226	200-286				
	Before CO2 addition							146-952		
	After CO2 addition						42-338	122-472		
PO ₄ -P	Total treat. period	mg L ⁻¹	2.68-11.2	2.23-9.27	1.74-7.38	0.005— 0.081	0.007-0.093	0.02-2.46	0.007-1.74	
	Phase 1		2.68-10.6	2.23-6.39	1.74-3.26	0.005-0.065	0.005-0.013	0.01-2.47	0.007-1.74	
	Phase 2		3.26-11.2	5.30-9.27	3.82-7.37	0.005-0.08	0.003-0.09	0.02-1.08	0.08-0.98	
NH ₃ -N	Phase 1	Conc. range	mg L ⁻¹	0.10-15.3	0.05-4.3	0.02-0.13	0.07-0.60	0.10-0.40	1.80-6.50	0.10-6.30
		Mean Conc.		8.18	1.13	0.04	0.21	0.25	3.97	2.01
		Removal efficiency*		%	-	86	100	97	97	51
	Phase 2	Conc. range	mg L ⁻¹	24.9-77.0	10.8-57.6	0.03-6.10	0.06-3.60	0.02-5.60	0.60-3.70	0.26-2.80
		Mean Concentration		52.01	32.61	0.83	0.53	0.97	1.54	0.65
		Removal efficiency*		%	-	37	98	99	98	97
NO ₃ -N	Phase 1	Conc. range	mg L ⁻¹	0.05-5.84	1.66-11.2	2.99-9.97	1.40-9.17	3.28-3.47	0.05-2.86	0.05-3.70
		Mean Conc.		1.41	6.74	6.47	5.2	3.37	0.57	0.67
		Removal efficiency*		%		-378	-359	-269	-139	60
	Phase 2	Conc. range	mg L ⁻¹	0.05-0.73	0.05-5.57	11.4-92.5	7.79-78.3	4.76-51.6	0.84-41.3	1.02-38.1
		Mean Conc.		0.16	1.5	41.3	31.6	21.6	14.6	13.6
		Removal efficiency*		%		-839	-25753	-19691	-13446	-9019
	Al	µg L ⁻¹	0.28-15.3	0.08-20.0	0.08-21.3	186-1183	5.98-1516			
	V	µg L ⁻¹	0.06-0.91	0.47-1.14	0.72-2.31	1.46-48.6	1.47-26.37			

* calculated with respect to Cell 1 effluent

Table 3.8 Concentration ranges of DO, cBOD₅, COD, *E. coli*, and total coliform in the effluents of Cell 1, 2, 3, 4, 4*, and 5.

		Unit	Cell 1	Cell 2	Cell 3	Cell 4	Cell 4*	Cell 5	Cell 6	
DO	Total treat. period	mg L ⁻¹	0.12-10	1.0-11	3.7-11	1.2-22	7.2-15	1.6-8.3	1.0-16	
	Phase 1		0.40-10	1.0-11	5.7-9.9	1.2-21	7.2-14	1.6-8.1	1.0-16	
	Phase 2		0.12-1.8	1.5-5.7	3.7-11	3.0-6.2	7.7-15	3.5-8.3	7.8-11	
cBOD ₅	Phase 1	Conc. range	6.0-40	4.0-48	0.50-42	0.50-0.50	0.50-0.50	0.50-18	0.16-30	
		Mean Conc.	16	13	11	0.5	0.5	3.4	5.7	
		Removal efficiency*	%	-	22	32	97	97	79	65
	Phase 2	Conc. range	mg L ⁻¹	13-168	9.7-58	1.7-9.9	0.50-0.50	0.50-6.3	0.50-6.7	3.9-12
		Mean Concentration	49	25	6.1	0.5	1.2	5.0	6.1	
		Removal efficiency*	%	-	49	87	99	97	90	88
COD	Phase 1	Conc. range	mg L ⁻¹	20-76	5.1-81	9.3-115	3.7-48	9.6-15	15-183	21-157
		Mean Conc.	38	31	36	13	13	54	51	
		Removal efficiency*	%	-	20	7	67	67	-40	-32
	Phase 2	Conc. range	mg L ⁻¹	25-231	37-127	21-44	5.0-27	5.3-27	5.0-31	12-32
		Mean Conc.	102	78	31	13	14	17	20	
		Removal efficiency*	%	-	24	70	87	86	84	81
<i>E. coli</i>		CFU 100	2.2x10 ⁴	1.1x10 ⁴	7.5x10 ¹	5.3x10 ⁰	3.0x10 ⁰	9.1x10 ⁰	5.1x10 ⁰	
Total Coliform		mL ⁻¹	8.9x10 ⁴	2.2x10 ⁴	6.9x10 ²	6.1x10 ⁰	3.0x10 ⁰	1.4x10 ¹	7.7x10 ²	

* calculated with respect to Cell 1 effluent

Chapter 4

Advanced Phosphorus Removal in a Demonstration-scale Engineered Wetland Wastewater Treatment System

4.1 Executive Summary

Integration of a phosphorus removal component in an engineered wetland (EW) wastewater treatment system provided enhanced treatment efficiencies of phosphorus, ammonia, cBOD₅, COD, *E. coli*, total coliform, and trace metals from septic system effluent. The phosphate removal component utilized basic oxygen furnace slag (BOFS) as a treatment medium. The effluent from a conventional septic system circulated through the treatment cells with an average flow rate of 1.1 m³ day⁻¹, which was approximately 25% of the capacity of the treatment system (4-5 m³ day⁻¹). The average influent concentrations of P, ammonia, cBOD₅, and COD were 7, 48, 63, and 143 mg L⁻¹, respectively. Removal efficiencies for P, ammonia, cBOD₅, and COD in the treatment system were > 99, >82, >98, and >76%, respectively. Removal efficiencies for *E. coli* and total coliform in the treatment system were >99%. The effluent of the phosphate treatment cell was elevated (pH, 10.88±1.47), and was neutralized by sparging with CO_{2(g)} prior to discharge to the local sewage system. A thin layer of ZVI imbedded at the bottom part of the BOFS cell was utilized to maintain low concentrations of dissolved metals and metalloids, including V, leached from basic oxygen furnace slag (BOFS). The pH neutralization process enhanced removal of Al. Fourier Transform Infrared (FTIR) spectra indicated the presence of calcium carbonate and calcium phosphate minerals on the spent BOFS. X-ray absorption near

edge structure (XANES) spectra also indicated the accumulation of calcium phosphate species on the spent BOFS. The results show the benefits of integrating complementary treatment technologies for the removal of nutrients and other constituents from domestic wastewater.

4.2 Introduction

Domestic and municipal wastewater often contains elevated concentrations of dissolved nutrients, including phosphorus (P) and nitrogen (N) species. Although N species may be removed in wastewater treatment systems, elevated concentrations of P are commonly discharged from wastewater treatment facilities and introduced to proximal water bodies, which may lead to eutrophication (U. S. EPA, 2007; Vymazal, 1997). Subsurface horizontal and vertical flow constructed wetland systems are effective for the removal of a wide range of wastewater pollutants (Vymazal, 2007; Vymazal, 2011). Although initial removal of ~46% P from wastewater was observed by Vymazal (2004) subsequent declines in P removal indicate that constructed wetlands are not suitable for treating P for extended periods (Kadlec and Knight, 1996; Knight et al., 2000; Vymazal, 2004). In recent years, research has explored compound specific treatment strategies and suitable P treatment media for engineered wetlands (EWs) (Vymazal et al., 2011).

Several studies concentrated on identifying potential substrates that can be used in EWs to improve the P removal efficiency (Johansson, 1999; Drizo et al., 1999; Drizo et al., 2002; Jenssen and Krogstad, 2003). Materials selected as substrates in EWs are based on high P sorption capacities and on the potential to precipitate phosphate-bearing phases. Potential substrate materials include industrial byproducts such as electric arc furnace (EAF) slag (Drizo et

al., 2002; Drizo et al., 2006), shale (Drizo et al., 1999), lightweight aggregates (Jenssen and Krogstad, 2003), and blast furnace steel slags (Vohla et al., 2011).

Basic oxygen furnace slag (BOFS), a waste by-product generated during steelmaking processes (Mikhail et al., 1994; Shi, 2004; Bowden et al., 2009), has been used as a reactive material for phosphate removal (Baker et al., 1998). The chemical composition of BOFS differs depending on the raw materials used at various steel production sites. Basic oxygen furnace slag is comprised of four dominant phases (>10 wt%) including Ca_2SiO_4 , Ca_3SiO_5 , FeO , and $(\text{Ca},\text{Mg},\text{Mn},\text{Zn})\text{Fe}_2\text{O}_4$; with major phases (5-10 wt%) including $\text{Ca}(\text{OH})_2$, $\text{Ca}_2\text{Fe}_2\text{O}_4$, and MgFe_2O_4 ; and minor phases (<5 wt%) including SiO_2 , $3\text{Al}_2\text{O}_3\text{SiO}_2$, $\text{CaO}\cdot\text{Al}_2\text{O}_3\cdot 2\text{SiO}_2$, MgO , CaO , $2\text{CaO}\cdot\text{Al}_2\text{O}_3\cdot\text{SiO}_2$, CaFeO_2 , $(\text{Mg},\text{Mn})\text{Fe}_2\text{O}_4$, MnFeO , and Fe (Mikhail et al., 1994). The major constituents (~70-80 wt. %) of BOFS are CaO , Fe_2O_3 , and SiO_2 ; and the minor constituents (20-30 wt. %) of the material are MgO , MnO , Al_2O_3 , P_2O_5 , TiO_2 , K_2O , Na_2O , and Cr_2O_3 (Cha et al., 2006; Kim et al., 2006; Bowden et al., 2009; Xue et al., 2009; Navarro et al., 2010; Stimson et al., 2010). Analysis of 17 BOFS samples indicate a mean composition of Ca (28.01%), Fe (18.43%), Si (5.97%), Mg (5.53%), Mn (3.29%), and Al (2.38%); with significant minor constituents of P (0.32%), C (0.26%), Cr-total (0.13%), S (0.11%), and V (0.10%) (Proctor et al., 2000). Blowes et al. (1996) identified BOFS as a low cost reactive material that has potential to remove phosphorus, arsenic and waterborne pathogens, from groundwater and wastewater. The treatment efficiencies of arsenic, phosphate and pathogen indicators (e.g., *E. coli*) are often over 99% in BOFS based on laboratory and field applications treating wastewater (Baker et al., 1997, 1998; McRae et al., 1999; Blowes et al., 2000; Smyth et al., 2002b, Stimson et al., 2010).

Based on a laboratory experiment, Baker et al. (1998) suggests hydraulic retention times of at least 24 hours in BOFS media may be required to ensure maximum phosphorus removal efficiency. Exceedingly alkaline effluent and the potential for metal leaching from BOFS are concerns that need to be considered when implementing a BOFS treatment system.

This paper describes the integration of a BOFS-based phosphate treatment system with a EW System in a demonstration-scale outdoor facility with a capacity of 4-5 m³ per day. The study investigated the removal of nutrients (PO₄ and NH₃), cBOD₅, COD, and pathogens (E.coli and Total coliform) in the treatment cells, and examined the release of V (potentially derived from BOFS) and subsequent removal using a zero valent iron (ZVI) layer. The pH of the effluent was neutralized by sparging CO₂ in a large volume of high pH effluent from the BOFS component of the treatment system. The hydraulic performance of the treatment system was monitored throughout the period of operation. The occurrence of calcium carbonate and calcium phosphate (CaP) minerals on the outer layer of the spent BOFS as well as the possible CaP speciation were also investigated through FTIR and XANES.

4.3 Materials and Methods

4.3.1 System configuration

The demonstration scale Engineered Wetland (EW)-phosphate treatment system was installed during the fall 2009 at the outdoor experimental facility at the Center for Alternative Wastewater Treatment, Fleming College, Lindsay, Ontario. Regular flow and monitoring of the system commenced in late January 2010. The feed wastewater for the system is derived from the

effluent from a pre-treatment septic tank (Cell 1). The septic tank effluent passed through a series of treatment components including a vegetated horizontal subsurface flow cell (Cell 2), a vegetated vertical subsurface flow aerated engineered wetland cell (Cell 3), a BOFS phosphate treatment cell (Cell 4), and a pH adjustment cell (Cell 5) before release into the City of Kawartha Lakes sewer system (Figure 4.1). The volume of Cell 2 was 24 m³ (dimensions: 6 m × 4 m × 1 m). Cell 2 was filled with a 0.81 m thick gravel layer which contained the inlet and outlet piping network, where inlet and out flow pipes were surrounded by coarse gravel. The gravel used in Cell 2 contained a small amount of organic carbon derived from the wetland plants and may contain biomass from previous loading (because this cell was previously used for another study). The pore volume of the media in Cell 2 (6.80 m³) was calculated from the media volume (19.44 m³, based on the thickness of the media) and porosity (~35%). Cell 3 was 24.2 m³ (dimensions: 2.7 m × 4 m × 2.24 m) and was filled with a 0.28 m thick layer of granitic gravel at the bottom that covered the collection pipe. An aeration grid was placed directly on the granite layer and covered by a second 1.51 m granitic gravel layer. The pore volume of the cell (6.77 m³) was calculated from the volume (19.33 m³, based on the thickness of the media) and porosity (~35%) of the media. A sewage distribution manifold was placed on top of the upper granitic gravel layer. Reeds (*Phragmites australis*) were planted at the level of the distribution manifold. A 0.45 m layer of insulating straw was placed on top of the distribution manifold (Figure 4.2). Cell 4 was a 27.4 m³ (dimensions: 4.1 m × 4 m × 1.67 m) tank operated in a downflow direction. A distribution manifold was placed in a 0.29 m layer at the top of the tank, which was underlain by a 0.55 m thick layer of BOFS. A thin layer of granitic gravel mixed with zero valent iron (ZVI) filings (Connelly GPM Inc., Chicago, Illinois, USA) was placed beneath the BOFS layer to

remove V from effluent derived from the overlying BOFS. A collection manifold was placed at the base of the tank within a 0.26 m thick layer of granitic gravel layer (Figure 4.3). The pore volume of Cell 4 (5.31 m^3) was calculated from the media volume (13.28 m^3 , based on the thickness of the media below the distribution network) and porosity ($\sim 40\%$) of the media. A small sacrificial container ($\sim 1/2 \text{ m}^3$) was placed before the BOFS cell. Cell 5 consisted of two connected plastic tanks (1000 L each), used to adjust the high pH effluent derived from the BOFS in Cell 4. An automatic flow monitor was employed to monitor the flow continuously excluding the period when the monitor was malfunctioning due to clogging. Flow volume was calculated from the automatically monitored data during the period when the flow monitor was functioning. Flow volume was calculated assuming constant flow during the periods when the monitor was malfunctioning.

4.3.2 Characterization of the reactive material and reaction products

Basic oxygen furnace slag (BOFS) was collected from the US Steel Stelco Hilton Works facility, Hamilton, ON, Canada. Zero valent iron was obtained from the Connelly-GPM, Chicago, Illinois, USA. The particle density of BOFS and ZVI were determined using a pycnometer (Air Comparison Beckman Model 930). Surface area was determined with a surface area analyzer (Micromeritics Gemini[®] VII 2390 Series).

The chemical and mineralogical composition of the BOFS were determined by X-ray fluorescence (XRF; MiniPal4, PANalytical), and X-ray diffraction (XRD, Rigaku D/MAX 2500 rotating anode powder diffractometer). Samples of precipitates from Cell 4 effluent (accumulated at the bottom of the Cell 4 collection chamber) and from Cell 5 (accumulated at the

bottom of a plastic tank) were examined using a Leo 1530 field emission scanning electron microscopy (FE-SEM) with energy dispersive X-ray (EDX) analysis.

The samples of the spent media were collected from nine sampling locations in Cell 4 for solid-phase analyzes. At each location, samples were collected in 8-10 cm vertical intervals from the surface of the reactive material (Profiles 1-9, Figure 4.4). Materials accumulated (adsorbed or precipitated) on the spent BOFS were analyzed using FTIR and XANES. The FTIR spectra were collected for the top-most samples from all nine sampling profiles using a Bruker Tensor 27 infrared spectrometer.

Phosphorus K absorption edge data was recorded using the Soft X-Ray Micro-characterization Beam line (SXRMB; 06B1-1) on two samples collected from the influent zone (Profile 1, samples 1 and 2) and a sample from the effluent zone of Cell 4 (Profile 8, sample 1) at the Canadian Light Source, Saskatoon, Canada using the 2.9 GeV storage ring. XANES spectra were processed and analyzed using the Athena (version 0.8.56) data processing package (Ravel and Newville, 2005). Linear combination fitting was used to compare the spectra from spent BOFS and the reference materials based on the goodness of fit criteria. Detailed methods for collection and interpretation of FTIR and XANES are described in Chapter 3. Reference materials, including hydroxylapatite (HAP-S), tricalcium phosphate (α -TCP & β -TCP), calcium phosphate dihydrite (CPD), calcium phosphate dihydrite dibasic (CPDD), and iron phosphate (FeP) used for FTIR and XANES analysis were obtained from Sigma Aldrich, Canada. In addition, hydroxyapatite (HAP-WM) was synthesized in the laboratory following a liquid mix technique described in Pena and Vallet-Regi (2003) and used as reference material.

4.3.3 Sample collection and analysis

The demonstration-scale treatment system was monitored regularly over two years from January 2010 to December 2011. A flow meter was installed between Cell 4 and Cell 5 to measure flow rate of the system. Influent and effluent samples from the overall system, and effluent samples from each cell were collected more frequently in year 1 (weekly) than in year 2 (monthly).

Samples were collected with polyethylene containers after purging at least three times to avoid cross contamination and ensure representative samples. The values of pH, Eh and alkalinity were measured in the field using the same instruments and following the procedures described in Chapter 3. Samples for cations, anions, phosphate, ammonia, COD, $cBOD_5$, total Coliform and *Escherichia coli* (*E.coli*) were collected, preserved, and analyzed using the methods described in Chapter 3.

4.3.4 Geochemical modeling

The geochemical modeling code PHREEQC Interactive was used to calculate the saturation indices (SI) for CaP phases (*e.g.*, hydroxylapatite) and other mineral phases relevant to the treatment system (Parkhurst and Appelo, 1999). The WATEQ4F database was used for these calculations. Solubility product values for brushite, monetite, octacalciumphosphate, β -tricalciumphosphate, and variscite (Table 4.1) were added to the database using published solubility constants (Baker et al., 1998). Saturation indices were calculated for four sampling events at the effluent of Cells 1, 2, 3, and 4.

4.4 Results and Discussion

4.4.1 Characteristics of the reactive materials

The BOFS particle size ranged from <0.5 to 8 mm. The finest fraction of the BOFS had the highest mass-weighted surface area (Table 4.2). The particle density of the BOFS was 3.43 g cm^{-3} . XRF analysis results indicate the composition of BOFS material, expressed as oxides, was 33.8 wt. % CaO, 24.3% Fe₂O₃, 11.3% SiO₂, 9.6% MgO, 4.1% MnO, and 7.4% Al₂O₃ (Table 4.2). XRD measurements of two BOFS samples collected from the source material indicated that BOFS material contained wuestite (FeO), lime (CaO), larnite (Ca(SiO₄)), srebrodolskite (Ca₂Fe₂O₅), anhydrite (CaSO₄) and possibly portlandite (Ca(OH)₂). However, only one of the samples analyzed contained both lime and anhydrite. The XRD analysis also indicated the presence of corundum (Al₂O₃), which was probably derived from the mortar and pestle used to prepare the samples (Table 4.2). The particle size, surface area and density of ZVI were 8 to 50 mesh (0.297- 2.38 mm), $4.4 \text{ m}^2 \text{ g}^{-1}$, and 6.7 g cm^{-3} .

4.4.2 Flow characteristics

The flow rate was highly variable throughout the study period due to variations in the size of student population at the college. The average flow rate was $0.89 \text{ m}^3 \text{ day}^{-1}$ and the flow rate varied between 0.02 and $4.3 \text{ m}^3 \text{ day}^{-1}$ ($\sigma=625$, Figure 4.5). Mean hydraulic retention time was 7.6 (minimum HRT of 1.59 days), 7.6 (minimum HRT of 1.59 days), and 6.0 (minimum HRT of 1.24 days) days in Cells 2, 3, and 4. Due to the formation of particulate CaCO₃ in Cell 4 effluent, the flow meter between Cells 4 and 5 clogged several times. High electrical conductivity and

high concentrations of TSS in the Cell 4 effluent (Figure 4.6) confirmed the presence of suspended and dissolved solids. Although no significant change in flow rate was observed during the experiment, a decrease in flow rate can be anticipated in cases of long-term operation without any maintenance.

4.4.3 pH and alkalinity

Mean pH values of effluent from Cells 1, 2, 3, and 4 were 7.61, 7.81, 7.84, and 11.4 respectively (Table 4.3). A gradual increase in pH was observed in Cells 2 and 3 effluents, which is probably due to respiration of CO₂ through plant roots in Cell 2 and through aeration in Cell 3 (Figure 4.6). The pH of the Cell 4 effluent was consistently over 9.4 (pH range, 10.9±1.47) throughout the experiment. The mean alkalinity in Cells 1, 2, 3, and 4 effluents were 534, 483, 222, and 802 mg L⁻¹ as CaCO₃, respectively (Table 4.3). The alkalinity values in Cell 4 effluent were very high (up to 2360 mg L⁻¹ as CaCO₃) during the initial stage of the experiment, which was probably due to the dissolution of CaO and Ca(OH)₂ on the outer layers of the BOFS. The alkalinity values gradually decreased over time as the labile calcium oxide and hydroxide phases were depleted by continuous flushing by the Cell 3 effluent. However, pH values did not change significantly over time as the hydraulic retention time (~5 days) probably was sufficient to dissolve the calcium species (CaO and Ca(OH)₂) from the BOFS. The high pH effluent from Cell 4 was neutralized in Cell 5 (pH adjustment tank) by sparging with CO₂ based on results from an indoor pilot-scale (~1 m³ capacity) treatment system (Chapter 3). A large volume of white precipitate accumulated in the bottom of the Cell 4 effluent collection chamber. The accumulation of these precipitates was anticipated due to very high average electrical conductivity (4050 μS cm⁻¹) and

total suspended solid (TSS) concentrations (245 mg L^{-1}) in the Cell 4 effluent relative to the effluent from the other cells effluents (Figure 4.6). The FTIR analysis suggests that these precipitates were mainly calcium carbonate and calcium phosphate (Table 4.4). The formation of these carbonate minerals was minimized when the pH was maintained between 6.5 and 7 (by sparging CO_2). The rate of CO_2 addition required to neutralize the effluent pH was determined on the basis of the difference between the OH^- concentration measured in Cell 4 effluent and the desired OH^- concentration. Typically 10^{-2} moles of CO_2 were required to reduce the pH from 12 to 7.5 per liter of effluent.

4.4.4 Phosphorus removal

Mean $\text{PO}_4\text{-P}$ concentrations in the effluent from Cells 1, 2, 3, and 4 were 5.49, 5.89, 3.49, and 0.07 mg L^{-1} respectively (Figure 4.6). The removal efficiency of PO_4 in Cells 2, 3, and 4 was 7%, 44%, and 62%, respectively (Figure 4.6). Thus the overall PO_4 removal efficiency in the treatment system was ~99%. The removal efficiency of PO_4 in Cell 3 (aerated EW cell) was 44%. Similar efficiencies (40-60%) have been reported for other aerated EW systems (Kadlec and Knight, 1996; Knight et al., 2000, and Vymazal, 2004). The extent of PO_4 removal was greatest (62%) in Cell 4. Furthermore, PO_4 removal efficiency in Cell 4 was about 98% with respect to the Cell 3 effluent. The concentrations of PO_4 in Cell 5 effluent were greater than in the Cell 4 effluent (Figure 4.7). Phosphorus mass retention was higher in Cell 4 (~94%), compared to Cell 2 (1.3%) and Cell 3 (27%) during the experiment (Figure 4.5, Table C 32 in Appendix C).

Adsorption of inorganic PO_4 on hydrous oxides of Fe and Al is favored in acidic environments; however, alkaline conditions are suitable for precipitation of calcium phosphate phases (Qualls and Richardson, 1995). Low removal efficiency of PO_4 in Cell 3 was probably due to the low abundances of Ca, Fe, and Al, in the granitic gravel, because these metals are commonly involved in formation of P-bearing phases (Vymazal, 2004). On the other hand, presence of significant quantities of Ca, Fe, Al, and Mg oxides (Table 4.2) in the BOFS probably enhanced removal of PO_4 in Cell 4.

Precipitation of Al-phosphate and Fe-phosphate phases is favoured in near neutral to acidic conditions (Stumm and Morgan, 1981). Whereas, Ca-rich alkaline conditions ($\text{pH} > 9$) favor the formation of calcium phosphate phases (e.g., hydroxyapatite) (Baker et al., 1998; Bowden et al., 2009). In BOFS based treatment systems, precipitation of calcium phosphate phases (i.e. hydroxyapatite) is found to be the most important PO_4 removal mechanism (Baker et al., 1998; Bowden et al., 2009). However, the formation of hydroxyapatite can be inhibited by high concentrations of dissolved Mg (Kim et al., 2006). In addition to calcium phosphate phases, iron, aluminum, and magnesium phosphate phases may also form in BOFS based treatment system.

Although adsorption of PO_4^{3-} is anticipated to be less significant at high pH, predominance of the negatively charged HPO_4^{2-} and PO_4^{3-} species at $\text{pH} > 9$ is reported (Stumm and Morgan, 1981). The scarcity of positively charged surfaces is more predominant at lower pH. However, the BOFS reactive media in Cell 4, contains an abundance of metal oxides, some of which have high pH greater than zero point of charge (pH_{ZPC}) values, including 11.2 % MgO (with pH_{ZPC} of 12.4; Parks, 1965) and 3.4 % Al_2O_3 (with pH_{ZPC} of 9.1; Parks, 1965). The removal efficiency for

PO₄ in Cell 4 did not decrease significantly because the reactive material consistently released effluent with high pH and high Ca during the investigation (Table C 6 in Appendix C).

The influent water was undersaturated with respect to brushite, monetite, and vivianite in all sampling events (Figure 4.8); undersaturated with respect to variscite in all sampling events except Jun 03, 2010; and supersaturated with respect to octacalciumphosphate, β -tricalciumphosphate, MnHPO₄, calcite, aragonite, gibbsite, goethite, ferrihydrite, hydroxyapatite and strengite in all sampling events except Jun 03, 2010. Very low phosphate concentrations in Cell 4 effluent and the supersaturation of the pore water with respect to calcium phosphate phases including hydroxyapatite, one of the major P-bearing phases in Ca- and P-rich environments (Yamada et al., 1986; Bowden et al., 2009; Stumm and Morgan, 1981), suggest that precipitation of calcium phosphate phases is likely mechanisms for P retention in the BOFS media.

4.4.4.1 FTIR

The FTIR spectra were collected for the outer layer materials of the spent media from top the 5 cm of the nine sampling locations in Cell 4. All of the spectra showed pronounced carbonate and phosphate bands. Sharp carbonate bands, including the ν_4 band at 712-713 cm⁻¹, the ν_2 band at 872-874 cm⁻¹, and a broad distinct carbonate ν_3 band at 1422-1426 cm⁻¹, carbonate overtones including the combination bands of ν_1 and ν_4 at 1797-1800 cm⁻¹ ($\nu_1 + \nu_4$; Gillet et al., 1996; Vongsavat et al., 2006; Tatzber et al., 2007; Gunasekaran and Anbalagan, 2008), and the combination bands of ν_1 and ν_3 or $2\nu_2$ and ν_4 at 2514-2515 cm⁻¹ were observed ($\nu_1 + \nu_3$; Vongsavat et al., 2006; $2\nu_2 + \nu_4$; Gunasekaran and Anbalagan, 2008). Relatively weaker

carbonate overtones were also observed at 2874-2876 cm^{-1} , and 2980-2982 cm^{-1} ($2\nu_3$; Gunasekaran and Anbalagan, 2008). The carbonate vibrational frequencies ν_4 , ν_2 , and ν_3 along with the overtones suggested that calcite was one of the predominant minerals in the outer layer materials accumulated on the spent reactive materials (Vagenas et al., 2003; Vongsavat et al., 2006; Ni and Ratner, 2008; Kurap et al., 2010). An example spectrum plotted with labelled carbonate vibrational bands for calcite and aragonite is shown in Figure 4.9. A broad phosphate ν_3 band at 1030-1039 cm^{-1} , several phosphate ν_4 bands at 632-635, 602-608, 595-597, 583-588, and 567-575 cm^{-1} , and a phosphate ν_2 band between 450-461 cm^{-1} and 475 cm^{-1} were also observed. However, none of these spectra showed any signature of phosphate ν_1 band (Table 4.4). Although phosphate ν_3 and ν_2 bands were well-defined, most of the phosphate ν_4 bands were weak to very weak. The FTIR spectra were compared with the reference materials including HAP-S and β -TCP (Figure 4.9). The wavenumbers of the phosphate vibrational bands obtained from the reference materials were similar to the HAP and β -TCP reported in the previous studies (Rehman and Bonfield, 1997; Ribeiro et al., 2006; Panda et al., 2003; Singh and Purohit, 2011, Matkovic et al., 2012; Kim et al., 2006; Pena and Vallet, 2003; and De Oliveira et al., 2005). The phosphate vibrational bands of β -TCP showed better match with the samples compare to HAP-S. However, due to inadequate concentration of P compared to the Ca concentration in the samples and the absence of appropriate conditions (e.g. high temperature, ~ 1000 $^{\circ}\text{C}$ for crystallization of HAP and β -TCP) during the formation of CaPO_4 , wavenumbers may not be the same as the crystalline reference materials.

4.4.4.2 XANES

XANES spectra were collected for samples P2-S1, P2-S2, and P8-S1 from the upper influent and effluent part of Cell 4 (Figure 4.10). The XANES spectra can show the presence of phosphate (oxidation state +5) bearing phases, by comparing primary fluorescence peak positions. The primary peak positions reported for the reference phosphate species are around 2149 eV (Hesterberg et al., 1999; Sato et al., 2005), 2150 eV (Shober et al., 2006, Güngör et al., 2007), 2151 eV (Brandes et al., 2007), and 2158.5 eV (Peak et al., 2002). This primary peak is also designated as absorption edges or white lines in XANES spectra (Brandes et al., 2007; Güngör et al., 2007) and is based on the charge, electronegativity, and interatomic distance of the coordinating cation; the white line may vary between ± 0.5 eV (Franke and Hormes, 1995). The pre- and post-edge spectral features characteristic of various phosphate phases including Ca-, Al-, and Al-phosphates are described in previous studies (Hesterberg et al., 1999; Ajiboye et al., 2008; Shober et al., 2006; Sato et al., 2005; Eveborn et al., 2009; Beauchemin et al., 2003).

The energy range of P K-edge of the CaP reference materials analysed in this study were between 2151.5 and 2151.7 eV. A well-defined post-edge shoulder at ~ 2154.7 eV and two other features at ~ 2162.5 eV, and ~ 2169.0 eV were observed in the spectra. The iron phosphate reference material, iron (III) phosphate, showed the white line at a higher energy (2152.2 eV) and also displayed a unique pre-edge feature at 2148.5 eV. The position of this pre-edge feature is consistent with previous studies (Hesterberg et al., 1999; Khare et al., 2007; Ajiboye et al., 2008; Shober et al., 2006, Sato et al., 2005, Eveborn et al., 2009; and Beauchemin et al., 2003).

The calcium phosphate phases all exhibited a shoulder at ~2154.7 eV (Figure 4.10 c) and a distinct feature at ~2162.5 eV (Figure 4.10 d). Although other studies reported different energies for these features, the relative positions of these features with respect to the white lines were within the same range (Peak et al., 2002; Sato et al., 2005). Another feature at ~2169 eV was observed at a similar position, relative to the white line, as a feature attributed to the oxygen oscillation by Peak et al. (2002) and Sato et al. (2005).

XANES spectra of the calcium phosphate reference materials and the spent BOFS samples are compared in a single plot (Figure 4.10). Phosphate sorbed on calcite (PSC) was synthesized in the laboratory and included as a reference material in this study. The XANES spectrum of this PSC sample closely resembled the PSC spectrum presented in Peak et al. (2002). The absorption edges of all of the spectra collected for the samples from Cell 4 were between 2151.5 and 2151.7 eV. This edge position is similar to that observed for the Ca-PO₄ reference materials. The samples obtained from Cell 4 also showed post-edge features including a shoulder at 2154.7 eV, a Ca-PO₄ peak at 2162.5 eV, and an oxygen oscillation peak at 2169.0 eV. Although the relative positions were similar to those observed in the reference materials, these features were not as distinct as observed in the reference materials. The sharpness of the spectral features is proportional to the degree of crystallinity (Peak et al., 2002; Sato et al 2005). The XANES spectra showed small differences between the samples, suggesting minor differences in composition or structure. There was no pre-edge feature observed in the XANES spectra of the samples, indicating an absence of iron phosphate phases.

The linear combination (LC) fitting tool of Athena was used to compare the XANES spectra of the samples and the reference materials. Binary and ternary combinations of Ca-PO₄ reference

materials were compared to the spectra for each sample. The Fe-PO₄ was considered in the LC fitting because it showed a unique pre-edge feature, which is not observed in the samples (Figure 4.11). Sample P2-S1 showed the best LC fit ($\chi^2 = 1.01$) with the combination of β -TCP, α -TCP, and CPDD. The contributions from β -TCP were greatest in the linear combination fit (70%), followed by α -TCP (~20%) and CPDD (~10%) (Figure 4.11, Table 4.5). Sample P8-S1 showed a similar LC fit with contributions from β -TCP, α -TCP, and CPDD of ~72%, ~16% and ~12%. The best LC fit ($\chi^2 = 2.71$) for sample P2-S2 was observed for the combination of α -TCP (~57%), β -TCP (~41%), and CPDD (~2%), suggesting that the greatest contribution was from α -TCP, rather than from β -TCP, as found in the other samples. Comparatively higher χ^2 values were observed in different combinations of Ca-PO₄ reference materials for sample P2-S2 than for the other samples. However, similar high values are not uncommon in the literature (Güngör et al., 2007).

4.4.5 Ammonia and nitrate

Mean concentrations of NH₃-N in Cells 1, 2, 3, and 4 effluents were 47.9, 38.8, 4.31 and 8.38 mg L⁻¹, respectively; and mean concentrations of NO₃-N in Cells 1, 2, 3, and 4 effluents were 3.55, 3.47, 38.0 and 32.6 mg L⁻¹, respectively. There were sharp differences observed in NH₃-N and NO₃-N concentrations between Cells 2 and 3 effluent during the experiment (Table 4.3). Removal efficiencies of NH₃-N in Cells 2, 3, and 4 were 19, 72, and -9.0%, respectively. Although Cell 4 contributed ~ 9.0% NH₃-N, the overall removal efficiency of the treatment system was ~82%.

Mean $\text{NO}_3\text{-N}$ concentrations decreased in Cell 2 by 2.3% and then increased sharply in Cell 3 (~ 11 times higher than the concentrations in the Cell 2 effluent). Finally, the $\text{NO}_3\text{-N}$ concentration decreased 14% in the Cell 4 with respect to the Cell 3 effluent (Figure 4.5). The 33.8 mg L^{-1} loss in $\text{NH}_3\text{-N}$ in Cell 2 corresponds closely to the 34.5 mg L^{-1} gain in $\text{NO}_3\text{-N}$. These sharp changes in $\text{NH}_3\text{-N}$ and $\text{NO}_3\text{-N}$ concentrations from Cell 2 to Cell 3 can be attributed to microbially mediated oxidation of NH_3 to NO_3^- . Nitrification is enhanced by the continuous supply of O_2 through the forced aeration system as was evident by the high DO (dissolved oxygen) concentrations in these cells (Figure 4.6, Table 4.6). Similar degrees of nitrification have been observed in other studies of EW systems (Green et al., 1998; Ye and Li, 2009).

The ZVI layer at the bottom of Cell 4 may play an important role in the increasing ammonia concentrations in Cell 4 effluent. Reduction of nitrate and nitrite by ZVI and release of NH_3 are reported in previous studies (Rahman and Agrawal, 1997; Cheo et al., 2004). A very low positive change in mass (2% N mass loss) was observed in this treatment system (Table C 36 in Appendix C).

4.4.6 Carbonaceous biochemical oxygen demand (cBOD₅) and chemical oxygen demand (COD)

Mean concentrations and the concentration ranges of cBOD₅ and COD of in Cells 1, 2, 3 and 4 are summarized in Table 4.6. The removal efficiencies of cBOD₅ in Cells 2, 3, and 4 were 58, 30, and 10%, respectively. Thus the overall removal efficiency of cBOD₅ in the treatment system was > 98%. However, the removal efficiency of cBOD₅ in Cell 3 was 71% compared to the Cell 2 effluent, which is about 20% less than values reported previously (Johnson and Mara, 2005).

Although Cell 4 contributed only 10% of the total cBOD₅ removal (>98%) in the treatment

system, this cell has potential for removing a higher percentage of the cBOD_5 (86% removal compared to Cell 3 effluent) of cBOD_5 . Thus all three treatment cells played important roles in degrading labile organic carbon compounds.

Mean concentrations of COD in Cells 1, 2, 3, and 4 were 143, 72.1, 28.4, and 34.0, respectively. Removal efficiencies of COD in Cells 2, 3, and 4 were 50, 31 and -4.0%, relative to the Cell 1 effluent. However, the COD removal efficiency in Cell 2 was 50% with respect to Cell 1 effluent; in Cell 3 removal was 61% with respect to Cell 2 effluent; and in Cell 4 was -20% with respect to Cell 3 effluent. Thus both Cells 2 and 3 were effective in removing COD from wastewater, whereas Cell 4 contributed COD to the effluent. Both cBOD_5 and COD loading fluctuate with the flow variation depending on the student population (Table C37, C38).

4.4.7 Major ion chemistry

Mean Ca concentrations in Cells 1, 2, 3, and 4 effluents were 100.8, 101.2, 105.1, and 193.2 mg L^{-1} , respectively. There were no significant changes in Ca concentrations between the Cell 1 and Cell 2 effluent. Calcium concentrations increased by 5% and 61% in the Cells 3 and 4. A sharp increase in Ca concentrations (as high as 568.2 mg L^{-1}) was observed in Cell 4 effluent at the initial stage of the trial. This sharp increase in Ca concentration was probably due to the dissolution of CaO and Ca(OH)_2 . Over time, as the cell continuously flushed, the Ca concentrations gradually decreased (Figure 4.12). In Cell 5, where CO_2 is introduced to the system by sparging, Ca concentrations decreased and precipitates accumulated (Figure 4.7). Mean Na concentrations in the Cell 1, 2, 3, and 4 effluents were 131.0, 126.3, 120.6, and 118.7 mg L^{-1} , respectively. Although Na concentrations gradually decreased from Cell 1 to Cell 4

(Figure 4.12), the small differences in concentrations (<5%) is consistent with the conservative nature of Na. Mean Mg concentrations were in the Cell 1, 2, 3, and 4 effluent were 11.8, 11.2, 14.1, and 4.3 mg L⁻¹, respectively. Although the Mg concentration decreased slightly in Cell 2 (5%), Mg concentrations in Cell 3 effluent increased by 25%. The Mg concentration decreased (70%) in Cell 4 effluent relative to the Cell 3 effluent (Figure 4.12). This decrease in Mg, may result from substitution of Mg for Ca in calcite or hydroxyapatite (Kim et al., 2006). Mean SO₄²⁻ concentrations in Cells 1, 2, 3, and 4 effluents were 42.3, 33.9, 45.6, and 30.5 mg L⁻¹, respectively (Figure 4.12). Mean SO₄²⁻ concentrations decreased by 20% in Cell 2 with respect to Cell 1 effluent, and increased by 35% in Cell 3 with respect to Cell 2 effluent, then decreased by 33% in Cell 4 with respect to Cell 3 effluent. Reducing conditions in Cell 4 (indicated by low Eh values; Figure 4.6) favour reduction of SO₄ and precipitation of metal sulfides. Chloride concentrations in Cells 1, 2, 3, and 4 did not significantly change (5% variation was observed) throughout the treatment system (Figure 4.12, Table 4.3), which indicate Cl is conservative in this system.

4.4.8 Trace metals

With few exceptions in the initial stage of the experiment, the concentrations of the dissolved trace metals (Zn, Fe, Mn, Cr, Ni, and Pb) remained at low concentrations below water quality guidelines for Ontario (Figure 4.13, MOEE, 1994).

Mean Al concentrations in Cells 1, 2, 3, and 4 were 17.1, 24.0, 28.4, and 32.3 µg L⁻¹, respectively. The concentrations of Al gradually increased along the flow path. The increase in Al concentrations observed in Cells 2, 3, and 4 probably were due to the progressive release

from the treatment materials, with the greatest concentrations derived from the BOFS media, where the pH increases to pH>11. However, Al concentrations decreased in Cell 5 as pH of the cell was adjusted to near neutral by sparging with CO₂ (Figure 4.7, Stumm & Morgan, 1981). Mean V concentrations in Cells 1, 2, 3, and 4 effluents were 0.63, 0.72, 5.15, and 2.77 µg L⁻¹, respectively (Figure 4.13).

The release of V from BOFS has been observed previously (Chaurand et al., 2007) and the observed increase in V, was probably derived from the BOFS. The V concentrations in Cell 3 effluent were abnormally high (as high as 13.76 µg L⁻¹) in the initial stage of the experiment. This elevated V concentration probably was derived from a small sacrificial container filled with BOFS installed immediately below the effluent pipe of Cell 3. However, the release of V from this chamber declined at later stages of the experiment. Although V concentrations increased to 10.45 µg L⁻¹ in the effluent from Cell 4, this increase was less than that observed in previous reports (Proctor et al. 2000; Chapter 2). The ZVI layer, placed at the base of Cell 4 probably reduced vanadate (VO₄³⁻) resulting in precipitation or adsorption of vanadium, yielding lower concentrations. Addition of this thin ZVI layer is not expected to have significant effect on flow.

Average Cu concentrations in the effluent from Cell 1, 2 3 and 4 were 26.9, 14.4, 17.6, and 24.8 µg L⁻¹. The Cu concentrations in the Cell 1 effluent (system influent) were up to 59.9 µg L⁻¹ and exceeded water quality guidelines for Ontario (1 µg L⁻¹; MOEE, 1994). The average Cu concentration in the Cell 4 effluent reached a maximum of 27.5 µg L⁻¹, but remained lower than in Cell 1 effluent suggesting the EW system removed Cu from the effluent water (Figure 4.13).

4.4.9 Removal of bacterial indicators (total coliforms and *E. coli*)

Concentrations of *E. coli* of 2.2×10^3 to 2.4×10^6 CFU 100 mL⁻¹ in Cell 1, decreased to 0.3×10^2 to 4.8×10^5 CFU 100 mL⁻¹ in Cell 2, 0.03×10^2 to 2.4×10^4 CFU 100 mL⁻¹ in Cell 3, and 0.03×10^2 to 2.4×10^3 CFU 100 mL⁻¹ in Cell 4 showing progressive removal of *E. coli* in the treatment system (Table 4.6). In addition, concentrations of total coliform of 3.8×10^3 to 1.2×10^7 CFU 100 mL⁻¹ in Cell 1 decreased to 0.5×10^2 to 1.2×10^6 CFU 100 mL⁻¹ in Cell 2, 0.03×10^2 to 2.4×10^4 CFU 100 mL⁻¹ in Cell 3, and 0.03×10^2 to 2.4×10^3 CFU 100 mL⁻¹ in Cell 4 (Table 4.6). Both *E.coli* and total coliform sharply decreased while passing through Cell 3 by aeration and the bacterial indicators were further removed in Cell 4 due to highly alkaline condition of the cell (Figure 4.14). Thus, Cell 4 may also be considered a disinfection component within the treatment system.

4.5 Conclusions

The removal efficiencies of cBOD₅, COD, PO₄, NH₃, *E. coli*, and total coliform in the demonstration-scale wastewater-treatment system were often >99%. Elevated pH and dissolved Al and V concentrations in the effluent from Cell 4, derived from the BOFS materials, were potential concerns associated with the treatment system. The high pH was neutralized by sparging with CO_{2(g)} prior to discharge to the sewer system. Dissolved Al concentrations decreased as the pH was neutralized. The ZVI layer placed at the bottom of Cell 4 maintained the V concentration below the PWQO value. There was no significant effect of seasonal temperature variation on the overall performance of the treatment system. The precipitates derived from Cell 4 effluent were separated from the effluent in a settling chamber prior to sparging with CO₂,

maintaining low total PO₄ concentrations in the final effluent. Removal of *E. coli* and total coliform in the treatment system is attributed to the high pH concentrations prevalent in Cell 4. The trace metal concentrations were mostly within the guideline ranges in Cell 4 effluent. FTIR data indicated the occurrence of Ca-PO₄ minerals on the outer layers of samples of the spent BOFS. XANES spectra and LC fit results showed the probable occurrence of β-TCP on the outer layers of samples of the spent BOFS.

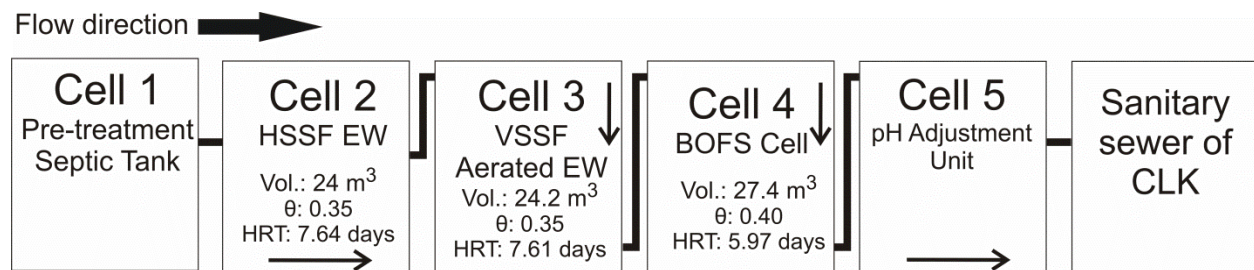


Figure 4.1 Schematic diagram of the EW-BOFS demonstration-scale treatment system. The treatment system comprises 4 outdoor cells (Cells 1-4) and an indoor cell (Cell 5). Wastewater continuously flushes through the system by a combination of gravity feed and pumping. In this diagram HSSF EW represents horizontal subsurface flow engineered wetland, VSSF aerated EW represents vertical subsurface flow aerated engineered wetland, BOFS represents basic oxygen furnace slag, and CLK represents City of lake Kawartha.

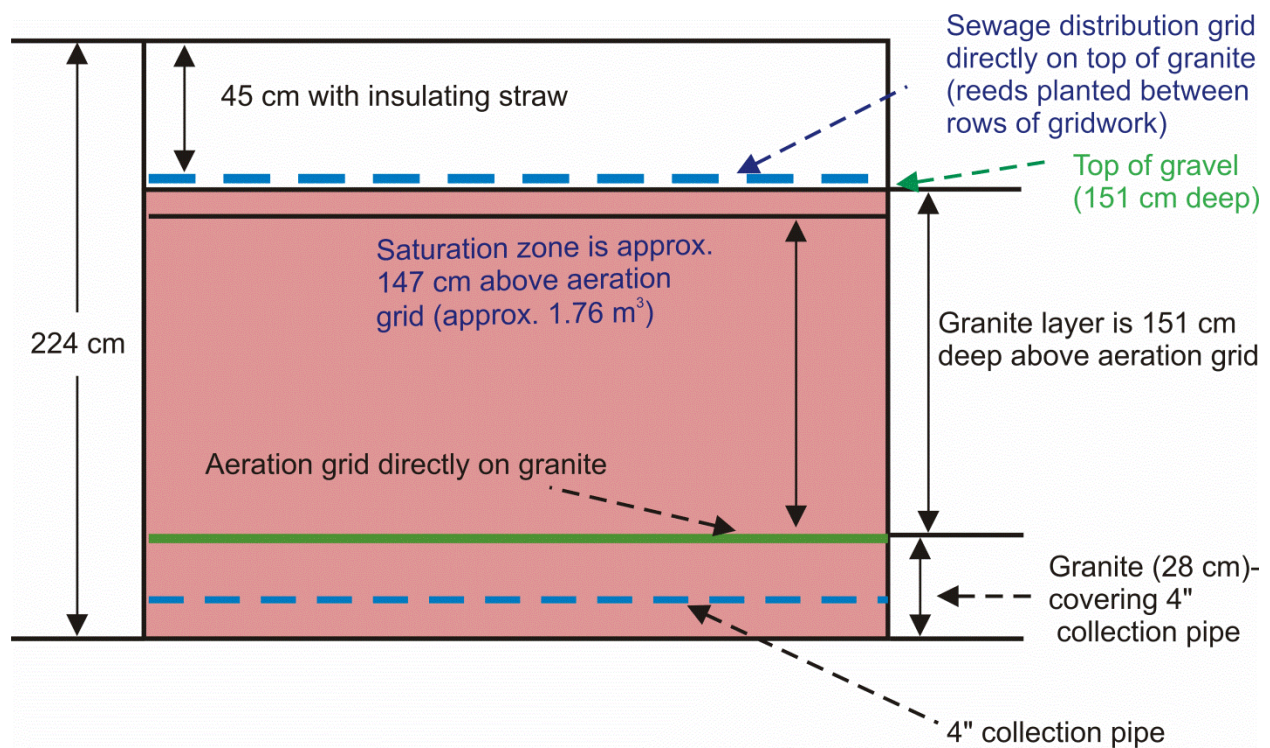


Figure 4.2 Cross-section of the Aerated EW cell (Cell 3) showing the thickness and vertical distribution of different components of the cell.

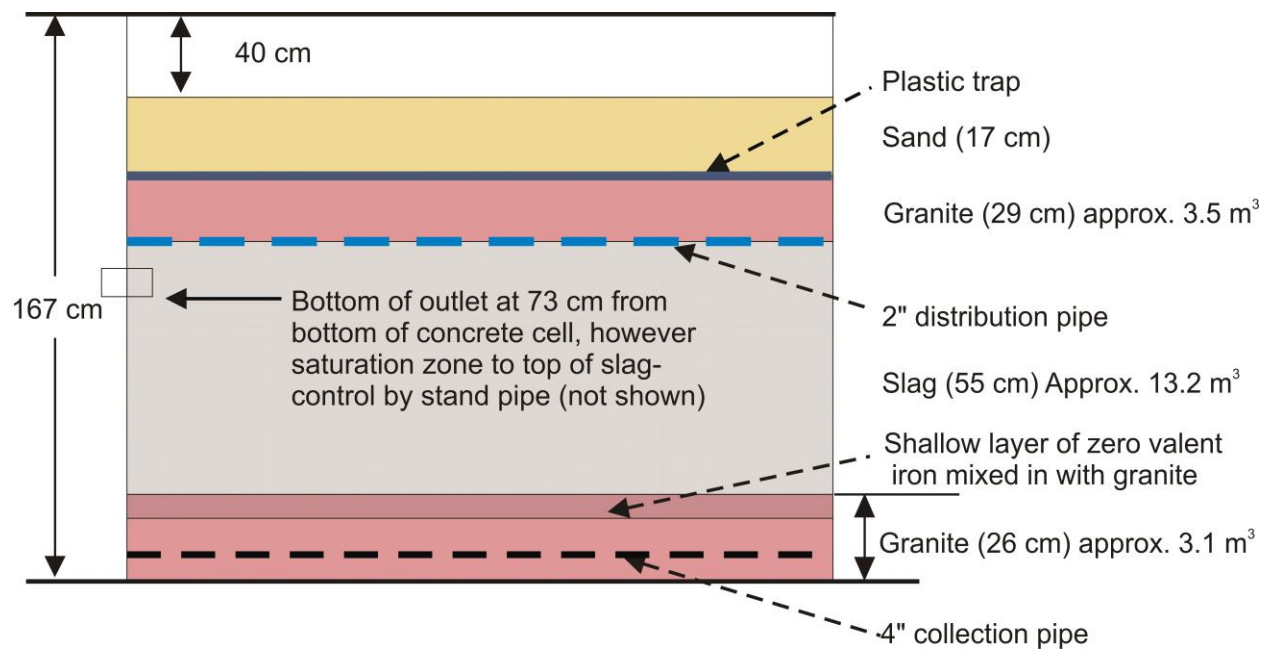


Figure 4.3 Cross-section of the BOFS cell (Cell 4) showing the thickness and vertical distribution of different components of the cell.

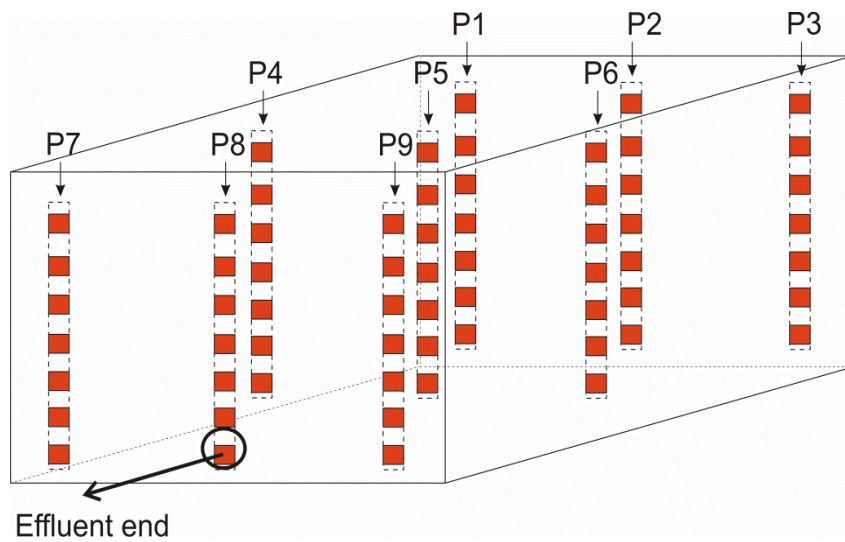


Figure 4.4 Locations of solid phase spent media collected from the BOFS cell.

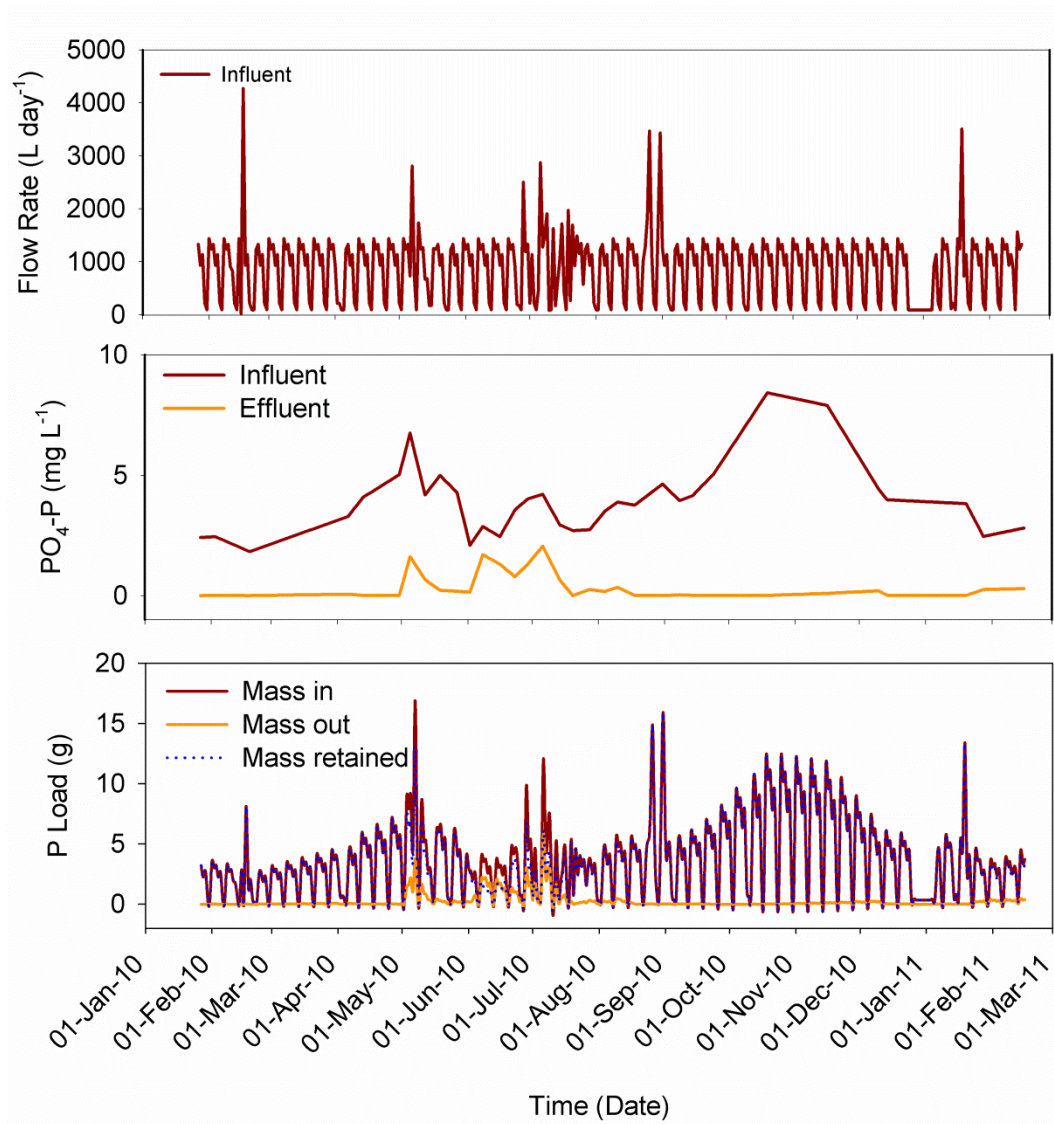


Figure 4.5 Flow rate, PO₄-P concentrations in the influent and effluent, and P load in BOFS Cell.

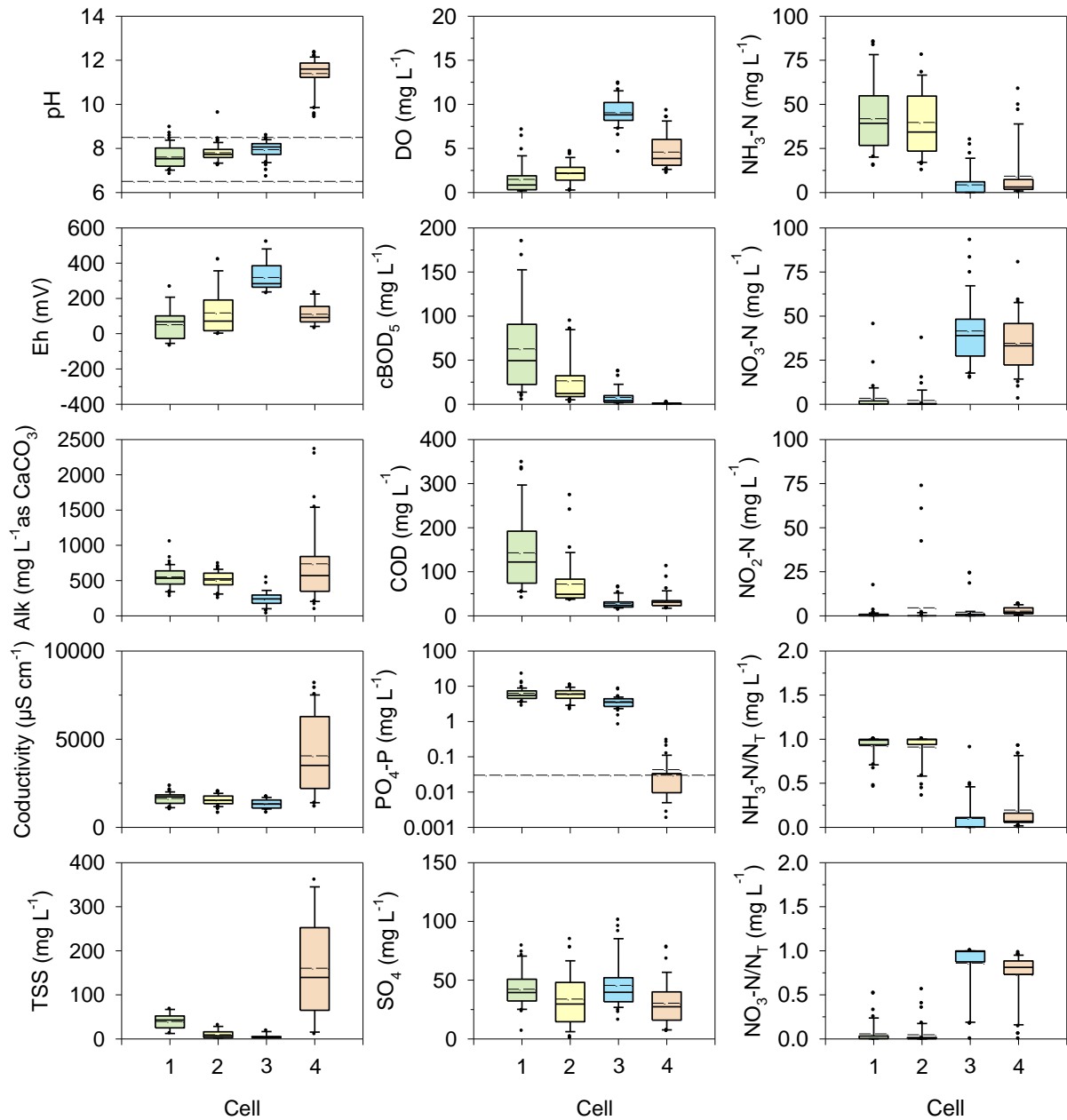


Figure 4.6 Box plots of pH values, Eh, conductivity, alkalinity, $\text{PO}_4\text{-P}$, DO, cBOD_5 , COD, Cl, SO_4 , $\text{NH}_3\text{-N}$, $\text{NO}_3\text{-N}$, $\text{NO}_2\text{-N}$, $\text{NH}_3\text{-N}/\text{N}_T$, $\text{NO}_3\text{-N}/\text{N}_T$ versus distance (Cells 1-4) along the treatment flow path. Dotted lines represent the Ontario Provincial Water Quality Objective (PWQO). Horizontal solid lines and broken lines on the boxes represent median and mean concentrations. Top and bottom most dots represent maximum observation above upper fence and minimum observation below lower fence.

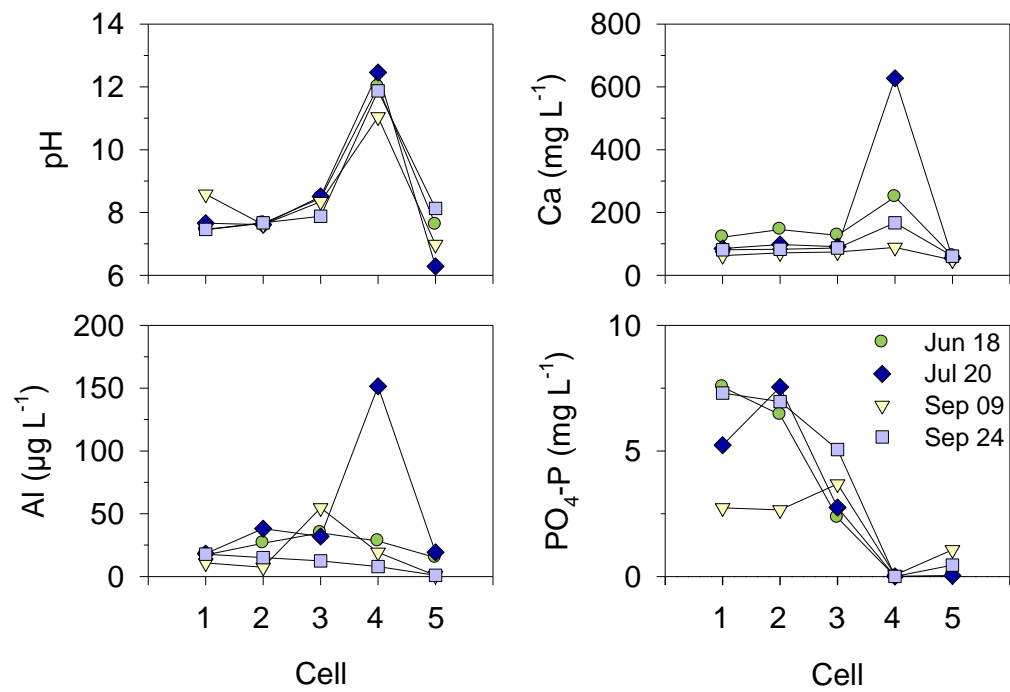


Figure 4.7 pH values, Ca, Al, and PO₄-P concentrations versus distance (Cells 1-5) along the flow path.

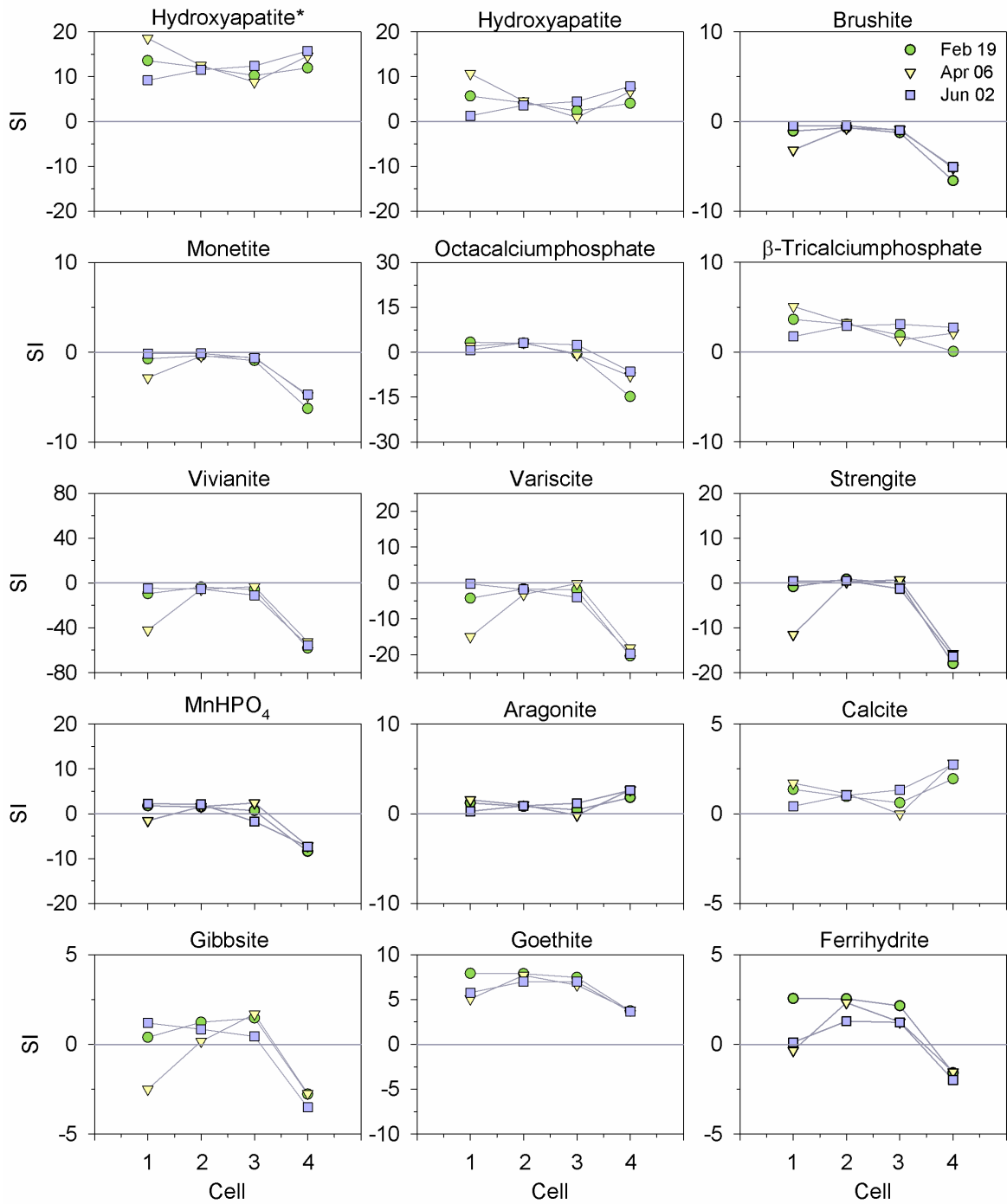


Figure 4.8 Saturation indices for calcium phosphate and other related phases (calculated using PHREEQCI) along the treatment cells during 3 sampling events. Saturation index of hydroxyapatite (indicated by *) was plotted using a modified log K_{sp} value (Baker et al., 1998).

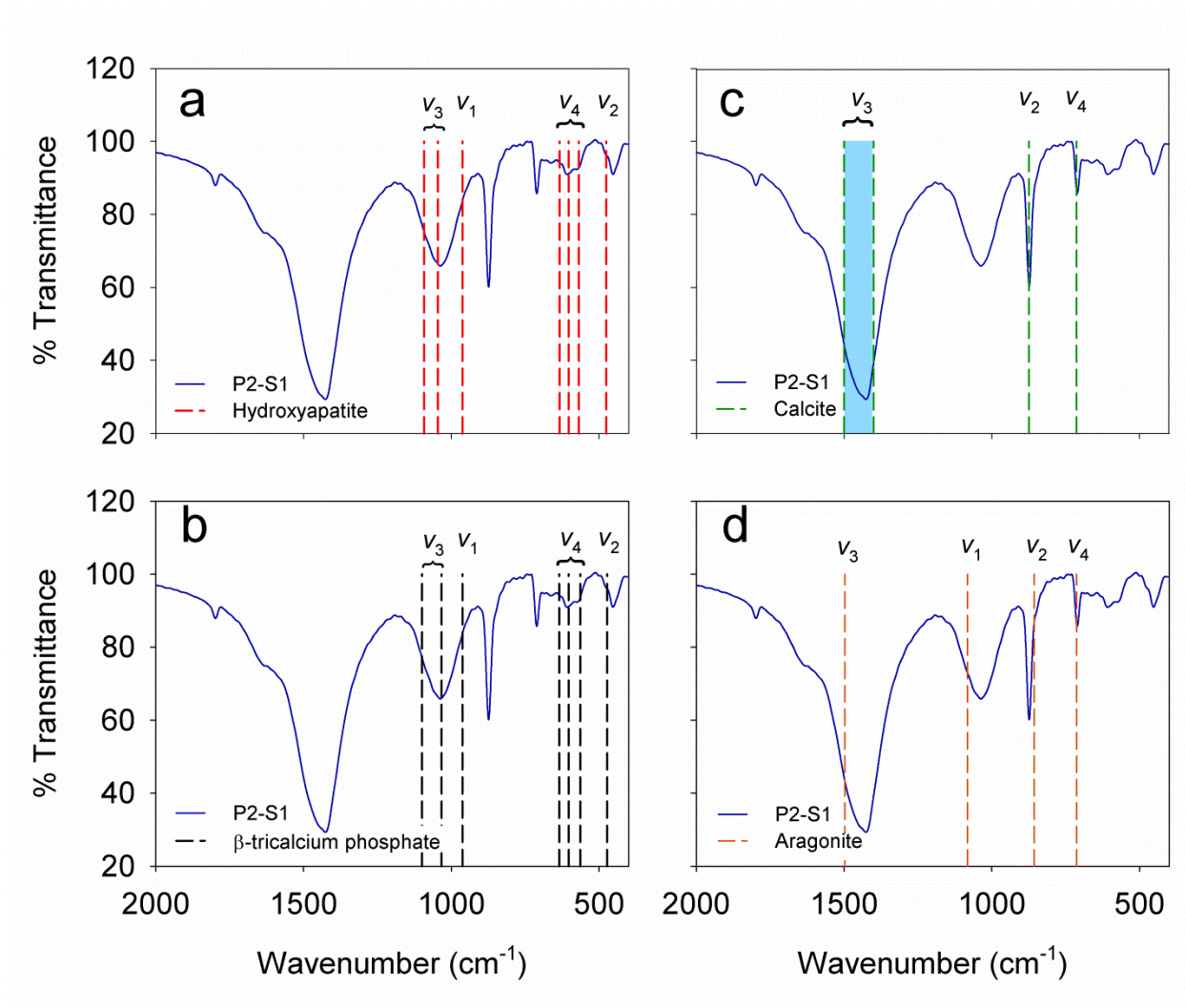


Figure 4.9 FTIR spectrum of sample with highest mass and reference materials and sample P2-S1, with phosphate vibrational bands for a) HAP-S, b) β-TCP, c) calcite, d) aragonite. Vertical dotted lines in “a” and “b” represent phosphate vibrational bands, while vertical dotted lines in “c” and “d” represent carbonate vibrational bands.

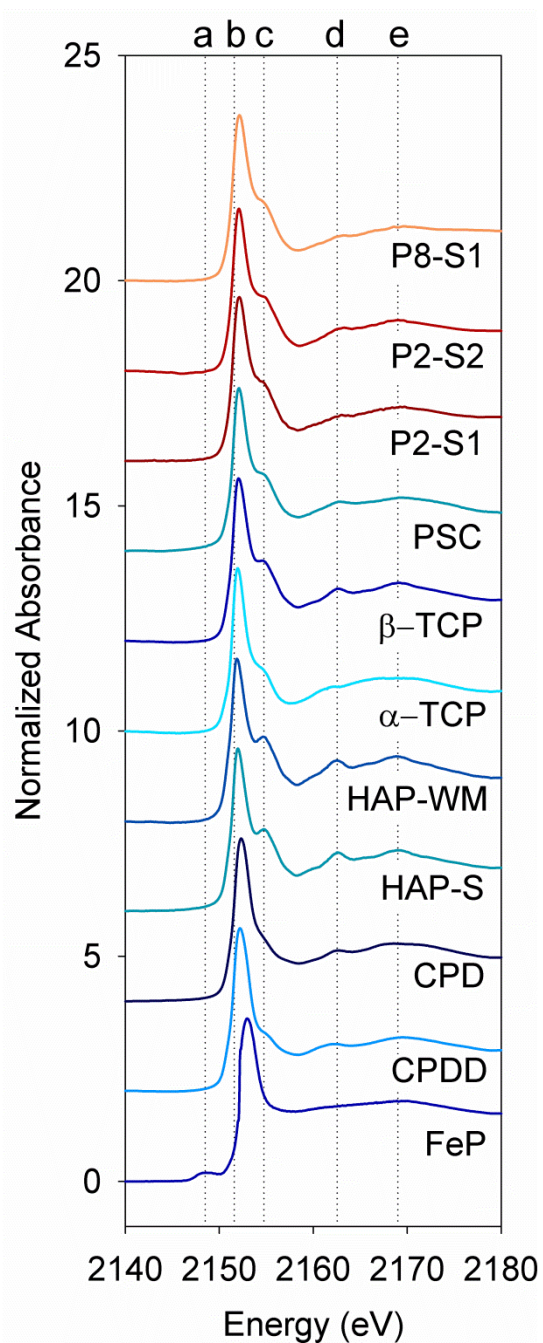


Figure 4.10 XANES spectra for reference materials, PO₄ sorbed on CaCO₃ (PSC; Peak et al., 2002), and samples P2-S1, P2-S2, P8-S1. Vertical lines represent various spectral features: a) pre edge feature for FeP; b) absorption edge (white line) for CaP species; c) shoulder (sharpness dependent on the degree of crystallinity); d) spectral feature common in HAP; e) oxygen oscillation.

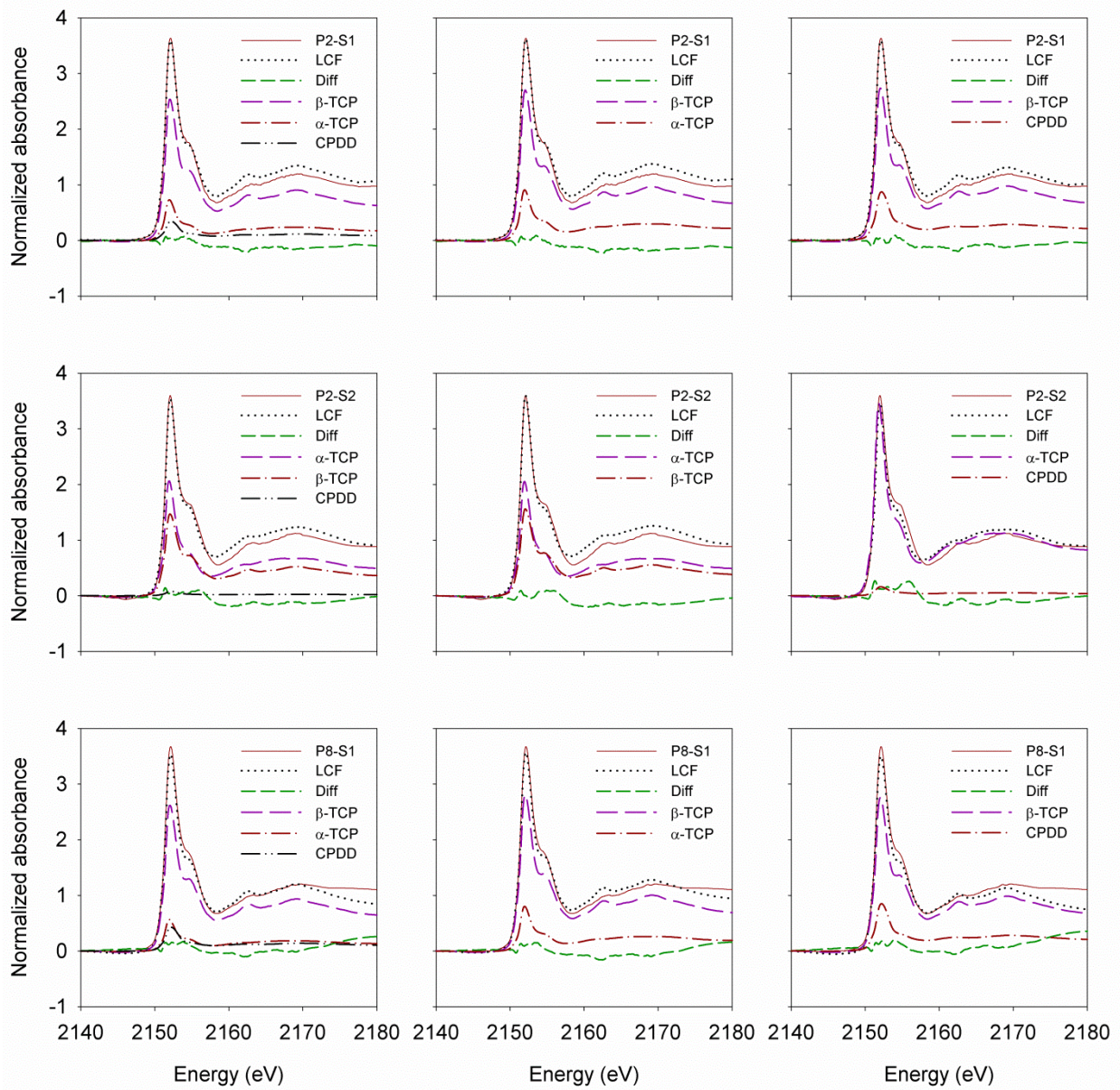


Figure 4.11 Linear combination fit results for spent BOFS samples P2-S1, P2-S2, and P8-S1.

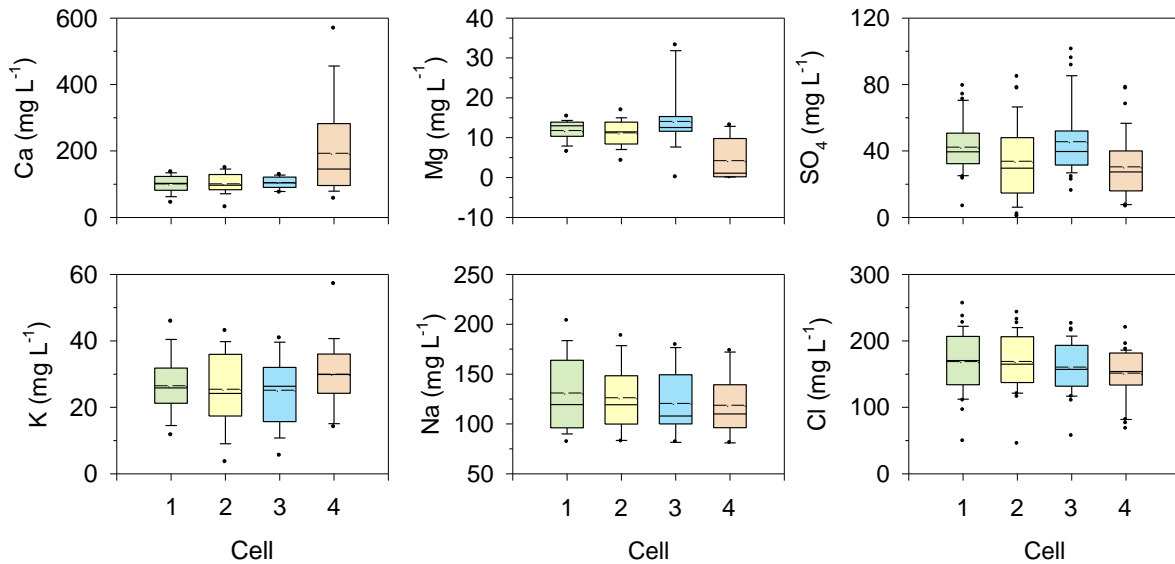


Figure 4.12 Box plots of Ca, Na, Mg, K, SO₄, and Cl concentrations versus distance (Cells 1-4) along the flow path. Horizontal solid lines and broken lines on the boxes represent median and mean concentrations. Top and bottom most dots represent maximum observation above upper fence and minimum observation below lower fence.

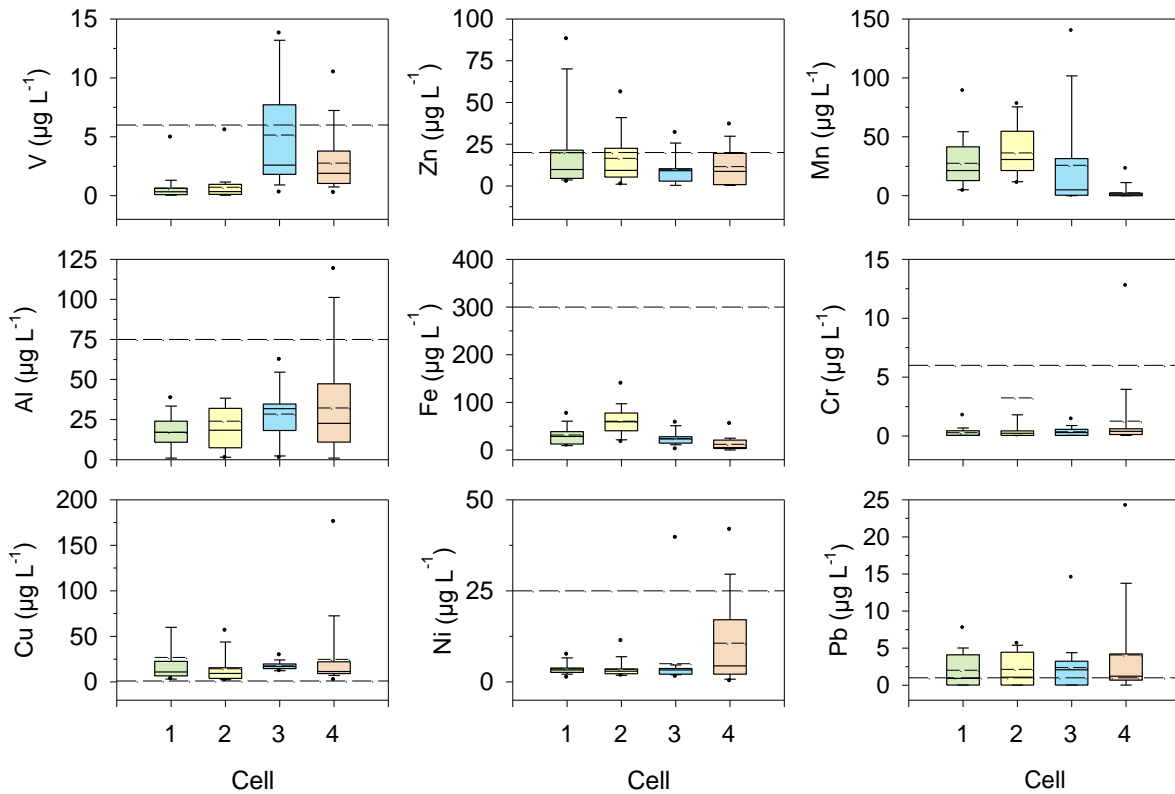


Figure 4.13 Box plots of V, Al, Cu, Zn, Fe, Ni, Mn, Cr, and Pb concentrations versus distance (Cells 1-4) along the flow path. Dotted lines represent the Ontario Provincial Water Quality Objective (PWQO). Horizontal solid lines and broken lines on the boxes represent median and mean concentrations. Top and bottom most dots represent maximum observation above upper fence and minimum observation below lower fence.

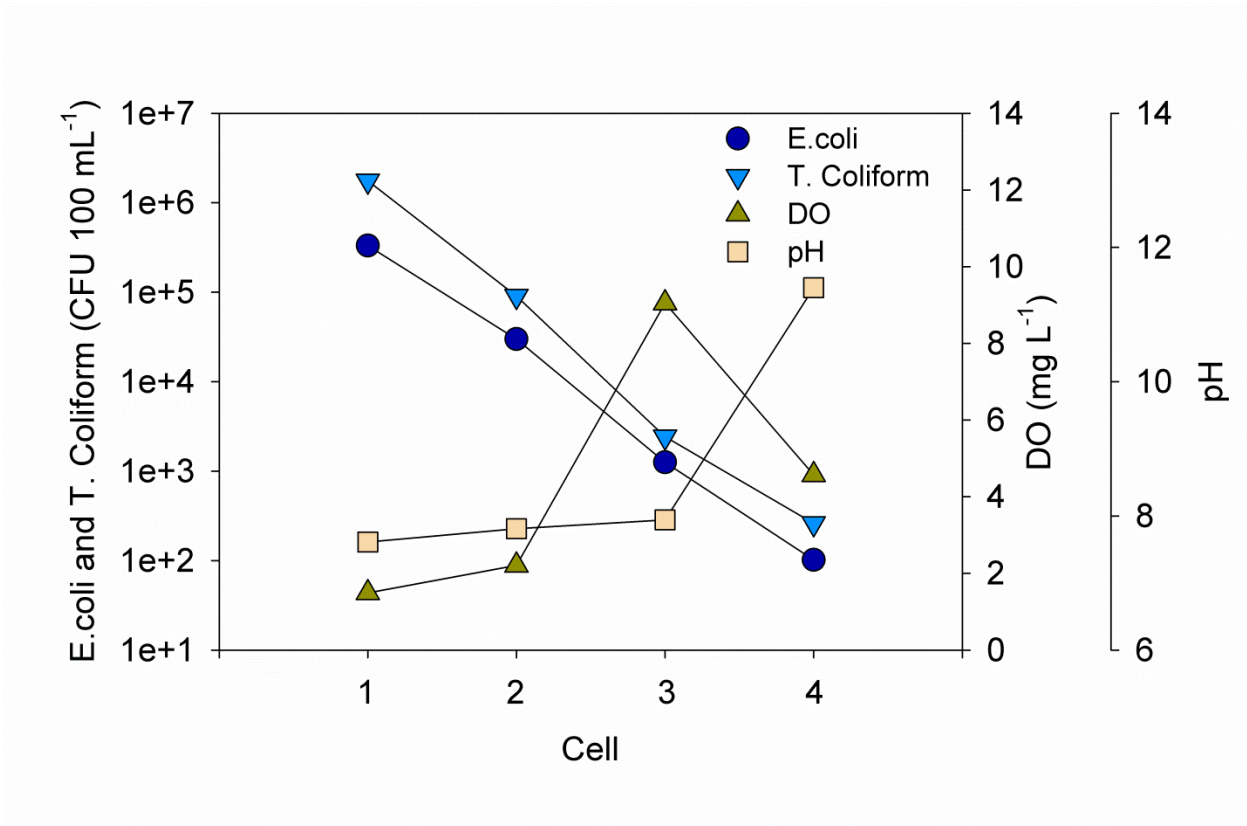


Figure 4.14 Concentrations of *E. coli*, total coliform (in the left Y-axis), DO, pH (in the right Y-axis) versus cells (1-4) along the flow path.

Table 4.1 K_{sp} values of the calcium phosphate minerals added to the PHREQCI database.

Mineral Phases	Reactions	log K _{sp}	References
Hydroxyapatite*	$\text{Ca}_5(\text{PO}_4)_3\text{OH} + \text{H}^+ = 5\text{Ca}^{+2} + 3\text{PO}_4^{-3} + \text{H}_2\text{O}$	-36.31	Baker et al., 1998
Brushite	$\text{CaHPO}_4 \cdot 2\text{H}_2\text{O} = \text{Ca}^{+2} + \text{PO}_4^{-3} + 2\text{H}_2\text{O} + \text{H}^+$	-18.91	Baker et al., 1998
Monetite	$\text{CaHPO}_4 = \text{Ca}^{+2} + \text{PO}_4^{-3} + \text{H}^+$	-19.24	Baker et al., 1998
Octacalciumphosphate	$\text{Ca}_8\text{H}_2(\text{PO}_4)_6 \cdot 5\text{H}_2\text{O} = 8\text{Ca}^{+2} + 5\text{H}_2\text{O} + 6\text{PO}_4^{-3} + 2\text{H}^+$	-93.95	Baker et al., 1998
β-tricalciumphosphate	$\text{Ca}_3(\text{PO}_4)_2 = 3\text{Ca}^{+2} + 2\text{PO}_4^{-3}$	-28.94	Baker et al., 1998
Variscite	$\text{AlPO}_4 \cdot 2\text{H}_2\text{O} = \text{Al}^{+3} + \text{PO}_4^{-3} + 2\text{H}_2\text{O}$	-21	Stumm and Morgan, 1981

Table 4.2 Physical and chemical properties of the BOFS materials used in the experiments.

Slag type: BOFS	
Slag source: Stelco Hamilton	
Physical properties	
Particle size (mm)	Surface area (m ² g ⁻¹)
4-2	6.05
2-1	8.98
1-0.5	11.5
<0.5	13.9
Particle size (mm)	Mass weighted surface area (m ² g ⁻¹)
4-2	154
2-1	196
1-0.5	250
<0.5	429
Density (g cm ⁻³):	3.49
Chemical properties	
Chemical composition	wt. %
CaO	33.8
Fe ₂ O ₃	24.3
SiO ₂	11.3
MgO	9.62
MnO	4.08
Al ₂ O ₃	7.43
P ₂ O ₅	-
TiO ₂	0.38
K ₂ O	0.03
Na ₂ O	0.07
Cr ₂ O ₃	-
Loss on ignition	8.96

Table 4.3 Mean concentrations and concentration ranges (expressed as average of maximum and minimum values) of pH, alkalinity, conductivity, and other target parameters including PO₄, NH₃-N, NO₃-N, NO₂-N, Cl, and SO₄ in the effluents of Cells 1, 2, 3, and 4.

	Unit		Effluents			
			Cell 1	Cell 2	Cell 3	Cell 4
pH		Average	7.61	7.81	7.94	11.4
		Range	7.89±1.06	8.42±1.20	7.65±0.94	10.88±1.47
Alk	mg L ⁻¹ as CaCO ₃	Average	534	483	222	802
		Range	661±389	494±246	284±256	1225±1135
Conductivity	µS cm ⁻¹	Average	1636	1546	1333	4052
		Range	1669±665	1412±610	1268±449	4661±3500
o-PO ₄	mg L ⁻¹	Average	7.00	6.74	3.86	0.33
		Range	12.9±9.32	8.40±6.21	5.12±3.29	1.03±1.03
o-PO ₄ _UW	mg L ⁻¹	Average	5.22	5.15	3.46	0.05
		Range	5.14±2.41	4.87±2.68	3.25±1.80	0.13±0.12
PO ₄ -P	mg L ⁻¹	Average	7.00	6.74	3.86	0.33
		Range	12.9±9.32	8.40±6.21	5.12±3.29	1.03±1.03
PO ₄ -P dissolved comb.	mg L ⁻¹	Average	5.22	5.15	3.46	0.05
		Range	7.20±4.71	7.68±6.02	4.69±3.88	0.24±0.24
TP	mg L ⁻¹	Average	8.41	7.23	3.64	1.13
		Range	13.5±9.83	10.2±8.16	4.98±3.01	3.67±3.64
NH ₃ -N	mg L ⁻¹	Average	47.9	38.8	4.79	8.38
		Range	62.2±47.2	54.7±46.9	15.0±15.0	29.4±29.2
NO ₃ -N	mg L ⁻¹	Average	3.59	3.47	37.3	32.1
		Range	22.6±22.6	31.2±31.2	51.3±41.6	41.6±38.8
NO ₂ -N	mg L ⁻¹	Average	0.83	4.53	2.07	2.62
		Range	8.59±8.58	36.73±36.72	12.04±12.04	3.48±3.24
Cl	mg L ⁻¹	Average	169.2	169.7	161.1	151.9
		Range	152±104	144±99	141±84.3	144±76.0
SO ₄	mg L ⁻¹	Average	42.25	33.9	45.6	30.5
		Range	42.8±36.3	42.6±42.0	58.5±42.6	42.3±35.8

Table 4.4 Vibrational bands of carbonate and phosphate and the corresponding wavenumbers in the FTIR spectra of the surface materials.

Carbonate	P1-S1	P2-S1	P 3-S1	P4-S1	P5-S1	P6-S1	P7-S1	P8-S1	P9-S1
ν_4	712	712	712	712	712	712	712	713	712
ν_2	873	874	873	873	873	872	873	874	873
ν_3	1426	1426	1425	1423	1426	1422	1425	1425	1426
$\nu_1+\nu_4$	1798	1797	1800	1799	1798	1799	1798	1798	1799
$\nu_1+\nu_3$ or $2\nu_2+\nu_4$	2514	2514	2515	2514	2515	2514	2514	2515	2515
$2\nu_3$	2874	2874	2875	2875	2874	2876	2875	2874	2875
$2\nu_3$	2980	2980	2980	2982	2981	2982	2978	2982	2980, 2924
Phosphate									
ν_3	1035	1037	1035	1037	1035	1037	1039	1034	1030
ν_1		-							
ν_4	602, 583, 567	632, 608, 574	604, 584, 572	604, 576, 568	635, 605, 588, 573	604, 578, 569	606, 580, 568	605, 597, 587, 579, 569	632, 604, 595, 587, 568
ν_2	450	475, 453	451	450	451	450	461	454	459

Table 4.5 Linear combination fitting results of spent BOFS samples.

Linear combination fits to P2-S1					
Combination	R-factor	χ^2	β -TCP (weight)	α -TCP (weight)	CPDD (weight)
β -TCP, α -TCP, CPDD	2.36E-03	1.01	0.703	0.202	0.095
β -TCP, α -TCP	2.45E-03	1.05	0.749	0.251	0
β -TCP, CPDD	2.76E-03	1.18	0.759	0	0.241
α -TCP, CPDD	7.96E-03	3.40	0	0.412	0.588
Linear combination fits to P2-S2					
Combination	R-factor	χ^2	α -TCP (weight)	β -TCP (weight)	CPDD (weight)
α -TCP, β -TCP, CPDD	7.10E-03	2.71	0.571	0.407	0.021
α -TCP, β -TCP	7.28E-03	2.78	0.568	0.432	0
α -TCP, CPDD	9.93E-03	3.79	0.956	0	0.044
β -TCP, CPDD	1.31E-02	4.99	0	0.984	0.016
Linear combination fits to P8-S1					
Combination	R-factor	χ^2	β -TCP (weight)	α -TCP (weight)	CPDD (weight)
β -TCP, α -TCP, CPDD	3.13E-03	1.34	0.726	0.156	0.118
β -TCP, α -TCP	3.24E-03	1.38	0.778	0.222	0
β -TCP, CPDD	3.36E-03	1.43	0.765	0	0.235
α -TCP, CPDD	9.10E-03	3.88	0	0.365	0.635

Table 4.6 Mean concentrations and concentration ranges (expressed as average of maximum and minimum values) of DO, cBOD₅, COD, total coliform, and *E. coli* in the effluents of Cells 1, 2, 3, and 4.

	Unit		Effluents			
			Cell 1	Cell 2	Cell 3	Cell 4
DO	mg L ⁻¹	Average	1.49	2.21	9.05	4.57
		Range	3.61±3.48	2.41±2.23	8.59±3.91	5.74±3.54
cBOD ₅	mg L ⁻¹	Average	62.71	26.4	7.61	1.05
		Range	103±98.5	48.1±46.2	18.9±18.2	1.59±0.59
COD	mg L ⁻¹	Average	143	72.1	28.4	34.0
		Range	194±154	154±119	39.2±26.0	64.2±47.8
Total coliform	CFU 100 mL ⁻¹	Average	1.76 x10 ⁶	9.04 x10 ⁴	2.42 x10 ³	2.61 x10 ²
		Range	6.06x10 ⁶ ±6.06x10 ⁶	5.87x10 ⁵ ±5.87x10 ⁵	1.21x10 ⁴ ±1.21x10 ⁴	1.21x10 ³ ±1.21x10 ³
<i>E. coli</i>	CFU 100 mL ⁻¹	Average	3.31 x10 ⁵	3.00 x10 ⁴	1.26 x10 ³	1.02 x10 ²
		Range	1.24x10 ⁶ ±1.24x10 ⁶	2.42x10 ⁵ ±2.42x10 ⁵	1.21x10 ⁴ ±1.21x10 ⁴	1.21x10 ³ ±1.21x10 ³

Chapter 5

Transport and Attenuation of Pharmaceutical Compounds and Acesulfame-K in a Demonstration-scale Wastewater Treatment System

5.1 Executive Summary

The occurrence of pharmaceutically active compounds (PhACs), an artificial sweetener, and other wastewater constituents derived from a septic system, and subsequent removal in an engineered wetland with an integrated phosphate-removal system were investigated. Water samples from four locations in the treatment system and effluent from three subsequent treatment cells were collected and analyzed to evaluate rates of removal. The PhACs evaluated in this study covered a range of octanol-water partition coefficients and acid dissociation constants, and included carbamazepine, caffeine, sulfamethoxazole, ibuprofen, and naproxen. The study also evaluated the occurrence and treatment of acesulfame-K, a commonly used artificial sweetener. The concentrations of caffeine, carbamazepine, sulfamethoxazole, ibuprofen, naproxen and acesulfame in the septic system effluent were between 5.2 and 61 $\mu\text{g L}^{-1}$, 0.15 and 9.3 $\mu\text{g L}^{-1}$, 0.003 and 0.1 $\mu\text{g L}^{-1}$, 19-70 $\mu\text{g L}^{-1}$, 2.3 and 13 $\mu\text{g L}^{-1}$, and 35 and 94 $\mu\text{g L}^{-1}$, respectively. Based on the removal efficiencies, the PhACs were classified into four different groups, including those that were a) efficiently removed with >75% removal (e.g. caffeine), b) moderately removed with 50-75% removal (e.g. ibuprofen), c) poorly removed with 25-50% removal (e.g. sulfamethoxazole and naproxen), and d) very poorly removed or recalcitrant with <25% removal

(e.g. carbamazepine). Acesulfame-K was classified as category “d”. Removal efficiencies of P, ammonia and cBOD₅ in the treatment system were 62 and >99%. The mean flow rate in the system was 0.89 m³ day⁻¹ (0.02 to 4.27 m³ day⁻¹) representing a hydraulic retention time of 5 days. Variability in concentrations and treatment efficiencies were observed in different sampling events, which may be due to variations in input concentrations or changes in flow rate.

5.2 Introduction

Pharmaceutically active compounds (PhACs) consumed by humans and animals for therapeutic purposes, and excreted as metabolized or non-metabolized forms, may be released from sewage treatment plants (STPs), and other wastewater treatment systems, and subsequently introduced to the aquatic environment (Daughton and Ternes, 1999). A wide variety of PhACs and/or their metabolites have been detected in wastewater (Ternes, 1998; Heberer, 2002; Lishman et al., 2006; Castiglioni et al., 2006; Carrara et al., 2008; Spongberg and Witter, 2008; Jelic et al., 2011), surface water (Ternes, 1998; Halling-Sørensen et al., 1998; Daughton and Ternes, 1999; Kolpin et al., 2002; Tixier et al., 2003; Sanderson, 2011), groundwater (Sacher et al., 2001; Ternes et al., 2007; Carrara et al., 2008; Fram and Belitz 2011), and drinking water (Ternes et al., 2002; Webb et al., 2003; Benotti et al., 2009; Bruce et al., 2010; Sanderson, 2011; Fram and Belitz 2011). The metabolized forms of some PhACs (derived from oxidation, reduction or hydrolysis reaction) often become more reactive and more toxic than the parent compounds (Halling-Sorensen et al., 1998). However, in the aquatic environment the metabolites may revert to the parent compounds or be modified further (Bendz et al., 2005). This chapter is focused on the occurrence, transport, and removal of PhACs including carbamazepine, sulfamethoxazole,

caffeine, ibuprofen, and naproxen as these are frequently observed in the environment. An artificial sweetener acesulfame-K is also included in the analysis for the same reason.

Caffeine, ibuprofen, and naproxen are typically removed in conventional wastewater treatment plants with high efficiencies (>99, 90, 69, and 66%); but carbamazepine (-25 to 96%) and sulfamethoxazole (-25%) are often highly persistent (Ternes, 1998; Heberer, 2002b; Metcalfe et al., 2003; Bendz et al., 2005; Dordio et al., 2010). There was no significant effect of hydraulic retention time on the removal efficiency of neutral drugs including carbamazepine in sewage treatment plants. Metcalfe et al. (2003) reported poor or negative removal of carbamazepine with increasing hydraulic retention time. The interpretation of concentration data for influent and effluent samples requires caution for these because of the potential for changes in influent concentrations within the hydraulic retention over a particular sampling event (Metcalfe et al., 2003). Although changes in influent concentration may occur for any component, these changes may be particularly significant for the PhACs because of the very low concentrations of these compounds.

Studies focused on removal of the selected PhACs in alternative wastewater treatment systems indicate variable results. For example, removal of PhACs in a series of mesocosm-scale constructed wetlands with different configurations was evaluated by Hijosa-Valsero et al. (2010). Results show that the concentrations of carbamazepine decreased by 24-36% in winter and 48% in summer, ibuprofen decreased by 51- 54% in winter and 85-96% in summer during flow through a floating-macrophyte surface-flow constructed wetland; concentrations of caffeine decreased by 58- 65% in winter and 99% in summer during flow through a horizontal subsurface

flow constructed wetland; and concentrations of naproxen decreased by 66% in winter and 83% in summer during flow through a planted horizontal subsurface flow constructed wetland.

Although a very high percentage of removal of individual PhACs was observed for each constructed wetland evaluated, no single constructed wetland is able to remove all compounds. However, a wastewater treatment plant with a combination of a series of aerated lagoons, constructed wetlands, a UV disinfection unit, and a natural forested wetland removed 51% of carbamazepine, >90% of sulfamethoxazole and gemfibrozil, and $\geq 99\%$ of caffeine, ibuprofen, and naproxen from wastewater (Conkle et al., 2008). Additional studies (Matamoros and Bayona, 2006; Matamoros et al., 2007, 2008; Hijosa-Valsero et al., 2010; Zhang et al., 2011) reported that wetlands constructed for PhAC removal are more efficient than conventional wastewater treatment plants not designed for PhAC removal.

Studies on the occurrence and fate of artificial sweeteners in the environment indicate relative persistence of these compounds in the environment. Acesulfame-K is one of the artificial sweeteners commonly used in food, beverages, and other products. Acesulfame-K is detected in a wide variety of water samples including untreated and treated wastewater (12-46 $\mu\text{g/L}$; Buerge et al., 2009; Van Stempvoort et al., 2011a), surface waters (Buerge et al., 2009), groundwater (Buerge et al., 2009; Scheurer et al., 2009; Van Stempvoort et al., 2011a), septic system plumes (Van Stempvoort et al., 2011b) and tap water (up to 2.6 $\mu\text{g/L}$; Buerge et al., 2009). Remediation of artificial sweeteners including Acesulfame-K was observed after natural organic matter and hydroxyl radical scavengers are removed from the water (Toth et al., 2012). Steel slag has been used in previous laboratory and field investigations to treat phosphorus-rich water (Baker et al., 1998; Smyth et al., 2002a; Kim et al., 2006; Bowden et al., 2009). This material was not

evaluated previously for treating wastewater containing PhACs and artificial sweeteners. In particular the removal of PhACs and artificial sweetener using BOFS and ZVI has not been considered.

In this study, the removal of selected PhACs (including carbamazepine, caffeine, sulfamethoxazole, ibuprofen, and naproxen) and acesulfame-K were evaluated in a demonstration-scale treatment system. The demonstration system consisted of four treatment cells. The first treatment cell is a horizontal subsurface flow cell filled with granitic gravel and vegetated with cattails, *Typha spp* (Figure 5.1). The second treatment cell is a down flowing, vertical surface flow force bed aerated cell filled with granitic gravel and vegetated with cattails, *Typha spp*. The third treatment cell is a down-flow vertical surface-flow cell filled with basic oxygen furnace slag (BOFS) and zero valent iron (ZVI). The fourth treatment cell is a pH adjustment cell equipped with a CO₂ sparger. Wastewater was sampled at different stages along the treatment system over six sampling events to evaluate the treatment effectiveness under a range of operational conditions.

5.3 Materials and Methods

5.3.1 Chemicals/ chemical standards

Carbamazepine, naproxen, sulfamethoxazole, ibuprofen and caffeine were obtained from Sigma Aldrich Canada Ltd., Oakville, Ontario, Canada. Isotope-labelled internal standards (IS) were used to quantify each analyte. The type of IS and the properties of each analyte and IS(s) are provided in Table 5.1. Sulfamethoxazole d₄ was obtained from Toronto Research Chemicals

(Toronto, ON, Canada) and all other IS(s) were obtained from CDN Isotopes (Quebec, Canada). Nanopure water (Milli-Q, Billerica, MA) was provided through the use of a 0.45 µm Millipore Q-Gard1 unit. High performance liquid chromatography (HPLC) grade methanol (MeOH) (99.9%), ammonium acetate, formic acid, acetic acid and acetonitrile were obtained from Caledon Laboratories Ltd. (Georgetown, ON, Canada).

5.3.2 Field methods

5.3.2.1 System configuration

Samples were collected from a multi-stage Engineered Wetland (EW)-Phosphate treatment system which was installed in Autumn 2009 at the Center for Alternative Wastewater Treatment, Fleming College, Lindsay, Ontario. A detailed description of these cells including dimensions of the cells, pore volume of each cell, and physical and chemical characteristics of the reactive materials including basic oxygen furnace slag (BOFS) and zero valent iron (ZVI) are provided in Chapter 4. Briefly, the influent of the treatment system, wastewater, was received from a pre-treatment septic tank (Cell 1). The treatment system consisted of four treatment stages including a vegetated horizontal subsurface flow engineered wetland (Cell 2), a vegetated vertical subsurface-flow aerated engineered wetland (Cell 3), a phosphate-treatment cell (Cell 4), and a pH-adjustment unit (Cell 5). The effluent from Cell 1 passed through Cells 2 through 5 in sequence prior to being released into the City of Kawartha Lakes sewer system (Figure 5.1). Flow was monitored continuously with an automatic flow meter with interruptions when the meter was clogged. Flow volume was calculated based on the periods when flow was

automatically monitored. During other times, flow rates were assumed to be consistent with the periods when monitoring data was available.

5.3.2.2 Sampling Procedure

Water samples were collected throughout the treatment system for analysis of PhACs, acesulfame-K, and other water quality parameters. All samples were filtered with 0.45 μm cellulose acetate filters prior to preservation. Samples for PhAC and acesulfame-K analyzes were collected in 500 ml amber glass bottles using a sampling pump with dedicated tubing and filters and acidified to $\text{pH} < 2$ with 18 N H_2SO_4 . The samples for PhACs and acesulfame-K were collected from each cell effluent except Cell 5 (pH adjustment cell), because this unit was not regulated systematically during the sampling events. Analyzes were performed within 3 days of sample collection. Duplicates of each sample were collected in the field and archived in a freezer. Field blanks for PhACs consisted of MilliQ water collected using the same collection and preservation methods like other samples in the field to evaluate whether contamination occurred during the filtering process or transport. The trip blanks for PhACs were unfiltered MilliQ water (brought to the field) samples collected directly from a plastic container in the field without using a pump and preserved in the same manner as the other samples to determine whether any contamination occurred in from the bottles and during the transport. All samples were maintained at 4⁰C until analysis. The results for six sampling events (SE), conducted between Feb 2010 and Jan 2011, are reported here.

The values of pH, Eh, and alkalinity were measured onsite immediately after the samples were collected following the same procedure as described in Chapter 3. Samples, field and trip blanks

were collected for analysis of cations, anions, PO₄-P, and NH₄-N following the same collection and preservation methods as describe in Chapter 3.

The samples were collected during winter and pre-spring period. The average minimum and maximum air temperatures were -4.0 and 17.6° C and the influent sample temperatures were between 4.3 and 14.2°C. There was a sampling event during the summer months as well. However, data obtained from this sampling event was not included in this discussion because of poor data quality. The samples were stored at 4° C (instead of freezing) for more than six months before analysis, jeopardizing data quality.

5.3.3 Analytical methods

Samples were analyzed to determine dissolved concentrations of major cations, trace metals, and Cl, NO₂, NO₃, SO₄, PO₄, and NH₃ using the methods described in Chapter 3. The concentrations of the PhACs including carbamazepine, caffeine, sulfamethoxazole, ibuprofen, and naproxen, were determined using high performance liquid chromatography electrospray tandem mass spectrometry (HPLC-ESI-MS/MS). The analytical procedure utilized was modified from procedures described by Vanderford et al. (2006) and Stafiej et al. (2007). Unique isotopically labelled compounds were added to each sample prior to analysis for use as IS(s).

Solid-phase extraction (SPE) was performed on samples (180 ml) spiked with a mixture of the six IS(s). Oasis HLB 5 mL glass cartridges were used for SPE and the pressure maintained below 10psi for the vacuum to facilitate percolation of the samples through the cartridges. Prior to loading the samples, the cartridges were prepared by loading 5 ml HPLC grade MeOH (5%, v/v) and 5 ml MilliQ water. After loading the samples the cartridges were washed with 5 ml HPLC

grade MeOH (5%, v/v). Finally, 6 ml of MeOH (2 ml at a time) was loaded to the cartridges and extracts were collected in amber glass bottles and preserved at 4°C until analysis. The samples were spiked to achieve a final concentration of 1 µg L⁻¹ of each IS after the extraction process. Internal standards were employed to account for potential loss of analyte during the SPE steps and to account for matrix effects during analysis (Gros et al., 2007).

The nebulizer gas at the ionization source and the collision gas used to fragment the parent ion was N₂. A multiple reaction monitoring scan (MRM) was utilized for quantification, using a ratio between the analyte peaks to that of the corresponding internal standard.

Analyzes of caffeine, carbamazepine and sulfamethoxazole were conducted in positive ESI mode. A Symmetry RP18 column (Waters Corporation, Mississauga, ON, Canada) with a length of 50 mm, an internal diameter of 4.6 mm, and a particle size of 3 µm was used for separation. The rate of solvent flow through the column was 1.25 mL min⁻¹, with an injection volume of 15 µL. Mobile phase “A” consisted of 5 mM ammonium acetate and 0.1 % formic acid in nanopure water. Mobile phase “B” was 100 % MeOH with 0.1 % formic acid. The gradient started at 15 % for mobile phase “B”, and after 0.76 min increased to 100 %, then at 2.5 min decreased back to 15 % until 4 min was reached.

Naproxen, gemfibrozil, ibuprofen, and acesulfame were analyzed in negative ESI mode. An XDB-C18 column (Agilent Technologies, Mississauga, ON, Canada) with a length of 150 mm, an internal diameter of 4.6 mm and a particle size of 5 µm was used. The flow rate through the column was 1 mL min⁻¹, with a total injection volume of 10 µL. Mobile phase “A”, at pH 4, was 30 % acetonitrile diluted with nanopure water with 6.9 mM acetic acid. Mobile phase “B” was

100 % acetonitrile. The gradient started at 0 % of mobile phase “B”, at 18 min increased to 3 %, at 22 min to 12%, 40 min to 40 %, and ended at 45 min at 0 %.

5.3.3.1 Quality Control and Quality Assurance

In addition to the use of internal standards, additional calibration blanks (CB) and calibration verification (CV) samples were analyzed on a continuous basis to ensure that cross contamination between injections was minimal and to assess recovery of the analytes. The CCB samples were MeOH/H₂O, 50/50 v/v. The CCV solutions were prepared from an independent stock solution than the calibration standards. A CCV sample (MeOH/H₂O, 50/50 v/v spiked with IS and analytes) was analyzed directly after each CCB to ensure ongoing acceptable calibration performance during analysis of each batch of samples. This calibration pair (CCB and CCV) was analyzed after initial calibration, after every ten samples, and at the end of the analysis. The CCV values were within ±15% of expected values (Table 5.2).

Standards prepared in water, including aqueous blanks which consisted of MilliQ water spiked with IS were analyzed for each batch of SPE. Quality control samples (QCS) were prepared from MilliQ water spiked with analytes of different concentrations and the mixture of ISs. An aqueous blank and a QCS were processed through the SPE with each set of 10 samples. The aqueous blank samples were used to check any cross contamination and the recovery of the IS. The QCSs were used to check whether there was any loss of IS or analytes during storage, SPE, and analysis.

The calibration range was 0.1-40 µg L⁻¹ with 9 calibrators and calibration curve was linear (R² > 0.9999). The LOD and LOQ for caffeine, carbamazepine, and sulfamethoxazol were 10 ng L⁻¹

and 20-100 ng L⁻¹. The LOD and LOQ for ibuprofen, and naproxen were 5-200 ng L⁻¹ and 10-500 ng L⁻¹, after correcting for dilution prior to reporting the concentration of the respective compounds. Recoveries of the internal standards in the CCV samples, QC samples, and samples from the treatment system were between 90 and 125% (Table 5.2). Recoveries of the IS in the QC samples for the selected PhACs were between 72 and 127% (Table 5.2). Recoveries of IS for caffeine and carbamazepine, with few exceptions, were between 82 and 121% in all of the samples collected during the sampling events except the fourth (between 52 and 68%). For sulfamethoxazole, IS recoveries were, with few exceptions, between 92 and 121% in SE 1, 2, and 3. However, recoveries for sulfamethoxazole were between 15 and 58% in SE 4, between 121 and 160% in SE 5, and between 55 and 75% in SE 6 (Table 5.3). Recoveries of IS for ibuprofen were between 75 and 86% in SE 1, 2, and 5, between 58 and 72 in SE 3 and 4, and between 32 and 45% in SE 4 (Table 5.3). Recoveries of IS for naproxen were between 86 and 96% in SE 1, between 62 and 74% in SE 5 and 6 and between 6 and 35% in SE 2, 3, and 4 (Table 5.3). The reported concentrations were corrected for the observed recoveries of IS for each event.

5.4 Results and Discussion

The physical and chemical characteristics of BOFS and ZVI used in this system are provided in Chapter 4. The flow rate was dependent on the availability of septic tank effluent, which was proportional to the on campus student population in different times of the year. The observed flow rate was highly variable ($\sigma=625$) during the study period. The mean flow rate was calculated to be 0.89 m³ day⁻¹ during the study period. Hydraulic retention time (HRT) is one of

the major factors for the removal efficiency of PhACs (Conkle et al., 2008). The average HRT in Cells 2, 3, and 4 were 7.6, 7.6, and 6.0 days.

5.4.1 Characteristics of wastewater

The chemical composition of the effluent of the treatment cells reflected the pH conditions in each of the cells (Table 5.4). The pH in Cells 1, 2, and 3 was slightly alkaline (8.17 ± 0.79 in cell 1, 8.66 ± 0.96 in cell 2, and 7.76 ± 0.35 in cell 3). In Cell 4, the pH increased substantially up to 10.87 ± 1.46 and a corresponding elevated total alkalinity was observed at the onset of the experiment (maximum 1620 mg L^{-1} as CaCO_3 ; Figure 5.2). The total alkalinity in Cell 4 effluent decreased with time as the cell was flushed with the near neutral effluent from Cell 3, likely due to leaching of free lime (CaO) and portlandite (Ca(OH)_2) from the outer layer of the BOFS during the course of the study. The high pH effluent from Cell 4 was neutralized in Cell 5 (indoor pH adjustment tanks; Figure 5.3). The highest mean Eh was observed in Cell 3 effluent and the lowest mean Eh was observed in Cell 1 effluent (Figure 5.2). Low mean dissolved oxygen (DO) concentrations were observed in the effluents of Cell 1 (1.61 mg L^{-1}) and Cell 2 (2.26 mg L^{-1}), indicating relatively anoxic conditions in these cells. High average DO concentrations, up to 8.93 mg L^{-1} , were observed in Cell 3 effluent. However, the DO concentrations decreased significantly (mean concentration, 4.70 mg L^{-1}) in Cell 4 effluent. Mean concentrations of $\text{NH}_3\text{-N}$ were 50, 53, 21, and 19 mg L^{-1} in effluent collected from Cells 1, 2, 3, and 4, indicating a decrease along the flow path (Figure 5.2). In contrast, concentrations of $\text{NO}_3\text{-N}$ were 9, 2, 49, and 43 mg L^{-1} , showing an increase along the flow path. The calculated ratios of $\text{NH}_3\text{-N}/\text{NO}_3\text{-N}$ decreased from 5.56 to 0.44, showing the influence of oxidation

reactions. The presence of the fresh ZVI layer added to Cell 4 may have initially led to the reduction of NO_3 to NH_3 . Reduction of NO_3 to NH_3 by ZVI is reported in previous studies (Rahman and Agrawal, 1997). Thus, the changes in Eh values were directly proportional to the changes in DO and $\text{NO}_3\text{-N}$ concentrations and inversely proportional to the changes in $\text{NH}_3\text{-N}$ concentration along the flow path.

5.4.2 Carbonaceous biochemical oxygen demand (cBOD₅)

High concentrations of cBOD₅ were observed in Cell 1 effluent (mean, 99.12 mg L⁻¹). Mean cBOD₅ concentrations in Cells 2, 3, and 4 were 49.5, 16.1, and 0.83 mg L⁻¹. The cBOD₅ removal efficiencies in Cells 2, 3, and 4 were 50, 34, and 15%. Thus the overall cBOD₅ removal efficiency in the treatment system was >99%. The removal of cBOD₅ in Cell 2 can be explained by the influence of plants, which introduced atmospheric O₂ in the system through the roots. The residual amount of cBOD₅ in the wastewater after treatment in Cell 3 was removed in Cell 4, which suggests that highly alkaline conditions in Cell 4 can successfully lead to degradation of the remaining labile organic compounds. Both cBOD₅ and NH₃ removal efficiencies in Cell 3 were considerably higher (33.7% and 63.9%; Figure 5.2) than in other cells. The high oxidation-reduction potential measurements in the Cell 3 effluent resulted from the aeration of the cell. The cBOD₅ removal efficiency in Cell 3 indicates that the aerobic degradation was the dominant mechanisms removing organic matter. These results are consistent with previous studies (Brix and Arias, 2005; Matamoros et al., 2007). A sharp increase in NO_3 and a decrease in NH_3 in Cell 3 suggest that higher NO_3 concentrations were derived from the oxidation of NH_3 (Figure 5.2).

5.4.3 Pharmaceutical compounds (PhACs)

The results of the analyses of effluent samples collected along the treatment system indicate a general decrease in concentrations of the majority of the PhACs analyzed (Figure 5.4, 5.5; Table 5.4), with the notable exception of carbamazepine which showed little change along the treatment system. The influent concentrations fluctuated, likely in response to changes in the student population in the college. For example, the presence of relatively high concentrations of pharmaceutical compounds including ibuprofen, naproxen and carbamazepine in the Cell 2 effluent compared to the Cell 1 effluent (system influent) in some of the sampling events suggests carryover from earlier loading events. The presence of trace concentrations of all of the PhACs in the last cell for most sampling events indicates some degree of persistence even for the more reactive compounds.

Mean initial concentrations of ibuprofen, naproxen, caffeine, carbamazepine, sulfamethoxazole, and acesulfame-K were 47, 8.8, 23, 3.6, 0.06, and 66 $\mu\text{g L}^{-1}$ (Figure 5.5, Table 5.4). The removal efficiencies of these PhACs and artificial sweetener are shown in Table 5.4.

The P-values from the t-tests (two-sample assuming unequal variance) for the pooled sample sets (concentrations of each chemical in 6 sampling events) were obtained from EXCEL. The p-values from the t-tests for the compounds (concentrations of caffeine between Cells 1 and 4, Cells 2 and 4; ibuprofen between Cells 1 and 3, Cells 1 and 4, Cells 2 and 3, and Cells 2 and 4; naproxen between Cells 2 and 4) were less than 0.05. Thus the null hypothesis would be rejected and there were statistically significant differences observed (Table 5.5). In contrast, the p-values from the t-tests for the the rest of the compounds (caffeine, ibuprofen, and naproxen with other

cell combinations and carbamazepine, sulfamethoxazole, and acesulfame-K with all cell combinations) were greater than 0.05. Thus the null hypothesis would not be rejected, indicating no significant differences were observed. However, for selected sampling dates (e.g. Feb, 09, 2010: caffeine, carbamazepine, ibuprofen and acesulfame-K; Apr 06, 2010: caffeine, ibuprofen, acesulfame-K; Apr 13, 2010: ibuprofen, naproxen, and acesulfame-K; Dec 10, 2010: ibuprofen, and naproxen; and Jan 28, 2011: ibuprofen and acesulfame-K) obvious decreases in concentrations were observed, suggesting removals on these dates.

5.4.3.1 Analgesic anti-inflammatory drugs

Ibuprofen is a non-steroidal anti-inflammatory drug. Ibuprofen is considered as one of the most biodegradable PhACs (Dordio et al., 2010). There were no significant changes in concentrations observed in Cell 2 effluent and the mean concentration increased slightly to $48.0 \mu\text{g L}^{-1}$ relative to the system influent. The concentration increase in Cell 2 can be explained by the carryover from the previous loads and the variation of input concentrations. A sharp decrease in concentrations with a mean concentration of $23.7 \mu\text{g L}^{-1}$ was observed in Cell 3 effluent. An additional decrease in concentrations with a mean concentration of $19.0 \mu\text{g L}^{-1}$ was observed in Cell 4 effluent. The concentration profile showed decreasing trend along the flow path from Cell 2 effluent. The removal efficiency for ibuprofen in Cell 3 (52%) was consistent with other studies (Matamoros and Bayona, 2006; Hijosa-Valsero et al., 2010). For example, Matamoros and Bayona (2006) observed similar to slightly greater removal of ibuprofen under more oxidizing conditions in a shallow bed subsurface flow constructed wetland (50-80% removal efficiency). In this study, all samples were collected in winter and early spring. The removal

efficiencies for ibuprofen observed in this study (range: 38-75%, mean: 60%) were slightly higher than the removal efficiencies observed by Hijosa-Valsero et al. (2010) (range: 27-74%) and by Castiglioni et al. (2006) (range: 25-72%, mean: 38%) in winter months. However, about 82% removal of ibuprofen in winter is reported by Dordio et al. (2010). The aeration process increased the amount of oxygen in Cell 3, which favoured the aerobic biodegradation of ibuprofen. A positive linear correlation between redox potential and the removal efficiency for ibuprofen was observed in this study, which is consistent with observations by Hijosa-Valsero et al. (2010).

Naproxen is also a non-steroidal anti-inflammatory drug. The concentration profile of naproxen was similar to that of ibuprofen along the flow path. The concentrations of naproxen increased in Cell 2 effluent relative to the system influent, with a mean concentration of 11.04 $\mu\text{g L}^{-1}$ then gradually decreased in Cells 3 and 4 effluents with mean concentrations of 7.82 and 5.44 $\mu\text{g L}^{-1}$. In this treatment system, naproxen showed much lower removal efficiency (39%) than ibuprofen (60%). However, this removal rate was consistent with values reported by Matamoros and Bayona (2006) and Hijosa-Valsero et al. (2010).

5.4.3.2 Stimulant

Caffeine is a stimulant drug ingested in food, beverages and medicinal products. A decreasing trend was observed along the flow path, where the mean concentrations in Cells 2, 3, and 4 effluents were 18.85, 6.64, and 4.14 $\mu\text{g L}^{-1}$. The sharp drop in concentrations in Cell 3 effluent compared to Cell 2 effluent was similar to the change observed for ibuprofen.

The total removal efficiency for caffeine was 82%, which was the highest removal observed for the drugs investigated in this study. The removal efficiencies for caffeine observed in this study (sampled in winter and early spring time) were higher than removal efficiencies reported for winter months in a previous study (Hijosa-Valsero et al., 2010), and approached the higher rates reported for summer months. Hijosa-Valsero et al. (2010) showed removal efficiency in summer (average temperature 19.9 °C) was approximately three times greater than the rates observed in winter (average temperature 7 °C).

5.4.3.3 Anti-epileptic drug

Carbamazepine is an anticonvulsant and antidepressant drug. Mean concentrations of carbamazepine in the effluent from Cells 2, 3, and 4 were 4.07, 3.77, and 3.89 $\mu\text{g L}^{-1}$. An increase in concentrations was observed in the Cell 2 effluent compared to the Cell 2 influent. A small decrease in concentrations was observed in the Cell 3 effluent with respect to the Cell 2 effluent. In the first two cells, carbamazepine concentrations showed a trend that was similar to the trends observed for caffeine, ibuprofen, and naproxen. However, this drug did not show similar decreasing trend in Cell 4 effluent. Although the mean removal efficiency for carbamazepine was about 8% in Cell 3 with respect to Cell 2 effluent, the overall mean removal efficiency for this compound in the treatment system was negative 9% (Figure 5.6). This was the most recalcitrant pharmaceutical compound analyzed in this study. The recalcitrant nature of carbamazepine is widely reported in the available literature (Matamoros et al., 2007; Conkle et al., 2008; Matamoros et al., 2008, Zhang et al., 2011). However, about 96% removal in summer and 88% removal in winter are reported by Dordio et al. (2010).

5.4.3.4 Sulfonamide

Sulfamethoxazole is an antibiotic drug. A decrease in concentrations of 32% was observed in Cell 2 effluent ($0.003\text{-}0.08\ \mu\text{g L}^{-1}$). This removal may be explained by oxidation reactions in this aerated cell. However, the actual cause of this attenuation was unclear. The mean concentrations remain the same in Cells 3 and 4 effluent. Neither Cell 3 (6% removal) nor Cell 4 (4% removal) provided significant removal of sulfamethoxazole. Sulfamethoxazole has been reported to be relatively recalcitrant, closely resembling carbamazepine, in terms of biodegradation (Benotti and Brownawell, 2009; Suarez et al., 2010). Removal efficiencies for sulfamethoxazole were 24% in a conventional sewage treatment plant (Ternes et al., 2007). Higher removals have been observed in other studies (as high as 78%) especially in systems with long hydraulic retention times of 30 days (Conkle et al., 2008). In this study, removal efficiencies of sulfamethoxazole were about 32% in Cell 2 at a mean HRT of 7.6 days, about 5.6% in Cell 3 at a mean HRT of 7.6 days, and about 4.4% in Cell 4 at a mean HRT of 6.0 days.

The removal efficiencies of sulfamethoxazole in Cells 3 and 4 were similar to the extent of removal (38%) reported in a laboratory experiment at a low biomass concentration (Alexy et al., 2004). However, Al-Ahmad et al. (1999) reported no biodegradation of sulfamethoxazole in a closed bottle test and also noted that only a small group of bacteria present in the inoculum are affected by sulfamethoxazole. High biomass conditions usually favor biodegradation of sulfamethoxazole (Batt et al., 2007). Thus, >30% removal efficiency for sulfamethoxazole in Cell 2 (32%) is attributed to the higher biomass in this cell because it was well vegetated and existed long before the other cells were reconstructed.

Among the treatment cells, the removal of caffeine, carbamazepine, and naproxen was greater in Cell 3 compared to other cells, likely due to the oxidizing conditions in this cell, which favoured aerobic degradation. Based on the removal efficiency observed during this study, the selected PhACs can be classified in to four different groups a) efficiently removed with >75% removal (e.g. caffeine), b) moderately removed with 50-75% removal (e.g. ibuprofen), c) poorly removed with 25-50% removal (e.g. sulfamethoxazole and naproxen), and d) very poorly removed or recalcitrant with <25% removal (carbamazepine).

5.4.4 Artificial sweetener

Acesulfame-K is a commonly used artificial sweetener. The concentrations of this sweetener were gradually decreased along the flow path, where the mean concentrations of Cells 2, 3, and 4 were 58.5, 54.2, and 48.7 $\mu\text{g L}^{-1}$. The removal efficiencies of acesulfame-K in Cells 2, 3, and 4 were 12.0, 6.4 and 8.4%. Thus the treatment system removed ~27% acesulfame-K from wastewater. The presence of hydroxyl radicals (due to dissociation of CaO and Ca(OH)₂) and low natural organic matter (very low cBOD₅ concentrations) in Cell 4 was expected to favor Acesulfame-K removal (Toth et al., 2012). However, the removal was not very extensive. The mechanism of Acesulfame-K removal in Cell 2 was not clear.

5.4.5 Removal mechanisms

5.4.5.1 Acid dissociation constant (pK_a) and ionic forms

Although the target PhACs have similar molecular weights, the octanol-water partitioning coefficients and hydrophobicity of these compounds are different. The compounds analyzed in

this study covered a range of octanol-water partition coefficients and acid dissociation constants. Ibuprofen, naproxen, and sulfamethoxazole are expected to dissociate predominantly into their anionic forms in the treatment system, as the pH values of each treatment cell effluent including the septic tank effluent (system influent) were greater than the pK_a values of these compounds (Table 5.1, Figure 5.7). The pH values in the first 3 cells (Cells 1, 2, and 3) were less than the pK_a value of caffeine, whereas the pH in Cell 4 was greater than the pK_a value of caffeine (Figure 5.7). These conditions indicated that this compound was predominantly in a neutral form in the first 3 cells and in its anionic form in the 4th cell. The pH values of each cell effluent were substantially less than the pK_a value of carbamazepine, thus, the compound was predominantly in its neutral form in all of the cells (Figure 5.7). Adsorption of negatively charged compounds onto aquifer materials (including calcium carbonate and calcium phosphate) is generally not expected under high pH conditions. However, due to the presence of metal oxides with a high pH of zero point charge (pHzpc) including 33% CaO (pHzpc=8.1; Hanawa et al., 1998), 24% Fe₂O₃ (pHzpc=6.9; Parks, 1965), 8-9% MgO (pHzpc=12.4; Parks, 1965), and 4-6% Al₂O₃ (pHzpc=9.1; Parks, 1965) in BOFS media, adsorption of the negatively charged compounds in Cell 4 may still be possible. Moreover, upon continuous flushing with wastewater, labile CaO and Ca(OH)₂ would be removed from the outer layer of the BOFS, and would lead to a decrease in generation of alkalinity. Adsorption and/or precipitation of other inorganic compounds may coat the outer layer of the BOFS grains and restrict the CaO and Ca(OH)₂ from dissolving to create alkaline condition. Precipitation of calcite (CaCO₃, pHzpc= 9.5; Parks, 1965), and hydroxyapatite (Ca₅OH(PO₄)₃, pHzpc=7.6; Davis and Kent, 1990) on the outer layer of BOFS, was indicated by FTIR spectra, may also favor adsorption of negatively charged compounds. Based on the

decreasing trend of pH it can be predicted that over time with continuous flushing the pH of Cell 4 is expected to decrease potentially leading to improved removal of PhACs.

5.4.5.2 Hydrophobicity

Compounds can be classified on the basis of log K_{ow} values as hydrophilic (log K_{ow}<1; Verliefe et al., 2008; Ney, 1990), intermediate or transphilic (1>log K_{ow}<3; Verliefe et al., 2008), and hydrophobic (log K_{ow} >3; Verliefe et al., 2008). Amiard-Triquet et al. (2011) further classified the hydrophobic compounds as moderately hydrophobic (3<log K_{ow} <7) and very hydrophobic (log K_{ow} >7). Due to acid-base transformation of the insoluble organic compounds, pH-dependent octanol-water distribution coefficients (log D_{ow} values) can be calculated and are usually distinctly different than the intrinsic hydrophobicity when partial or complete dissociation takes place (log K_{ow}, Nghiem and Hawkes, 2009). The log D_{ow} expresses the relationship between K_{ow}, pH and pK_a and can be calculated using the following equation (Stuer-Lauridsen et al., 2000).

$$(5.1) \quad \log D_{ow} = \frac{K_{ow}}{1 + 10^{pH - pKa}}$$

The log D_{ow} values vary substantially from the log K_{ow} for acidic drugs that dissociate under the pH conditions at the site. This difference has important implications on the fate and transport of the PhACs. It is anticipated that caffeine, sulfamethoxazole, and naproxen would display a hydrophilic nature in the treatment cells (with pH between 7.38 and 12.32) based on the log D_{ow} values (<1) (Figure 5.8). Carbamazepine showed intermediate hydrophobicity and did not show any significant change (log D_{ow} from 2.45 to 2.44) under the range of pH values observed in the treatment system (Figure 5.8). Ibuprofen showed very low to low hydrophobicity (log D_{ow}>1)

below pH 7.82 (Figure 5.8). However, carbamazepine was transported through the system, despite its low to moderate hydrophobicity.

5.4.5.3 Aeration

Aeration, which creates oxidizing conditions, is an important factor affecting the attenuation of several PhACs. Removal of caffeine, acetaminophen, and naproxen often exceeds 99% from the influent concentrations (Conkle et al., 2008). Aeration also facilitates volatilization, a function of Henry's coefficient (K_H) and the air flow contacting the wastewater, which is one of the removal mechanisms of pharmaceutical compounds in STPs (Carballa et al., 2007). The compounds studied are not expected to be volatile, nor was the aeration aggressive. Therefore, attenuation of these compounds, particularly in Cell 3, is attributed to the presence of oxidizing conditions. Moreover, based on the decreasing trend of pH it can be predicted that over time with continuous flushing the pH of Cell 4 is expected to decrease potentially leading to improved removal of PhACs.

5.4.5.4 Reduction through ZVI

Constructed wetland treatment systems designed for the removal of pharmaceutical compounds commonly use gravel and/ or sand as a substrate (Matamoros and Bayona, 2006; Matamoros et al., 2007; Hijosa-Valsero et al., 2010; Zhang et al., 2011). ZVI has been used as reactive media for the removal of metals from groundwater (Blowes et al., 2000; Morrison et al., 2002) and occasionally for the removal of antibiotics from aqueous solution (Ghauch et al., 2009) and for the degradation of the pharmaceutical diazepam (Bautitz et al., 2012). In Cell 4, a reactive zone containing ZVI was placed at the bottom of Cell 4 and the DO concentration in the effluent of

Cell 4 was much lower than Cell 3 effluent. Zero valent iron promotes the reduction of water through the reaction



ZVI is oxidized to Fe^{2+} in the presence of H_2O (predominant electron receptor), leading to an increase in pH and a decrease in redox potential (Zhang, 2003; Reardon, 2005; Wei et al., 2010). Although an increase in the pH does not favor adsorption of the pharmaceutical compounds on the surfaces of the substrates, reducing conditions created due to the presence of ZVI may have contributed to additional treatment in Cell 4.

5.4.5.5 Other potential removal mechanisms

In addition to the above removal mechanisms, there is potential for removal of pharmaceuticals compounds through degradation reactions. Hydrolytic degradation is one of the most common degradation pathways for organic contaminants in the environment. The hydrolysis of organic compounds involves substitution of an atom or group of atoms by water or hydroxide ions. Hydrolysis reactions, however, are not expected to be an important degradation process in the environment for caffeine, carbamazepine, and naproxen due to the lack of hydrolysable functional groups in these chemicals (Lyman et al., 1990). Ibuprofen is not expected to undergo hydrolysis as carboxylic acid functional groups are generally resistant to hydrolysis (Lyman et al., 1990). Under field conditions, hydrolysis also is not a likely degradation process for sulfamethoxazole (Lam et al., 2004) or acesulfame-K (Buerge et al. 2009). While there is potential for additional removal mechanisms, this study did not focus on delineation of those mechanisms.

5.5 Conclusions

The overall treatment efficiencies observed in the multi-cell system evaluated in this study were similar to those observed in large scale wastewater treatment systems and comparable to mesocosm-scale constructed wetlands. The removal of the PhACs was strongly correlated to the measured pH and Eh values. The highly alkaline condition of Cell 4 likely promoted dissociation of some compounds, enhancing the mobility (i.e. sulfamethoxazole and ibuprofen). Aeration is an important factor affecting the attenuation of caffeine, carbamazepine, ibuprofen, and naproxen. Incorporation of BOFS and ZVI may have provided this additional removal. Although the system was operated during the winter and early spring, the treatment performance observed for caffeine and ibuprofen were higher than that observed in similar wastewater treatment systems during winter periods.

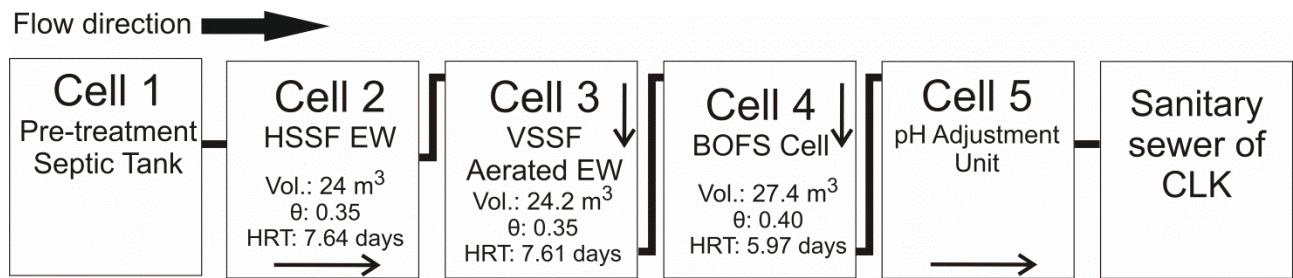


Figure 5.1 Schematic diagram of the outdoor cells of the EW-BOFS pilot-scale treatment system. Cell 2 represents a horizontal subsurface flow constructed wetland, Cell 3 represents a vertical subsurface flow aerated engineered wetland, and Cell 4 contains a mixture of BOFS and ZVI. Wastewater was continuously flushed through the system by a combination of gravity feed and pumping (from Chapter 4). In this diagram HSSF EW represents horizontal subsurface flow engineered wetland, VSSF aerated EW represents vertical subsurface flow aerated engineered wetland, BOFS represents basic oxygen furnace slag, and CLK represents City of lake Kawartha.

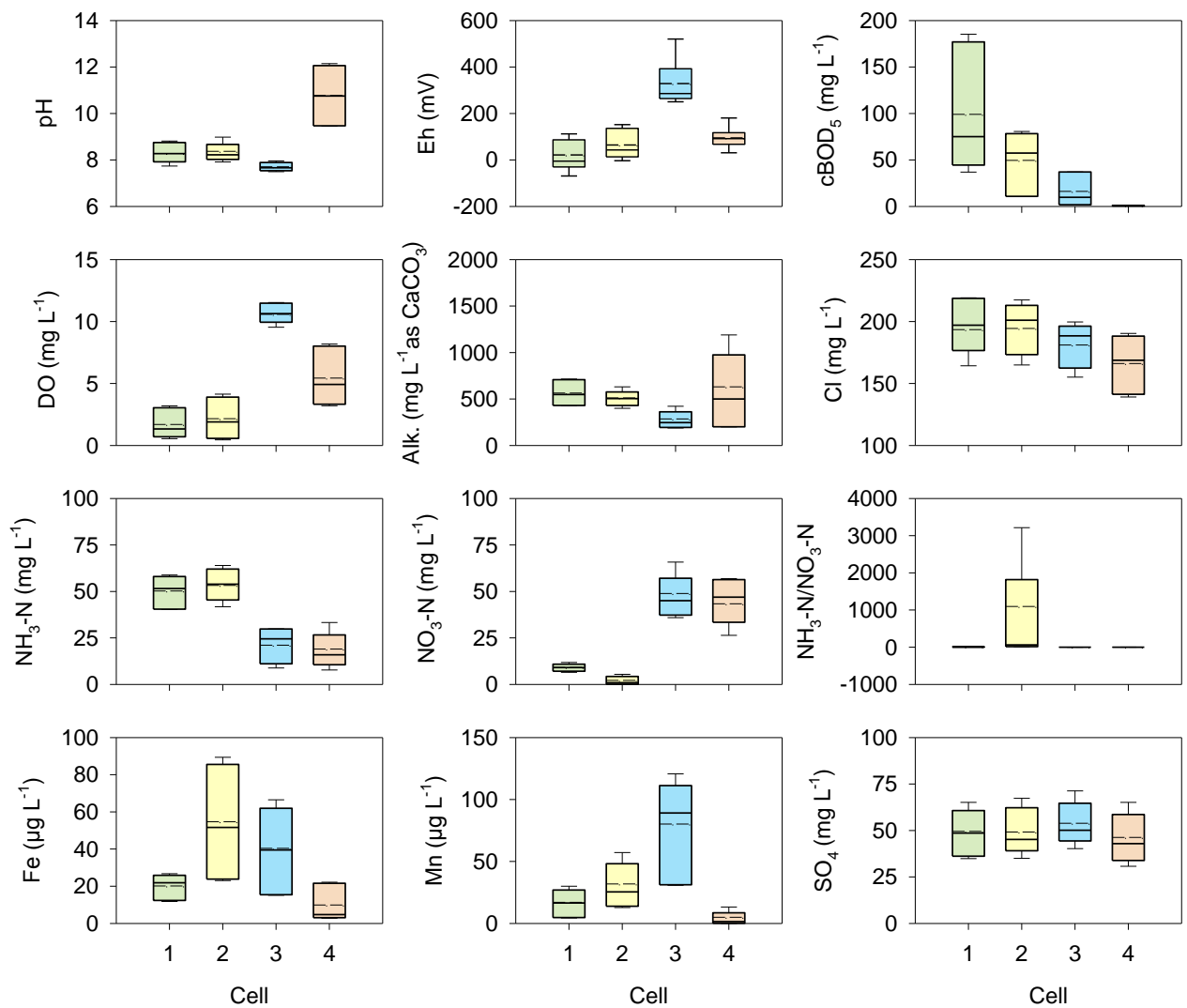


Figure 5.2 Box plots of pH, alkalinity, Eh, cBOD₅, DO, Cl, NH₃-N, NO₃-N, NH₃-N/NO₃-N, Fe, Mn, and SO₄ versus distance (Cells 1-4) along the treatment flow path. Horizontal solid lines and broken lines on the boxes represent median and mean concentrations.

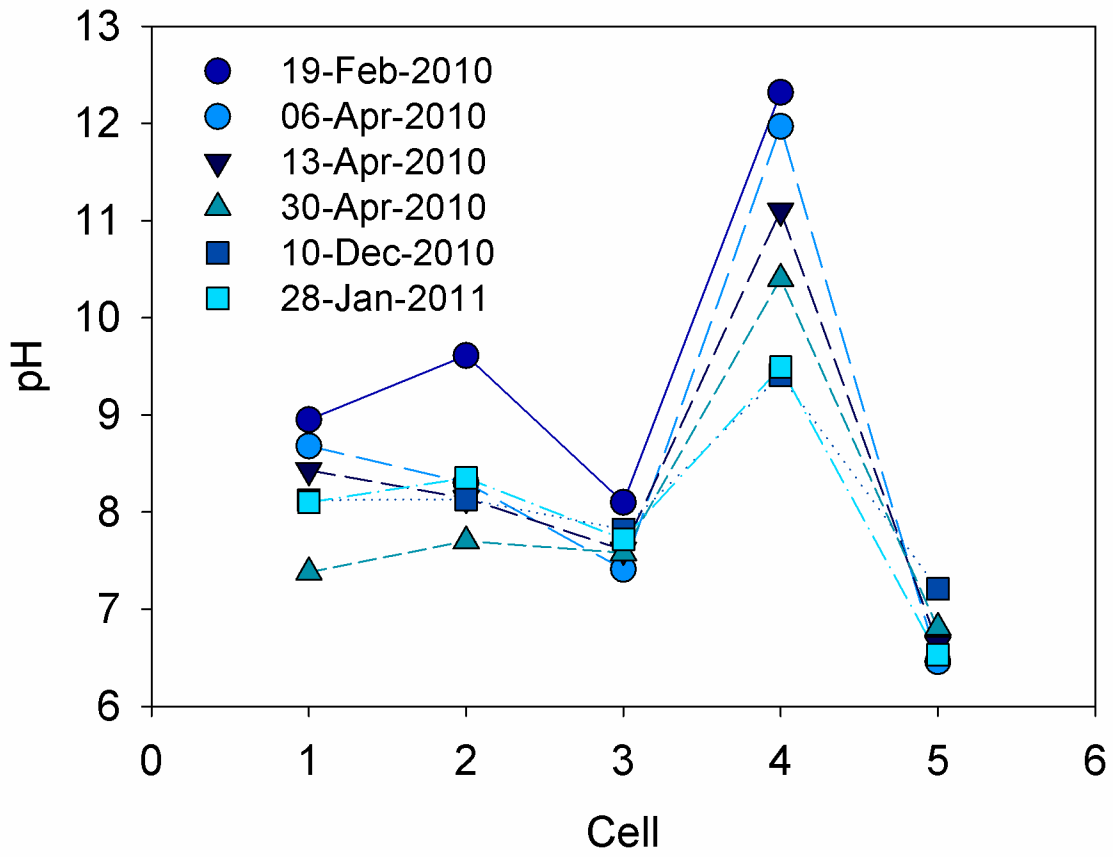


Figure 5.3 pH versus distance (Cells 1-5) along the treatment flow path.

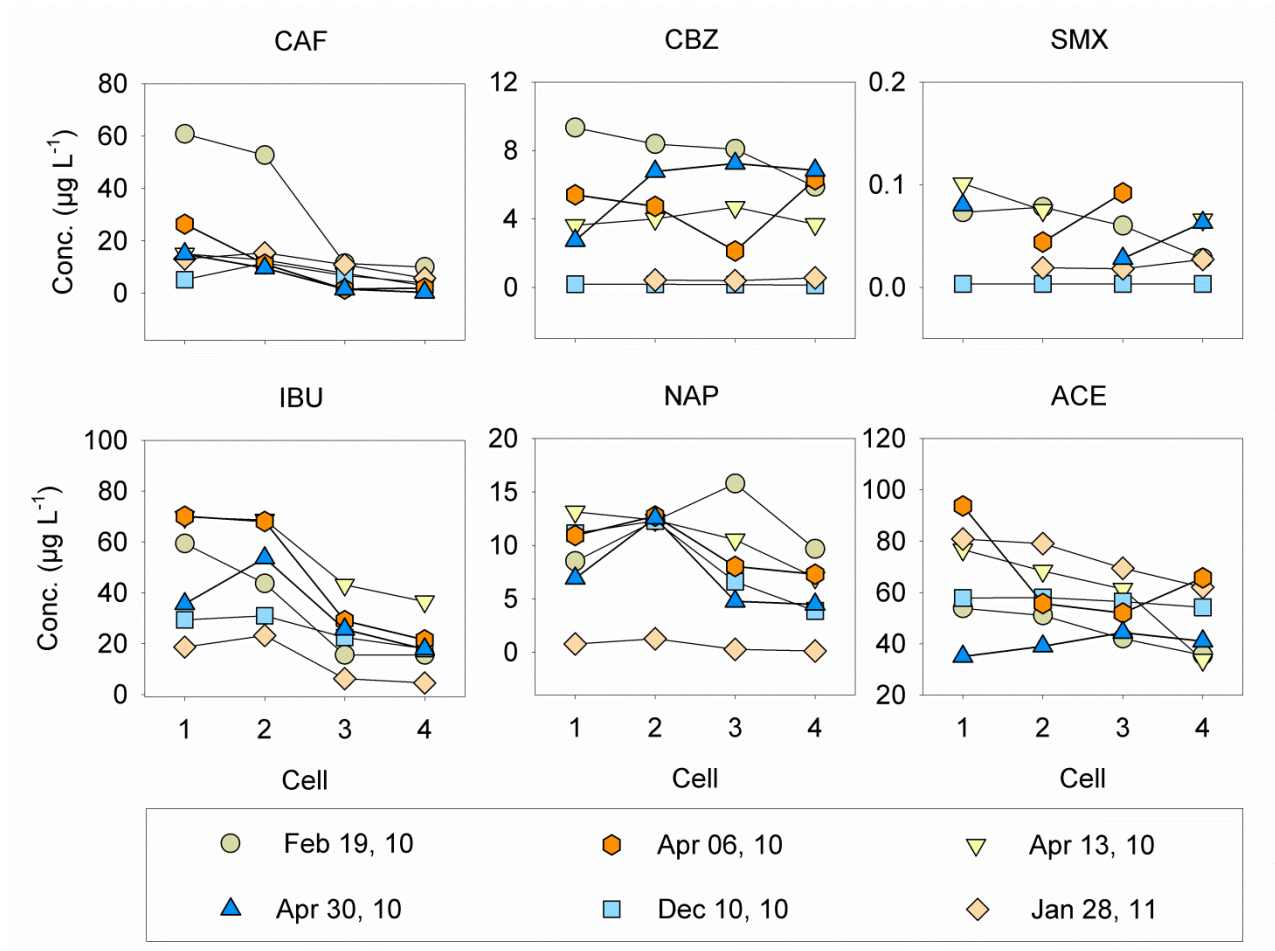


Figure 5.4 Selected pharmaceutical compounds, caffeine (CAF), carbamazepine (CBZ), sulfamethoxazole (SMX), ibuprofen (IBU), naproxen (NAP), and an artificial sweetener, acesulfame-K (ACE), along the treatment flow path.

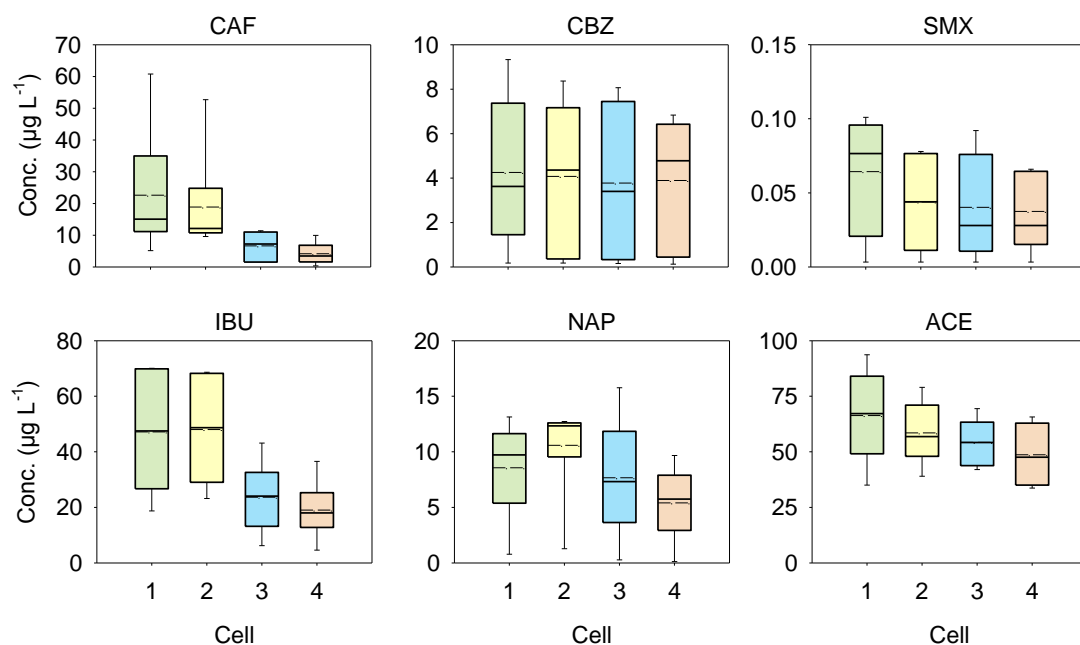


Figure 5.5 Box plots of selected pharmaceutical compounds, caffeine (CAF), carbamazepine (CBZ), sulfamethoxazole (SMX), ibuprofen (IBU), naproxen (NAP), and an artificial sweetener, acesulfame-K (ACE), along the treatment flow path. Horizontal solid lines and broken lines on the boxes represent median and mean concentrations.

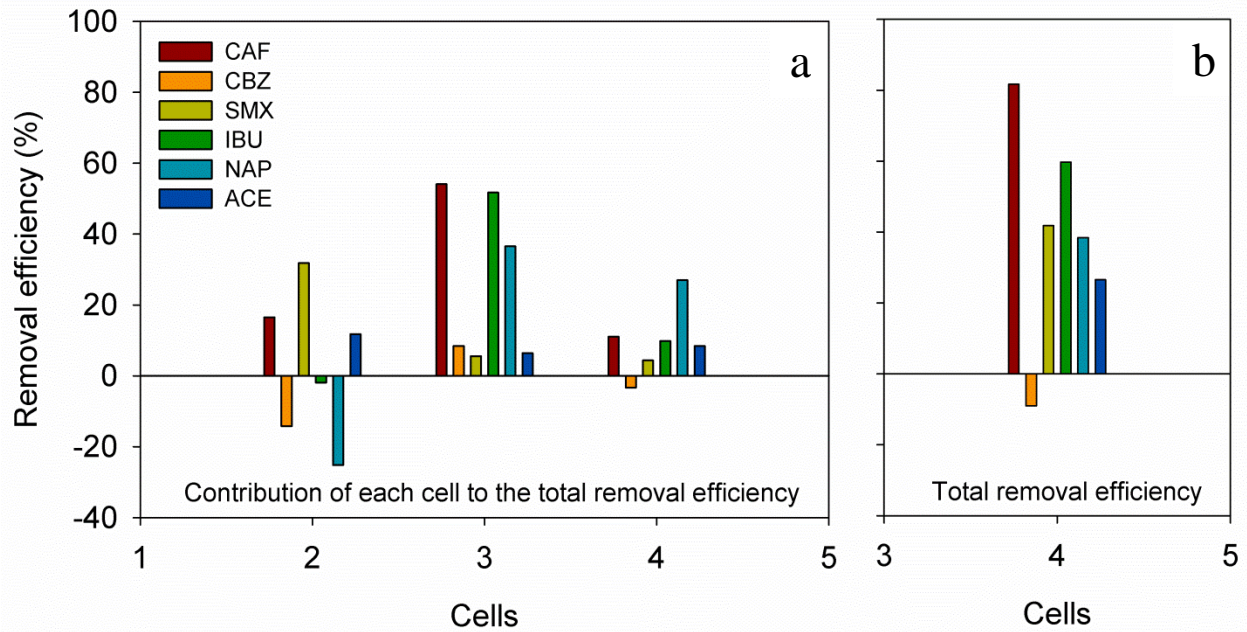


Figure 5.6 Selected pharmaceutical compounds, caffeine (CAF), carbamazepine (CBZ), sulfamethoxazole (SMX), ibuprofen (IBU), naproxen (NAP), and an artificial sweetener, acesulfame-K (ACE), along the treatment flow path. a) Contribution of each cell to the total removal efficiency, b) total removal efficiency.

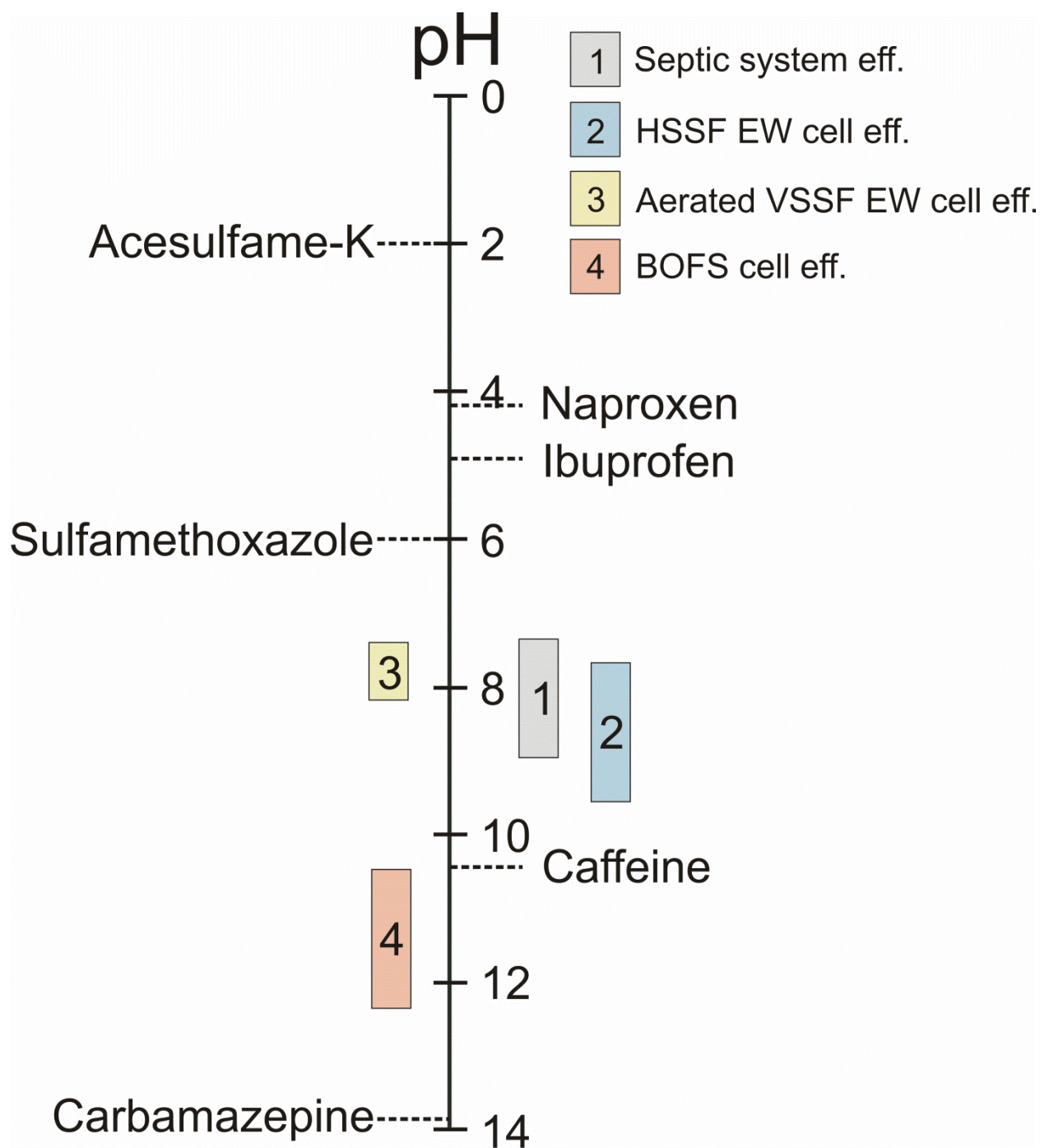


Figure 5.7 pKa of each pharmaceutical of interest plotted on the pH scale with dotted lines and the pH range of the treatment cells (Cells 1-4) shown with vertical bars.

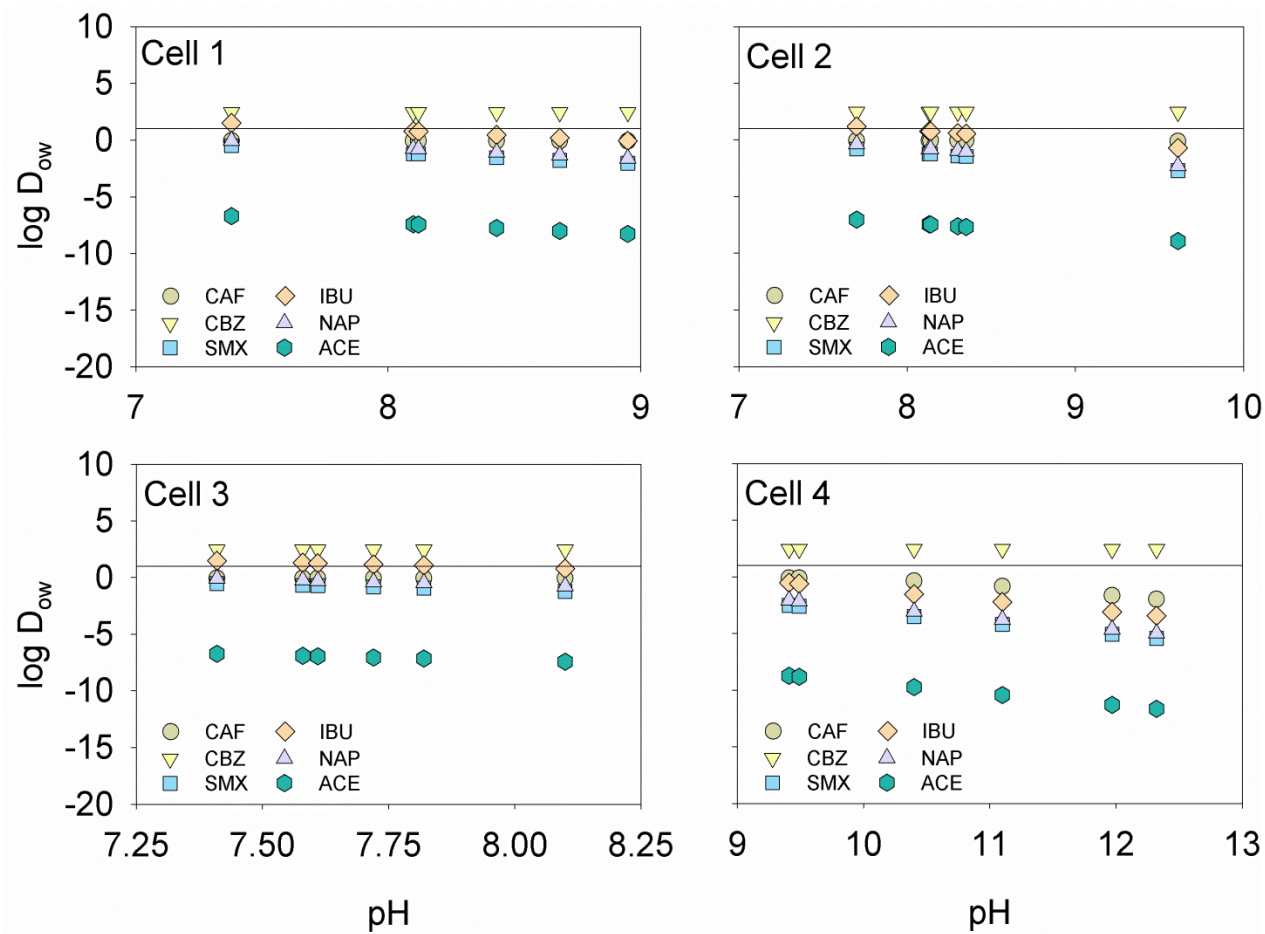
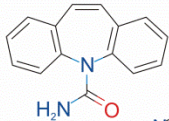
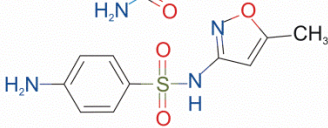
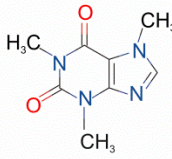
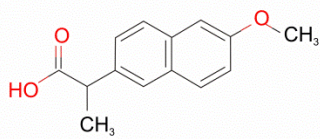
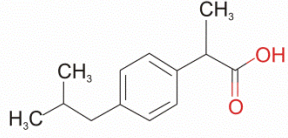
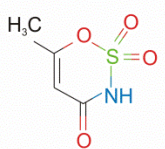


Figure 5.8 Calculated values of $\log D_{ow}$ versus pH in the influent (Cell 1 effluent) and three other treatment cells (Cells 2, 3, and 4).

Table 5.1 Chemical properties and structures of pharmaceutically active compounds (Trenholm et al., 2006) and artificial sweetener, along with their molecular weights. Molecular weights of the internal standards are also provided.

	Drug Class	Chemical Structure of Analyte	Molecular Weight (g mol ⁻¹)	log K _{ow}	Solubility (mg L ⁻¹)	pK _a
Carbamazepine Carbamazepine d ₁₀	Anticonvulsant, antidepressant		236.27 246.33	2.45	17.7	13.9
Sulfamethoxazole Sulfamethoxazole d ₄	Antibiotic		253.28 257.30	0.89	610	6
Caffeine Caffeine d ₃	Stimulant		194.19 197.21	-0.07	21.6	10.4
Naproxen Naproxen ¹³ C	Non-steroidal anti-inflammatory		230.26	3.18	15.9	4.15
Ibuprofen Ibuprofen d ₃	Non-steroidal anti-inflammatory		206.28 209.30	3.97	21	4.91
Acesulfame-K	Artificial sweetener		163.20 ^a	-1.33 ^b	270000 ^c	~2 ^d

^aScheurer et al., 2009; ^bToxnet; ^cVon Rymon Lipinski, 1985; ^dRudan-Tasic et al. 2011

Table 5.2 Quality control samples and preparation blanks, continuing calibration verification and continuing calibration blanks.

	ACE	CBZ	CAF	SMX	IBU	GEM	NAP
LOD (ng L-1) Limit of detection	50	0.1	3	3	10	3	30
LOQ (ng L-1) Limit of quantification	70	9	30	10	80	10	250
<hr/>							
Internal Standard Recovery %	ACE	CBZ	CAF	SMX	IBU	GEM	NAP
Samples	33	119	101	104	113	119	81
Trip Blank	59	97	104	84	88	90	80
Field Blank	50	96	73	108	95	78	93
Preparation Blank (PRB)	12	90	98	102	122	113	74
Quality control samples (QCS)	20	95	98	98	118	94	72
Continuing calibration verification (CCV)	20	113	97	116	120	125	90
<hr/>							
Analyte Recovery %	ACE	CBZ	CAF	SMX	IBU	GEM	NAP
Quality control samples (QCS)	105	106	127	118	105	105	72
Continuing calibration verification (CCV)	85	97	102	103	98	91	87
Continuing calibration blank (CCB)	<LOD	<LOD	<LOD	<LOD	<LOD	<LOD	<LOD
Recovery sample different dilutions %	115	117	110	200	127	111	105
<hr/>							
Standards Range (ng L-1)	1000- 100000	20- 2000	50- 2000	50- 2000	100- 40000	10- 40000	50- 40000
Correlation coefficient %	0.9998	0.9999	0.9993	0.9998	0.9997	0.9993	0.9991
<hr/>							
<p>Quality control samples and preparation blank samples were prepared with every set of samples. Continuing calibration verification and continuing calibration blank samples were analyzed every 5 or 10 samples. SPE factor (30) and the dilution factor (10) were considered on the calculation of LOD and LOQ.</p>							

Table 5.3 Internal standard recoveries of laboratory blanks, trip blanks, field blanks, continuous calibration blank (CCB), and continuous calibration verification (CCV) of each analysis during the study period.

Sampling event 1(SE 1): 19-Feb-10										
Standard Recovery	Lab Blank		Trip Blank		Field Blank		CCB		CCV	
	Conc. (µg/L)	IS Rec. (%)	Conc. (µg/L)	IS Rec. (%)	Conc. (µg/L)	IS Rec. (%)	b Conc. (µg/L)	Comments	Conc. (µg/L)	Accuracy (%)
CAF	0.125	117	<0	128	0.027	90	3.1	<LOD	2	101
							1.8		20	102
							5.3		0.02	92
CBZ	0.063	110	0.0096	97	0.011	96	-	<LOD	2	N/A
							-		20	100
							-		0.02	90
SMX	0.007	N/A	No Peak	N/A	No Peak	N/A	No Peak	<LOD	2	105
							0.88		20	101
							0.60		0.02	87
IBU	<0	84	0.004	88	0.021	95	-	<LOD	0.05	N/A
							-		0.5	101
							-		10	102
NAP	0.023	45	0.83	86	0.041	99	-	<LOD	0.05	188
							-		0.5	95
							-		10	87

Table 5.3 continued

SE 2: 6-Apr-10										
Standard Recovery	Preparation Blank		Trip Blank		Field Blank		CCB		CCV	
	Conc. (µg/L)	IS Rec. (%)	Conc. (µg/L)	IS Rec. (%)	Conc. (µg/L)	IS Rec. (%)	b Conc. (µg/L)	Comments	Conc. (µg/L)	Accuracy (%)
CAF	<0	106	<0	120	<0	105	17	-	-	-
							101		10	113
							12		1	107
CBZ	0.06	105	0.036	109	0.048	122	-	-	-	-
							-		10	77
							-		1	102
SMX	0.022	131	No Peak	123	No Peak	144	-	-	-	-
							4.0		10	82
							-		1	79
IBU	No Peak	28	No Peak	45	No Peak	54	-	-	-	-
							-		5	96
							-		10	112
NAP	0.607	8	No Peak	29	0.26	16	-	-	-	-
							-		5	94
							-		10	71

Table 5.3 continued

SE 3: 13-Apr-10										
Standard Recovery	Lab Blank		Trip Blank		Field Blank		CCB		CCV	
	Conc. (µg/L)	IS Rec. (%)	Conc. (µg/L)	IS Rec. (%)	Conc. (µg/L)	IS Rec. (%)	b Conc. (µg/L)	Comments	Conc. (µg/L)	Accuracy (%)
CAF	<0	106	<0	133	<0	95	17	-	-	-
							101		10	113
							12		1	107
CBZ	0.0597	105	No Peak	118	0.009	95	-	-	-	-
							-		10	77
							-		1	102
SMX	0.0217	131	No Peak	169	No Peak	107	-	-	-	-
							-		-	-
							-		-	-
IBU	No Peak	28	No Peak	47	No Peak	26	-	-	-	-
							-		-	-
							-		-	-
NAP	0.607	8	No Peak	16	No Peak	8	-	-	-	-
							-		-	-
							-		-	-

Table 5.3 continued

SE 4: 30-Apr-10										
Standard Recovery	Lab Blank		Trip Blank		Field Blank		CCB		CCV	
	Conc. (µg/L)	IS Rec. (%)	Conc. (µg/L)	IS Rec. (%)	Conc. (µg/L)	IS Rec. (%)	b Conc. (µg/L)	Comments	Conc. (µg/L)	Accuracy (%)
CAF	-	-	-	-	-	-	74	-	-	-
							No Peak		2	83
							80		10	99
CBZ	-	-	-	-	-	-	-	-	-	-
							2.5		2	96
							-		0.2	95
SMX	-	-	-	-	-	-	1.3	-	-	-
							5.2		2	99
							2.1		0.1	99
IBU	No Peak	40	-	-	-	-	-	-	-	-
							-		5	108
							-		10	107
NAP	No peak	7	-	-	-	-	-	-	-	-
							-		5	99
							-		10	89

Table 5.3 continued

SE 5: 10-Dec-10										
Standard Recovery	Lab Blank		Trip Blank		Field Blank		CCB (b conc. in µg/L)		CCV	
	Conc. (µg/L)	IS Rec. (%)	Conc. (µg/L)	IS Rec. (%)	Conc. (µg/L)	IS Rec. (%)	b Conc. (µg/L)	Comments	Conc. (µg/L)	Accuracy (%)
CAF	-	-	-	-	<10	85	-	-	-	-
							-		0.5	114
							-		2	109
CBZ	-	-	-	-	<10	128	-	-	-	-
							-		0.5	84
							-		2	107
SMX	-	-	-	-	<10	147	-	-	-	-
							-		0.5	106
							-		2	103
IBU	No Peak	66	-	-	-	-	-	-	-	-
							-		0.5	207
							-		1	211
NAP	-	-	-	-	-	-	-	-	-	-
							-		-	-
							-		-	-

Table 5.3 continued

SE 6: 28-Jan-11										
Standard Recovery	Lab Blank		Trip Blank		Field Blank		CCB (b conc. in µg/L)		CCV	
	Conc. (µg/L)	IS Rec. (%)	Conc. (µg/L)	IS Rec. (%)	Conc. (µg/L)	IS Rec. (%)	b Conc. (µg/L)	Comments	Conc. (µg/L)	Accuracy (%)
CAF	-	-	-	-	<10	84	-	-	-	-
							-		-	
							-		-	
CBZ	-	-	-	-	<10	117	-	-	-	-
							-		-	
							-		-	
SMX	-	-	-	-	<10	114	-	-	-	-
							-		-	
							-		-	
IBU	No Peak	70	-	-	-	-	-	-	-	-
							-		-	
							-		-	
NAP	-	-	-	-	-	-	-	-	-	-
							-		-	
							-		-	

Table 5.4 Values of pH, Eh, alkalinity and the concentration range of the pharmaceuticals and acesulfame-K in the influent and the treatment cells.

	Unit	Cell 1 effluent (System influent)	Cell 2 (HSSF-EW cell) effluent	Cell 3 (VSSF-AEW cell) effluent	Cell 4 (BOFS cell) effluent	Removal efficiency contributed by each cell with respect to mean initial concentration (%)			Overall Removal efficiency
						Cell 2	Cell 3	Cell 4	
pH		7.38-8.96	7.70-9.65	7.41-8.11	12.32-				
Eh	mV	-69 to 112	-4 to 152	250 to 520	30 to 180				
Alkalinity	mg L ⁻¹ as	425-729	340-740	175-540	200-1620				
Caffeine	μg L ⁻¹	range	5.2-61	9.6-53	1.5-11	0.32-10			
		mean	23	19	6.6	4.1	17	54	11
Carbamazepine	μg L ⁻¹	range	0.15-9.3	0.17-8.4	0.16-8.1	0.12-6.8			
		mean	3.6	4.1	3.8	3.9	-14	8.4	-3.3
Sulfamethoxazole	μg L ⁻¹	range	0.003-0.1	0.003-0.08	0.003-0.09	0.003-0.07			
		mean	0.06	0.04	0.4	0.04	32	5.6	4.4
Ibuprofen	μg L ⁻¹	range	19-70	23-69	6.2-43	4.6-37			
		mean	47	48	24	19	-1.9	52	9.8
Naproxen	μg L ⁻¹	range	2.3-13	4.0-13	1.2-16	0.29-9.7			
		mean	8.8	11	7.8	5.4	-25	37	27
Acesulfame-K	μg L ⁻¹	range	35-94	39-79	42-69	34-66			
		mean	66	59	54	49	12	6.4	8.4

Table 5.5 P-values obtained from t-Test, two-sample assuming unequal variances, for Cells 1-2, 2-3, 3-4, 1-3, 1-4, and 2-4 for the selected chemicals

P(T<=t) two-tail	Cell 1-2	Cell 1-3	Cell 1-4	Cell 2-3	Cell 2-4	Cell 3-4
CAF	0.73	0.11	0.08	0.13	0.09	0.29
CBZ	0.93	0.82	0.86	0.88	0.92	0.95
SMX	0.46	0.40	0.32	0.87	0.75	0.89
IBU	0.59	0.05	0.03	0.03	0.01	0.50
NAP	0.45	0.75	0.19	0.33	0.05	0.40
ACE	0.47	0.25	0.12	0.56	0.25	0.45

Chapter 6

Conclusions

6.1 Summary of Findings

Removal of phosphorus (P) from hypolimnetic water and from wastewater is dependent on the pore water chemistry and the composition of the reactive media. Basic Oxygen Furnace Slag (BOFS) based treatment materials removed 83 to >99 % of the initial P from the influent surface water and wastewater. In addition to BOFS cells, the upstream aerated cells in the constructed wetland systems contributed to removal of P from wastewater.

Geochemical modelling (using PHREEQCI) calculations based on the representative water chemistry data from the treatment systems (described in Chapters 2, 3, and 4) indicated supersaturation of the pore water with respect to hydroxyapatite, β -tricalciumphosphate, brucite, calcite, and aragonite. The presence of calcium phosphate mineral(s) on the outer layers of the spent reactive media was confirmed through multiple analytical techniques including FE-SEM-EDX, XPS, FTIR, and XANES analysis, which was consistent with the geochemical modelling results. FE-SEM-EDX techniques were used to estimate the elemental composition of the fresh BOFS and the precipitates collected from the outer layer of the spent media. The solid-phase P contents (in wt. %) were proportional to the aqueous P concentrations in the influent water for the treatment systems described in Chapters 2 and 3. X-ray photoelectron spectroscopic analysis showed limited indications of the formation of CaP minerals on the spent media (described in Chapters 2 and 3) possibly due to the low penetration depth of this technique and interference of calcium carbonate. Fourier transform infrared (FTIR) spectroscopy was used to identify

phosphate and carbonate functional groups on the outer layer samples of the spent media. FTIR spectra reported for phosphate and carbonate minerals in previous studies and those obtained from the standard materials analyzed in this study were used to infer the mineralogical composition of the precipitates. The presence of calcite in the samples was confirmed by FTIR spectroscopy (Chapters 2, 3, and 4). Although some samples showed well defined phosphate peaks (Chapter 3), it was not possible to confirm the presence of any specific CaP mineral. Very weak peaks of phosphate in the FTIR spectra for samples collected from the hypolimnetic treatment system (Chapter 2) reflect the low P concentration of the influent lake water.

Accumulation of P at the interfaces between spent BOFS grains was confirmed through elemental maps of polished cut-sections which indicated an abundance of P at the edges of the grains and low concentrations of P in the inner parts of the grains. ATR-FTIR spectra indicated the occurrence of P-bearing minerals at corresponding locations. However, samples with low P contents did not show distinct differences between the outer layers of the spent BOFS grains and the interior of the grains. X-ray absorption near edge structure (XANES) spectra indicated the occurrence of CaP minerals on the outer layers of the spent reactive media. Linear combination fitting allowed a comparison of spectra from the treatment system samples with the CaP and FeP standards, and calculation of the proportions of the contributing phosphate species. The predicted CaP minerals included hydroxyapatite, β -TCP, CPD, CPDD, and α -TCP depending on the locations and concentrations of solid phase P of the samples.

In addition to phosphate removal, the removal of other wastewater components was observed in the constructed wetland systems. Aeration processes in the force bed aerated cells enhanced the oxidation of ammonia and sharp decreases in $\text{NH}_4\text{-N}$ concentrations were observed. Although a significant positive mass change of total nitrogen (N mass loss, ~72%) was observed

in the indoor treatment system as discussed in chapter 3, a very low positive mass change (only 2%) was observed in the outdoor treatment system as described in chapter 4. Extensive decreases in (>99% removal) in concentrations of pathogens (*E.coli* and total coliform) were observed in the aerated cells of the constructed wetland systems. High pH conditions generated in BOFS-containing P-treatment cells (Cell 4 in Chapter 3 and Cell 4 in Chapter 4) provided further disinfection.

Concerns associated with the use of BOFS include the release of high pH effluent and dissolved Al and V following contact with the BOFS media. Effluent pH values varied between 8.08 and 12.35 depending upon the source and age of the slag. The elevated pH (often >12) was adjusted to near neutral conditions through sparging with CO₂. Neutral pH conditions favoured a decrease in the concentration of Al (leached from BOFSs) due to its amphoteric nature. A ZVI layer at the end of the BOFS layer removed excess V leached from BOFS effluent.

The PhACs, including caffeine, ibuprofen, naproxen, carbamazepine, sulfamethoxazole, and an artificial sweetener acesulfame-K were detected in the influents of the demonstration-scale wastewater treatment system. An aerated cell (Cell 3 in Chapter 5) was more effective at removing caffeine, carbamazepine, ibuprofen, and naproxen than the other treatment cells. However, concentrations of caffeine, sulfamethoxazole, and acesulfame-K were observed to increase in Cell 2 (in Chapter 5); whereas concentrations of caffeine, sulfamethoxazole, ibuprofen and naproxen decreased in the BOFS cell (Cell 4).

6.2 Scientific Contributions

This thesis presented research related to surface water and wastewater treatment and provided information regarding geochemical changes in aqueous- and solid-phases during the treatment processes. The principal scientific contributions from this thesis include:

- Demonstrating that BOFS is very effective for removing P from surface water and wastewater in pilot-scale systems.
- Demonstrating that the performance of BOFS can be enhanced by restricting atmospheric CO₂ into the reaction columns and cells.
- Identifying reaction products on the outer layers of the spent reactive media (described in Chapters 2, 3, and 4) through the application of surface analytical techniques including FE-SEM-EDX, XPS, FTIR, ATR-FTIR, and synchrotron radiation based XANES methods.
- Evaluating the application of ZVI for the removal of V (leached from the BOFS) from the BOFS column and cell effluents.
- Demonstrating that pH adjustment can be effectively performed by sparging CO_{2(g)} and that this neutralization process also removed Al from BOFS column and cell effluents.
- Demonstrating that attenuation of certain PhACs (caffeine, ibuprofen, naproxen, sulfamethoxazole) and an artificial sweetener (acesulfame-K) was achieved through a combination of an anaerobic EW cell, an aerated EW cell and a BOFS based cell. The persistence of carbamazepine also was observed in these treatment cells.

6.3 Recommendations and Future Work

The BOFS treatment columns and cells were effective in removing P from lake water and wastewater. However, there are some important factors that should be considered in future research, which include potential clogging and subsequent decrease in hydraulic performance in long-term applications. Tight sealing of the BOFS columns/cells restricted the entry of atmospheric CO₂. Thus, no significant decrease in hydraulic performance was noted after sealing the BOFS columns/ cells. However, low to moderate cementation observed in the BOFS columns and cells when these were uncovered to collect spent BOFS for solid-phase analyzes. Despite tight sealing, this cementation may have been taken place when dissolved CO₂ from the previous cells or the ingress of atmospheric CO_{2(g)} through leakage interacted with Ca-rich pore water and/or with the BOFS grains containing lime and portlandite. Although the degree of cementation in the BOFS columns and cells was not critical for the limited flow volumes during the study periods, continuous cementation and subsequent clogging may decrease the hydraulic performance in long-term treatment. This cementation was observed at the inlet part of the BOFS columns and cells in this study. Introducing sacrificial and removable BOFS blocks at the inlet of the system would allow replacement of lower permeability BOFS and ensure the long-term use of this material. Incorporation of a sacrificial chamber of BOFS before the main BOFS column/cell is recommended for future research.

Although BOFS materials are inexpensive, transportation of these materials may be costly. In addition, reuse of the BOFS material would reduce the dumping cost of the spent media. Future research should be directed at evaluating the potential benefits of crushing the spent BOFS materials to smaller sizes, which would increase the surface area and provide fresh reactive

surfaces. The total cost of the BOFS-based treatment system would decrease significantly if the reuse of BOFS can be demonstrated through field-scale experiments.

The addition of ZVI layers used in this study after the BOFS columns/cells was effective in removing V and PhACs (to some extent). Although 5 wt. % ZVI, used in this study led to removal of V for a limited time only, future research should focus on the benefits of increasing the thickness of the ZVI layer and the percentage of ZVI to between 10 and 20%.

The basic oxygen furnace oxide (BOFO) may also be considered in future experiments as BOFO is locally available in some areas where BOFS is not available. Application of BOFO from local sources would also offer lower transport costs. This material potentially could be used with gravel and also with 10-20% BOFS to enhance the efficiency of P removal and ensure adequate hydraulic performance.

References

- Aguilar, M. I., Saez, J., Llorens, M., Soler, A., Ortuno, J. F., 2002. Nutrient removal and sludge production in the coagulation-flocculation process. *Water Res.* 36, 2910-2919.
- Ajiboye, B., Akinremi, O. O., Hu, Y. and Jürgensen, A., 2008. XANES speciation of phosphorus in organically amended and fertilized Vertisol and Mollisol. *Soil Sci. Soc. Am. J.* 72, 1256-1262.
- Al-Ahmad, A., Daschner, F. D., Kümmerer, K., 1999. Biodegradability of Cefotiam, Ciprofloxacin, Meropenem, Penicillin G, and Sulfamethoxazole and inhibition of waste water bacteria. *Arch. Environ. Contam. Toxicol.* 37, 158-163.
- Alexy, R., Kumpel, T., Kümmerer, K., 2004. Assessment of degradation of 18 antibiotics in the Closed Bottle Test. *Chemosphere* 57, 505-512.
- Amiard-Triquet, C., Rainbow, P. S., Roméo, M., 2011. Tolerance to environmental contaminants. In: Newman, M.C. (Ed.), *Environmental and Ecological Risk Assessment*, CRC Press, Boca Raton, Florida, USA, 299-332.
- Andersen, F. A. and Brecevic, L., 1991. Infrared spectra of amorphous and crystalline calcium carbonate. *Acta Chem. Scand.*, 45, 1018-24.
- Andreozzi, R., Marotta, R., Pinto, G., Pollio, A., 2002. Carbamazepine in water: persistence in the environment, ozonation treatment, and preliminary assessment on algal toxicity. *Water Res.* 36, 2869-2877.
- Antonakos, A., Liarokapis, E., Leventouri, T., 2007. Micro-Raman and FTIR studies of synthetic and natural apatites. *Biomaterials.* 28, 3043-3054.
- APHA (American Public Health Association), 1998. *Standard Methods for the Examination of Water and Wastewater*, 20th ed., Washington, D.C.
- APHA (American Public Health Association), AWWA (American Water Works Association), WEF (Water Environmental Federation), 2005. *Standard Methods for the Examination of Water and Wastewater*, Washington, D. C.

- Arvin, E., 1983. Observations supporting phosphate removal by biologically mediated chemical precipitation - a review. *Water Sci. Technol.* 15, 43-63.
- Baker, M. J., Blowes, D. W., Ptacek, C. J., 1997. Phosphorous adsorption and precipitation in a permeable reactive wall: Applications for wastewater disposal systems. *Land Contam. Reclam.* 5, 189-193.
- Baker, M. J., Blowes, D. W., Ptacek, C. J., 1998. Laboratory development of permeable reactive mixtures for the removal of phosphorus from onsite wastewater disposal systems. *Environ. Sci. Technol.* 32, 2308-2316.
- Balan, E., Delattre, S., Roche, D., Segalen, L., Morin, G., Guillaumet, M., Blanchard, M., Lazzeri, M., Brouder, C., Salje, E. K. H., 2011. Line-broadening effects in the powder infrared spectrum of apatite. *Phys. Chem. Minerals.* 38, 111-122.
- Barnes, K. K., Kolpin, D. W., Furlong, E. T., Zaugg, S. D., Meyer, M. T., Barber, L. B., 2008. A national reconnaissance of pharmaceuticals and other organic wastewater contaminants in the United States -I) Groundwater. *Sci. Total Environ.* 402, 192-200.
- Batt, A. L., Kim, S., Aga, D. S., 2007. Comparison of the occurrence of antibiotics in four full-scale wastewater treatment plants with varying designs and operations. *Chemosphere* 68, 428-435.
- Bautitz, I. R., Velosa, A. C., Nogueira, R. F. P., 2012. Zero valent iron mediated degradation of the pharmaceutical diazepam. *Chemosphere.* 88, 688-692.
- Beauchemin, S., Hesterberg, D., Chou, J., Beauchemin, M., Simard, R. R., Sayers, D. E., 2003. Speciation of phosphorus in phosphorus-enriched agricultural soils using X-ray absorption near-edge structure spectroscopy and chemical fractionation. *J. Environ. Qual.* 32, 1809-819.
- Belhadj, E., Diliberto, C., Lecomte, A., 2012. Characterization and activation of Basic Oxygen Furnace slag. *Cement. Concrete. Comp.* 34, 34-40.
- Bendz, D., Paxéus, N. A., Ginn, T. R., Loge, F. J., 2005. Occurrence and fate of pharmaceutically active compounds in the environment, a case study: Høje River in Sweden. *J. Hazard. Mater.* 122, 195-204.

- Benotti, M. J., and Brownawell B. J., 2009. Microbial degradation of pharmaceuticals in estuarine and coastal seawater. *Environ. Pollut.* 157, 994-1002.
- Benotti, M. J., Trenholm, R. A., Vanderford, B. J., Holady, J. C., Stanford, B. D., Snyder, S. A., 2009. Pharmaceuticals and endocrine disrupting compounds in U.S. drinking water. *Environ. Sci. Technol.* 43, 597-603.
- Blowes, D. W., Ptacek, C. J., Baker, M. J., 1996, Treatment of Wastewater. G. B. Patent 2,306,954 issued Dec. 1, 1999, 1996; Canadian Patent 2,190,933, filed November 11, 1996; U.S. Patent 5,876,606, issued March 9, 1999, Phosphex™ Canadian trademark registration 1,051,185 filed March 17, 2000, Phosphex™ U.S trademark registration 78/015,068 filed June 30, 2000.
- Blowes, D. W., Ptacek, C. J., Benner, S. G., McRae, C. W. T., Bennett, T. A., Puls, R. W., 2000. Treatment of inorganic contaminants using permeable reactive barriers. *J. Contam. Hydrol.* 45, 123-137.
- Bowden, L. I., Jarvis, A. P., Younger, P. L., Johnson, K. L., 2009. Phosphorus removal from waste waters using basic oxygen steel slag. *Environ. Sci. Technol.* 43, 2476-2481.
- Bostrom, B. and Pettersson, K., 1982. Different patterns of phosphorus release from lake sediments in laboratory experiments. *Hydrobiologia.* 92, 415-429.
- Bostrom, B., Andersen, J. M., Fleischer, S., Jansson, M., 1988. Exchange of phosphorus across the sediment-water interface. *Hydrobiologia.* 170, 229-244.
- Brandes, J. A., Ingall, E., Paterson, D., 2007. Characterization of minerals and organic phosphorus species in marine sediments using soft X-ray fluorescence spectromicroscopy. *Mar. Chem.* 103, 250-265.
- Brix, H., Arias, C. A., 2005. The use of vertical flow constructed wetlands for on-site treatment of domestic wastewater: New Danish guidelines. *Ecol. Eng.* 25, 491-500.
- Bruce, G. M., Pleus, R. C., Snyder, S. A., 2010. Toxicological relevance of pharmaceuticals in drinking water. *Environ. Sci. Technol.* 44, 5619-5626.

- Buerge, I. J., Buser, H., Kahle, M., Müller, M. D., Poiger, T., 2009. Ubiquitous occurrence of the artificial sweetener acesulfame in the aquatic environment: An ideal chemical marker of domestic wastewater in groundwater. *Environ. Sci. Technol.* 43, 4381-4385.
- Cameron, K., Madramootoo, C., Crolla, A., Kinsley, C., 2003. Pollutant removal from municipal sewage lagoon effluents with a free-surface wetland. *Water Res.* 37, 2803-2812.
- Caraco, N. F., Cole, J. J., and Likens, G. E., 1993. Sulfate control of phosphorus availability in lakes. *Hydrobiologia* 253: 275–280.
- Carpenter, S. R., Caraco, N. F., Correll, D. L., Howarth, R. W., Sharpley, A. N., Smith, V. H., 1998. Nonpoint pollution of surface waters with phosphorus and nitrogen. *Ecol. Appl.* 8, 559-568.
- Carrara, C., Ptacek, C. J., Robertson, W. D., Blowes, D. W., Moncur, M. C., Sverko, E., Backus, S., 2008. Fate of pharmaceutical and trace organic compounds in three septic system plumes, Ontario, Canada. *Environ. Sci. Technol.* 42, 2805-2811.
- CCME (Canadian Council of Ministers of the Environment), 2004. Canadian water quality guidelines for the protection of aquatic life: Phosphorus: Canadian Guidance Framework for the Management of Freshwater Systems. In: *Canadian Environmental Quality Guidelines*, Canadian Council of Ministers of the Environment, Winnipeg.
- Carballa, M., Omil, F., Lema, J. M., 2007. Calculation methods to perform mass balances of micropollutants in sewage treatment plants. Application to pharmaceutical and personal care products (PPCPs). *Environ. Sci. Technol.* 41, 884-890.
- Castiglioni, S., Bagnati, R., Fanelli, R., Pomati, F., Calamari, D., Zuccato, E., 2006. Removal of pharmaceuticals in sewage treatment plants in Italy. *Environ. Sci. Technol.* 40, 357-363.
- Cha, W., Kim, J., Choi, H., 2006. Evaluation of steel slag for organic and inorganic removals in soil aquifer treatment. *Water Res.* 40, 1034-1042.
- Chaurand, P., Rose, J., Briois, V., Olivi, L., Hazemann, J-L, Proux, O., Domas, J., Bottero, J-Y, 2007. Environmental impacts of steel slag reused in road construction: A crystallographic and molecular (XANES) approach. *J. Hazard. Mater.* B139, 537-542.

- Choe, S., Liljestrand, H. M., Khim, J., 2004. Nitrate reduction by zero-valent iron under different pH regimes. *Appl. Geochem.* 19, 335-342.
- Conkle, J. L., White, J. R., Metcalfe, C. D., 2008. Reduction of pharmaceutically active compounds by a lagoon wetland wastewater treatment system in Southeast Louisiana. *Chemosphere* 73, 1741-1748.
- CWQG (Canadian Water Quality Guidelines), 2005. National Guidelines and Standards Office, Environment Canada.
- Daughton, C. D., 2003. Cradle-to-cradle stewardship of drugs for minimizing their environmental disposition while promoting human health. II. Drug disposal, waste reduction, and future directions. *Environ. Health Perspect.* 111, 775-785.
- Daughton, C. G. and Ternes, T. A., 1999. Pharmaceuticals and personal care products in the environment: Agents of subtle change? *Environ. Health Perspect.* 107, 907-938.
- Davies, T. H. and Hart, B. T., 1990. Use of aeration to promote nitrification in reed beds treating wastewater. *Advanced Water Pollut. Control.* 11, 77-84.
- Davis, J. A. and Kent, D. B., 1990. Surface complexation modeling in aqueous geochemistry. *Rev. Mineral.* 23, 177-260.
- De Oliveira Ugarte, J. F., De Sena, L. Á., De Castro Pérez, C. A., De Aguiar, P. F., Rossi, A. M., Soares, G. A., 2005. Influence of processing parameters on structural characteristics of porous calcium phosphate samples: A study using an experimental design method. *Mat. Res.* 8, 71-76.
- Dordio, A., Carvalho, A. J. P., Teixeira, D. M., Dias, C. B., Pinto, A. P., 2010. Removal of pharmaceuticals in microcosm constructed wetlands using *Typha* spp. and LECA. *Bioresource Technol.* 101, 886-892.
- Drizo, A., Frost, C. A., Grace, J., Smith, K. A., 1999. Physico-chemical screening of phosphate-removing substrates for use in constructed wetland systems. *Water Res.* 33, 3595-3602.
- Drizo, A., Comeau, Y., Forget, C., Chapuis, R. P., 2002. Phosphorus saturation potential: A parameter for estimating the longevity of constructed wetland systems. *Environ. Sci. Technol.* 36, 4642-4648.

- Drizo, A., Forget, C., Chapuis, R. P., Comeau, Y., 2006. Phosphorus removal by electric arc furnace steel slag and serpentinite. *Water Res.* 40, 1547-1554.
- Eveborn, D., Gustafsson, J. P., Hillier, S., 2009. XANES speciation of P in environmental samples: An assessment of filter media for on-site wastewater treatment. *Environ. Sci. Technol.* 43, 6515-6521.
- Fernandez, F. B. Shenoy, S., Babu, S. S., Varma, H. K., and John, A., 2012. Short-term studies using ceramic scaffolds in lapine model for osteochondral defect amelioration. *Biomed. Mater.* 7 (035005), 1-8.
- Focazio, M. J., Kolpin, D. W., Barnes, K. K., Furlong, E. T., Meyer, M. T., Zaugg, S. D., Barber, L. B., Thurman, M. E., 2008. A national reconnaissance for pharmaceuticals and other organic wastewater contaminants in the United States -II) Untreated drinking water sources. *Sci. Total Environ.* 402, 201-216.
- Fram, M. S. and Belitz, K., 2011. Occurrence and concentrations of pharmaceutical compounds in groundwater used for public drinking-water supply in California. *Sci. Total Environ.* 409, 3409-3417.
- Franke, R. and Hormes, J., 1995. The P K-edge absorption spectra of phosphates. *Physica B: Phys. of Condens. Matter*, 216, 85-95.
- Ghauch, A., Tuqan, A., Assi, H. A., 2009. Antibiotic removal from water: Elimination of amoxicillin and ampicillin by microscale and nanoscale iron particles. *Environ. Pollut.*, 157, 1626-1635.
- Gillet, P., McMillan, P., Schott, J., Badro, J., Grzechnik, A., 1996. Thermodynamic properties and isotopic fractionation of calcite from vibrational spectroscopy of ¹⁸O-substituted calcite. *Geochim. Cosmochim. Acta.* 60, 3471-3485.
- Green, M., Friedler, E., Safrai, I., 1998. Enhancing nitrification in vertical flow constructed wetland utilizing a passive air pump. *Water Res.* 32, 3513-3520.
- Gross, B., Montgomery-Brown, J., Naumann, A., Reinhard, M., 2004. Occurrence and fate of pharmaceuticals and alkylphenol ethoxylate metabolites in an effluent-dominated river and wetland. *Environ. Toxicol. Chem.* 23, 2074-2083.

- Grüneberg, B. and Kern, J., 2001. Phosphorus retention capacity of iron-ore and blast furnace slag in subsurface flow constructed wetlands. *Water Sci. Technol.*, 44, 69-75.
- Gunasekaran, S. and Anbalagan, G, 2008. Spectroscopic study of phase transitions in natural calcite mineral. *Spectrochim. Acta. A*, 69, 1246-1251.
- Güngör, K., Jürgensen, A., Karthikeyan, K. G., 2007. Determination of phosphorus speciation in dairy manure using XRD and XANES spectroscopy. *J. Environ. Qual.* 36, 1856–1863.
- Gustafsson, J. P., Renman, A., Renman, G., Poll, K., 2008. Phosphate removal by mineral-based sorbents used in filters for small-scale wastewater treatment. *Water Res.* 42, 189-197.
- Halling-Sorensen, B., Nors Nielsen, S., Lanzky, P. F., Ingerslev, F., Holten Lutzhoft, H. C., Jorgensen, S. E., 1998. Occurrence, fate and effects of pharmaceutical substances in the environment – A review. *Chemosphere.* 36, 357-393.
- Hanawa, T., Kon, M., Doi, H., Ukai, H., Murakami, K., Hamanaka, H., Asaoka, K., 1998. Amount of hydroxyl radical on calcium-ion-implanted titanium and point of zero charge of constituent oxide of the surface-modified layer. *J. Mater. Sci. Mater. Med.* 9, 89-92.
- Heberer, T., 2002a. Occurrence, fate, and removal of pharmaceutical residues in the aquatic environment: a review of recent research data. *Toxicol. Lett.* 131, 5-17.
- Heberer, T., 2002b. Tracking persistent pharmaceutical residues from municipal sewage to drinking water. *J. Hydrol.* 266, 175-189.
- Heberer, T., Reddersen, K., and Mechlinski, A., 2002. From municipal sewage to drinking water: fate and removal of pharmaceutical residues in the aquatic environment in urban areas. *Water Sci. Technol.* 46, 81-88.
- Hendricks, R., and Pool, E. J., 2012. The effectiveness of sewage treatment processes to remove faecal pathogens and antibiotic residues. *J. Environ. Sci. Health, A.* 47, 289-297.
- Hesterberg, D., Zhou, W., Hutchison, K. J., Beauchemin, S., Sayers, D. E. 1999. XAFS study of adsorbed and mineral forms of phosphate. *J. Synchrotron Rad.* 6, 636-638.
- Hijosa-Valsero, M., Matamoros, V., Martín-Villacorta, J., Bécares, E., Bayona, J. M., 2010. Assessment of full-scale natural systems for the removal of PPCPs from wastewater in small communities. *Water Res.* 44, 1429-1439.

- Hosomi, M., Okada, M., and Sudo, R., 1982. Release of phosphorus from lake. *Environ. Int.* 7, 93-98.
- Hupfer, M., and Lewandowski, J., 2008. Oxygen Controls the phosphorus release from lake sediments - a long-lasting paradigm in limnology. *Int. Rev. Hydrobiol.* 93, 415-432.
- Jalota, S., Tas, A. C., and Bhaduri, S. B., 2005. Synthesis of HA-Seeded TTCP ($\text{Ca}_4(\text{PO}_4)_2\text{O}$) Powders at 1230°C from $\text{Ca}(\text{CH}_3\text{COO})_2 \cdot \text{H}_2\text{O}$ and $\text{NH}_4\text{H}_2\text{PO}_4$. *J. Am. Ceram. Soc.* 88, 3353-3360.
- Jelic, A., Gros, M., Ginebreda, A., Cespedes-Sanchez, R., Ventura, F., Petrovic, M., Barcelo, D., 2011. Occurrence, partition and removal of pharmaceuticals in sewage water and sludge during wastewater treatment. *Water Res.* 45, 1165-1176.
- Jenssen, P. D. and Krogstad, T., 2003. Design of constructed wetlands using phosphorus sorbing lightweight aggregate (LWA). In: Mander, Ü., Jenssen, P. D. (Eds.), *Constructed Wetlands for Wastewater Treatment in Cold Climates*, *Adv. Ecol. Sci.*, vol. 11. WIT Press, Southampton, Boston, pp. 259-272.
- Johansson, L., 1999. Industrial by-products and natural substrata as phosphorus sorbents. *Environ. Technol.* 20, 309-316.
- Johansson, L. and Gustafsson, J. P., 2000. Phosphate removal using blast furnace slags and opoka-mechanisms. *Water Res.* 34, 259-265.
- Johnson, M., and Mara, D. D., 2005. Aerated rock filters for enhanced nitrogen and faecal coliform removal from facultative waste stabilization pond effluents. *Water Sci. Technol.* 51, 99-102.
- Kadlec, R. and Knight, R., 1996. *Treatment Wetlands*, CRC Lewis Publishers, Boca Raton, FL., 1996.
- Kadlec, R., Knight, R., Vymazal, J., Brix, H., Cooper, P., Haberl, R., 2000. *Constructed Wetlands for Water Pollution Control: Processes, Performance, Design and Operation*; Scientific and Technical Report No. 8; IWA Publishing, London, UK.

- Kelly, S., Hesterberg, D., Ravel, B., 2008. Analysis of soils and minerals using x-ray absorption spectroscopy. In Ulery, A. L., Drees, R., (Eds); *Methods of Soil Analysis*; Soil Science Society of America: Madison, WI. pp. 387-463.
- Khare, N., Hesterberg, D., Beauchemin, S., Wang, S., 2007. XANES determination of adsorbed phosphate distribution between ferrihydrite and boehmite in mixtures. *Soil Sci. Soc. Am. J.* 68, 460-469.
- Khetan, S. K. and Collins, T. J., 2007. Human Pharmaceuticals in the aquatic environment: A challenge to green chemistry. *Chem. Rev.* 107, 2319-2364.
- Kim, E-H., Hwang, H-K., Yim, S-B., 2006. Phosphorus removal characteristics in hydroxyapatite crystallization using converter slag. *J. Environ. Sci. Health, A*, 41, 2531-2545.
- Knight, R. L., Payne Jr., V. W. E., Borer, R. E., Clarke Jr., R. A., Pries, J. H., 2000. Constructed wetlands for livestock wastewater management. *Ecol. Eng.* 15, 41-55.
- Kolpin, D. W., Furlong, E. T., Meyer, M. T., Thurman, E. M., Zaugg, S. D., Barber, L. B., Buxton, H. T., 2002. Pharmaceuticals, hormones, and other organic wastewater contaminants in U.S. streams, 1999-2000: A national reconnaissance. *Environ. Sci. Technol.* 36, 1202-1211.
- Korkusuz, E. A., Beklioğlu, M., Demirer, G. N., 2005. Comparison of the treatment performances of blast furnace slag-based and gravel-based vertical flow wetlands operated identically for domestic wastewater treatment in Turkey. *Ecol. Eng.* 24, 187-200.
- Kortmann, R. W., Davis, E., Frink, C. R., Henry, D. D., 1983. Hypolimnetic Withdrawal: Restoration of Lake Wononscopomuc, Connecticut. In: *Lake Restoration, Protection, and Management*, U.S. Environmental Protection Agency, 46-55.
- Kurap, G., Akyuz, S., Akyuz, T., Basaran, S., Cakan, B., 2010. FT-IR spectroscopic study of terra-cotta sarcophagi recently excavated in Ainos (Enez) Turkey. *J. Mol. Struct.* 976, 161-167.
- Lam, M. W., Young, C. J., Brain, R. J., Johnson, D. J., Hanson, M. A., Wilson, C. J., Richards, S.M., Solomon, K.R., and Mabury, S. A., 2004. Aquatic Persistence of Eight Pharmaceuticals in a Microcosm Study. *Environmental Toxicology and Chemistry*, Vol. 23, No. 6, pp. 1431-1440.

- Lishman, L., Smyth, S. A., Sarafin, K., Kleywegt, S., Toito, J., Peart, T., Lee, B., Servos, M., Beland, M., Seto, P., 2006. Occurrence and reductions of pharmaceuticals and personal care products and estrogens by municipal wastewater treatment plants in Ontario, Canada. *Sci. Total Environ.* 367, 544-558.
- Lu, H. B., Campbell, C. T., Graham, D. J., Ratner, B. D., 2000. Surface characterization of hydroxyapatite and related calcium phosphates by XPS and TOF-SIMS. *Anal. Chem.* 72, 2886-2894.
- Lyman, W. J., Reehl, W., and Rosenblatt, D., 1990. *Handbook of Chemical Property Estimation Methods*. Washington, DC: Amer. Chem. Soc. pp. 4-9, 7-4, 7-5, 8-12, 15-1 to 15-29.
- Mahieux, P., Aubert, J., Escadeillas, G., 2009. Utilization of weathered basic oxygen furnace slag in the production of hydraulic road binders. *Constr. Build. Mater.* 23, 742-747.
- Mann, R. A. and Bavor, H. J., 1993. Phosphorus removal in constructed wetlands using gravel and industrial waste substrata. *Water Sci. Technol.* 27, 107-113.
- Matamoros, V., Garcia, J., Bayona, J. M., 2005. Behavior of Selected pharmaceuticals in subsurface flow constructed wetlands: A pilot-scale study. *Environ. Sci. Technol.* 39, 5449-5454.
- Matamoros, V. and Bayona, J. M., 2006. Elimination of pharmaceuticals and personal care products in subsurface flow constructed wetlands. *Environ. Sci. Technol.* 40, 5811-5816.
- Matamoros, V., Arias, C., Brix, H., Bayona, J. M., 2007. Removal of pharmaceuticals and personal care products (PPCPs) from urban wastewater in a pilot vertical flow constructed wetland and a sand filter. *Environ. Sci. Technol.* 41, 8171-8177.
- Matamoros, V., Caselles-Osorio, A., García, J., Bayona, J. M., 2008. Behaviour of pharmaceutical products and biodegradation intermediates in horizontal subsurface flow constructed wetland. A microcosm experiment. *Sci. Total Environ.* 394, 171-176.
- Matamoros, V., Hijosa, M., Bayona, J. M., 2009. Assessment of the pharmaceutical active compounds removal in wastewater treatment systems at enantiomeric level. Ibuprofen and naproxen. *Chemosphere.* 75, 200-205.

- Matković, I., Maltar-Strmečki, N., Babić-Ivančić, V., Dutour Sikirić, M., Noethig-Laslo, V., 2012. Characterisation of β -tricalcium phosphate-based bone substitute materials by electron paramagnetic resonance spectroscopy. *Radiat. Phys. Chem.* 81, 1621–1628.
- McRae, C. W. T., 1999. Evaluation of Reactive Materials for In Situ Treatment of Arsenic(III), Arsenic(V) And Selenium(VI) using Permeable Reactive Barriers: Laboratory Study, MSc Thesis, University of Waterloo, Waterloo, Ontario, Canada.
- Metcalf and Eddy Inc., 2003. Wastewater engineering, collection, treatment disposal, McGraw-Hill, New York.
- Metcalf, C. D., Miao, X., Koenig, B. G., Struger, J., 2003. Distribution of acidic and neutral drugs in surface waters near sewage treatment plants in the lower Great Lakes, Canada. *Environ. Toxicol. Chem.* 22, 2881-2889.
- McRae, C. W. T., 1999. Evaluation of Reactive Materials for In Situ Treatment of Arsenic(III), Arsenic(V) And Selenium(VI) using Permeable Reactive Barriers: Laboratory Study. MSc Thesis, University of Waterloo, Waterloo, Ontario, Canada.
- Miao, X-S., and Metcalfe, C. D., 2003. Determination of carbamazepine and Its metabolites in aqueous samples using liquid chromatography electrospray tandem mass spectrometry. *Anal. Chem.* 75, 3731-3738.
- Mikhail, S. A.; Owens, D. R.; Wang, S. S. B.; Lastra, R.; Van Huyssteen, E., 1994. Characterization of basic oxygen furnace dust and slag in steelmaking. Mineral Sciences Laboratories, Canada Centre for Mineral and Energy Technology, Division, Ottawa, ON, Report No. 94-18 (R), MSL Project. 691, 1-41.
- MOEE (Ministry of Environment and Energy), 1994. Water Management Policies, Guidelines, Provincial Water Quality Objectives. Tech. Rep. Ontario Ministry of Environment and Energy, Toronto, Ontario, Canada, 9-28.
- Morrison, S. J., Metzler, D. R., Dwyer, B. P., 2002. Removal of As, Mn, Mo, Se, U, V and Zn from groundwater by zero-valent iron in a passive treatment cell: reaction progress modeling. *J. Contam. Hydrol.* 56, 99-116.
- Morse, G. K., Brett, S. W., Guy, J. A., Lester, J. N., 1998. Review: Phosphorus removal and recovery technologies. *Sci. Total Environ.* 212, 69-81.

- Mortula, M., Gibbons, M., Gagnon, G. A., 2007. Phosphorus adsorption by naturally-occurring materials and industrial by-products. *J. Environ. Eng. Sci.* 6, 157-164.
- Navarro, C., Diaz, M., Villa-Garcia, M. A., 2010. Physico-chemical characterization of steel slag. study of its behavior under simulated environmental conditions. *Environ. Sci. Technol.* 44, 5383-5388.
- Ney, R. E., 1990. *Where did that Chemical Go: A Practical Guide to Chemical Fate and Transport in the Environment.* Van Nostrand Reinhold, 192.
- Nghiem, L. D. and Hawkes, S., 2009. Effects of membrane fouling on the nanofiltration of trace organic contaminants. *Desalination.* 236, 273-281.
- Ni, M. and Ratner, B. D., 2008. Differentiating calcium carbonate polymorphs by surface analysis techniques - An XPS and TOF-SIMS study. *Surf. Interface. Anal.* 40, 1356-1361.
- Nikolaou, A., Meric, S. and Fatta, D., 2007. Occurrence patterns of pharmaceuticals in water and wastewater environments. *Anal. Bioanal. Chem.* 387, 1225-1234.
- Nishikawa, H., 2001. Thermal behavior of hydroxyapatite in structural and spectrophotometric characteristics. *Mat Lett.* 50, 364-370.
- Nürnberg, G. K., 1984. The prediction of internal phosphorus load in lakes with anoxic hypolimnia. *Limnol. Oceanog.* 29, 111-124.
- Nürnberg, G. K., Peters, R. H., 1984. The importance of internal phosphorus load to the eutrophication of lakes with anoxic hypolimnia. *Verh. Int. Verein. Limnol.* 22, 190-194.
- Nürnberg, G. K., Hartley, R., Davis, E., 1987. Hypolimnetic withdrawal in two north american lakes with anoxic phosphorus release from the sediment. *Water Res.* 21, 923-928.
- Nürnberg, G. K., 1988. Prediction of phosphorus release rates from total and reductant soluble phosphorus in anoxic lake sediments. *Can. J. Fish. Aquat. Sci.* 45, 453-462.
- Nürnberg, G. K., LaZerte, B. D., Olding, D. D., 2003. An artificially induced *Planktothrix rubescens* surface bloom in a small kettle lake in Southern Ontario compared to blooms world-wide. *Lake Reserv. Manage.* 19, 307-322.

- Panda, R. N., Hsieh, M. F., Chung, R. J., Chin, T. S., 2003. FTIR, XRD, SEM and solid state NMR investigations of carbonate-containing hydroxyapatite nano-particles synthesized by hydroxide-gel technique. *J. Phys. Chem. Solids.* 64, 193-199.
- Parkhurst, D. L. and Appelo, C. A. J., 1999. Users Guide to PHREEQC (Version2)-A computer program for speciation, batch-reaction, one-dimensional transport, and inverse geochemical calculations. U.S. Geological Survey Water-Resources Investigations Report 99-4259: 312; U.S. Geological Survey: Washington, D.C.
- Parks, G. A., 1965. The isoelectric points of solid oxides, solid hydroxides, and aqueous hydroxo complex systems. *Chem. Rev.* 65, 177-198.
- Parry, R., 1998. Agricultural phosphorus and water quality: A U.S. Environmental Protection Agency perspective. *J. Environ. Qual.* 27, 258-261.
- Peak, D., Sims, J. T., Sparks, D. L., 2002. Solid-state speciation of natural and alum-amended poultry litter using XANES spectroscopy. *Environ. Sci. Technol.* 36, 4253-4261.
- Pearson, H. W., Mara, D. D., Mills, S. W., Smallman, D. J., 1987. Physico-chemical parameters influencing faecal bacterial survival in waste stabilization ponds. *Water Sci. Technol.* 19, 145-152.
- Pena, J. and Vallet-Regi, M., 2003. Hydroxyapatite, tricalcium phosphate and biphasic materials prepared by a liquid mix technique. *J. Eur. Ceram. Soc.* 23, 1687-1696.
- Petra, M., Anastassopoulou, J., Theologis, T., Theophanides, T., 2005. Synchrotron micro-FT-IR spectroscopic evaluation of normal paediatric human bone. *J. Mol. Struct.* 733, 101-110.
- Poh, H., Ghataora, G., Ghazireh, N., 2006. Soil Stabilization Using Basic Oxygen Steel Slag Fines. *J. Mater. Civ. Eng.* 18, 229-240.
- Proctor, D. M., Fehling, K. A., Shay, E. C., Wittenborn, J. L., Green, J. J., Avent, C., Bigham, R. D., Connolly, M., Lee, B., Shepker, T. O., Zak, M. A., 2000. Physical and chemical characteristics of blast furnace, basic oxygen furnace, and electric arc furnace steel industry slags. *Environ. Sci. Technol.* 34, 1576-1582.
- Qualls, R. G. and Richardson, C. J., 1995. Forms of soil phosphorus along a nutrient enrichment gradient in the northern everglades. *Soil Sci.* 160, 183-198.

- Rabiet, M., Togola, A., Brissaud, F., Seidel, J-L., Budzinski, H., Elbaz-Poulichet, F., 2006. Consequences of treated water recycling as regards pharmaceuticals and drugs in surface and ground waters of a medium-sized Mediterranean catchment. *Environ. Sci. Technol.* 40, 5282-5288.
- Rahman, A. and Agrawal, A., 1997. Reduction of nitrate and nitrite by iron metal: Implications for ground water remediation. Preprint of papers presented at the 213th ACS National meeting, Sanfrancisco, CA. 37, 157-159.
- Rapacz-Kmita, A., Paluszkiwicz, C., Slosarczyka, A., Paszkiewicz, Z., 2005. FTIR and XRD investigations on the thermal stability of hydroxyapatite during hot pressing and pressureless sintering processes. *J. Mol. Struct.* 744-747, 653-656.
- Ravel, B. and Newville, M., 2005. Athena, Artemis, Hephaestus: data analysis for X-ray absorption spectroscopy using IFEFFIT. *J. Synchrotron Rad.* 12, 537-541.
- Reardon, E. J., 2005. Zerovalent irons: styles of corrosion and inorganic control on hydrogen pressure buildup. *Environ. Sci. Technol.* 39, 7311-7317.
- Reed, D.C., Slomp, C.P., Gustafsson, B.G., 2011. Sedimentary phosphorus dynamics and the evolution of bottom-water hypoxia: A coupled benthic-pelagic model of a coastal system. *Limnol. Oceanogr.* 56, 1075-1092.
- Rehman, I. and Bonfield, W., 1997. Characterization of hydroxyapatite and carbonated apatite by photo acoustic FTIR spectroscopy. *J. Mater. Sci.-Mater. M.* 8, 1-4.
- Ribeiro, C. C., Gibson, I., Barbosa, M. A., 2006. The uptake of titanium ions by hydroxyapatite particles - Structural changes and possible mechanisms. *Biomater.* 27, 1749-1761.
- Robertson, W. D., Van Stempvoort, D. R., Solomon, D. K., Homewood, J., Brown, S. J., Spoelstra, J., Schiff, S. L., 2013. Persistence of artificial sweeteners in a 15-year-old septic system plume. *J. Hydrol.* 477, 43-54.
- Sabourin, L., Beck, A., Duenk, P. W., Kleywegt, S., Lapen, D. R., Li, H., Metcalfe, C. D., Payne, M., Topp, E., 2009. Runoff of pharmaceuticals and personal care products following application of dewatered municipal biosolids to an agricultural field. *Sci. Total Environ.* 407, 4596-4604.

- Sacher, F., Lange, F. T., Brauch, H., Blankenhorn, I., 2001. Pharmaceuticals in groundwaters: Analytical methods and results of a monitoring program in Baden-Württemberg, Germany. *J. Chromatogr. A.* 938, 199-210.
- Sakadevan, K. and Bavor, H. J., 1998. Phosphate adsorption characteristics of soils, slags and zeolite to be used as substrates in constructed wetland systems. *Water Res.* 32, 393-399.
- Sanderson, H., 2011. Presence and risk assessment of pharmaceuticals in surface water and drinking water. *Water Sci. Technol.* 63, 2143-2148.
- Sargin, Y., Kizilyalli, M., Telli, C., Guler, H., 1997. A new method for the solid-state synthesis of tetracalcium phosphate, a dental cement: X-Ray powder diffraction and IR studies. *J. Eur. Ceram. Soc.* 17, 963-970.
- Sato, S., Solomon, D., Hyland, C., Ketterings, Q. M., Lehmann, J., 2005. Phosphorus speciation in manure and manure-amended soils using XANES spectroscopy. *Environ. Sci. Technol.* 39, 7485-7491.
- Scheurer, M., Brauch, H., Lange, F. T., 2009. Analysis and occurrence of seven artificial sweeteners in German waste water and surface water and in soil aquifer treatment (SAT). *Anal. Bioanal. Chem.* 394, 1585-1594.
- Schindler, D. W., 1974. Eutrophication and Recovery in Experimental Lakes: Implications for Lake Management. *Science, New Series*, 184, 897-899.
- Schindler, D. W., 1977. Evolution of phosphorus limitation in lakes. Natural mechanisms compensate for deficiencies of nitrogen and carbon in eutrophied lakes. *Science.* 195, 260-262.
- Seaman, L., Sherif, R., Parker, W. J., Kennedy, K., Seto, P., 2009. Sludge pretreatment before aerobic digestion to enhance pathogen destruction. *Can. J. Civ. Eng.* 36, 871-880.
- Sedlak, R., 1991. *Phosphorus and Nitrogen Removal from Municipal Wastewater: Principles and Practice*, 2nd ed, Lewis Publishers, NY.
- Shannon, E. E., 1980. Physical-chemical phosphorus removal processes. Nutrient control technology seminar, Calgary, Alberta, 7-8 February.

- Sharpley, A. N., Chapra, S. C., Wedepohl, R., Sims, J. T., Daniel, T. C., Reddy, K. R., 1994. Managing agricultural phosphorus for protection of surface waters: Issues and options. *J. Environ. Qual.* 23, 437-451.
- Shen, D-H., Wu, C-M., Du, J-C., 2009. Laboratory investigation of basic oxygen furnace slag for substitution of aggregate in porous asphalt mixture. *Constr.Build. Mater.* 23, 453-461.
- Shi, C., 2004. Steel slag - Its production, processing, characteristics, and cementitious properties. *J. Mater. Civ. Eng.* 16, 230-236.
- Shober, A. L., Hesterberg, D. L., Sims, J. T., and Gardner, S., 2006. Characterization of phosphorus species in biosolids and manures using XANES spectroscopy. *J. Environ. Qual.* 35, 1983-993.
- Singh, A. and Purohit, K. M., 2011. Chemical synthesis, characterization and bioactivity evaluation of hydroxyapatite prepared from Garden snail (*Helix aspersa*). *J. Bioprocess. Biotechniq.* 1:104 doi: 10.4172/2155-9821.1000104.
- Søndergaard, M., Jensen, J. P., Jeppesen, E., 2003. Role of sediment and internal loading of phosphorus in shallow lakes. *Hydrobiologia.* 506-509, 135–145.
- Smyth, D. J. A., Blowes, D. W., Ptacek, C. J., Baker, M. J., McRae, C. W. T., 2002a. Steel production wastes for use in permeable reactive barriers (PRBs). In: *Proceedings of the Third International Conference on Remediation of Chlorinated and Recalcitrant Compounds*, 435-442.
- Smyth, D. J. A., Blowes, D. W., Ptacek, C. J., Baker, M. J., Ford, G., Foss, S., Bernstene, E., 2002b. Removal of phosphate and waterborne pathogens from wastewater effluent using permeable reactive materials. In *Proceedings of the 55th Canadian Geotechnical and 3rd Joint IAHCNC and CGS Groundwater Specialty Conference*. 1123-1127.
- Snoeyink, V. L., and Jenkins, D., 1980. *Water Chemistry*. John Wiley and Sons. 463pp.
- Snyder, S. A., Leising, J., Westerhoff, P., Yoon, Y., Mash, H., Vanderford, B., 2004. Biological and physical attenuation of endocrine disruptors and pharmaceuticals: Implications for water reuse. *Ground Water Monit. Remed.* 24 (2), 108-118.

- Spongberg, A. L. and Witter J. D., 2008. Pharmaceutical compounds in the wastewater process stream in Northwest Ohio. *Sci. Total Environ.* 397, 148-157.
- Stafiej, A., Pyrzynska, K., Regan, F., 2007. Determination of anti-inflammatory drugs and estrogens in water by HPLC with UV detection. *J. Sep. Sci.* 30, 985-991.
- Stimson, J., Chae, G., Ptacek, C. J., Emelko, M. B., Mesquita, M. M., Hirata, R. A., Blowes, D. W., 2010. Basic oxygen furnace slag as a treatment material for pathogens: Contribution of inactivation and attachment in virus attenuation. *Water Res.* 44, 1150-1157.
- Stuer-Lauridsen, F., Birkved, M., Hansen, L. P., Holten Lützhøft, H., Halling-Sørensen, B., 2000. Environmental risk assessment of human pharmaceuticals in Denmark after normal therapeutic use. *Chemosphere.* 40, 783-793.
- Stumm, W., Morgan, J. J., 1981. *Aquatic Chemistry*, 2nd ed., New York, 780pp.
- Stumpf, M., Ternes, T. A., Wilken, R-D., Rodrigues, S. V., Baumann, W., 1999. Polar drug residues in sewage and natural waters in the state of Rio de Janeiro, Brazil. *Sci. Total Environ.* 225, 135-141.
- Suarez, S., Carballa, M., Omil, F., Lema, J. M. 2008. How are pharmaceutical and personal care products (PPCPs) removed from urban wastewaters? *Rev. Environ. Sci. Biotechnol.* 7, 125-138.
- Suarez, S., Lema, J. M., Omil, F., 2010. Removal of pharmaceutical and personal care products (PPCPs) under nitrifying and denitrifying conditions. *Water Res.*, 44, 3214-3224.
- Tatzber, M., Stemmer, M., Spiegel, H., Katzlberger, C., Haberhauer, G., Gerzabek, M. H., 2007. An alternative method to measure carbonate in soils by FT-IR spectroscopy. *Environ. Chem. Lett.* 5, 9-12.
- Ternes, T. A., 1998. Occurrence of drugs in German sewage treatment plants and rivers. *Water Res.* 32, 3245-3260.
- Ternes, T. A., 2001. Analytical methods for the determination of pharmaceuticals in aqueous environmental samples. *T. Anal. Chem.* 20, 419-434.

- Ternes, T. A., Meisenheimer, M., McDowell, D., Sacher, F., Brauch, H., Haist-Gulde, B., Preuss, G., Wilme, U., Zulei-Seibert, N., 2002. Removal of pharmaceuticals during drinking water treatment. *Environ. Sci. Technol.* 36, 3855-3863.
- Ternes, T. A., Bonerz, M., Herrmann, N., Teiser, B., Andersen, H. R., 2007. Irrigation of treated wastewater in Braunschweig, Germany: An option to remove pharmaceuticals and musk fragrances. *Chemosphere* 66, 894-904.
- Tixier, C., Singer, H. P., Oellers, S., Müller, S. R., 2003. Occurrence and fate of carbamazepine, clofibric acid, diclofenac, ibuprofen, ketoprofen, and naproxen in surface waters. *Environ. Sci. Technol.* 37, 1061-1068.
- Tomson, M. B. and Vignona, L., 1984. Precipitation of phosphate minerals in wastewater treatment systems. In: Nriagu, J.O. and Moore, P.B. (ed.) *Phosphate Minerals*, Springer-Verlag, New York.
- Toth, J. E., Rickman, K. A., Venter, A. R., Kiddle, J. J., Mezyk, S. P., 2012. Reaction kinetics and efficiencies for the hydroxyl and sulfate radical based oxidation of artificial sweeteners in water. *J. Phys. Chem. A.* 116, 9819-9824.
- U. S. EPA (U.S. Environmental Protection Agency), 1986. Quality criteria for water 1986: Washington, D.C., U.S. Environmental protection Agency Report 440/5-86-001, Office of Water.
- U. S. EPA (U.S. Environmental Protection Agency), 2007. Advanced Wastewater Treatment to Achieve Low Concentration of Phosphorus, EPA 910-R-07-002. U.S. Environmental Protection Agency, Office of Water and Watersheds.
- Vagenas, N. V., Gatsouli, A., Kontoyannis, C. G., 2003. Quantitative analysis of synthetic calcium carbonate polymorphs using FT-IR spectroscopy. *Talanta.* 59, 831-836.
- van Stempvoort, D. R., Roy, J. W., Brown, S. J., Bickerton, G., 2011a. Artificial sweeteners as potential tracers in groundwater in urban environments. *J. Hydrol.* 401, 126-133.
- van Stempvoort, D. R., Robertson, W. D., Brown, S. J., 2011b. Artificial sweeteners in a large septic plume. *Ground Water Monit. Remediat.* 31, 95-102.

- Vance, E. D., 2000a. Recycling paper mill by-products on forest lands: by-product composition, potential applications, and industry case studies. In: *The Forest Alternative: Principles and Practice of Residuals Use*, Henry, C.L., Harrison, R.B., Bastian, R.K. (Eds.), University of Washington College of Forest Resources, Seattle, Washington, 567.
- Vance, E. D., 2000b. Utilizing paper mill bi-products as forest soil amendments: forest responses, recommendations and industry case studies. NCASI Technical Bulletin, No.798 NCASI.
- Vanderford, B. J. and Snyder, S. A., 2006. Analysis of pharmaceuticals in water by isotope dilution liquid chromatography/tandem mass spectrometry. *Environ. Sci. Technol.* 40, 7312-7320.
- Verenitch, S. S., Lowe, C. J., Mazumder, A., 2006. Determination of acidic drugs and caffeine in municipal wastewaters and receiving waters by gas chromatography-ion trap tandem mass spectrometry. *J. Chromatogr. A.* 116, 193-203.
- Verliefde, A. R. D., Heijman, S. G. J., Cornelissen, E. R., Amy, G. L., Van Der Brugge, B., Van Dijk, J. C., 2008. Rejection of trace organic pollutants with high pressure membranes (NF/RO). *Environ. Prog.* 27, 180-188.
- Vieno, N. M., Tuhkanen, T., Kronberg, L., 2006. Analysis of neutral and basic pharmaceuticals in sewage treatment plants and in recipient rivers using solid phase extraction and liquid chromatography–tandem mass spectrometry detection. *J. Chromatogr. A.* 1134, 101-111.
- Vohla, C., Kõiv, M., Bavor, H. J., Chazarenc, F., Mander, Ü., 2011. Filter materials for phosphorus removal from wastewater in treatment wetlands-A review. *Ecol. Eng.* 37, 70-89.
- Vongsavat, V., Winotai, P., Meejoo, S., 2006. Phase transitions of natural corals monitored by ESR spectroscopy. *Nucl. Instrum. Meth. B.* 243, 167-173.
- Vymazal, J., 1997. Subsurface horizontal-flow constructed wetlands for wastewater treatment: the Czech experience. *Wetl. Ecol. Manag.* 4, 199-206.
- Vymazal, J., 2004. Removal of phosphorus in constructed wetlands with horizontal sub-surface flow in the Czech Republic. *Water, Air, Soil Pollut.: Focus.* 4, 657-670.

- Vymazal, J., 2007. Removal of nutrients in various types of constructed wetlands. *Sci. Total Environ.* 380, 48-65.
- Vymazal, J., 2011. Constructed wetlands for wastewater treatment: Five decades of experience. *Environ. Sci. Technol.* 2011, 45, 61-69.
- Waligora, J., Bulteel, D., Degrugilliers, P., Damidot, D., Potdevin, J.L., Measson, M., 2010. Chemical and mineralogical characterizations of LD converter steel slags: A multi-analytical techniques approach. *Mater. Charact.* 61, 3 9-4 8.
- Webb, S., Ternes, T., Gibert, M., Olejniczak, K., 2003. Indirect human exposure to pharmaceuticals via drinking water. *Toxicol. Lett.* 142, 157-167.
- Wei, Y-T., Wu, S-C., Chou, C-M., Che, C-H., Tsai, S-M., Lien, H-L., 2010. Influence of nanoscale zero-valent iron on geochemical properties of groundwater and vinyl chloride degradation: A field case study. *Water Res.* 44, 131-140.
- Xue, Y., Hou, H., Zhu, S., 2009. Characteristics and mechanisms of phosphate adsorption onto basic oxygen furnace slag. *J. Hazard. Mater.* 162, 973-980.
- Yamada, H., Kayama, M., Saito, K., Hara, M., 1986. A fundamental research on phosphate removal by using slag. *Water Res.* 20, 547-557.
- Ye, F. and Li, Y., 2009. Enhancement of nitrogen removal in towery hybrid constructed wetland to treat domestic wastewater for small rural communities. *Ecol. Eng.* 35, 1043-1050.
- Yeoman, S., Stephenson, T., Lester, J. N., Perry, R., 1988. The removal of phosphorus during wastewater treatment: A review. *Environ. Pollut.* 49, 183-233.
- Yildirim, I. Z. and Prezzi, M., 2011. Chemical mineralogical and morphological properties of steel slag. *Adv. Civil Eng.* Published by: Hindawi Publishing, New York, NY, USA. 1-13.
- Zhang, D. Q., Tan, S. K., Gersberg, R. M., Sadreddini, S., Zhu, J., Tuan, N. A., 2011. Removal of pharmaceutical compounds in tropical constructed wetlands. *Ecol. Eng.* 37, 460-464.
- Zhang, W-X, 2003. Nanoscale iron particles for environmental remediation: An overview. *J. Nanopart. Res.* 5, 323-332.

Appendix A
Summary of Data Presented in Chapter 2

Table A 1: pH values along the treatment flow path in year 1 (2005) of the hypolimnetic withdrawal P treatment experiment.

Sample ID	Distance (cm)	20-Jul	18-Aug	26-Aug	02-Sep	16-Sep	23-Sep	29-Sep	06-Oct	11-Nov
C1-Inf	0	7.20	7.36	7.85	7.31	7.35	7.31	7.24	7.33	7.65
C1-P1	36	7.63	7.56	-	-	-	-	-	-	-
C1-P2	68	8.00	7.83	-	7.41	7.53	7.71	7.89	8.95	8.31
C1-P3	99	8.20	8.11	-	7.67	7.94	7.82	8.04	8.90	8.20
C1-P4	130	8.34	8.39	-	7.79	7.83	7.98	8.23	8.81	8.27
C2-Inf	151	8.39	8.42	7.80	7.72	8.16	8.12	8.30	8.54	8.06
C2-P1	238	8.55	8.53	8.14	8.13	8.10	8.46	8.56	8.84	8.60
C2-P2	299	8.74	8.57	8.19	8.01	8.48	8.42	8.61	8.51	8.61
C3-Inf	320	8.90	8.53	8.14	8.34	8.15	8.47	8.51	8.51	8.39
C3-P1	406	9.01	8.50	8.00	8.16	8.42	8.48	8.54	8.59	8.46
C3-P2	468	9.12	8.50	8.09	8.26	8.11	8.53	8.59	8.67	8.56
C3-Eff	509	-	-	-	-	-	-	-	-	-
Final Eff	610	9.64	8.74	7.72	8.31	8.38	8.43	8.44	8.15	8.38

Table A 2: pH values along the treatment flow path in year 2 (2006) of the hypolimnetic withdrawal P treatment experiment.

Sample ID	Distance (cm)	19-Jul	26-Jul	03-Aug	10-Aug	17-Aug	25-Aug	02-Sep	09-Sep	30-Sep	10-Oct	17-Oct	27-Oct
C1-Inf	0	7.38	7.34	7.34	7.37	7.32	7.18	7.19	7.26	7.25	7.20	7.22	7.58
C1-P1	36	7.59	7.58	7.62	7.51	7.38	7.40	7.38	7.48	8.77	7.29	7.32	7.78
C1-P2	68	8.41	8.50	8.58	8.53	8.14	7.60	7.73	8.02	9.09	7.63	7.83	8.61
C1-P3	99	9.26	9.00	8.96	8.94	8.55	8.45	8.44	8.58	9.45	7.91	8.35	8.98
C1-P4	130	10.10	9.85	9.83	9.30	8.71	8.75	8.71	8.80	9.57	8.27	8.79	9.22
C2-Inf	151	10.83	10.75	10.83	10.80	9.31	9.12	8.91	8.86	-	-	-	-
C2-P1	238	11.41	11.58	11.34	11.45	10.48	9.82	9.51	9.36	9.95	8.62	8.95	9.34
C2-P2	299	11.56	11.59	11.50	11.62	11.22	11.27	10.78	10.37	11.20	9.40	9.36	9.83
C3-Inf	320	11.41	11.47	11.41	11.41	10.97	11.07	10.86	10.58	-	-	-	-
C3-P1	406	11.50	11.53	11.44	11.51	11.17	11.18	11.04	10.82	-	-	-	-
C3-P2	468	11.53	11.62	11.48	11.63	11.37	11.40	11.31	11.20	11.20	9.40	9.36	9.83
C3-Eff	509	8.44	8.79	10.01	10.41	8.36	8.36	8.54	9.31	6.13	8.99	8.89	8.95
Final Eff	610	8.07	8.58	9.17	9.64	8.51	8.54	8.68	9.22	8.44	9.09	9.06	9.03

Table A 3: pH values along the treatment flow path in year 3 (2007) of the hypolimnetic withdrawal P treatment experiment.

Sample ID	Distance (cm)	01-Aug	09-Aug	15-Aug	22-Aug	28-Aug	13-Sep	21-Sep	26-Sep	01-Oct	06-Oct	11-Oct	17-Oct	22-Oct
C1-Inf	0	7.33	7.69	7.36	9.11	10.94	7.25	7.30	7.28	7.15	7.23	7.28	7.22	7.34
C1-P1	36	8.70	7.70	7.51	11.76	11.96	7.31	-	7.42	7.55	7.57	7.61	7.52	7.76
C1-P2	68	8.75	8.22	7.78	12.03	12.07	7.41	7.34	7.56	7.57	7.81	7.77	7.68	8.05
C1-P3	99	9.55	8.92	8.88	11.83	11.96	7.74	-	7.92	8.07	8.24	8.47	8.32	8.49
C1-P4	130	11.72	11.59	11.33	11.80	11.88	9.68	11.00	9.84	9.97	10.04	10.35	10.23	10.02
C2-Inf	151	11.64	11.64	11.55	12.46	12.40	10.60	10.96	10.55	9.67	9.60	9.60	9.58	9.40
C2-P1	238	12.13	11.85	11.78	12.32	12.34	11.57	-	11.48	11.38	11.32	11.32	11.24	11.09
C2-P2	299	12.19	11.92	11.89	12.29	-	11.68	11.60	11.57	11.52	11.52	11.65	11.66	11.51
C3-Inf	320	12.10	12.07	12.02	12.45	12.41	11.82	11.67	11.76	11.69	11.64	11.82	11.78	11.56
C3-P1	406	12.16	12.12	12.10	12.42	-	11.93	-	11.81	11.77	11.71	11.87	11.88	11.71
C3-P2	468	12.11	12.11	12.13	12.19	-	12.00	11.84	11.80	11.84	11.79	11.98	11.96	11.79
C3-Eff	509	12.15	12.17	12.15	-	-	12.02	11.78	11.80	11.85	11.80	11.96	11.98	11.80
Final Eff	610	8.78	12.17	11.58	6.18	-	6.67	-	7.82	7.70	7.38	7.18	7.02	6.99

Table A 4: Alkalinity ($\text{mg L}^{-1} \text{CaCO}_3$) concentrations along the treatment flow path in year 1(2005) of the hypolimnetic withdrawal P treatment experiment.

Sample ID	Distance (cm)	20-Jul	18-Aug	26-Aug	02-Sep	16-Sep	23-Sep	29-Sep	06-Oct	11-Nov
C1-Inf	0	118	140	150	280	240	172	130	156	140
C1-P1	36	157	158	-	-	-	-	-	-	-
C1-P2	68	162	151	-	200	220	142	164	154	160
C1-P3	99	158	152	-	140	240	180	166	138	180
C1-P4	130	170	166	-	220	260	136	176	158	160
C2-Inf	151	146	174	-	200	220	174	190	170	180
C2-P1	238	156	178	246	200	220	180	196	174	180
C2-P2	299	154	178	170	160	200	216	198	184	180
C3-Inf	320	98	180	208	180	200	188	166	180	220
C3-P1	406	94	182	170	180	240	234	181	156	240
C3-P2	468	78	152	362	180	200	144	172	136	220
C3-Eff	509	-	-	-	-	-	-	-	-	-
Final Eff	610	70	108	-	170	230	150	162	128	240

Table A 5: Alkalinity ($\text{mg L}^{-1} \text{CaCO}_3$) concentrations along the treatment flow path in year 2 (2006) of the hypolimnetic withdrawal P treatment experiment.

Sample ID	Distance (cm)	19-Jul	20-Jul	03-Aug	10-Aug	17-Aug	25-Aug	02-Sep	09-Sep	30-Sep	10-Oct	17-Oct	27-Oct
C1-Inf	0	142	154	126	124	136	142	262	150	178	154	170	126
C1-P1	36	154	146	138	146	148	154	162	160	129	164	164	102
C1-P2	68	156	170	166	150	154	153	157	178	128	166	150	104
C1-P3	99	110	116	120	132	177	156	174	160	133	168	184	110
C1-P4	130	74	76	78	92	162	166	186	166	125	180	194	104
C2-Inf	151	92	94	112	82	118	128	140	144	171	110	-	-
C2-P1	238	176	218	170	172	112	86	96	116	78	178	184	92
C2-P2	299	240	218	262	196	144	134	118	118	87	132	138	82
C3-Inf	320	190	178	216	152	107	96	91	94	51	98	-	-
C3-P1	406	194	192	237	166	122	88	86	79	84	70	-	-
C3-P2	468	258	252	254	212	150	128	122	108	134	144	-	-
C3-Eff	509	-	-	-	-	-	-	-	-	-	-	-	-
Final Eff	610	116	106	84	108	134	122	132	94	122	110	120	78

Table A 6: Alkalinity ($\text{mg L}^{-1} \text{CaCO}_3$) concentrations along the treatment flow path in year 3 (2007) of the hypolimnetic withdrawal P treatment experiment.

Sample ID	Distance (cm)	01-Aug	09-Aug	15-Aug	13-Sep	21-Sep	26-Sep	01-Oct	06-Oct	11-Oct	17-Oct	22-Oct
C1-Inf	0	160	200	280	360	200	200	160	180	210	250	170
C1-P1	36	156	200	180	280	-	230	230	220	160	200	190
C1-P2	68	140	200	200	190	230	240	190	180	160	170	160
C1-P3	99	134	180	180	200		220	220	200	260	220	180
C1-P4	130	376	340	280	190	180	330	170	160	170	140	130
C2-Inf	151	348	420	280	190	180	240	220	130	170	170	150
C2-P1	238	1100	500	420	220	-	280	220	170	155	130	130
C2-P2	299	1210	580	440	290	240	320	320	190	230	190	210
C3-Inf	320	1030	800	520	340	280	330	210	220	220	200	200
C3-P1	406	1150	900	760	420	-	420	280	250	200	230	220
C3-P2	468	1050	920	680	518	370	360	440	280	300	250	230
C3-Eff	509	1150	1000	780	620	130	440	370	330	330	260	250
Final Eff	610	96	1020	420	360	-	330	270	200	220	260	250

Table A 7: Concentrations of PO₄-P (mg L⁻¹) along the treatment flow path in year 1 (2005) of the hypolimnetic withdrawal P treatment experiment.

Sample ID	Distance (cm)	20-Jul	18-Aug	26-Aug	02-Sep	16-Sep	23-Sep	29-Sep	06-Oct	11-Nov
C1-Inf	0	0.36	0.29	0.31	0.30	0.32	0.35	0.36	0.51	0.55
C1-P1	36	0.46	0.29	-	-	-	-	-	-	-
C1-P2	68	0.49	0.25	-	0.30	0.33	0.34	0.35	0.26	0.55
C1-P3	99	0.27	0.22	-	0.30	0.32	0.33	0.34	0.26	0.54
C1-P4	130	0.20	0.17	-	0.23	0.25	0.30	0.32	0.25	0.53
C2-Inf	151	0.21	0.19	-	0.24	0.26	0.29	0.31	0.27	0.33
C2-P1	238	0.14	0.13	0.15	0.18	0.22	0.24	0.27	0.21	0.41
C2-P2	299	0.17	0.077	0.12	0.17	0.19	0.24	0.24	0.17	0.33
C3-Inf	320	0.040	0.038	0.035	0.13	0.15	0.18	0.18	0.24	0.20
C3-P1	406	0.046	0.023	0.085	0.074	0.11	0.14	0.16	0.13	0.13
C3-P2	468	0.035	0.020	0.020	0.039	0.085	0.11	0.12	0.075	0.080
C3-Eff	509	0.039	-	-	-	-	-	-	-	-
Final Eff	610	<DL	<DL	<DL	<DL	0.038	0.060	0.058	0.059	0.040

DL: 0.02 mg L⁻¹

Table A 8: Concentrations of PO₄-P (mg L⁻¹) along the treatment flow path in year 2 (2006) of the hypolimnetic withdrawal P treatment experiment.

Sample ID	Distance (cm)	19-Jul	26-Jul	03-Aug	10-Aug	17-Aug	25-Aug	02-Sep	09-Sep	30-Sep	10-Oct	17-Oct	27-Oct
C1-Inf	0	0.31	0.30	0.26	0.28	0.30	0.32	0.36	0.37	0.49	0.49	0.35	0.02
C1-P1	36	0.30	0.29	0.26	0.29	0.31	0.33	0.37	0.39	0.49	0.49	0.28	0.03
C1-P2	68	0.25	0.22	0.21	0.25	0.29	0.32	0.36	0.38	0.48	0.47	0.37	0.14
C1-P3	99	0.11	0.077	0.087	0.15	0.25	0.28	0.32	0.34	0.32	0.45	0.47	0.20
C1-P4	130	0.046	0.035	0.032	0.048	0.20	0.23	0.27	0.29	0.25	0.44	0.44	0.24
C2-Inf	151	0.033	<DL	<DL	<DL	0.083	0.11	0.12	0.14	-	-	-	-
C2-P1	238	0.021	<DL	<DL	<DL	0.034	0.046	0.052	0.061	0.063	0.33	0.30	0.21
C2-P2	299	<DL	<DL	<DL	<DL	<DL	0.023	0.023	0.024	<DL	0.12	0.15	0.11
C3-Inf	320	<DL	<DL	<DL	<DL	<DL	0.021	<DL	0.020	-	-	-	-
C3-P1	406	<DL	<DL	<DL	<DL	<DL	<DL	<DL	<DL	-	-	-	-
C3-P2	468	<DL	<DL	<DL	<DL	<DL	<DL	<DL	<DL	<DL	0.12	0.15	-
C3-Eff	509	0.025	<DL	<DL	<DL	<DL	<DL	<DL	<DL	<DL	<DL	0.064	0.060
Final Eff	610	<DL	<DL	<DL	<DL	<DL	<DL	<DL	<DL	<DL	<DL	0.064	0.063

DL: 0.02 mg L⁻¹

Table A 9: Concentrations of PO₄-P (mg L⁻¹) along the treatment flow path in year 3 (2007) of the hypolimnetic withdrawal P treatment experiment.

Sample ID	Distance (cm)	01-Aug	09-Aug	15-Aug	13-Sep	21-Sep	26-Sep	01-Oct	06-Oct	11-Oct	17-Oct	22-Oct
C1-Inf	0	0.33	0.32	0.36	0.33	0.34	0.32	0.32	0.37	0.31	0.36	0.36
C1-P1	36	0.30	0.29	0.35	0.32	-	0.30	0.31	0.35	0.28	0.32	0.32
C1-P2	68	0.23	0.25	0.28	0.30	0.31	0.30	0.30	0.32	0.28	0.31	0.31
C1-P3	99	0.11	0.18	0.22	0.29	-	0.28	0.29	0.31	0.28	0.30	0.31
C1-P4	130	<DL	<DL	<DL	0.12	0.087	0.12	0.15	0.11	0.085	0.084	0.10
C2-Inf	151	<DL	<DL	<DL	0.084	0.025	0.060	0.098	0.16	0.14	0.20	0.17
C2-P1	238	<DL	<DL	<DL	<DL	-	<DL	<DL	<DL	<DL	<DL	<DL
C2-P2	299	<DL	<DL	<DL	<DL	<DL	<DL	<DL	<DL	<DL	<DL	<DL
C3-Inf	320	<DL	<DL	<DL	<DL	<DL	<DL	<DL	<DL	<DL	<DL	<DL
C3-P1	406	<DL	<DL	<DL	<DL	-	<DL	<DL	<DL	<DL	<DL	<DL
C3-P2	468	<DL	<DL	<DL	<DL	<DL	<DL	<DL	<DL	<DL	<DL	<DL
C3-Eff	509	<DL	<DL	<DL	<DL	<DL	<DL	<DL	<DL	<DL	<DL	<DL
Final Eff	610	<DL	<DL	<DL	<DL	-	<DL	<DL	<DL	<DL	<DL	<DL

DL: 0.02 mg L⁻¹

Table A 10: Concentrations of Ca (mg L^{-1}) along the treatment flow path in year 1 (2005) of the hypolimnetic withdrawal P treatment experiment.

Sample ID	Distance (cm)	20-Jul	18-Aug	02-Sep	23-Sep	06-Oct
C1-Inf	0	54.6	53.5	54.2	55.6	58.1
C1-P1	36	59.1	58.3	-	-	-
C1-P2	68	59.9	60.0	58.9	59.3	50.4
C1-P3	99	53.0	63.7	60.4	61.2	-
C1-P4	130	58.8	61.8	61.3	61.2	54.2
C2-Inf	171	58.0	61.1	63.1	61.6	60.2
C2-P1	238	55.2	60.1	61.1	66.6	53.9
C2-P2	299	52.6	55.8	61.1	65.2	56.2
C3-Inf	340	32.1	47.5	62.4	63.0	54.3
C3-P1	406	24.3	44.3	59.7	60.7	50.6
C3-P2	468	22.7	39.0	56.0	57.9	47.0
C3-Eff	509	20.7	-	-	-	-
Final Eff	610	20.2	26.6	47.6	54.2	42.6

DL: 0.21 mg L^{-1}

Table A 11: Concentrations of Ca (mg L^{-1}) along the treatment flow path in year 2 (2006) of the hypolimnetic withdrawal P treatment experiment.

Sample ID	Distance (cm)	19-Jul	03-Aug	17-Aug	09-Sep	30-Sep
C1-Inf	0	71.4	50.3	49.0	48.9	54.3
C1-P1	36	67.0	52.0	53.6	50.4	40.4
C1-P2	68	60.9	55.7	52.2	53.2	42.4
C1-P3	99	65.8	38.9	51.9	55.7	38.9
C1-P4	130	62.2	27.1	53.2	54.9	34.9
C2-Inf	171	56.0	40.5	34.1	41.1	44.0
C2-P1	238	85.0	71.0	30.8	27.4	21.4
C2-P2	299	60.4	102.7	55.6	41.8	27.2
C3-Inf	340	83.2	79.4	46.0	27.6	8.2
C3-P1	406	97.1	50.7	52.1	27.1	29.4
C3-P2	468	-	-	-	44.3	45.1
C3-Eff	509	-	-	-	43.2	52.9
Final Eff	610	64.4	30.3	61.3	39.5	40.7

DL: 0.21 mg L^{-1}

Table A 12: Concentrations of Ca (mg L^{-1}) along the treatment flow path in year 3 (2007) of the hypolimnetic withdrawal P treatment experiment.

Sample ID	Distance (cm)	01-Aug	15-Aug	13-Sep	01-Oct	22-Oct
C1-Inf	0	51.7	49.9	52	51.4	55.4
C1-P1	36	53.9	55.0	52.4	53.1	57.0
C1-P2	68	51.1	56.1	52.6	53.4	58.0
C1-P3	99	43.3	50.1	54.6	55.9	60.2
C1-P4	130	155	104	48.5	47.5	45.6
C2-Inf	151	136	102	49.9	46.4	47.0
C2-P1	238	427	152	70.4	53.7	42.3
C2-P2	299	489	174	89.7	71.6	65.7
C3-Inf	320	410	246	113	83.8	68.4
C3-P1	406	472	294	131	96.8	83.0
C3-P2	468	426	297	147	108	92.7
C3-Eff	509	476	318	158	113	94.7
Final Eff	610	30.1	162	117	84.2	98.8

DL: 0.21 mg L^{-1}

Table A 13: Concentrations of Na (mg L^{-1}) along the treatment flow path in year 1 (2005) of the hypolimnetic withdrawal P treatment experiment.

Sample ID	Distance (cm)	20-Jul	18-Aug	02-Sep	23-Sep	06-Oct
C1-Inf	0	51.0	48.6	48.9	49.9	48.0
C1-P1	36	52.5	50.1	-	-	-
C1-P2	68	53.1	49.8	49.3	48.4	48.0
C1-P3	99	45.1	51.5	49.6	48.9	54.8
C1-P4	130	51.8	50.3	49.7	48.3	48.2
C2-Inf	171	50.4	49.8	50.6	48.3	51.5
C2-P1	238	50.7	50.3	49.0	51.2	48.6
C2-P2	299	52.8	49.2	48.5	50.4	49.6
C3-Inf	340	51.5	48.9	50.6	49.6	48.4
C3-P1	406	50.6	49.2	49.8	48.4	48.4
C3-P2	468	51.4	50.2	49.3	48.0	49.8
C3-Eff	509	51.2	-	-	-	-
Final Eff	610	50.0	49.9	49.9	48.7	48.1

DL: 0.62 mg L^{-1}

Table A 14: Concentrations of Na (mg L^{-1}) along the treatment flow path in year 2 (2006) of the hypolimnetic withdrawal P treatment experiment.

Sample ID	Distance (cm)	19-Jul	03-Aug	17-Aug	09-Sep	30-Sep
C1-Inf	0	58.8	43.9	42.6	41.7	41.3
C1-P1	36	55.8	44.1	44.8	41.1	36.7
C1-P2	68	48.3	45.2	42.2	41.7	37.4
C1-P3	99	56.8	42.9	41.5	42.6	37.7
C1-P4	130	63.4	42.2	44.2	42.4	37.2
C2-Inf	171	57.1	45.2	44.3	41.4	38.7
C2-P1	238	47.3	43.9	41.8	41.0	38.2
C2-P2	299	48.0	46.2	41.2	41.4	36.5
C3-Inf	340	45.3	41.7	42.0	42.0	38.2
C3-P1	406	49.8	43.2	43.9	41.0	39.4
C3-P2	468	-	-	-	41.6	37.2
C3-Eff	509	-	-	-	40.3	37.7
Final Eff	610	57.8	43.3	41.4	39.8	37.9

DL: 0.21 mg L^{-1}

Table A 15: Concentrations of Na (mg L^{-1}) along the treatment flow path in year 3 (2007) of the hypolimnetic withdrawal P treatment experiment.

Sample ID	Distance (cm)	01-Aug	15-Aug	13-Sep	01-Oct	22-Oct
C1-Inf	0	76.5	41.5	59.5	38.6	39.4
C1-P1	36	76.2	43.4	58.8	38.6	39.4
C1-P2	68	76.3	42.9	58.5	38.4	40.5
C1-P3	99	75.9	42.0	58.9	38.3	40.6
C1-P4	130	78.1	44.2	59.4	39.0	39.5
C2-Inf	151	76.9	42.8	59.9	38.9	39.1
C2-P1	238	80.1	44.3	60.5	38.7	40.2
C2-P2	299	80.6	42.2	61.1	39.3	40.7
C3-Inf	320	79.5	43.8	61.2	39.7	41.9
C3-P1	406	80.9	42.9	61.2	40.0	41.5
C3-P2	468	80.0	44.4	61.4	40.0	41.2
C3-Eff	509	79.7	43.6	62.3	40.3	41.1
Final Eff	610	76.6	41.8	56.6	38.7	39.0

DL: 0.21 mg L^{-1}

Table A 16: Concentrations of Mg (mg L⁻¹) along the treatment flow path in year 1 (2005) of the hypolimnetic withdrawal P treatment experiment.

Sample ID	Distance (cm)	20-Jul	18-Aug	02-Sep	23-Sep	06-Oct
C1-Inf	0	7.40	7.11	7.17	7.39	7.51
C1-P1	36	8.27	7.70	-	-	-
C1-P2	68	8.83	8.11	7.56	7.65	6.34
C1-P3	99	7.73	8.72	7.83	7.88	6.81
C1-P4	130	9.44	9.13	8.17	7.96	6.68
C2-Inf	171	8.96	8.79	8.41	7.99	8.05
C2-P1	238	9.39	9.29	8.55	9.07	7.66
C2-P2	299	10.2	9.57	8.53	8.93	8.10
C3-Inf	340	9.78	10.1	9.18	8.86	8.55
C3-P1	406	8.95	10.8	9.35	8.88	8.04
C3-P2	468	9.19	11.9	9.71	8.95	8.29
C3-Eff	509	6.35	-	-	-	-
Final Eff	610	5.91	12.7	10.8	9.49	9.42

DL: 0.22 mg L⁻¹

Table A 17: Concentrations of Mg (mg L⁻¹) along the treatment flow path in year 2 (2006) of the hypolimnetic withdrawal P treatment experiment.

Sample ID	Distance (cm)	19-Jul	03-Aug	17-Aug	09-Sep	30-Sep
C1-Inf	0	6.87	6.46	6.28	6.11	6.59
C1-P1	36	6.91	6.82	6.71	6.21	4.86
C1-P2	68	7.30	8.05	6.77	6.90	5.71
C1-P3	99	5.90	6.76	7.62	8.08	5.88
C1-P4	130	5.24	4.49	8.40	8.49	5.77
C2-Inf	171	2.60	1.46	7.44	8.72	8.93
C2-P1	238	-	<DL	4.21	8.44	4.96
C2-P2	299	-	<DL	1.70	3.74	-
C3-Inf	340	-	<DL	1.35	3.98	4.80
C3-P1	406	0.94	<DL	0.35	1.29	0.49
C3-P2	468	-	-	-	<DL	<DL
C3-Eff	509	-	-	-	<DL	0.45
Final Eff	610	<DL	<DL	<DL	<DL	0.94

DL: 0.22 mg L⁻¹

Table A 18: Concentrations of Mg (mg L^{-1}) along the treatment flow path in year 3 (2007) of the hypolimnetic withdrawal P treatment experiment.

Sample ID	Distance (cm)	01-Aug	15-Aug	13-Sep	01-Oct	22-Oct
C1-Inf	0	6.89	6.82	6.71	6.80	7.06
C1-P1	36	6.96	6.97	6.60	6.72	6.77
C1-P2	68	6.70	6.51	6.53	6.83	6.74
C1-P3	99	5.59	7.57	7.19	7.46	7.77
C1-P4	130	0.41	0.77	6.00	5.29	6.12
C2-Inf	171	< DL	0.26	3.21	4.35	4.89
C2-P1	238	< DL	< DL	< DL	0.40	1.50
C2-P2	299	< DL	< DL	< DL	< DL	0.30
C3-Inf	340	< DL	< DL	< DL	< DL	0.26
C3-P1	406	< DL	< DL	< DL	< DL	< DL
C3-P2	468	< DL	< DL	< DL	< DL	< DL
C3-Eff	509	< DL	< DL	< DL	< DL	< DL
Final Eff	610	< DL	< DL	< DL	< DL	< DL

DL: 0.22 mg L^{-1}

Table A 19: Concentrations of Mn (mg L^{-1}) along the treatment flow path in year 1 (2005) of the hypolimnetic withdrawal P treatment experiment.

Sample ID	Distance (cm)	20-Jul	18-Aug	02-Sep	23-Sep	06-Oct
C1-Inf	0	0.73	0.86	0.92	1.0	0.94
C1-P1	36	0.83	0.91	-	-	-
C1-P2	68	0.71	0.97	0.97	1.1	0.29
C1-P3	99	0.52	0.89	1.0	1.1	0.28
C1-P4	130	0.45	0.72	1.0	1.1	0.34
C2-Inf	171	0.45	0.67	0.80	1.1	0.46
C2-P1	238	0.33	0.45	0.78	0.99	0.33
C2-P2	299	0.17	0.21	0.66	0.78	0.36
C3-Inf	340	0.058	0.11	0.48	0.56	0.35
C3-P1	406	0.043	0.14	0.25	0.31	0.21
C3-P2	468	0.054	0.11	0.15	0.21	0.13
C3-Eff	509	-	-	-	-	-
Final Eff	610	<DL	0.066	0.12	0.15	0.10

DL: 0.027 mg L^{-1}

Table A 20: Concentrations of Mn (mg L^{-1}) along the treatment flow path in year 2 (2006) of the hypolimnetic withdrawal P treatment experiment.

Sample ID	Distance (cm)	19-Jul	03-Aug	17-Aug	09-Sep	30-Sep
C1-Inf	0	0.63	0.71	0.76	0.82	0.89
C1-P1	36	0.67	0.76	0.79	0.87	0.26
C1-P2	68	0.77	0.70	0.98	0.96	0.33
C1-P3	99	0.21	0.19	1.1	0.99	0.35
C1-P4	130	0.20	0.06	0.83	0.79	0.32
C2-Inf	171	<DL	<DL	0.24	0.32	0.44
C2-P1	238	<DL	<DL	<DL	0.091	0.020
C2-P2	299	<DL	<DL	<DL	<DL	<DL
C3-Inf	340	<DL	<DL	<DL	<DL	<DL
C3-P1	406	0.058	<DL	<DL	<DL	<DL
C3-P2	468	-	-	-	<DL	<DL
C3-Eff	509	-	-	-	-	-
Final Eff	610	<DL	<DL	<DL	<DL	0.035

DL: 0.027 mg L^{-1}

Table A 21: Concentrations of Mn (mg L^{-1}) along the treatment flow path in year 3 (2007) of the hypolimnetic withdrawal P treatment experiment.

Sample ID	Distance (cm)	01-Aug	15-Aug	13-Sep	01-Oct	22-Oct
C1-Inf	0	0.99	0.94	0.92	0.83	0.89
C1-P1	36	0.94	0.95	0.86	0.82	0.81
C1-P2	68	0.72	0.80	0.92	0.84	0.81
C1-P3	99	0.27	0.58	0.94	0.83	0.80
C1-P4	130	<DL	<DL	0.34	0.23	0.19
C2-Inf	171	<DL	<DL	0.22	0.37	0.42
C2-P1	238	<DL	<DL	<DL	<DL	<DL
C2-P2	299	<DL	<DL	<DL	<DL	<DL
C3-Inf	340	<DL	<DL	<DL	<DL	<DL
C3-P1	406	<DL	<DL	<DL	<DL	<DL
C3-P2	468	<DL	<DL	<DL	<DL	<DL
C3-Eff	509	<DL	<DL	<DL	<DL	<DL
Final Eff	610	<DL	<DL	<DL	<DL	0.036

DL: 0.027 mg L^{-1}

Table A 22: Concentrations of SO₄ (mg L⁻¹) along the treatment flow path in year 1 (2005) of the hypolimnetic withdrawal P treatment experiment.

Sample ID	Distance (cm)	20-Jul	18-Aug	23-Sep
C1-Inf	0	12.3	11.1	9.47
C1-P1	36	10.8	9.14	-
C1-P2	68	10.2	7.18	6.19
C1-P3	99	9.63	6.63	5.11
C1-P4	130	9.83	6.11	5.64
C2-Inf	171	9.57	5.31	-
C2-P1	238	9.57	5.42	3.19
C2-P2	299	-	5.31	4.11
C3-Inf	340	8.69	5.16	3.30
C3-P1	406	9.16	5.85	3.18
C3-P2	468	9.43	5.50	3.57
C3-Eff	509	-	-	-
Final Eff	610	10.0	5.74	3.05

DL: 0.01 mg L⁻¹

Table A 23: Concentrations of SO₄ (mg L⁻¹) along the treatment flow path in year 2 (2006) of the hypolimnetic withdrawal P treatment experiment.

Sample ID	Distance (cm)	19-Jul	17-Aug	09-Sep	10-Oct
C1-Inf	0	12.6	11.0	10.8	11.3
C1-P1	36	11.8	11.4	9.42	9.91
C1-P2	68	8.08	8.87	6.16	6.82
C1-P3	99	8.61	6.07	3.53	3.71
C1-P4	130	10.2	6.29	2.28	3.46
C2-Inf	171	9.72	6.81	2.77	1.76
C2-P1	238	10.7	6.67	1.82	2.25
C2-P2	299	9.62	7.04	2.98	2.33
C3-Inf	340	8.80	7.03	2.56	2.76
C3-P1	406	9.93	7.52	3.68	2.68
C3-P2	468	9.95	6.30	3.79	2.92
C3-Eff	509	-	-	-	-
Final Eff	610	10.2	7.49	2.83	3.09

DL: 0.01 mg L⁻¹

Table A 24: Concentrations of SO₄ (mg L⁻¹) along the treatment flow path in year 3(2007) of the hypolimnetic withdrawal P treatment experiment.

Sample ID	Distance (cm)	01-Aug	15-Aug	13-Sep	01-Oct	22-Oct
C1-Inf	0	10.1	11.9	13.3	10.9	13.6
C1-P1	36	10.1	11.4	12.7	10.4	12.7
C1-P2	68	5.44	9.14	12.8	9.99	12.1
C1-P3	99	5.98	5.62	10.3	6.44	8.68
C1-P4	130	5.42	5.17	4.75	5.58	2.41
C2-Inf	171	5.94	3.94	3.48	8.48	9.57
C2-P1	238	3.80	3.95	10.1	6.49	7.67
C2-P2	299	3.23	3.75	4.51	5.32	8.15
C3-Inf	340	2.81	4.42	7.00	8.06	7.89
C3-P1	406	2.52	3.58	3.80	7.69	8.04
C3-P2	468	3.39	2.62	5.28	8.12	8.00
C3-Eff	509	1.97	3.48	5.02	3.72	8.14
Final Eff	610	2.77	3.48	4.36	6.60	7.25

DL: 0.01 mg L⁻¹

Table A 25: Concentrations of V (µg L⁻¹) along the treatment flow path in year 1 (2005) of the hypolimnetic withdrawal P treatment experiment.

Sample ID	Distance (cm)	20-Jul	18-Aug	02-Sep	23-Sep	06-Oct
C1-Inf	0	0.109	0.109	<DL	<DL	<DL
C1-P1	36	1.92	1.67	-	-	-
C1-P2	68	3.31	3.06	1.79	1.88	-
C1-P3	99	3.42	3.10	3.03	2.32	2.64
C1-P4	130	5.33	3.29	3.14	2.37	1.93
C2-Inf	171	4.21	2.18	3.96	1.96	5.86
C2-P1	238	7.05	2.53	2.75	2.87	-
C2-P2	299	8.14	2.22	2.64	2.50	1.02
C3-Inf	340	13.1	2.03	2.99	2.40	2.51
C3-P1	406	10.9	0.900	3.50	3.00	-
C3-P2	468	9.30	1.45	1.75	1.93	2.21
C3-Eff	509	19.9	-	-	-	-
Final Eff	610	20.7	3.91	4.77	2.06	8.22

DL: 0.025 µg L⁻¹

Table A 26: Concentrations of V ($\mu\text{g L}^{-1}$) along the treatment flow path in year 2 (2006) of the hypolimnetic withdrawal P treatment experiment.

Sample ID	Distance (cm)	19-Jul	03-Aug	17-Aug	09-Sep	30-Sep
C1-Inf	0	26.8	<DL	<DL	<DL	<DL
C1-P1	36	25.0	1.15	0.441	0.271	2.48
C1-P2	68	14.2	3.37	4.01	1.49	2.85
C1-P3	99	48.5	13.1	2.39	1.75	2.48
C1-P4	130	60.4	35.1	4.07	2.15	3.11
C2-Inf	171	92.1	78.3	26.3	5.71	7.32
C2-P1	238	118	120	32.2	9.37	19.8
C2-P2	299	-	-	-	-	-
C3-Inf	340	113	102	95.5	50.8	35.2
C3-P1	406	112	92.3	108	71.5	91.4
C3-P2	468	-	-	-	-	-
C3-Eff	509	-	-	-	-	-
Final Eff	610	112	84.5	127	91.8	73.0

DL: $0.025 \mu\text{g L}^{-1}$

Table A 26: Concentrations of V ($\mu\text{g L}^{-1}$) along the treatment flow path in year 3 (2007) of the hypolimnetic withdrawal P treatment experiment.

Sample ID	Distance (cm)	01-Aug	15-Aug	13-Sep	01-Oct	22-Oct
C1-Inf	0	0.30	0.30	0.41	0.24	0.30
C1-P1	36	3.20	1.40	1.11	2.35	3.86
C1-P2	68	7.30	3.90	2.38	3.16	4.28
C1-P3	99	27.4	9.20	2.30	2.22	2.38
C1-P4	130	30.1	44.0	39.3	49.4	30.8
C2-Inf	171	40.3	53.1	41.0	27.8	22.0
C2-P1	238	5.00	34.7	72.7	87.3	69.8
C2-P2	299	-	-	-	-	-
C3-Inf	340	2.70	6.10	21.3	87.1	90.0
C3-P1	406	2.00	3.70	11.1	83.2	101
C3-P2	468	-	-	-	-	-
C3-Eff	509	-	-	-	-	-
Final Eff	610	0.20	0.100	2.15	46.2	85.7

DL: $0.025 \mu\text{g L}^{-1}$

Table A 26: Concentrations of Al ($\mu\text{g L}^{-1}$) along the treatment flow path in year 1 (2005) of the hypolimnetic withdrawal P treatment experiment.

Sample ID	Distance (cm)	20-Jul	18-Aug	02-Sep	23-Sep	06-Oct
C1-Inf	0	<DL	1.1	8.4	0.64	5.8
C1-P1	36	19	12	14	-	-
C1-P2	68	44	35	18	8.4	53
C1-P3	99	52	27	28	14	66
C1-P4	130	63	27	32	18	46
C2-Inf	171	62	26	21	28	33
C2-P1	238	81	45	12	32	50
C2-P2	299	47	35	23	21	31
C3-Inf	340	11	18	14	12	8.4
C3-P1	406	28	21	-	23	28
C3-P2	468	30	22	14	14	24
C3-Eff	509	23	-	-	-	-
Final Eff	610	25	19	<DL	14	22

DL: $0.64 \mu\text{g L}^{-1}$

Table A 27: Concentrations of Al ($\mu\text{g L}^{-1}$) along the treatment flow path in year 2 (2006) of the hypolimnetic withdrawal P treatment experiment.

Sample ID	Distance (cm)	19-Jul	03-Aug	17-Aug	09-Sep	30-Sep
C1-Inf	0	5	2	2	<DL	1
C1-P1	36	15	16	6	5	66
C1-P2	68	46	46	16	11	63
C1-P3	99	54	60	18	10	12
C1-P4	130	55	53	22	15	17
C2-Inf	171	108	158	14	28	8
C2-P1	238	400	436	21	33	52
C2-P2	299	525	849	266	128	71
C3-Inf	340	400	599	109	49	19
C3-P1	406	466	526	107	15	21
C3-P2	468	616	-	-	118	137
C3-Eff	509	616	-	-	159	108
Final Eff	610	622	843	265	150	122

DL: $0.606 \mu\text{g L}^{-1}$

Table A 28: Concentrations of Al ($\mu\text{g L}^{-1}$) along the treatment flow path in year 3 (2007) of the hypolimnetic withdrawal P treatment experiment.

Sample ID	Distance (cm)	01-Aug	15-Aug	13-Sep	01-Oct	22-Oct
C1-Inf	0	10	<DL	<DL	<DL	<DL
C1-P1	36	30	10	<DL	10	20
C1-P2	68	50	50	20	9.9	20
C1-P3	99	70	40	20	30	20
C1-P4	130	370	40	70	60	60
C2-Inf	171	290	230	80	40	50
C2-P1	238	300	400	190	70	30
C2-P2	299	310	670	350	170	110
C3-Inf	340	390	690	510	260	140
C3-P1	406	340	660	600	350	180
C3-P2	468	350	650	660	460	260
C3-Eff	509	370	590	660	530	290
Final Eff	610	350	570	140	100	140

DL: $10 \mu\text{g L}^{-1}$

Appendix B
Summary of Data Presented in Chapter 3

Table B 1: pH values along the treatment flow path of the EW-BOFS pilot-scale treatment system experiment.

Date	Cell 1	Cell 2	Cell 3	Cell 4	Cell 5
1-Jun-09	7.37	8.54	8.54	12.19	11.67
17-Jun-09	7.53	8.30	8.62	12.35	11.90
22-Jun-09	7.38	8.09	8.62	12.34	12.07
24-Jun-09	7.43	8.15	8.62	12.32	12.01
26-Jun-09	7.11	7.96	8.61	12.28	12.01
29-Jun-09	7.25	7.98	8.66	12.36	12.14
2-Jul-09	7.47	8.02	8.57	12.35	12.17
2-Jul-09	7.96	8.17	8.46	12.30	12.00
8-Jul-09	7.42	8.09	8.60	12.35	12.07
9-Jul-09	7.48	8.38	8.62	12.19	12.05
15-Jul-09	-	8.17	8.53	12.30	11.85
15-Jul-09	-	7.94	8.31	11.80	11.49
22-Jul-09	7.19	7.70	8.24	11.70	11.48
30-Jul-09	6.91	7.92	8.48	11.95	11.76
5-Aug-09	7.19	7.68	8.41	11.78	11.45
12-Aug-09	7.36	7.49	8.49	11.65	10.22
19-Aug-09	7.38	7.52	8.45	11.72	11.11
26-Aug-09	7.54	7.53	8.29	11.87	11.40
9-Sep-09	7.51	7.68	8.41	11.64	-
16-Sep-09	7.87	7.82	8.33	11.69	6.80
23-Sep-09	7.69	8.00	8.58	11.88	7.25
24-Sep-09	-	-	-	11.50	-
25-Sep-09	-	-	-	11.37	7.07
28-Sep-09	-	-	-	11.71	7.26
29-Sep-09	-	-	-	11.44	6.84
30-Sep-09	7.28	7.49	8.09	11.03	6.95
1-Oct-09	-	-	-	11.35	7.14
2-Oct-09	-	-	-	11.25	7.14
5-Oct-09	-	-	-	11.65	7.11
6-Oct-09	-	-	-	11.86	7.28
7-Oct-09	7.71	7.74	8.40	11.59	7.18
8-Oct-09	-	-	-	11.92	7.34
9-Oct-09	-	-	-	11.80	7.04
13-Oct-09	-	-	-	11.32	7.29
14-Oct-09	7.59	7.86	8.50	11.80	7.28
15-Oct-09	-	-	-	11.77	7.33
15-Oct-09	-	8.01	8.62	11.98	7.51
16-Oct-09	-	-	-	11.42	7.38

Table B 1 continued: pH values along the treatment flow path of the EW-BOFS pilot-scale treatment system experiment.

Date	Cell 1	Cell 2	Cell 3	Cell 4	Cell 5
19-Oct-09	-	-	-	11.78	7.41
20-Oct-09	-	-	-	11.89	7.44
21-Oct-09	-	-	-	11.58	7.44
22-Oct-09	7.39	7.71	8.41	11.50	7.00
23-Oct-09	7.38	7.65	8.41	11.60	7.34
26-Oct-09	-	-	-	11.61	7.27
27-Oct-09	-	-	-	11.63	7.24
28-Oct-09	-	-	-	11.29	7.33
29-Oct-09	-	-	-	11.64	7.45
2-Nov-09	-	-	-	11.64	7.33
3-Nov-09	-	-	-	11.21	7.31
6-Nov-09	-	-	-	11.17	7.18
9-Nov-09	-	-	-	11.14	7.07
10-Nov-09	-	-	-	11.52	7.43
13-Nov-09	-	-	-	11.54	7.30
16-Nov-09	-	-	-	11.55	7.42
17-Nov-09	-	7.73	8.39	11.74	7.53
19-Nov-09	-	-	-	11.46	6.87
20-Nov-09	-	-	-	11.40	6.94
23-Nov-09	-	-	-	11.23	6.82
24-Nov-09	-	-	-	11.66	7.13
26-Nov-09	-	-	-	11.50	6.91
27-Nov-09	-	-	-	11.27	6.88
30-Nov-09	-	-	-	11.62	7.16
2-Dec-09	7.44	7.42	7.85	11.15	7.24
3-Dec-09	-	-	-	11.36	7.39
7-Dec-09	-	-	-	11.31	7.50
9-Dec-09	7.60	7.91	8.11	11.41	7.90
14-Dec-09	-	-	-	11.52	7.72
15-Dec-09	-	-	-	11.44	7.55
16-Dec-09	7.49	7.63	7.99	11.35	7.46
17-Dec-09	-	-	-	11.47	-
14-Jan-10	7.74	7.72	7.59	11.60	7.91
20-Jan-10	7.75	7.94	7.75	11.11	7.34
27-Jan-10	7.89	7.66	7.58	10.96	6.97
3-Feb-10	7.90	7.82	7.70	11.12	7.14
9-Feb-10	-	7.99	7.57	11.46	7.47

Table B 2: Measurements of alkalinity (mg L⁻¹ CaCO₃) along the treatment flow path of the EW-BOFS pilot-scale treatment system experiment.

Date	Cell 1	Cell 2	Cell 3	Cell 4	Cell 5
1-Jun-09	305	243	175	1560	342
17-Jun-09	308	248	220	1290	952
24-Jun-09	333	256	220	1030	582
2-Jul-09	316	252	224	1050	556
2-Jul-09	347	254	241	995	621
8-Jul-09	324	236	232	964	528
9-Jul-09	-	221	250	920	659
15-Jul-09	284	224	220	880	324
22-Jul-09	240	212	228	744	356
30-Jul-09	312	224	220	680	400
5-Aug-09	340	232	212	592	352
12-Aug-09	316	276	236	524	292
19-Aug-09	352	284	236	480	216
26-Aug-09	302	256	222	478	164
2-Sep-09	285	268	226	422	146
9-Sep-09	214	222	224	420	-
16-Sep-09	248	240	240	340	688
23-Sep-09	264	256	248	424	472
30-Sep-09	276	266	252	386	258
1-Oct-09	-	-	-	374	227
2-Oct-09	-	-	-	378	206
5-Oct-09	-	-	-	426	200
7-Oct-09	274	266	254	446	196
13-Oct-09	-	-	-	456	194
14-Oct-09	334	284	270	410	182
15-Oct-09	-	230	330	520	230
16-Oct-09	-	-	-	410	194
19-Oct-09	-	-	-	442	208
21-Oct-09	-	-	-	435	195
22-Oct-09	284	268	268	426	198
29-Oct-09	-	-	-	398	174
2-Nov-09	-	-	-	354	152
13-Nov-09	-	-	-	278	230
30-Nov-09	-	-	-	280	348
2-Dec-09	433	398	225	265	335
3-Dec-09	-	-	-	264	252
7-Dec-09	-	-	-	286	292
9-Dec-09	500	450	225	228	238

Table B 2 continued: Measurements of alkalinity ($\text{mg L}^{-1} \text{CaCO}_3$) along the treatment flow path of the EW-BOFS pilot-scale treatment system experiment.

Date	Cell 1	Cell 2	Cell 3	Cell 4	Cell 5
14-Dec-09	-	-	-	244	200
15-Dec-09	-	-	-	254	184
16-Dec-09	528	488	205	280	200
20-Jan-10	633	560	170	203	175
27-Jan-10	688	620	168	210	122
3-Feb-10	670	625	194	200	130

Table B 3: Measurements of Eh (mV) along the treatment flow path of the EW-BOFS pilot-scale treatment system experiment.

Date	Cell 1	Cell 2	Cell 3	Cell 4	Cell 6
1-Jul-09	120	287	305	126	136
10-Aug-09	90	179	310	130	170
1-Oct-09	118	205	305	124	141
17-Nov-09	88	181	310	113	181

Table B 4: Concentrations of PO₄-P (mg L⁻¹) along the treatment flow path of the EW-BOFS pilot-scale treatment system experiment.

Date	Cell 1	Cell 2	Cell 3	Cell 4	Cell 5
3-Jun-09	7.77	4.34	2.50	0.07	0.31
10-Jun-09	8.75	5.16	2.19	0.007	0.27
18-Jun-09	8.55	4.48	1.97	0.03	0.72
19-Jun-09	10.6	5.22	2.33	0.01	0.26
24-Jun-09	8.62	5.18	1.97	0.03	0.85
2-Jul-09	8.94	4.99	2.32	0.03	0.03
3-Jul-09	8.95	4.99	2.32	0.03	0.03
2-Jul-09	8.55	4.97	2.49	0.03	0.03
8-Jul-09	8.95	5.11	2.39	0.03	0.03
9-Jul-09	7.93	3.60	0.22	0.005	0.02
10-Jul-09	8.03	4.27	2.06	0.007	0.10
15-Jul-09	7.40	3.27	2.13	0.03	0.03
21-Jul-09	6.90	2.94	1.84	0.03	0.03
22-Jul-09	6.52	3.10	2.16	0.03	0.03
24-Jul-09	6.40	3.33	2.25	0.03	0.11
30-Jul-09	6.29	2.85	1.84	0.03	0.03
30-Jul-09	6.21	3.03	2.12	0.03	0.03
5-Aug-09	5.63	2.82	1.74	0.03	0.03
7-Aug-09	6.13	3.15	1.93	0.03	0.03
10-Aug-09	6.11	2.99	1.79	0.009	0.04
12-Aug-09	5.62	3.19	1.90	0.03	0.03
14-Aug-09	7.96	6.40	2.89	0.03	0.30
19-Aug-09	7.37	4.08	2.20	0.03	0.36
21-Aug-09	7.18	4.01	2.24	0.03	0.35
26-Aug-09	6.53	4.96	2.76	0.03	0.24
31-Aug-09	5.26	3.90	2.08	0.03	0.03
2-Sep-09	5.18	3.97	2.40	0.03	0.03
3-Sep-09	3.92	4.18	2.35	0.03	0.30
9-Sep-09	4.89	3.26	2.43	0.03	0.03
10-Sep-09	2.78	2.85	2.23	0.03	0.03
16-Sep-09	2.68	2.23	2.16	0.03	2.47
15-Oct-09	4.44	2.83	2.33	0.005	1.62
30-Oct-09	6.40	4.11	2.79	0.007	1.98
4-Nov-09	6.46	4.67	3.26	0.007	1.27
11-Nov-09	7.65	6.04	3.82	0.04	0.62
17-Nov-09	8.81	6.37	3.63	0.01	0.38
18-Nov-09	9.17	6.82	4.41	0.05	0.63
25-Nov-09	9.40	9.20	6.33	0.08	1.08

Table B 4 continued: Concentrations of PO₄-P (mg L⁻¹) along the treatment flow path of the EW-BOFS pilot-scale treatment system experiment.

Date	Cell 1	Cell 2	Cell 3	Cell 4	Cell 5
2-Dec-09	11.2	9.27	6.85	0.06	0.18
9-Dec-09	10.8	7.61	5.55	0.007	0.23
16-Dec-09	3.26	5.25	4.49	0.005	0.005
14-Jan-10	4.97	8.06	7.37	0.04	0.38
20-Jan-10	7.11	7.62	5.34	0.01	0.15
20-Jan-10	6.26	6.07	6.00	0.07	0.20
27-Jan-10	6.00	5.45	4.50	0.07	0.17
3-Feb-10	6.78	5.64	4.83	0.02	0.18
19-Feb-10	-	5.41	3.99	0.007	0.10

Table B 5: Concentrations of Ca (mg L⁻¹) along the treatment flow path during the EW-BOFS pilot-scale wastewater treatment experiment.

Date	Cell 1	Cell 2	Cell 3	Cell 4	Cell 4*	Cell 5	Cell 6	DL
09-Jul-09	96	82	79	294	-	228	89	0.20
10-Aug-09	95	83	78	228	-	102	23	0.20
15-Oct-09	91	85	82	164	30	54	-	0.13
04-Nov-09	93	89	85	123	17	41	51	0.23
17-Nov-09	99	103	92	128	93	88	75	0.08
03-Feb-10	157	132	125	140	68	81	73	0.08

Table B 6: Concentrations of Na (mg L⁻¹) along the treatment flow path during the EW-BOFS pilot-scale wastewater treatment experiment.

Date	Cell 1	Cell 2	Cell 3	Cell 4	Cell 4*	Cell 5	Cell 6	DL
09-Jul-09	63.2	68.3	72.6	78.3	-	86.3	86.6	0.10
10-Aug-09	87.3	75.9	72.4	67.9	-	72.3	72.2	0.10
15-Oct-09	114	114	117	111	108	105	-	0.03
04-Nov-09	108	109	110	109	109	106	107	0.10
17-Nov-09	124	134	130	130	130	134	137	0.10
03-Feb-10	179	162	162	147	142	144	144	0.10

Table B 7: Concentrations of Mg (mg L^{-1}) along the treatment flow path during the EW-BOFS pilot-scale wastewater treatment experiment.

Date	Cell 1	Cell 2	Cell 3	Cell 4	Cell 4*	Cell 5	Cell 6	DL
09-Jul-09	11	11	10	<DL	-	0.14	0.10	0.10
10-Aug-09	10	11	10	<DL	-	0.18	0.07	0.02
15-Oct-09	11	11	11	<DL	0.63	<DL	-	0.02
04-Nov-09	11	11	11	<DL	0.62	0.02	0.64	0.02
17-Nov-09	13	13	13	<DL	<DL	0.77	0.75	0.10
03-Feb-10	16	14	16	0.41	0.52	0.65	0.51	0.10

Table B 8: Concentrations of SO_4 (mg L^{-1}) along the treatment flow path during the EW-BOFS pilot-scale wastewater treatment experiment.

Date	Cell 1	Cell 2	Cell 3	Cell 4	Cell 4*	Cell 5	Cell 6	MDL
09-Jul-09	28	25	25	9	10	17	6	0.018
10-Aug-09	47	47	50	24	30	33	32	0.018
15-Oct-09	61	64	67	51	51	45	46	0.018
04-Nov-09	61	64	67	54	52	52	48	0.018
17-Nov-09	52	57	59	50	50	54	53	0.018
03-Feb-10	29	22	23	29	34	46	43	0.018

Table B 9: Concentrations of V ($\mu\text{g L}^{-1}$) along the treatment flow path during the EW-BOFS pilot-scale wastewater treatment experiment.

Date	Cell 1	Cell 2	Cell 3	Cell 4	Cell 5	DL ($\mu\text{g L}^{-1}$)
9-Jul-09	0.40	0.63	1.8	1.9	1.8	0.006
10-Aug-09	0.53	0.15	2.2	5.0	5.2	0.035
15-Oct-09	0.91	1.1	1.3	13	2.1	0.015
4-Nov-09	0.40	0.61	1.0	16	7.0	0.015
11-Nov-09	0.06	0.56	1.5	37	8.5	0.009
17-Nov-09	0.29	0.70	1.3	32	9.9	0.007
16-Dec-09	0.20	0.53	0.73	49	24	0.004
27-Jan-10	0.66	0.53	1.0	44	26	0.004
3-Feb-10	0.35	0.47	0.72	47	24	0.020

Table B 10: Concentrations of Al ($\mu\text{g L}^{-1}$) along the treatment flow path during the EW-BOFS pilot-scale wastewater treatment experiment.

Date	Cell 1	Cell 2	Cell 3	Cell 4	Cell 5	DL ($\mu\text{g L}^{-1}$)
9-Jul-09	6.14	4.41	21.0	821	1334	0.030
10-Aug-09	5.70	<DL	21.3	1183	1516	0.449
15-Oct-09	3.54	2.03	5.16	955	23.4	0.055
4-Nov-09	0.93	10.6	3.31	818	27.8	0.453
11-Nov-09	0.28	0.08	2.22	637	10.7	0.080
17-Nov-09	15.2	0.08	0.13	708	5.98	0.082
16-Dec-09	5.70	6.08	0.08	425	40.0	0.227
27-Jan-10	15.3	7.77	0.82	186	22.2	0.227
3-Feb-10	3.72	5.63	0.42	431	13.3	0.280

Table B 11: Concentrations of Zn ($\mu\text{g L}^{-1}$) along the treatment flow path during the EW-BOFS pilot-scale wastewater treatment experiment.

Date	Cell 1	Cell 2	Cell 3	Cell 4	Cell 5	DL ($\mu\text{g L}^{-1}$)
9-Jul-09	3.79	2.91	3.40	6.64	4.66	0.057
10-Aug-09	5.40	5.93	4.53	4.67	12.2	0.067
15-Oct-09	12.8	16.4	5.56	2.07	6.47	0.083
4-Nov-09	15.9	8.58	4.61	1.60	5.11	0.025
11-Nov-09	19.9	12.1	8.32	23.7	10.9	0.072
17-Nov-09	21.9	35.3	3.17	1.27	23.3	0.086
16-Dec-09	9.32	22.4	4.44	3.47	14.2	1.559
27-Jan-10	5.32	5.93	5.79	4.37	5.57	1.559
3-Feb-10	3.39	4.39	3.67	1.39	7.22	0.920

Table B 12: Concentrations of Mn ($\mu\text{g L}^{-1}$) along the treatment flow path during the EW-BOFS pilot-scale wastewater treatment experiment.

Date	Cell 1	Cell 2	Cell 3	Cell 4	Cell 5	DL ($\mu\text{g L}^{-1}$)
9-Jul-09	59	3.7	0.56	2.6	7.5	0.011
10-Aug-09	43	0.04	0.33	1.9	5.9	0.035
15-Oct-09	32	9.7	0.47	0.89	85	0.019
4-Nov-09	4	16	0.39	0.77	68	0.008
11-Nov-09	79	41	1.1	1.6	90	0.012
17-Nov-09	96	47	1.0	1.3	101	0.012
16-Dec-09	93	101	0.65	0.75	8.1	0.012
27-Jan-10	55	84	1.0	0.32	54	0.012
3-Feb-10	46	65	0.47	0.92	49	0.030

Table B 13: Concentrations of Cr ($\mu\text{g L}^{-1}$) along the treatment flow path during the EW-BOFS pilot-scale wastewater treatment experiment.

Date	Cell 1	Cell 2	Cell 3	Cell 4	Cell 5	DL ($\mu\text{g L}^{-1}$)
9-Jul-09	0.06	0.04	0.06	2.13	0.46	0.009
10-Aug-09	0.03	0.03	0.03	3.85	0.03	0.031
15-Oct-09	0.07	0.13	0.11	3.94	2.10	0.019
4-Nov-09	0.02	0.39	0.05	3.59	0.13	0.001
11-Nov-09	0.27	0.23	0.25	4.38	0.37	0.012
17-Nov-09	1.16	0.18	0.26	4.71	0.57	0.011
16-Dec-09	0.35	0.38	0.10	4.21	1.32	0.015
27-Jan-10	0.23	0.31	0.22	4.03	1.06	0.015
3-Feb-10	0.23	0.25	0.16	4.32	1.14	0.040

Table B 14: Concentrations of Cu ($\mu\text{g L}^{-1}$) along the treatment flow path during the EW-BOFS pilot-scale wastewater treatment experiment.

Date	Cell 1	Cell 2	Cell 3	Cell 4	Cell 5	DL ($\mu\text{g L}^{-1}$)
9-Jul-09	3.2	21	20	6.7	6.4	0.021
10-Aug-09	5.5	18	24	12	10	0.029
15-Oct-09	12	25	15	6.4	4.0	0.043
4-Nov-09	7.9	9.6	12	6.3	4.4	0.021
11-Nov-09	8.2	15	18	15	11	0.020
17-Nov-09	14	26	25	16	16	0.020
16-Dec-09	17	8.2	22	25	17	0.027
27-Jan-10	4.2	4.3	16	7.9	6.8	0.027
3-Feb-10	2.6	4.3	11	8.3	7.7	0.050

Table B 15: Concentrations of Fe ($\mu\text{g L}^{-1}$) along the treatment flow path during the EW-BOFS pilot-scale wastewater treatment experiment.

Date	Cell 1	Cell 2	Cell 3	Cell 4	Cell 5	DL ($\mu\text{g L}^{-1}$)
9-Jul-09	47	14	15	8.3	42	0.050
10-Aug-09	47	14	8.6	5.0	37	0.062
15-Oct-09	34	16	40	3.7	317	0.050
4-Nov-09	57	39	10	8.6	117	0.089
11-Nov-09	64	25	9.4	5.0	37	0.081
17-Nov-09	156	43	11	4.2	50	0.100
16-Dec-09	98	118	19	4.6	20	0.066
27-Jan-10	140	68	14	9.3	17	0.066
3-Feb-10	107	55	13	8.5	18	0.660

Table B 16: Concentrations of Ni ($\mu\text{g L}^{-1}$) along the treatment flow path during the EW-BOFS pilot-scale wastewater treatment experiment.

Date	Cell 1	Cell 2	Cell 3	Cell 4	Cell 5	DL ($\mu\text{g L}^{-1}$)
9-Jul-09	2.2	2.1	1.9	0.36	1.3	0.015
10-Aug-09	2.2	1.9	1.9	0.43	1.3	0.042
15-Oct-09	3.0	2.7	2.1	0.78	1.6	0.018
4-Nov-09	2.3	3.8	1.9	0.71	1.2	0.008
11-Nov-09	3.5	2.7	2.8	1.5	1.3	0.021
17-Nov-09	5.7	2.5	2.5	1.7	1.7	0.016
16-Dec-09	4.3	3.9	2.3	1.3	1.4	0.047
27-Jan-10	3.3	3.3	2.6	1.8	1.4	0.047
3-Feb-10	2.5	2.5	2.0	1.0	1.4	0.050

Table B 17: Concentrations of Pb ($\mu\text{g L}^{-1}$) along the treatment flow path during the EW-BOFS pilot-scale wastewater treatment experiment.

Date	Cell 1	Cell 2	Cell 3	Cell 4	Cell 5	DL ($\mu\text{g L}^{-1}$)
9-Jul-09	0.08	0.05	0.05	0.33	0.15	0.002
10-Aug-09	0.04	0.01	0.14	0.14	0.10	0.005
15-Oct-09	0.08	0.71	0.07	0.08	0.10	0.006
4-Nov-09	0.03	0.03	0.02	0.05	0.06	0.002
11-Nov-09	0.28	0.45	0.33	0.58	0.47	0.002
17-Nov-09	1.5	6.3	0.23	0.15	0.50	0.002
16-Dec-09	0.43	0.47	0.90	0.22	1.1	0.003
27-Jan-10	0.22	2.3	0.20	0.17	0.14	0.003
3-Feb-10	0.30	0.64	0.45	0.36	1.1	0.014

Table B 18: Concentrations of NH₃-N (mg L⁻¹) along the treatment flow path during the EW-BOFS pilot-scale wastewater treatment experiment.

Date	Cell 1	Cell 2	Cell 3	Cell 4	Cell 5
1-Jun-09	4.5	0.06	0.05	0.6	5.9
17-Jun-09	8.8	0.16	0.02	0.41	6.4
24-Jun-09	12	0.4	0.02	0.29	6.5
2-Jul-09	11	0.15	0.02	0.22	3.6
2-Jul-09	13	0.5	0.1	0.2	3.7
8-Jul-09	8.2	0.37	0.02	0.2	4.5
15-Jul-09	7.3	0.37	0.02	0.25	3.6
22-Jul-09	1.8	0.05	0.03	0.17	3.7
30-Jul-09	11	0.77	0.06	0.19	4.5
5-Aug-09	9.1	0.65	0.02	0.15	2.9
12-Aug-09	8.7	1.2	0.02	0.07	2.6
19-Aug-09	15	4.3	0.02	0.23	6.3
2-Sep-09	9.2	4.2	0.08	0.12	2.8
9-Sep-09	0.1	0.11	0.13	0.22	-
16-Sep-09	0.2	0.4	0.02	0.08	2.6
30-Oct-09	-	-	0.02	0.14	2.1
4-Nov-09	12	4.3	0.02	0.07	1.8
11-Nov-09	25	11	0.04	0.11	1.5
18-Nov-09	28	16	0.07	0.06	1.5
25-Nov-09	32	18	0.25	0.09	2.1
2-Dec-09	42	31	0.38	0.06	0.95
9-Dec-09	77	40	0.03	0.07	1.5
16-Dec-09	51	40	0.06	0.09	0.98
14-Jan-10	68	46	0.4	3.6	3.7
20-Jan-10	58	14	0.8	0.4	1.4
27-Jan-10	63	53	6.1	0.57	0.6
3-Feb-10	76	58	0.2	0.23	1.1

DL: 0.02 mg L⁻¹

Table B 19: Concentrations of NO₃-N (mg L⁻¹) along the treatment flow path during the EW-BOFS pilot-scale wastewater treatment experiment.

Date	Cell 1	Cell 2	Cell 3	Cell 4	Cell 5
1-Jun-09	0.15	1.7	2.3	1.6	0.53
17-Jun-09	0.05	5.4	3.4	1.4	0.05
24-Jun-09	0.05	7.5	5.1	2.9	0.05
2-Jul-09	0.05	11	7.8	4.6	0.05
2-Jul-09	0.05	9.3	7.3	4.4	0.06
8-Jul-09	0.05	11	8.6	4.8	0.05
15-Jul-09	0.22	9.5	7.5	6.9	0.05
22-Jul-09	3.2	8.0	6.9	6.5	0.08
29-Jul-09	0.05	7.1	6.2	5.8	0.28
30-Jul-09	0.05	7.3	6.6	5.9	0.18
5-Aug-09	0.05	7.0	6.3	5.3	0.63
7-Aug-09	0.30	7.9	7.1	6.4	0.71
12-Aug-09	0.19	6.4	6.8	6.4	0.24
19-Aug-09	0.05	3.8	5.1	5.0	1.7
26-Aug-09	2.0	3.5	7.5	5.3	2.4
2-Sep-09	4.9	5.3	10	7.5	2.9
9-Sep-09	5.8	7.3	8.3	9.2	
16-Sep-09	5.7	5.4	4.1	6.0	
30-Oct-09	1.7	5.0	5.5	3.5	0.05
4-Nov-09	3.4	5.2	6.9	4.7	0.28
11-Nov-09	0.73	5.6	11	7.8	0.84
18-Nov-09	0.29	4.0	14	11	2.2
25-Nov-09	0.05	2.6	26	18	3.7
2-Dec-09	0.23	1.3	33	26	12
9-Dec-09	0.05	1.3	39	31	11
16-Dec-09	0.05	0.08		17	11
14-Jan-10	0.05	0.05	43	28	11
20-Jan-10	0.05	0.05	52	42	19
27-Jan-10	0.05	0.05	92	78	41
3-Feb-10	0.05	0.05	60	57	33

DL: 0.05 mg L⁻¹

Table B 20: Concentrations of DO (mg L^{-1}) along the treatment flow path during the EW-BOFS pilot-scale wastewater treatment experiment.

Date	Cell 1	Cell 2	Cell 3	Cell 4	Cell 5
1-Jun-09	1.9	11	8.1	2.0	3.5
17-Jun-09	2.5	7.3	7.4	2.1	4.3
24-Jun-09	1.2	5.4	5.7	1.4	1.6
2-Jul-09	1.2	6.2	7.0	1.4	3.2
2-Jul-09	5.2	5.3	7.0	6.6	4.4
8-Jul-09	1.1	6.5	7.0	1.2	1.8
15-Jul-09	1.3	6.7	6.9	1.6	2.1
22-Jul-09	1.8	7.0	7.0	1.4	1.7
30-Jul-09	0.8	6.6	7.0	1.7	2.2
5-Aug-09	1.1	6.5	7.2	1.7	2.5
12-Aug-09	0.92	3.0	6.9	1.8	3.4
19-Aug-09	0.40	1.0	7.4	1.8	1.8
26-Aug-09	1.5	1.1	7.2	2.2	2.2
2-Sep-09	3.1	4.0	8.7	1.7	2.9
9-Sep-09	4.6	5.5	7.7	2.2	
16-Sep-09	7.1	5.9	8.0	2.9	3.5
23-Sep-09	2.8	5.1	7.7	2.1	3.5
30-Sep-09	5.6	4.8	8.9	2.7	3.9
1-Oct-09	-	-	-	6.8	3.6
2-Oct-09	-	-	-	3.1	6.1
5-Oct-09	-	-	-	4.4	3.8
6-Oct-09	-	-	-	2.7	
7-Oct-09	4.4	4.9	8.7	2.0	3.7
8-Oct-09	-	-	-	3.2	3.7
9-Oct-09	-	-	-	2.5	4.2
13-Oct-09	-	-	-	2.9	5.6
14-Oct-09	3.4	5.7	8.7	2.1	4.1
15-Oct-09	-	-	-	2.2	4.0
16-Oct-09	-	-	-	2.7	5.2
19-Oct-09	-	-	-	2.3	5.0
20-Oct-09	-	-	-	2.7	4.6
21-Oct-09	-	-	-	2.5	8.1
22-Oct-09	4	6.7	9.7	2.9	3.9
23-Oct-09	10	9.9	9.9	22	8.1
26-Oct-09	-	-	-	3.5	5.4
27-Oct-09	-	-	-	2.7	5.0
28-Oct-09	-	-	-	3.0	4.2
29-Oct-09	-	-	-	2.5	4.4

Table B 20 continued: Concentrations of DO (mg L^{-1}) along the treatment flow path during the EW-BOFS pilot-scale wastewater treatment experiment.

Date	Cell 1	Cell 2	Cell 3	Cell 4	Cell 5
2-Nov-09	-	-	-	4.8	4.9
3-Nov-09	-	-	-	3.0	4.7
6-Nov-09	-	-	-	4.9	4.7
9-Nov-09	-	-	-	6.2	7.7
10-Nov-09	-	-	-	5.7	4.9
13-Nov-09	-	-	-	4.2	5.8
16-Nov-09	-	-	-	3.2	5.0
19-Nov-09	-	-	-	3.9	5.9
20-Nov-09	-	-	-	4.0	5.6
23-Nov-09	-	-	-	4.9	4.8
24-Nov-09	-	-	-	4.6	4.6
26-Nov-09	-	-	-	4.3	4.7
27-Nov-09	-	-	-	6.0	8.0
30-Nov-09	-	-	-	4.3	7.9
2-Dec-09	1.8	5.7	9.7	4.9	7.9
3-Dec-09	-	-	-	4.9	7.3
7-Dec-09	-	-	-	3.8	7.1
9-Dec-09	0.57	3.1	11	5.6	7.1
14-Dec-09	-	-	-	5.5	8.3
15-Dec-09	-	-	-	5.5	7.2
16-Dec-09	0.46	1.9	9.4	4.3	6.9
14-Jan-10	0.84	3.4	3.7	3.0	6.4
20-Jan-10	0.21	1.5	7.2	3.8	3.5
27-Jan-10	0.76	3.6	6.9	4.8	4.4
3-Feb-10	0.12	2.7	7.6	5.3	4.5

Table B 21: Concentrations of cBOD₅ (mg L⁻¹) along the treatment flow path during the EW-BOFS pilot-scale wastewater treatment experiment.

Date	Cell 1	Cell 2	Cell 3	Cell 4	Cell 5
1-Jun-09	40	48	42	1.0	18
17-Jun-09	15	37	39	1.0	7.6
24-Jun-09	20	11	5.0	1.0	5.2
2-Jul-09	15	12	8.2	1.0	1.9
2-Jul-09	6.0	4.0	4.0	4.0	4.0
8-Jul-09	14	8.3	4.1	1.0	1.0
15-Jul-09	11	6.3	7.9	1.0	1.0
22-Jul-09	8.9	4.7	6.6	1.0	1.0
30-Jul-09	23	8.3	8.9	1.0	1.0
5-Aug-09	16	6.0	11	1.0	1.0
12-Aug-09	17	8.5	11	1.0	1.0
19-Aug-09	20	17	8.3	1.0	1.0
26-Aug-09	16	9.6	3.9	1.0	1.0
2-Sep-09	12	9.5	6.9	1.0	3.1
9-Sep-09	8.8	4.3	7.4	1.0	11
4-Nov-09	15	7.6	1.0	1.0	-
11-Nov-09	18	9.8	1.7	1.0	4.0
18-Nov-09	15	12	3.9	1.0	5.9
25-Nov-09	13	10	6.1	1.0	5.3
2-Dec-09	21	11	7.1	1.0	6.7
9-Dec-09	53	27	7.3	1.0	6.1
16-Dec-09	21	24	2.8	1.0	5.4
20-Jan-10	80	46	9.7	1.0	6.1
3-Feb-10	168	57	9.9	1.0	1.0

DL: 1 mg L⁻¹

Table B 22: Concentrations of COD (mg L⁻¹) along the treatment flow path during the EW-BOFS pilot-scale wastewater treatment experiment.

Date	Cell 1	Cell 2	Cell 3	Cell 4	Cell 5
1-Jun-09	76	81	115	48	183
17-Jun-09	57	32	25	16	111
24-Jun-09	52	56	27	15	91
2-Jul-09	40	33	27	9.1	50
2-Jul-09	44	30	32	9.0	46
8-Jul-09	38	29	27	15	51
15-Jul-09	33	24	23	7.0	47
22-Jul-09	25	27	29	8.1	42
30-Jul-09	30	5.1	9.3	3.0	27
5-Aug-09	23	11	12	3.0	15
12-Aug-09	37	29	22	8.6	32
19-Aug-09	58	32	31	3.7	63
26-Aug-09	40	27	27	11	40
2-Sep-09	37	32	42	12	34
9-Sep-09	20	25	36	14	-
16-Sep-09	29	23	80	13	55
23-Sep-09	27	26	36	13	36
30-Sep-09	29	25	58	10	43
30-Oct-09	37	31	26	12	23
4-Nov-09	35	34	32	14	31
11-Nov-09	48	38	32	15	19
18-Nov-09	50	37	30	14	20
25-Nov-09	70	42	30	9.3	18
2-Dec-09	53	51	30	10	7.5
9-Dec-09	127	78	27	16	14
16-Dec-09	74	79	21	3.0	3.0
14-Jan-10	152	113	32	8.7	31
20-Jan-10	194	105	36	13	15
27-Jan-10	231	127	44	27	22
3-Feb-10	25	113	28	15	15

DL: 3 mg L⁻¹

Table B 23: Concentrations of *E.coli* (CFU/100mL) along the treatment flow path during the EW-BOFS pilot-scale wastewater treatment experiment.

Date	Cell 1	Cell 2	Cell 3	Cell 4	Cell 5
1-Jun-09	1.1E+04	1.5E+03	1.0E+02	6.0E+01	3.0E+01
17-Jun-09	6.5E+02	3.0E+02	1.7E+02	1.0E+01	6.0E+00
24-Jun-09	4.0E+02	1.4E+02	1.5E+01	3.0E+00	3.0E+00
2-Jul-09	4.7E+03	3.0E+02	8.0E+00	3.0E+00	3.0E+00
2-Jul-09	1.3E+03	1.9E+02	8.0E+00	2.0E+00	3.0E+00
8-Jul-09	2.0E+02	1.5E+01	1.3E+01	3.0E+00	3.0E+00
15-Jul-09	2.7E+04	5.9E+03	3.9E+02	3.0E+00	3.0E+00
22-Jul-09	1.0E+02	1.6E+02	2.8E+01	3.0E+00	3.0E+00
30-Jul-09	4.8E+04	1.4E+04	1.0E+03	3.0E+00	3.0E+00
5-Aug-09	3.0E+02	6.0E+01	1.5E+01	3.0E+00	3.0E+00
12-Aug-09	1.1E+04	1.6E+03	2.0E+01	3.0E+00	3.0E+00
19-Aug-09	2.4E+04	2.1E+03	8.0E+00	3.0E+00	3.0E+00
26-Aug-09	4.7E+03	3.8E+02	3.2E+01	3.0E+00	3.0E+00
2-Sep-09	8.0E+02	2.2E+02	2.2E+01	3.0E+00	3.0E+00
9-Sep-09	8.0E+02	2.6E+02	2.6E+01	3.0E+00	-
16-Sep-09	2.5E+02	6.0E+01	1.0E+01	3.0E+00	3.0E+00
30-Oct-09	6.5E+01	2.5E+01	3.0E+00	3.0E+00	3.0E+00
4-Nov-09	8.0E+01	3.2E+01	3.0E+00	3.0E+00	9.0E+01
11-Nov-09	1.5E+00	3.0E+00	3.0E+00	3.0E+00	3.0E+00
18-Nov-09	1.6E+03	1.1E+02	3.0E+00	3.0E+00	3.0E+00
25-Nov-09	4.6E+03	2.5E+02	3.0E+00	3.0E+00	3.9E+01
2-Dec-09	2.5E+03	3.0E+01	3.0E+00	3.0E+00	3.0E+00
9-Dec-09	2.4E+05	2.4E+04	3.0E+00	3.0E+00	3.0E+00
16-Dec-09	7.9E+03	4.2E+03	3.0E+00	3.0E+00	3.0E+00
14-Jan-10	1.5E+00	1.3E+02	5.0E+00	3.0E+00	-
20-Jan-10	3.9E+03	9.8E+02	3.0E+01	3.0E+00	3.0E+00
27-Jan-10	3.0E+04	1.7E+03	1.9E+01	3.0E+00	3.0E+00
3-Feb-10	1.3E+05	1.2E+04	6.9E+01	3.0E+00	3.0E+00

DL: 3CFU/100 ml

Table B 24: Concentrations of Total coliform (CFU/100mL) along the treatment flow path during the EW-BOFS pilot-scale wastewater treatment experiment.

Date	Cell 1	Cell 2	Cell 3	Cell 4	Cell 5
1-Jun-09	7.7E+04	4.3E+03	1.0E+02	6.0E+01	3.0E+01
17-Jun-09	4.2E+03	3.3E+02	3.5E+02	3.0E+01	6.0E+00
24-Jun-09	9.7E+03	3.3E+03	2.2E+02	3.0E+00	3.0E+00
2-Jul-09	4.7E+03	4.0E+03	2.8E+02	3.0E+00	3.0E+00
8-Jul-09	1.1E+04	1.9E+03	1.1E+03	3.0E+00	3.0E+00
15-Jul-09	4.8E+04	1.2E+04	2.9E+03	3.0E+00	3.0E+00
22-Jul-09	2.1E+03	7.6E+02	6.1E+03	3.0E+00	3.0E+00
30-Jul-09	4.8E+04	2.4E+04	4.8E+03	3.0E+00	3.0E+00
5-Aug-09	1.3E+06	2.1E+03	1.9E+03	3.0E+00	3.0E+00
12-Aug-09	2.6E+04	6.7E+03	5.5E+01	3.0E+00	3.0E+00
19-Aug-09	2.3E+04	2.8E+03	7.5E+00	3.0E+00	3.0E+00
26-Aug-09	5.9E+04	1.0E+03	2.0E+02	3.0E+00	3.0E+00
2-Sep-09	4.4E+03	1.0E+03	1.2E+02	3.0E+00	3.0E+00
9-Sep-09	2.5E+03	1.4E+03	2.6E+01	3.0E+00	-
16-Sep-09	2.0E+03	4.4E+02	2.6E+01	3.0E+00	1.6E+01
30-Oct-09	2.2E+03	1.7E+02	3.0E+00	3.0E+00	-
4-Nov-09	5.3E+02	6.6E+01	3.0E+00	3.0E+00	1.1E+02
11-Nov-09	4.7E+03	2.3E+02	3.0E+00	3.0E+00	3.0E+00
18-Nov-09	5.1E+04	1.2E+03	5.0E+00	3.0E+00	4.6E+01
25-Nov-09	1.7E+04	1.3E+03	1.9E+01	3.0E+00	4.6E+01
2-Dec-09	8.7E+03	1.1E+03	5.0E+00	3.0E+00	2.2E+01
9-Dec-09	2.4E+05	2.4E+05	5.0E+00	3.0E+00	5.0E+00
16-Dec-09	1.6E+04	2.4E+05	5.0E+00	3.0E+00	3.0E+00
14-Jan-10	1.3E+04	1.6E+03	9.0E+01	3.0E+00	-
20-Jan-10	8.7E+03	1.8E+03	3.3E+01	3.0E+00	3.0E+00
27-Jan-10	6.9E+04	3.4E+03	4.9E+01	3.0E+00	2.5E+01
3-Feb-10	3.4E+05	1.9E+04	1.3E+02	3.0E+00	3.0E+00

DL: 3CFU/100 ml

Table B 25: Mass change of P observed in different components of the treatment system. The +ve values indicate mass loses from the system component and the -ve values indicate mass gains within the system component.

	P mass in (mg)	P mass out (mg)	P mass change (mg)	P mass change (Kg)	P mass % change
Overall treatment system	100409	5944	94465	0.095	94.08
Cell 2	100409	69828	30580	0.031	30.46
Cell 3	69828	44940	24888	0.025	35.64
Cell 4	44940	269	44671	0.045	99.40
Cell 4*	269	155	114	0.0001	42.35
Cell 5	155	8568	-8413	-0.008	-5430.9
Cell 6	8568	5944	2624	0.003	30.63

Table B 26: Mass change of NH₃ observed in different components of the treatment system. The +ve values indicate mass loses from the system component and the -ve values indicate mass gains within the system component.

	NH₃-N mass in (mg)	NH₃-N mass out (mg)	NH₃-N mass change (mg)	NH₃-N mass change (Kg)	NH₃-N mass % change
Overall treatment system	256661	20875	235786	0.236	91.87
Cell 2	256661	132030	124631	0.125	48.56
Cell 3	132030	3910	128120	0.128	97.04
Cell 4	3910	3984	-74	-0.0001	-1.90
Cell 4*	3984	3533	452	0.0005	11.33
Cell 5	3533	44641	-41108	-0.041	-1163.6
Cell 6	44641	20875	23766	0.024	53.24

Table B 27: Mass change of NO₃ observed in different components of the treatment system. The +ve values indicate mass loses from the system component and the -ve values indicate mass gains within the system component.

	NO ₃ -N mass in (mg)	NO ₃ -N mass out (mg)	NO ₃ -N mass change (mg)	NO ₃ -N mass change (Kg)	NO ₃ -N mass % change
Overall treatment system	19258	56237	-36980	-0.037	-192.03
Cell 2	19258	72637	-53380	-0.053	-277.19
Cell 3	72637	199369	-126732	-0.127	-174.47
Cell 4	199369	167114	32255	0.032	16.18
Cell 4*	167114	80371	86743	0.087	51.91
Cell 5	80371	56912	23459	0.024	29.19
Cell 6	56912	56237	675	0.001	1.19

Table B 28: Mass change of N_T(NO₃+ NH₃) observed in different components of the treatment system. The +ve values indicate mass loses from the system component and the -ve values indicate mass gains within the system component.

	N _T mass in (mg)	N _T mass out (mg)	N _T mass change (mg)	N _T mass change (Kg)	N _T mass % change
Overall treatment system	275919	77112	198806	0.199	72.05
Cell 2	275919	204667	71251	0.072	25.82
Cell 3	204667	203279	1388	0.001	0.68
Cell 4	203279	171098	32181	0.0319	15.83
Cell 4*	171098	83904	87195	0.0875	50.96
Cell 5	83904	101553	-17649	-0.017	-21.03
Cell 6	101553	77112	24441	0.025	24.07

Table B 29: Mass change of cBOD₅ observed in different components of the treatment system. The +ve values indicate mass losses from the system component and the -ve values indicate mass gains within the system component.

	cBOD₅ mass in (mg)	cBOD₅ mass out (mg)	cBOD₅ mass change (mg)	cBOD₅ mass change (Kg)	cBOD₅ mass % change
Overall treatment system	285884	67420	218464	0.219	76.42
Cell 2	285884	196336	89548	0.090	31.32
Cell 3	196336	129195	67141	0.067	34.20
Cell 4	129195	6630	122565	0.123	94.87
Cell 4*	6630	3612	3018	0.003	45.52
Cell 5	3612	59702	-56090	-0.056	-1552.8
Cell 6	59702	67420	-7718	-0.008	-12.93

Table B 30: Mass change of COD observed in different components of the treatment system. The +ve values indicate mass losses from the system component and the -ve values indicate mass gains within the system component.

	COD mass in (mg)	COD mass out (mg)	COD mass change (mg)	COD mass change (Kg)	COD mass % change
Overall treatment system	798257	615341	182916	0.183	22.91
Cell 2	798257	604761	193496	0.194	24.24
Cell 3	604761	494256	110505	0.111	18.27
Cell 4	494256	182028	312228	0.312	63.17
Cell 4*	182028	80100	101928	0.102	56.00
Cell 5	80100	622831	-542731	-0.543	-677.57
Cell 6	622831	615341	7490	0.008	1.20

Appendix C

Summary of Data Presented in Chapter 4

Table C 1: pH values along the treatment flow path of the EW-BOFS demonstration-scale treatment system experiment.

Date	Cell 1	Cell 2	Cell 3	Cell 4
27-Jan-10	7.53	7.79	7.48	11.35
3-Feb-10	7.98	8.11	8.10	11.83
19-Feb-10	8.95	9.61	8.10	12.32
6-Apr-10	8.68	8.30	7.40	11.97
13-Apr-10	8.43	8.14	7.61	11.10
30-Apr-10	7.38	7.70	7.58	10.40
5-May-10	7.23	7.63	7.80	11.52
12-May-10	7.19	7.63	8.06	11.29
19-May-10	7.02	7.66	8.17	11.60
27-May-10	7.22	7.69	8.13	11.53
2-Jun-10	6.83	7.64	8.29	11.89
8-Jun-10	7.04	7.55	8.26	11.29
16-Jun-10	7.15	7.33	8.29	11.85
23-Jun-10	6.98	7.33	7.76	11.52
29-Jun-10	7.70	7.71	8.22	11.39
6-Jul-10	7.01	7.22	8.14	11.56
14-Jul-10	7.27	7.61	8.07	11.96
20-Jul-10	7.50	7.55	8.45	11.86
28-Jul-10	7.60	7.93	8.58	11.81
4-Aug-10	7.62	7.95	8.25	11.84
10-Aug-10	7.46	7.78	8.40	12.20
18-Aug-10	7.68	7.84	8.21	11.88
31-Aug-10	7.73	7.87	8.10	11.69
8-Sep-10	8.04	7.80	7.95	11.37
14-Sep-10	7.75	7.69	7.98	11.54
19-Oct-10	7.67	7.65	7.35	9.81
16-Nov-10	8.12	7.74	7.01	10.03
10-Dec-10	8.12	8.13	7.82	9.41
14-Dec-10	8.13	8.08	7.22	11.69
20-Jan-11	8.11	7.94	7.92	11.15
28-Jan-11	8.10	8.35	7.72	9.49
16-Feb-11	8.56	8.43	6.71	9.56
23-Mar-11	7.99	8.14	-	10.52
13-Apr-11	7.52	7.96	7.59	11.07
18-May-11	7.11	7.45	8.05	11.72
22-Jun-11	7.56	7.25	8.16	12.10
13-Jul-11	7.08	7.27	8.43	12.35
16-Aug-11	6.97	7.46	8.33	11.68
27-Oct-11	7.22	7.81	8.03	11.87
29-Nov-11	7.20	7.56	7.81	12.10
13-Dec-11	7.45	7.73	8.19	12.16

Table C 2: Measurements of alkalinity ($\text{mg L}^{-1} \text{CaCO}_3$) along the treatment flow path of the EW-BOFS demonstration-scale treatment system experiment.

Date	Cell 1	Cell 2	Cell 3	Cell 4
27-Jan-10	636	455	195	2300
3-Feb-10	763	538	225	2360
19-Feb-10	635	489	230	1620
6-Apr-10	460	520	200	640
30-Apr-10	700	740	540	360
5-May-10	728	248	250	403
12-May-10	594	564	240	343
19-May-10	650	450	275	768
21-May-10	520	630	460	230
27-May-10	536	638	320	682
2-Jun-10	638	605	253	1530
3-Jun-10	700	700	360	800
8-Jun-10	613	688	295	443
16-Jun-10	578	660	323	1670
18-Jun-10	540	650	360	600
23-Jun-10	533	550	288	713
29-Jun-10	493	570	350	255
6-Jul-10	470	605	300	1230
14-Jul-10	368	470	275	825
20-Jul-10	420	470	248	1530
20-Jul-10	520	480	260	1540
19-Aug-10	532	388	265	271
31-Aug-10	310	340	241	823
8-Sep-10	333	305	215	543
14-Sep-10	448	344	208	678
19-Oct-10	590	575	160	530
16-Nov-10	605	605	65	90
10-Dec-10	432	340	302	200
14-Dec-10	425	438	100	470
20-Jan-11	510	468	188	450
28-Jan-11	425	460	175	200
16-Feb-11	273	295	73	160
23-Mar-11	340	388	-	258
13-Apr-11	605	525	188	313
18-May-11	506	646	176	442
22-Jun-11	473	485	190	948
13-Jul-11	1050	540	178	1440
16-Aug-11	825	280	190	395
27-Oct-11	480	463	28	500
29-Nov-11	675	545	145	713
13-Dec-11	725	530	155	845

Table C 3: Measurements of Eh (mV) along the treatment flow path of the EW-BOFS demonstration-scale treatment system experiment.

Date	Cell 1	Cell 2	Cell 3	Cell 4
19-Feb-10	-33	-4	279	31
6-Apr-10	90	144	364	180
13-Apr-10	83	128	311	130
30-Apr-10	68	71	286	79
19-May-10	-6	43	267	101
2-Jun-10	-69	14	250	63
3-Jun-10	-28	19	421	105
16-Jun-10	-26	13	261	72
20-Jul-10	112	152	520	92
28-Jan-11	7	37	284	76
13-Jul-11	82	229	228	59
27-Oct-11	119	263	270	215
29-Nov-11	265	419	407	232

Table C 4: Measurements of Conductivity ($\mu\text{S}/\text{cm}$) along the treatment flow path of the EW-BOFS demonstration-scale treatment system experiment.

Date	Cell 1	Cell 2	Cell 3	Cell 4
27-Jan-10	2118	1441	1349	8160
3-Feb-10	2048	1504	1192	7500
5-May-10	1818	1903	1706	2262
12-May-10	1728	1706	1574	2258
19-May-10	1947	1840	1699	4350
27-May-10	1841	2000	1716	4720
2-Jun-10	1830	1971	1686	7040
8-Jun-10	1948	2021	1630	2489
16-Jun-10	1705	1845	1540	7520
23-Jun-10	1821	1852	1630	4020
29-Jun-10	1579	1671	1510	1929
6-Jul-10	1569	1774	1544	6280
14-Jul-10	1360	1541	1440	7890
20-Jul-10	1004	1468	1303	7480
28-Jul-10	1256	1330	1231	4160
4-Aug-10	1207	1337	1197	7360
10-Aug-10	1222	1225	1128	6050
18-Aug-10	1121	1187	1113	4500
31-Aug-10	1101	1168	1093	2500
8-Sep-10	1111	1030	999	1766
14-Sep-10	1423	1171	1032	2930
19-Oct-10	1777	1772	1424	1161
16-Nov-10	1772	1865	1483	1347
14-Dec-10	1580	1498	1297	2390
20-Jan-11	1791	1584	1351	1582
16-Feb-11	1754	1773	1694	1560
23-Mar-11	1513	1536	-	1350
13-Apr-11	1815	1589	1337	1431
18-May-11	1448	1646	1256	2790
22-Jun-11	1332	1307	1066	5030
13-Jul-11	2334	1416	1058	6950
16-Aug-11	1977	802	819	2202
27-Oct-11	1587	1374	1095	2855
29-Nov-11	1881	1514	1096	3511
13-Dec-11	1953	1444	1044	4508

DL:5 $\mu\text{S}/\text{cm}$

Table C 5: Concentrations of TSS (mg L^{-1}) along the treatment flow path during the EW-BOFS demonstration-scale wastewater treatment experiment.

Date	Cell 1	Cell 2	Cell 3	Cell 4
14-Sep-10	66	16	6	220
14-Dec-10	27	11	5	283
20-Jan-11	50	7	3	360
16-Feb-11	25	5	3	140
23-Mar-11	12	2		252
13-Apr-11	67	19	18	216
18-May-11	43	31	3	79
22-Jun-11	13	8	3	38
27-Oct-11	32	3	3	65
29-Nov-11	50	3	3	100
13-Dec-11	52	3	3	10

Table C 6: Concentrations of PO₄-P (mg L⁻¹) along the treatment flow path of the EW-BOFS demonstration-scale treatment system experiment.

Date	Cell 1	Cell 2	Cell 3	Cell 4
27-Jan-10	6.47	4.26	2.42	<DL
3-Feb-10	7.16	4.89	2.31	<DL
19-Feb-10	4.50	2.19	1.45	<DL
6-Apr-10	3.91	4.79	3.28	0.06
13-Apr-10	4.36	5.05	4.08	0.01
30-Apr-10	5.28	7.47	5.02	0.01
5-May-10	3.35	5.04	4.41	0.12
12-May-10	4.66	4.77	3.32	0.03
19-May-10	6.33	6.24	2.69	0.03
21-May-10	5.42	6.17	4.66	<DL
27-May-10	5.16	5.41	2.58	0.03
2-Jun-10	6.55	5.24	0.81	0.03
8-Jun-10	8.52	6.83	2.88	0.03
16-Jun-10	8.24	7.36	4.39	0.03
18-Jun-10	7.54	6.44	2.34	<DL
23-Jun-10	7.76	5.33	3.21	0.03
29-Jun-10	7.50	8.82	4.79	0.03
6-Jul-10	7.64	9.49	1.99	0.03
14-Jul-10	5.48	8.86	3.23	0.03
20-Jul-10	5.47	7.85	2.66	0.03
20-Jul-10	5.22	7.55	2.75	0.01
28-Jul-10	5.48	7.22	2.50	0.03
4-Aug-10	4.62	5.09	3.43	0.03
10-Aug-10	5.51	5.55	4.21	0.03
18-Aug-10	4.82	7.50	3.37	0.03
19-Aug-10	4.73	6.76	4.48	0.01
31-Aug-10	3.59	4.34	4.63	0.01
8-Sep-10	3.65	3.39	3.95	0.03
9-Sep-10	2.73	2.65	3.68	0.06
14-Sep-10	5.06	4.92	4.14	0.02
24-Sep-10	7.30	6.96	5.06	<DL
19-Oct-10	6.29	7.04	8.41	<DL
16-Nov-10	7.11	5.97	7.89	0.09
10-Dec-10	4.58	4.24	4.43	0.20
14-Dec-10	3.95	3.03	3.98	0.02

DL: 0.005 mg L⁻¹

Table C 6 Continued: Concentrations of PO₄-P (mg L⁻¹) along the treatment flow path of the EW-BOFS demonstration-scale treatment system experiment.

Date	Cell 1	Cell 2	Cell 3	Cell 4
20-Jan-11	5.28	3.49	3.82	<DL
28-Jan-11	3.80	2.68	2.46	0.25
16-Feb-11	3.54	2.35	2.80	0.29
23-Mar-11	4.40	3.07	-	0.04
13-Apr-11	9.39	7.18	3.25	0.05
22-Jun-11	6.72	10.6	3.64	<DL
13-Jul-11	22.2	10.4	2.40	0.01
27-Oct-11	8.22	9.26	3.75	0.01
29-Nov-11	12.0	10.9	4.44	<DL
13-Dec-11	12.9	9.31	4.82	<DL

DL: 0.005 mg L⁻¹

Table C 7: Concentrations of Ca (mg L^{-1}) along the treatment flow path during the EW-BOFS demonstration-scale wastewater treatment experiment.

Date	Cell 1	Cell 2	Cell 3	Cell 4	DL (mg L^{-1})
27-Jan-10	136	81	109	568	0.2
3-Feb-10	134	92	-	116	0.2
19-Feb-10	44	30	79	282	0.2
6-Apr-10	77	83	101	315	0.2
13-Apr-10	82	94	105	98	0.2
30-Apr-10	131	139	126	96	0.2
21-May-10	109	129	127	146	0.2
3-Jun-10	123	134	120	316	0.2
18-Jun-10	121	146	127	250	0.2
20-Jul-10	85	98	91	456	0.2
19-Aug-10	87	86	89	97	0.2
9-Sep-10	62	71	74	88	0.2
24-Sep-10	81	83	87	167	0.2
19-Oct-10	97	106	100	56	0.2
16-Nov-10	93	86	112	79	0.2
10-Dec-10	103	106	99	85	0.2
14-Dec-10	102	97	103	183	0.2
20-Jan-11	124	148	128	121	0.2
28-Jan-11	125	113	116	151	0.2

Table C 8: Concentrations of Na (mg L^{-1}) along the treatment flow path during the EW-BOFS demonstration-scale wastewater treatment experiment.

Date	Cell 1	Cell 2	Cell 3	Cell 4	DL ($\mu\text{g L}^{-1}$)
27-Jan-10	159	123	100	118	0.2
3-Feb-10	157	134	107	126	0.2
19-Feb-10	119	114	136	131	0.2
6-Apr-10	164	147	126	110	0.2
13-Apr-10	147	148	149	135	0.2
30-Apr-10	203	171	152	139	0.2
21-May-10	184	179	179	172	0.2
3-Jun-10	181	188	177	173	0.2
18-Jun-10	168	165	171	157	0.2
20-Jul-10	125	137	128	143	0.2
19-Aug-10	96	102	109	110	0.2
9-Sep-10	95	91	92	96	0.2
24-Sep-10	102	103	102	95	0.2
19-Oct-10	107	119	106	101	0.2
16-Nov-10	93	98	100	99	0.2
10-Dec-10	82	83	82	81	0.2
14-Dec-10	90	82	82	81	0.2
20-Jan-11	106	100	87	85	0.2
28-Jan-11	112	113	108	104	0.2

Table C 9: Concentrations of K (mg L^{-1}) along the treatment flow path during the EW-BOFS demonstration-scale wastewater treatment experiment.

Date	Cell 1	Cell 2	Cell 3	Cell 4	DL ($\mu\text{g L}^{-1}$)
27-Jan-10	27	24	16	29	0.5
3-Feb-10	27	24	14	40	0.5
19-Feb-10	46	36	36	36	0.5
6-Apr-10	36	37	31	30	0.5
13-Apr-10	32	36	39	57	0.5
30-Apr-10	24	33	41	41	0.5
21-May-10	22	23	26	32	0.5
3-Jun-10	19	23	26	39	0.5
18-Jun-10	24	20	25	26	0.5
20-Jul-10	21	14	16	30	0.5
19-Aug-10	12	9	11	14	0.5
9-Sep-10	17	3	5	15	0.5
24-Sep-10	26	17	15	16	0.5
19-Oct-10	38	40	32	32	0.5
16-Nov-10	40	43	40	34	0.5
10-Dec-10	15	25	32	30	0.5
14-Dec-10	22	16	27	25	0.5
20-Jan-11	26	21	17	20	0.5
28-Jan-11	31	38	31	24	0.5

Table C 10: Concentrations of Mg (mg L^{-1}) along the treatment flow path during the EW-BOFS demonstration-scale wastewater treatment experiment.

Date	Cell 1	Cell 2	Cell 3	Cell 4	DL ($\mu\text{g L}^{-1}$)
27-Jan-10	13	7.4	33	<DL	0.2
3-Feb-10	14	8.4	32	<DL	0.2
19-Feb-10	7.9	4.2	12	<DL	0.2
6-Apr-10	11	10	12	0.37	0.2
13-Apr-10	11	11	13	7.7	0.2
30-Apr-10	14	15	16	10	0.2
21-May-10	13	13	15	6.0	0.2
3-Jun-10	15	14	14	<DL	0.2
18-Jun-10	14	15	15	<DL	0.2
20-Jul-10	10	11	0.03	2.5	0.2
19-Aug-10	8.1	8.6	10	0.34	0.2
9-Sep-10	6.4	7.1	7.6	4.9	0.2
24-Sep-10	9.5	8.4	8.8	0.23	0.2
19-Oct-10	11	13	12	11	0.2
16-Nov-10	11	10	12	13	0.2
10-Dec-10	13	13	12	10	0.2
14-Dec-10	13	12	13	<DL	0.2
20-Jan-11	14	17	15	1.1	0.2
28-Jan-11	14	14	14	13	0.2

Table C 11: Concentrations of Cl (mg L⁻¹) along the treatment flow path during the EW-BOFS demonstration-scale wastewater treatment experiment.

Date	Cell 1	Cell 2	Cell 3	Cell 4	DL (mg L ⁻¹)
27-Jan-10	215	151	120	81	0.0002
3-Feb-10	49	147	121	82	0.0002
19-Feb-10	189	182	185	154	0.0002
6-Apr-10	220	204	170	144	0.0002
13-Apr-10	189	198	193	186	0.0002
30-Apr-10	218	226	206	195	0.0002
5-May-10	256	232	204	185	0.0002
12-May-10	222	215	194	167	0.0002
19-May-10	227	220	217	175	0.0002
27-May-10	126	138	139	133	0.0002
2-Jun-10	200	204	198	157	0.0002
8-Jun-10	237	242	215	164	0.0002
16-Jun-10	208	212	205	187	0.0002
23-Jun-10	207	206	196	182	0.0002
29-Jun-10	197	194	191	182	0.0002
6-Jul-10	196	207	191	182	0.0002
14-Jul-10	185	182	180	184	0.0002
20-Jul-10	170	183	173	182	0.0002
28-Jul-10	151	157	163	165	0.0002
4-Aug-10	136	158	157	178	0.0002
10-Aug-10	133	137	142	166	0.0002
18-Aug-10	112	137	139	148	0.0002
31-Aug-10	118	126	125	132	0.0002
8-Sep-10	110	130	125	138	0.0002
14-Sep-10	127	121	117	122	0.0002
19-Oct-10	141	137	134	131	0.0002
16-Nov-10	154	173	158	150	0.0002
10-Dec-10	140	148	140	135	0.0002
14-Dec-10	153	147	140	134	0.0002
20-Jan-11	186	164	152	152	0.0002
28-Jan-11	205	209	192	184	0.0002
16-Feb-11	214	219	225	220	0.0002
23-Mar-11	169	167	-	155	0.0002
13-Apr-11	176	165	153	146	0.0002
18-May-11	134	136	138	128	0.0002
22-Jun-11	127	115	120	114	0.0002
13-Jul-11	136	120	110	145	0.0002
16-Aug-11	96	45	57	76	0.0002
29-Nov-11	152	142	116	68	0.0002

Table C 12: Concentrations of SO₄ (mg L⁻¹) along the treatment flow path during the EW-BOFS demonstration-scale wastewater treatment experiment.

Date	Cell 1	Cell 2	Cell 3	Cell 4	DL (mg L ⁻¹)
27-Jan-10	24	30	101	25	0.018
3-Feb-10	26	30	96	7.3	0.018
19-Feb-10	49	46	41	24	0.018
6-Apr-10	51	46	50	42	0.018
13-Apr-10	46	43	50	44	0.018
30-Apr-10	32	27	32	37	0.018
5-May-10	54	29	40	33	0.018
12-May-10	41	35	43	33	0.018
19-May-10	39	30	49	35	0.018
27-May-10	31	17	37	27	0.018
2-Jun-10	23	12	36	9.2	0.018
8-Jun-10	32	8.4	37	26	0.018
16-Jun-10	37	27	30	7.7	0.018
23-Jun-10	35	24	32	22	0.018
29-Jun-10	35	13	28	26	0.018
6-Jul-10	37	6.8	33	16	0.018
14-Jul-10	36	18	29	6.8	0.018
20-Jul-10	35	15	27	8	0.018
28-Jul-10	39	10	29	19	0.018
4-Aug-10	43	49	32	9	0.018
10-Aug-10	41	39	39	15	0.018
18-Aug-10	48	23	42	25	0.018
31-Aug-10	47	48	38	28	0.018
8-Sep-10	50	48	46	36	0.018
14-Sep-10	53	42	50	37	0.018
19-Oct-10	57	52	38	29	0.018
16-Nov-10	39	44	35	31	0.018
10-Dec-10	56	57	58	52	0.018
14-Dec-10	71	66	63	47	0.018
20-Jan-11	79	85	91	77	0.018
28-Jan-11	74	77	85	78	0.018
16-Feb-11	71	78	76	68	0.018
23-Mar-11	56	61	-	57	0.018
13-Apr-11	35	23	59	54	0.018
18-May-11	25	1.9	16	17	0.018
22-Jun-11	25	0.6	23	11	0.018
13-Jul-11	6.6	0.8	24	6.5	0.018
16-Aug-11	28	51	58	40	0.018
29-Nov-11	40	6.1	40	21	0.018

Table C 13: Concentrations of V ($\mu\text{g L}^{-1}$) along the treatment flow path during the EW-BOFS demonstration-scale wastewater treatment experiment.

Date	Cell 1	Cell 2	Cell 3	Cell 4	DL ($\mu\text{g L}^{-1}$)
27-Jan-10	0.03	13	10	0.42	0.022
3-Feb-10	<DL	14		0.42	0.022
6-Apr-10	0.48	7.1	5.5	0.74	0.026
13-Apr-10	1.3	6.3	4.7	1.0	0.026
30-Apr-10	1.1	7.4	7.2	0.11	0.026
5-May-10	<DL	10	<DL	<DL	5
12-May-10	<DL	11	<DL	<DL	5
19-May-10	<DL	13	<DL	<DL	5
21-May-10	<DL	12	3.6	0.13	0.026
27-May-10	<DL	12	<DL	<DL	5
2-Jun-10	<DL	14	<DL	<DL	5
8-Jun-10	<DL	12	<DL	<DL	5
16-Jun-10	<DL	11	<DL	<DL	5
18-Jun-10	0.16	10	3.8	0.32	0.026
23-Jun-10	<DL	10	<DL	<DL	5
29-Jun-10	<DL	8.2	5.3	<DL	5
6-Jul-10	<DL	11	5	<DL	5
14-Jul-10	<DL	8.9	5	<DL	5

Table C 14: Concentrations of Al ($\mu\text{g L}^{-1}$) along the treatment flow path during the EW-BOFS demonstration-scale wastewater treatment experiment.

Date	Cell 1	Cell 2	Cell 3	Cell 4	DL ($\mu\text{g L}^{-1}$)
27-Jan-10	4.6	-	24	<DL	0.149
3-Feb-10	<DL	1.5	19	<DL	0.149
6-Apr-10	<DL	1.3	<DL	1.4	0.155
13-Apr-10	6.7	2.5	<DL	6.3	0.155
30-Apr-10	<DL	<DL	<DL	<DL	0.155
5-May-10	44	14	<DL	12	10
12-May-10	20	25	<DL	<DL	10
19-May-10	27	27	<DL	<DL	10
21-May-10	<DL	36	<DL	<DL	0.155
27-May-10	11	36	<DL	<DL	10
2-Jun-10	16	51	34	<DL	10
8-Jun-10	42	60	10	<DL	10
16-Jun-10	15	37	90	<DL	10
18-Jun-10	<DL	24	<DL	<DL	0.155
23-Jun-10	<DL	21	<DL	<DL	10
29-Jun-10	<DL	31	<DL	<DL	10
6-Jul-10	<DL	39	12	<DL	10
14-Jul-10	<DL	33	57	<DL	10

Table C 15: Concentrations of Zn ($\mu\text{g L}^{-1}$) along the treatment flow path during the EW-BOFS demonstration-scale wastewater treatment experiment.

Date	Cell 1	Cell 2	Cell 3	Cell 4	DL ($\mu\text{g L}^{-1}$)
27-Jan-10	10	4.5	6.5	30	0.25
3-Feb-10	3.5	2.0	2.8	0.29	0.25
19-Feb-10	22	41	26	11	0.25
6-Apr-10	9.2	5.3	6.8	20	0.25
13-Apr-10	4.3	8.0	10	0.8	0.25
30-Apr-10	3.6	1.0	2.3	1.1	0.25
21-May-10	21	15	1.3	0.49	0.25
3-Jun-10	5.9	6.4	0.29	0.29	0.25
18-Jun-10	5.7	0.85	0.29	0.29	0.25
20-Jul-10	9.4	19	5.0	37	0.29
19-Aug-10	19	56	9.3	8.7	0.29
9-Sep-10	21	7.7	9.1	8.9	0.29
24-Sep-10	4.5	23	6.9	7.1	0.29
19-Oct-10	70	39	22	18	0.29
16-Nov-10	51	31	32	23	0.29
10-Dec-10	2.4	20	10	6.6	0.29
14-Dec-10	12	5.4	20	5.6	0.29
20-Jan-11	88	9.3	9.2	29	0.29
28-Jan-11	14	21	10	13	0.29

Table C 16: Concentrations of Mn ($\mu\text{g L}^{-1}$) along the treatment flow path during the EW-BOFS demonstration-scale wastewater treatment experiment.

Date	Cell 1	Cell 2	Cell 3	Cell 4	DL ($\mu\text{g L}^{-1}$)
27-Jan-10	44	12	44	11	0.04
3-Feb-10	42	14	22	0.03	0.04
19-Feb-10	89	11	4.9	0.15	0.04
6-Apr-10	16	25	102	0.04	0.04
13-Apr-10	17	39	140	2.1	0.04
30-Apr-10	36	75	89	0.84	0.04
21-May-10	31	63	8.2	0.73	0.04
3-Jun-10	54	55	0.03	0.03	0.04
18-Jun-10	54	78	0.04	0.03	0.04
20-Jul-10	21	35	0.35	0.28	0.03
19-Aug-10	16	56	0.41	0.03	0.03
9-Sep-10	12	33	0.27	0.8	0.03
24-Sep-10	24	27	4.0	0.04	0.03
19-Oct-10	8.1	25	7.8	2.3	0.03
16-Nov-10	13	31	3.9	0.91	0.03
10-Dec-10	4.0	25	31	3.8	0.03
14-Dec-10	5.1	21	1.8	0.24	0.03
20-Jan-11	13	51	0.58	0.75	0.03
28-Jan-11	24	15	30	23	0.03

Table C 17: Concentrations of Cr ($\mu\text{g L}^{-1}$) along the treatment flow path during the EW-BOFS demonstration-scale wastewater treatment experiment.

Date	Cell 1	Cell 2	Cell 3	Cell 4	DL ($\mu\text{g L}^{-1}$)
27-Jan-10	0.05	0.05	0.89	13	0.05
3-Feb-10	0.05	0.05	0.57	0.92	0.05
19-Feb-10	0.05	0.05	1.4	4.0	0.05
6-Apr-10	0.05	0.05	0.05	0.05	0.05
13-Apr-10	0.05	0.26	0.05	0.05	0.05
30-Apr-10	0.05	0.05	0.05	0.59	0.05
21-May-10	0.05	0.05	0.05	1.6	0.05
3-Jun-10	0.05	0.05	0.05	0.05	0.05
18-Jun-10	0.05	0.05	0.05	0.05	0.05
20-Jul-10	0.69	0.32	0.30	0.40	0.05
19-Aug-10	0.28	-	0.31	0.34	0.05
9-Sep-10	1.7	0.31	0.32	0.50	0.05
24-Sep-10	0.48	0.03	0.77	0.62	0.05
19-Oct-10	0.32	0.43	0.46	0.28	0.05
16-Nov-10	0.33	0.24	0.66	0.55	0.05
10-Dec-10	0.45	0.76	0.20	0.39	0.05
14-Dec-10	0.09	0.26	0.15	0.30	0.05
20-Jan-11	0.49	0.69	0.31	0.13	0.05
28-Jan-11	0.05	1.8	0.20	0.54	0.05

Table C 18: Concentrations of Cu ($\mu\text{g L}^{-1}$) along the treatment flow path during the EW-BOFS demonstration-scale wastewater treatment experiment.

Date	Cell 1	Cell 2	Cell 3	Cell 4	DL ($\mu\text{g L}^{-1}$)
27-Jan-10	4.9	4.5	29	27	0.04
3-Feb-10	2.8	3.7	21	22	0.04
19-Feb-10	60	44	24	14	0.04
6-Apr-10	8.3	3.9	17	11	0.04
13-Apr-10	9.1	3.9	15	12	0.04
30-Apr-10	4.5	2.6	12	10	0.04
21-May-10	10	9.1	14	2.0	0.04
3-Jun-10	10	2.4	16	8.0	0.04
18-Jun-10	6.5	2.0	15	7.8	0.04
20-Jul-10	14	16	15	176	0.10
19-Aug-10	13	56	18	19	0.10
9-Sep-10	23	14	19	27	0.10
24-Sep-10	11	12	18	16	0.10
19-Oct-10	26	12	23	10	0.10
16-Nov-10	23	8.5	18	7.1	0.10
10-Dec-10	3.1	9.3	14	9.2	0.10
14-Dec-10	11	20	15	11	0.10
20-Jan-11	252	14	12	73	0.10

Table C 19: Concentrations of Fe ($\mu\text{g L}^{-1}$) along the treatment flow path during the EW-BOFS demonstration-scale wastewater treatment experiment.

Date	Cell 1	Cell 2	Cell 3	Cell 4	DL ($\mu\text{g L}^{-1}$)
27-Jan-10	28	78	41	55	0.07
3-Feb-10	9.5	60	23	3.4	0.07
19-Feb-10	76	97	22	3.4	0.07
6-Apr-10	21	39	28	2.2	0.07
13-Apr-10	29	64	51	21	0.07
30-Apr-10	25	82	57	4.7	0.07
21-May-10	37	75	11	0.81	0.07
3-Jun-10	48	49	28	0.26	0.07
18-Jun-10	61	78	1.4	0.26	0.07
20-Jul-10	37	62	25	25	0.26
19-Aug-10	39	56	28	20	0.26
9-Sep-10	39	139	25	24	0.26
24-Sep-10	32	60	27	8.1	0.26
19-Oct-10	19	53	17	20	0.26
16-Nov-10	57	58	14	3.9	0.26
10-Dec-10	13	25	15	23	0.26
14-Dec-10	9.3	17	15	5.1	0.26
20-Jan-11	11	41	12	7.3	0.26
28-Jan-11	11	21	16	4.7	0.26

Table C 20: Concentrations of Ni ($\mu\text{g L}^{-1}$) along the treatment flow path during the EW-BOFS demonstration-scale wastewater treatment experiment.

Date	Cell 1	Cell 2	Cell 3	Cell 4	DL ($\mu\text{g L}^{-1}$)
27-Jan-10	2.6	4.4	4.6	42	0.04
3-Feb-10	2.6	3.5	4.3	28	0.04
19-Feb-10	7.4	11	40	30	0.04
6-Apr-10	6.6	3.1	3.7	9.8	0.04
13-Apr-10	6.5	3.5	4.3	9.0	0.04
30-Apr-10	3.8	2.7	2.9	8.7	0.04
21-May-10	3.6	3.0	2.4	0.17	0.04
3-Jun-10	3.2	3.8	2.1	16	0.04
18-Jun-10	3.7	2.9	2.0	17	0.04
20-Jul-10	3.3	2.3	1.4	20	0.08
19-Aug-10	3.1	-	1.9	4.4	0.08
9-Sep-10	3.7	1.8	2.1	3.4	0.08
24-Sep-10	2.7	2.3	3.2	3.7	0.08
19-Oct-10	2.3	1.7	3.5	1.6	0.08
16-Nov-10	2.1	2.2	2.8	1.5	0.08
10-Dec-10	1.1	2.5	3.3	2.1	0.08
14-Dec-10	3.3	3.0	3.3	2.1	0.08
20-Jan-11	3.1	6.4	3.5	2.7	0.08
28-Jan-11	3.8	2.2	3.6	0.72	0.08

Table C 21: Concentrations of Pb ($\mu\text{g L}^{-1}$) along the treatment flow path during the EW-BOFS demonstration-scale wastewater treatment experiment.

Date	Cell 1	Cell 2	Cell 3	Cell 4	DL ($\mu\text{g L}^{-1}$)
27-Jan-10	0.03	0.03	3.8	14	0.01
3-Feb-10	4.3	5.1	0.07	8.3	0.01
19-Feb-10	0.74	0.98	14	3.8	0.01
6-Apr-10	0.03	0.03	0.03	0.33	0.01
13-Apr-10	0.03	0.03	0.03	0.03	0.01
30-Apr-10	0.03	0.03	0.03	0.03	0.01
21-May-10	0.03	0.15	0.03	0.87	0.01
3-Jun-10	0.03	0.03	0.03	0.69	0.01
18-Jun-10	0.03	0.03	0.03	0.14	0.01
20-Jul-10	7.7	4.5	3.0	24	0.03
19-Aug-10	4.1	5.6	3.8	4.2	0.03
9-Sep-10	4.7	4.9	3.2	4.0	0.03
24-Sep-10	4.0	3.2	4.4	2.6	0.03
19-Oct-10	2.0	2.4	2.1	1.2	0.03
16-Nov-10	4.1	1.1	2.6	0.83	0.03
10-Dec-10	0.72	0.85	1.5	0.73	0.03
14-Dec-10	1.1	3.5	1.3	1.7	0.03
20-Jan-11	-	3.1	2.2	9.3	0.03
28-Jan-11	2.9	5.4	2.5	1.1	0.03

Table C 22: Concentrations of NH₃-N (mg L⁻¹) along the treatment flow path during the EW-BOFS demonstration-scale wastewater treatment experiment.

Date	Cell 1	Cell 2	Cell 3	Cell 4
27-Jan-10	85	64	10	59
3-Feb-10	85	61	8.0	50
19-Feb-10	61	35	13	47
6-Apr-10	47	59	22	14
13-Apr-10	57	68	30	20
30-Apr-10	40	60	27	13
5-May-10	27	55	0.80	4.6
12-May-10	15	21	0.30	4.2
19-May-10	32	25	0.40	5.5
27-May-10	29	40	0.02	5.6
2-Jun-10	45	40	0.06	8.0
8-Jun-10	42	39	0.02	2.5
16-Jun-10	46	34	0.02	4.7
23-Jun-10	50	31	0.02	2.3
29-Jun-10	39	18	0.02	5.3
6-Jul-10	29	30	0.02	2.8
14-Jul-10	28	27	0.02	3.4
20-Jul-10	32	25	0.02	2.8
28-Jul-10	20	21	0.02	1.6
4-Aug-10	29	28	0.02	2.3
10-Aug-10	26	22	0.02	1.8
18-Aug-10	24	17	0.02	1.4
31-Aug-10	16	16	0.02	1.3
8-Sep-10	27	13	0.02	0.19
14-Sep-10	20	22	0.02	1.1
19-Oct-10	70	78	0.02	
16-Nov-10	83	102	0.02	2.4
14-Dec-10	53	51	0.02	3.5
20-Jan-11	57	33	0.02	2.3
16-Feb-11	42	54	0.02	21
23-Mar-11	21	27	0.02	0.68
13-Apr-11	68	44	0.02	0.75
18-May-11	37	53	0.02	1.8
22-Jun-11	32	27	0.02	2.2
13-Jul-11	108	27	0.02	3.3
16-Aug-11	98	7.9	0.02	1.6
27-Oct-11	55	36	0.02	5.1
29-Nov-11	85	42	0.02	2.6
13-Dec-11	109	41	0.02	5.2

DL: 0.02 mg L⁻¹

Table C 23: Concentrations of NO₃-N (mg L⁻¹) along the treatment flow path during the EW-BOFS demonstration-scale wastewater treatment experiment.

Date	Cell 1	Cell 2	Cell 3	Cell 4
27-Jan-10	0.05	12	62	10
3-Feb-10	0.05	0.05	63	3.0
19-Feb-10	5.3	7.7	83	12
6-Apr-10	10	1.0	48	56
13-Apr-10	7.7	0.16	48	48
30-Apr-10	8.9	0.00	43	58
5-May-10	4.4	0.03	64	59
12-May-10	0.05	0.05	46	41
19-May-10	0.05	0.05	47	41
27-May-10	0.10	0.05	23	28
2-Jun-10	0.05	0.05	38	36
8-Jun-10	0.12	0.05	40	31
16-Jun-10	0.05	0.05	37	39
23-Jun-10	0.29	0.04	36	35
29-Jun-10	0.58	0.23	36	35
6-Jul-10	0.05	0.05	39	33
14-Jul-10	0.56	0.05	34	30
20-Jul-10	0.09	0.05	29	28
28-Jul-10	0.52	0.04	27	23
4-Aug-10	0.67	0.03	25	26
10-Aug-10	0.03	0.03	22	23
18-Aug-10	0.03	0.03	21	21
31-Aug-10	2.2	0.05	18	18
8-Sep-10	1.5	2.7	15	16
14-Sep-10	0.03	1.9	15	15
19-Oct-10	1.4	0.03	59	50
16-Nov-10	0.29	0.03	93	80
14-Dec-10	-	0.82	-	-
20-Jan-11	9.1	0.74	39	40
16-Feb-11	45	37	75	58
23-Mar-11	23	15	-	51
13-Apr-11	0.03	0.03	44	46
18-May-11	0.03	0.03	55	46
22-Jun-11	0.44	0.13	33	32
13-Jul-11	0.12	0.09	36	42
16-Aug-11	0.03	0.03	17	21
29-Nov-11	0.03	0.05	44	20
13-Dec-11	0.04	0.09	43	31

DL: 0.05 mg L⁻¹

Table C 24: Concentrations of NO₂-N (mg L⁻¹) along the treatment flow path during the EW-BOFS demonstration-scale wastewater treatment experiment.

Date	Cell 1	Cell 2	Cell 3	Cell 4
27-Jan-10	<DL	<DL	2.5	1.9
3-Feb-10	<DL	<DL	1.1	1.2
19-Feb-10	1.1	60	0.76	1.2
6-Apr-10	17	42	24	0.37
13-Apr-10	<DL	73	24	0.60
30-Apr-10	<DL	<DL	18	0.77
5-May-10	1.4	<DL	1.4	1.6
12-May-10	<DL	<DL	<DL	2.3
19-May-10	<DL	<DL	<DL	2.0
27-May-10	0.14	<DL	<DL	2.1
2-Jun-10	3.2	<DL	<DL	5.5
8-Jun-10	<DL	<DL	<DL	5.7
16-Jun-10	<DL	<DL	<DL	6.7
23-Jun-10	<DL	<DL	0.82	1.9
29-Jun-10	<DL	<DL	<DL	1.6
6-Jul-10	<DL	<DL	<DL	5.1
14-Jul-10	<DL	<DL	<DL	6.6
20-Jul-10	<DL	<DL	<DL	6.4
28-Jul-10	0.43	<DL	<DL	6.4
4-Aug-10	0.75	<DL	<DL	5.9
10-Aug-10	<DL	<DL	<DL	4.6
18-Aug-10	<DL	<DL	<DL	3.2
31-Aug-10	0.82	0.08	<DL	1.8
8-Sep-10	1.6	0.07	<DL	1.2
14-Sep-10	<DL	0.29	0.54	2.0
19-Oct-10	0.05	<DL	2.5	3.1
16-Nov-10	<DL	<DL	0.26	1.8
10-Dec-10	0.32	0.53	0.11	0.47
14-Dec-10	0.68	0.90	0.30	0.69
20-Jan-11	1.0	0.20	<DL	0.41
28-Jan-11	0.98	<DL	<DL	0.25
16-Feb-11	1.6	1.9	1.8	1.3
23-Mar-11	1.2	0.59	-	0.42
13-Apr-11	<DL	0.07	1.8	1.5
18-May-11	<DL	<DL	<DL	0.84
22-Jun-11	<DL	<DL	<DL	4.5
13-Jul-11	<DL	<DL	<DL	4.8
16-Aug-11	<DL	<DL	<DL	1.9
29-Nov-11	0.06	<DL	0.11	1.9
13-Dec-11	0.05	<DL	<DL	2.5

DL: 0.05 mg L⁻¹

Table C 25: Concentration ratio of ammonia and total nitrogen ($\text{NH}_3\text{-N}/\text{N}_\text{T}$) along the treatment flow path during the EW-BOFS demonstration-scale wastewater treatment experiment.

Date	Cell 1	Cell 2	Cell 3	Cell 4
27-Jan-10	1.0E+00	8.5E-01	1.4E-01	8.3E-01
3-Feb-10	1.0E+00	1.0E+00	1.1E-01	9.2E-01
19-Feb-10	9.6E-01	3.6E-01	4.1E-01	9.2E-01
6-Apr-10	7.1E-01	5.8E-01	3.9E-01	5.1E-01
13-Apr-10	9.7E-01	4.8E-01	4.6E-01	6.4E-01
30-Apr-10	9.5E-01	1.0E+00	4.9E-01	4.9E-01
5-May-10	8.2E-01	1.0E+00	1.2E-02	7.1E-02
12-May-10	9.9E-01	1.0E+00	6.5E-03	8.9E-02
19-May-10	1.0E+00	1.0E+00	8.4E-03	1.1E-01
27-May-10	9.9E-01	1.0E+00	8.5E-04	1.6E-01
2-Jun-10	9.3E-01	1.0E+00	1.6E-03	1.6E-01
8-Jun-10	1.0E+00	1.0E+00	4.9E-04	6.5E-02
16-Jun-10	1.0E+00	1.0E+00	5.4E-04	9.4E-02
23-Jun-10	9.9E-01	1.0E+00	5.5E-04	5.9E-02
29-Jun-10	9.8E-01	9.8E-01	5.5E-04	1.3E-01
6-Jul-10	1.0E+00	1.0E+00	5.1E-04	6.8E-02
14-Jul-10	9.8E-01	1.0E+00	5.8E-04	8.4E-02
20-Jul-10	1.0E+00	1.0E+00	2.7E-03	7.4E-02
28-Jul-10	9.6E-01	1.0E+00	7.5E-04	5.0E-02
4-Aug-10	9.5E-01	1.0E+00	1.2E-03	6.8E-02
10-Aug-10	1.0E+00	1.0E+00	9.0E-04	6.1E-02
18-Aug-10	1.0E+00	1.0E+00	1.3E-02	5.7E-02
31-Aug-10	8.4E-01	9.9E-01	1.1E-02	6.2E-02
8-Sep-10	9.0E-01	8.2E-01	4.7E-03	1.1E-02
14-Sep-10	1.0E+00	9.1E-01	1.8E-01	5.9E-02
19-Oct-10	9.8E-01	1.0E+00	1.4E-01	0.0E+00
16-Nov-10	1.0E+00	1.0E+00	2.1E-04	2.9E-02
10-Dec-10	7.5E-01	9.3E-01	4.7E-01	2.8E-01
14-Dec-10	9.9E-01	9.7E-01	9.1E-01	8.4E-01
20-Jan-11	8.5E-01	9.7E-01	2.1E-03	5.4E-02
28-Jan-11	6.6E-01	4.4E-01	6.7E-02	3.6E-02
16-Feb-11	4.7E-01	5.8E-01	8.3E-02	2.6E-01
23-Mar-11	4.6E-01	6.4E-01	-	1.3E-02
13-Apr-11	1.0E+00	1.0E+00	4.0E-02	1.6E-02
18-May-11	1.0E+00	1.0E+00	1.8E-04	3.6E-02
22-Jun-11	9.9E-01	9.9E-01	6.0E-04	5.6E-02
13-Jul-11	1.0E+00	1.0E+00	8.2E-04	6.5E-02
16-Aug-11	1.0E+00	9.9E-01	1.2E-03	6.4E-02
29-Nov-11	1.0E+00	1.0E+00	5.6E-03	1.0E-01
13-Dec-11	1.0E+00	1.0E+00	4.7E-04	1.3E-01

Table C 26: Concentration ratio of ammonia and total nitrogen ($\text{NO}_3\text{-N}/\text{N}_\text{T}$) along the treatment flow path during the EW-BOFS demonstration-scale wastewater treatment experiment.

Date	Cell 1	Cell 2	Cell 3	Cell 4
27-Jan-10	5.8E-04	1.5E-01	8.3E-01	1.4E-01
3-Feb-10	5.7E-04	8.0E-04	8.7E-01	5.5E-02
19-Feb-10	1.9E-02	1.8E-02	5.7E-01	5.5E-02
6-Apr-10	3.4E-02	2.3E-03	1.9E-01	4.7E-01
13-Apr-10	2.9E-02	2.6E-04	1.7E-01	3.4E-01
30-Apr-10	4.8E-02	0.0E+00	1.8E-01	4.8E-01
5-May-10	1.4E-01	5.9E-04	9.7E-01	9.0E-01
12-May-10	3.1E-03	2.4E-03	9.9E-01	8.6E-01
19-May-10	1.5E-03	1.9E-03	9.9E-01	8.4E-01
27-May-10	3.4E-03	1.2E-03	1.0E+00	7.8E-01
2-Jun-10	1.0E-03	1.2E-03	1.0E+00	7.3E-01
8-Jun-10	2.9E-03	1.3E-03	1.0E+00	7.9E-01
16-Jun-10	1.1E-03	1.4E-03	1.0E+00	7.7E-01
23-Jun-10	5.9E-03	1.2E-03	9.8E-01	8.9E-01
29-Jun-10	1.5E-02	1.3E-02	1.0E+00	8.4E-01
6-Jul-10	1.7E-03	1.6E-03	1.0E+00	8.1E-01
14-Jul-10	2.0E-02	1.8E-03	1.0E+00	7.5E-01
20-Jul-10	2.8E-03	2.0E-03	1.0E+00	7.6E-01
28-Jul-10	2.4E-02	1.9E-03	1.0E+00	7.5E-01
4-Aug-10	2.2E-02	1.1E-03	1.0E+00	7.6E-01
10-Aug-10	1.2E-03	1.4E-03	1.0E+00	7.9E-01
18-Aug-10	1.3E-03	1.8E-03	9.9E-01	8.2E-01
31-Aug-10	1.2E-01	3.3E-03	9.9E-01	8.5E-01
8-Sep-10	5.0E-02	1.8E-01	9.9E-01	9.2E-01
14-Sep-10	1.5E-03	7.9E-02	8.0E-01	8.3E-01
19-Oct-10	2.0E-02	4.1E-04	8.3E-01	9.4E-01
16-Nov-10	3.5E-03	3.0E-04	1.0E+00	9.5E-01
10-Dec-10	2.5E-01	5.9E-02	5.2E-01	7.1E-01
14-Dec-10	-	1.6E-02	-	-
20-Jan-11	1.4E-01	2.2E-02	1.0E+00	9.4E-01
28-Jan-11	3.2E-01	5.6E-01	9.3E-01	9.6E-01
16-Feb-11	5.1E-01	4.0E-01	9.0E-01	7.3E-01
23-Mar-11	5.2E-01	3.5E-01	-	9.8E-01
13-Apr-11	4.4E-04	6.7E-04	9.2E-01	9.5E-01
18-May-11	8.1E-04	5.7E-04	1.0E+00	9.5E-01
22-Jun-11	1.4E-02	4.8E-03	1.0E+00	8.3E-01
13-Jul-11	1.1E-03	3.3E-03	1.0E+00	8.4E-01
16-Aug-11	3.1E-04	3.8E-03	1.0E+00	8.6E-01
29-Nov-11	3.5E-04	1.3E-03	9.9E-01	8.2E-01
13-Dec-11	3.6E-04	2.2E-03	1.0E+00	8.0E-01

Table C 27: Concentrations of DO (mg L⁻¹) along the treatment flow path during the EW-BOFS demonstration-scale wastewater treatment experiment.

Date	Cell 1	Cell 2	Cell 3	Cell 4
27-Jan-10	1.4	1.4	12	3.0
3-Feb-10	0.26	0.20	11	3.8
5-May-10	3.5	0.70	8.7	6.0
12-May-10	0.85	2.4	11	3.4
19-May-10	0.20	2.2	12	4.0
27-May-10	1.8	1.6	9.0	2.6
2-Jun-10	0.13	1.0	8.8	2.7
8-Jun-10	0.22	2.4	9.2	6.8
16-Jun-10	0.42	2.0	9.0	2.6
23-Jun-10	0.14	1.4	7.2	4.6
29-Jun-10	4.9	3.1	8.5	5.0
6-Jul-10	0.35	2.3	8.4	4.3
14-Jul-10	2.4	0.18	6.5	3.0
20-Jul-10	0.19	0.26	8.4	2.4
28-Jul-10	1.5	4.3	8.4	3.7
4-Aug-10	2.5	4.5	8.2	3.8
10-Aug-10	0.85	1.3	8.2	3.1
18-Aug-10	0.51	2.3	8.9	3.2
31-Aug-10	3.7	2.5	8.4	6.1
8-Sep-10	1.2	2.6	8.8	6.7
14-Sep-10	0.41	2.8	7.5	5.1
19-Oct-10	0.49	1.4	4.6	2.7
16-Nov-10	0.53	0.3	9.4	3.3
14-Dec-10	2.9	3.7	10	7.8
20-Jan-11	1.3	4.6	10	8.5
16-Feb-11	6.4	3.7	7.7	4.2
23-Mar-11	7.1	3.7	-	9.3
13-Apr-11	0.43	2.9	9.5	8.5
18-May-11	0.20	3.8	9.9	5.7
22-Jun-11	1.9	1.6	8.1	3.6
13-Jul-11	1.2	1.9	8.6	3.4
16-Aug-11	0.18	1.4	8.0	3.9
27-Oct-11	1.0	2.4	10	2.2
29-Nov-11	0.84	2.2	10	6.6
13-Dec-11	0.31	2.2	12	4.2

Table C 28: Concentrations of cBOD₅ (mg L⁻¹) along the treatment flow path during the EW-BOFS demonstration-scale wastewater treatment experiment.

Date	Cell 1	Cell 2	Cell 3	Cell 4
27-Jan-10	169	52	37	1.0
3-Feb-10	202	85	37	1.0
5-May-10	59	63	10	1.0
12-May-10	92	76	9.0	1.0
19-May-10	79	94	32	1.0
27-May-10	60	51	4.0	1.0
2-Jun-10	124	85	13	1.0
8-Jun-10	49	30	10	1.0
16-Jun-10	91	32	11	1.0
23-Jun-10	43	20	10	1.0
29-Jun-10	30	17	8.0	1.0
6-Jul-10	34	9.0	6.0	1.0
14-Jul-10	18	18	3.0	1.0
20-Jul-10	10	6.0	4.0	1.0
28-Jul-10	5.0	2.0	1.0	<DL
4-Aug-10	16	15	6.0	<DL
10-Aug-10	25	15	10	<DL
18-Aug-10	20	12	5.0	<DL
31-Aug-10	9.0	9.0	5.0	<DL
8-Sep-10	25	10	2.0	<DL
14-Sep-10	55	9.0	4.0	<DL
19-Oct-10	39	25	5.0	1.0
16-Nov-10	52	24	2.0	<DL
14-Dec-10	22	10	2.0	<DL
20-Jan-11	52	11	1.0	<DL
16-Feb-11	26	10	4.0	2.0
23-Mar-11	18	5.0		1.0
13-Apr-11	84	7.0	2.0	1.0
18-May-11	105	84	2.0	1.0
22-Jun-11	22	9.0	2.0	<DL
13-Jul-11	185	8.0	2.0	<DL
16-Aug-11	42	5.0	3.0	<DL
27-Oct-11	142	9.0	3.0	<DL
29-Nov-11	78	4.0	2.0	<DL
13-Dec-11	114	6.0	3.0	<DL

DL: 1 mg L⁻¹

Table C 29: Concentrations of COD (mg L⁻¹) along the treatment flow path during the EW-BOFS demonstration-scale wastewater treatment experiment.

Date	Cell 1	Cell 2	Cell 3	Cell 4
27-Jan-10	332	273	65	112
3-Feb-10	335	240	64	88
5-May-10	109	128	38	36
12-May-10	118	82	30	32
19-May-10	167	85	50	24
27-May-10	131	89	26	30
2-Jun-10	174	76	19	36
8-Jun-10	128	71	25	31
16-Jun-10	123	59	24	33
29-Jun-10	90	46	18	17
6-Jul-10	118	49	23	27
14-Jul-10	73	44	18	33
20-Jul-10	104	74	52	61
28-Jul-10	41	46	22	32
4-Aug-10	60	38	20	33
10-Aug-10	66	39	19	34
18-Aug-10	73	45	20	27
31-Aug-10	53	38	21	34
8-Sep-10	75	35	21	21
14-Sep-10	137	37	21	28
19-Oct-10	122	90	37	35
16-Nov-10	155	86	32	34
14-Dec-10	86	49	24	30
20-Jan-11	150	45	22	18
16-Feb-11	94	61	43	50
23-Mar-11	54	40	-	21
13-Apr-11	210	50	24	22
18-May-11	242	154	19	17
22-Jun-11	56	49	30	28
16-Aug-11	348	46	28	29
27-Oct-11	244	38	25	35
29-Nov-11	244	37	13	20
13-Dec-11	210	41	16	16

DL: 3 mg L⁻¹

Table C 30: Concentrations of *E.coli* (CFU/100mL) along the treatment flow path during the EW-BOFS demonstration-scale wastewater treatment experiment.

Date	Cell 1	Cell 2	Cell 3	Cell 4
27-Jan-10	-	3.0E+02	3.0E+00	1.1E+01
3-Feb-10	3.1E+05	5.0E+01	1.6E+01	<DL
5-May-10	4.9E+04	2.5E+03	1.4E+02	<DL
12-May-10	1.5E+05	3.0E+03	7.5E+02	<DL
19-May-10	1.6E+05	2.2E+03	3.0E+01	<DL
27-May-10	7.8E+04	5.9E+03	1.5E+01	<DL
2-Jun-10	3.0E+04	6.0E+02	1.5E+01	<DL
8-Jun-10	3.2E+04	3.0E+02	1.1E+01	<DL
16-Jun-10	1.7E+05	9.5E+02	6.0E+01	<DL
23-Jun-10	5.2E+04	3.0E+03	1.3E+01	<DL
29-Jun-10	1.4E+05	2.9E+04	<DL	<DL
14-Jul-10	3.3E+04	1.5E+02	<DL	<DL
28-Jul-10	2.2E+03	1.3E+03	<DL	<DL
4-Aug-10	9.4E+04	1.3E+03	8.0E+00	<DL
10-Aug-10	3.3E+03	2.2E+03	5.0E+00	<DL
18-Aug-10	5.5E+04	1.0E+03	8.0E+00	<DL
31-Aug-10	5.9E+04	8.6E+02	3.8E+02	<DL
8-Sep-10	7.4E+05	5.1E+03	4.9E+02	<DL
14-Sep-10	2.5E+05	1.2E+05	5.1E+03	<DL
19-Oct-10	6.2E+05	1.0E+05	2.1E+03	7.9E+02
16-Nov-10	2.4E+06	4.8E+05	6.0E+00	3.0E+00
14-Dec-10	7.2E+04	7.9E+04	5.5E+03	6.0E+00
20-Jan-11	2.5E+06	3.2E+04	2.5E+02	3.0E+00
16-Feb-11	3.5E+05	1.4E+04	2.4E+04	2.4E+03
23-Mar-11	5.2E+04	9.2E+04	-	3.0E+01
13-Apr-11	1.4E+05	4.0E+03	6.0E+01	6.0E+00
18-May-11	8.5E+05	6.0E+02	3.0E+01	3.0E+00
22-Jun-11	2.2E+04	1.0E+03	3.0E+00	3.0E+00
13-Jul-11	7.6E+04	1.2E+03	3.0E+01	3.0E+00
16-Aug-11	8.1E+05	3.0E+01	3.0E+01	3.0E+00
27-Oct-11	4.4E+04	1.5E+02	8.0E+01	3.0E+00
29-Nov-11	2.5E+05	1.5E+02	3.0E+01	3.0E+00
13-Dec-11	2.0E+04	5.0E+01	3.0E+01	3.0E+00

DL: 3CFU/100 ml

Table C 31: Concentrations of Total coliform (CFU/100mL) along the treatment flow path during the EW-BOFS demonstration-scale wastewater treatment experiment.

Date	Cell 1	Cell 2	Cell 3	Cell 4
27-Jan-10	9.7E+06	1.3E+03	1.4E+02	<DL
3-Feb-10	6.9E+05	5.0E+01	7.6E+01	<DL
5-May-10	1.6E+05	2.4E+04	2.4E+03	<DL
12-May-10	1.2E+06	1.9E+04	1.5E+03	<DL
19-May-10	1.2E+06	1.8E+04	5.0E+02	<DL
27-May-10	4.8E+06	4.2E+04	2.2E+02	<DL
2-Jun-10	4.3E+05	3.8E+03	3.6E+02	<DL
8-Jun-10	1.5E+05	6.5E+03	2.1E+02	<DL
16-Jun-10	1.7E+06	1.5E+04	1.3E+02	<DL
23-Jun-10	3.4E+05	1.6E+04	2.0E+02	<DL
29-Jun-10	4.7E+05	8.1E+04	3.3E+01	<DL
14-Jul-10	1.9E+05	4.7E+03	5.2E+01	8.0E+00
28-Jul-10	3.8E+03	3.8E+03	4.9E+01	<DL
4-Aug-10	1.8E+05	7.0E+04	1.1E+02	<DL
10-Aug-10	8.6E+04	4.7E+04	9.8E+01	<DL
18-Aug-10	9.4E+05	9.8E+03	8.7E+01	<DL
31-Aug-10	4.3E+05	3.3E+03	1.0E+03	<DL
8-Sep-10	9.4E+05	1.0E+04	6.5E+02	<DL
14-Sep-10	3.4E+06	2.4E+05	1.9E+04	<DL
19-Oct-10	8.6E+05	1.3E+05	2.7E+03	-
16-Nov-10	2.4E+06	4.8E+05	4.8E+03	-
14-Dec-10	1.9E+06	1.2E+06	9.7E+03	<DL
20-Jan-11	6.8E+06	2.5E+05	1.5E+03	<DL
16-Feb-11	1.4E+06	5.4E+04	2.4E+03	-
23-Mar-11	4.9E+05	1.6E+05	-	3.0E+01
13-Apr-11	3.5E+05	6.7E+03	9.8E+02	6.0E+00
18-May-11	9.7E+06	8.1E+04	1.6E+03	3.0E+00
22-Jun-11	5.6E+05	1.5E+04	9.8E+01	3.0E+00
13-Jul-11	1.6E+06	1.2E+03	1.9E+03	3.0E+00
16-Aug-11	1.2E+07	2.1E+03	8.7E+02	2.4E+03
27-Oct-11	2.2E+05	8.6E+03	5.9E+02	3.0E+00
29-Nov-11	5.8E+05	8.0E+02	9.4E+02	3.0E+00
13-Dec-11	1.7E+05	1.3E+02	3.0E+01	3.0E+00

DL: 3CFU/100 ml

Table C 32: Mass change of PO₄-P observed in different components of the treatment system. The +ve values indicate mass loses from the system component and the -ve values indicate mass gains within the system component.

	PO ₄ -P mass in (mg)	PO ₄ -P mass out (mg)	PO ₄ -P mass change (mg)	PO ₄ -P mass change (Kg)	PO ₄ -P mass % change
Overall treatment system	2003663	89904	1913759	1.91	95.51
Cell 2	2003663	1978166	25497	0.03	1.27
Cell 3	1978166	1450086	528080	0.53	26.70
Cell 4	1450086	89904	1360182	1.36	93.80

Table C 33: Mass change of NH₃-N observed in different components of the treatment system. The +ve values indicate mass loses from the system component and the -ve values indicate mass gains within the system component.

	NH ₃ -N mass in (mg)	NH ₃ -N mass out (mg)	NH ₃ -N mass change (mg)	NH ₃ -N mass change (Kg)	NH ₃ -N mass % change
Overall treatment system	16487032	3516451	12970581	12.97	78.67
Cell 2	16487032	16298910	188122	0.19	1.14
Cell 3	16298910	937765	15361145	15.36	94.25
Cell 4	937765	3516451	-2578686	-2.58	-274.98

Table C 34: Mass change of NO₃-N observed in different components of the treatment system. The +ve values indicate mass losses from the system component and the -ve values indicate mass gains within the system component.

	NO₃-N mass in (mg)	NO₃-N mass out (mg)	NO₃-N mass change (mg)	NO₃-N mass change (Kg)	NO₃-N mass % change
Overall treatment system	1257749	13219591	-11961842	-11.96	-951.05
Cell 2	1257749	656414	601335	0.60	47.81
Cell 3	656414	17408976	-16752562	-16.75	-2552.13
Cell 4	17408976	13219591	4189385	4.19	24.06

Table C 35: Mass change of NO₂-N observed in different components of the treatment system. The +ve values indicate mass losses from the system component and the -ve values indicate mass gains within the system component.

	NO₂-N mass in (mg)	NO₂-N mass out (mg)	NO₂-N mass change (mg)	NO₂-N mass change (Kg)	NO₂-N mass % change
Overall treatment system	176941	814301	-637360	-0.64	-360.21
Cell 2	176941	66841	110100	0.11	62.22
Cell 3	66841	244506	-177665	-0.18	-265.80
Cell 4	244506	814301	-569795	-0.57	-233.04

Table C 36: Mass change of N_T observed in different components of the treatment system. The +ve values indicate mass losses from the system component and the -ve values indicate mass gains within the system component.

	N_T mass in (mg)	N_T mass out (mg)	N_T mass change (mg)	N_T mass change (Kg)	N_T mass % change
Overall treatment system	17921722	17550343	371379	0.37	2.07
Cell 2	17921722	17022165	899557	0.90	5.02
Cell 3	17022165	18591246	-1569081	-1.57	-9.22
Cell 4	18591246	17550343	1040904	1.04	5.60

Table C 37: Mass change of $cBOD_5$ observed in different components of the treatment system. The +ve values indicate mass losses from the system component and the -ve values indicate mass gains within the system component.

	$cBOD_5$ mass in (mg)	$cBOD_5$ mass out (mg)	$cBOD_5$ mass change (mg)	$cBOD_5$ mass change (Kg)	$cBOD_5$ mass % change
Overall treatment system	22388542	361100	22027443	22.03	98.39
Cell 2	22388542	12029514	10359029	10.36	46.27
Cell 3	12029514	3510693	8518820	8.52	70.82
Cell 4	3510693	361100	3149594	3.15	89.71

Table C 38: Mass change of COD observed in different components of the treatment system. The +ve values indicate mass losses from the system component and the -ve values indicate mass gains within the system component.

	COD mass in (mg)	COD mass out (mg)	COD mass change (mg)	COD mass change (Kg)	COD mass % change
Overall treatment system	48819048	13549821	35269227	35.27	72.24
Cell 2	48819048	32135788	16683260	16.68	34.17
Cell 3	32135788	11550415	20585373	20.59	64.06
Cell 4	11550415	13549821	-1999405	-2.00	-17.31

Appendix D
Summary of Data Presented in Chapter 5

Table D 1: Concentrations of caffeine ($\mu\text{g L}^{-1}$) along the treatment flow path of the EW-BOFS demonstration-scale treatment system experiment.

Date	Cell 1	Cell 2	Cell 3	Cell 4
19-Feb-10	61	53	11	10
6-Apr-10	26	11	1.5	2.0
13-Apr-10	15	13	7.6	2.9
30-Apr-10	15	10	1.6	0.32
10-Dec-10	5.1	12	6.8	3.9
28-Jan-11	13	15	11	5.8

Table D 2: Concentrations of carbamazepine ($\mu\text{g L}^{-1}$) along the treatment flow path of the EW-BOFS demonstration-scale treatment system experiment.

Date	Cell 1	Cell 2	Cell 3	Cell 4
19-Feb-10	9.3	8.4	8.1	5.9
6-Apr-10	5.4	4.7	2.1	6.3
13-Apr-10	3.6	4.0	4.7	3.7
30-Apr-10	2.7	6.8	7.2	6.8
10-Dec-10	0.17	0.17	0.16	0.12
28-Jan-11	-	0.42	0.38	0.55

Table D 3: Concentrations of sulfamethoxazole ($\mu\text{g L}^{-1}$) along the treatment flow path of the EW-BOFS demonstration-scale treatment system experiment.

Date	Cell 1	Cell 2	Cell 3	Cell 4
19-Feb-10	0.073	0.078	0.060	0.028
6-Apr-10	-	0.044	0.092	-
13-Apr-10	0.101	0.075	-	0.066
30-Apr-10	0.080		0.028	0.063
10-Dec-10	0.003	0.003	0.003	0.003
28-Jan-11	-	0.019	0.018	0.027

Table D 4: Concentrations of ibuprofen ($\mu\text{g L}^{-1}$) along the treatment flow path of the EW-BOFS demonstration-scale treatment system experiment.

Date	Cell 1	Cell 2	Cell 3	Cell 4
19-Feb-10	59	44	16	16
6-Apr-10	70	68	29	22
13-Apr-10	70	69	43	37
30-Apr-10	36	54	26	18
10-Dec-10	29	31	22	18
28-Jan-11	19	23	6.2	4.6

Table D 5: Concentrations of naproxen ($\mu\text{g L}^{-1}$) along the treatment flow path of the EW-BOFS demonstration-scale treatment system experiment.

Date	Cell 1	Cell 2	Cell 3	Cell 4
19-Feb-10	8.5	12	16	9.7
6-Apr-10	11	13	8.0	7.3
13-Apr-10	13	12	11	7.0
30-Apr-10	7	13	4.8	4.5
10-Dec-10	11	12	6.6	3.9
28-Jan-11	0.78	1.3	0.27	0.12

Table D 6: Concentrations of acesulfame-K ($\mu\text{g L}^{-1}$) along the treatment flow path of the EW-BOFS demonstration-scale treatment system experiment.

Date	Cell 1	Cell 2	Cell 3	Cell 4
19-Feb-10	54	51	42	36
6-Apr-10	94	56	52	66
13-Apr-10	77	68	61	34
30-Apr-10	35	39	44	41
10-Dec-10	58	58	56	54
28-Jan-11	81	79	69	62

Table D 7: pH values along the treatment flow path of the EW-BOFS demonstration-scale treatment system experiment.

Date	Cell 1	Cell 2	Cell 3	Cell 4
19-Feb-10	8.95	9.61	8.10	12.32
6-Apr-10	8.68	8.30	7.41	11.97
13-Apr-10	8.43	8.14	7.61	11.10
30-Apr-10	7.38	7.70	7.58	10.40
10-Dec-10	8.12	8.13	7.82	9.41
28-Jan-11	8.10	8.35	7.72	9.49

Table D 8: Measurements of alkalinity ($\text{mg L}^{-1} \text{CaCO}_3$) along the treatment flow path of the EW-BOFS demonstration-scale treatment system experiment.

Date	Cell 1	Cell 2	Cell 3	Cell 4
19-Feb-10	630	490	230	1620
6-Apr-10	729	520	260	760
13-Apr-10	460	520	200	640
30-Apr-10	700	740	540	360
10-Dec-10	430	340	300	200
28-Jan-11	425	460	175	200

Table D 9: Measurements of Eh (mV) along the treatment flow path of the EW-BOFS demonstration-scale treatment system experiment.

Date	Cell 1	Cell 2	Cell 3	Cell 4
19-Feb-10	-33	-4	279	31
6-Apr-10	90	144	364	180
13-Apr-10	83	128	311	130
30-Apr-10	68	71	286	79
19-May-10	-6	43	267	101
2-Jun-10	-69	14	250	63
3-Jun-10	-28	19	421	105
16-Jun-10	-26	13	261	72
20-Jul-10	112	152	520	92
28-Jan-11	7	37	284	76
13-Jul-11	82	229	228	59
27-Oct-11	119	263	270	215
29-Nov-11	265	419	407	232

Table D 10: Concentrations of DO (mg L^{-1}) along the treatment flow path of the EW-BOFS demonstration-scale treatment system experiment.

Date	Cell 1	Cell 2	Cell 3	Cell 4
19-Feb-10	1.4	1.4	12	3.0
6-Apr-10	0.26	0.20	11	3.8
13-Apr-10	3.5	0.70	8.7	6.0
30-Apr-10	0.85	2.4	11	3.4
10-Dec-10	2.9	3.7	10	7.8
28-Jan-11	1.3	4.6	10	8.5

Table D 11: Concentrations of cBOD_5 (mg L^{-1}) along the treatment flow path of the EW-BOFS demonstration-scale treatment system experiment.

Date	Cell 1	Cell 2	Cell 3	Cell 4
19-Feb-10	169	52	37	<DL
6-Apr-10	202	85	37	<DL
13-Apr-10	59	63	10	<DL
30-Apr-10	92	76	9.2	<DL
10-Dec-10	22	10	2.0	<DL
28-Jan-11	52	11	1.0	<DL

DL: 1 mg L^{-1}

Table D 12: Concentrations of $\text{NH}_3\text{-N}$ (mg L^{-1}) along the treatment flow path during the EW-BOFS demonstration-scale wastewater treatment experiment.

Date	Cell 1	Cell 2	Cell 3	Cell 4
19-Feb-10	61	35	13	47
6-Apr-10	47	59	22	14
13-Apr-10	57	68	30	20
30-Apr-10	40	60	27	13
10-Dec-10	41	49	30	18
28-Jan-11	57	49	4.4	2.0

DL: 0.02 mg L^{-1}

Table D 13: Concentrations of NO₃-N (mg L⁻¹) along the treatment flow path during the EW-BOFS demonstration-scale wastewater treatment experiment.

Date	Cell 1	Cell 2	Cell 3	Cell 4
19-Feb-10	5.3	7.7	83	12
6-Apr-10	10	1.0	48	56
13-Apr-10	7.7	0.16	48	48
30-Apr-10	8.9	0.01	43	58
10-Dec-10	14	3.1	33	46
28-Jan-11	9.1	0.74	39	40

DL: 0.05 mg L⁻¹

Table D 14: Concentrations of Cl (mg L⁻¹) along the treatment flow path during the EW-BOFS demonstration-scale wastewater treatment experiment.

Date	Cell 1	Cell 2	Cell 3	Cell 4
19-Feb-10	189	182	185	154
6-Apr-10	220	204	170	144
13-Apr-10	189	198	193	186
30-Apr-10	218	226	206	195
10-Dec-10	140	148	140	135
28-Jan-11	205	209	192	184

Table D 15: Concentrations of SO₄ (mg L⁻¹) along the treatment flow path during the EW-BOFS demonstration-scale wastewater treatment experiment.

Date	Cell 1	Cell 2	Cell 3	Cell 4
19-Feb-10	37	45	49	25
6-Apr-10	51	46	50	42
13-Apr-10	46	43	50	44
30-Apr-10	32	27	32	37
10-Dec-10	56	57	58	52
28-Jan-11	74	77	85	78

DL: 0.018 mg L⁻¹

Table D 16: Concentrations of Fe ($\mu\text{g L}^{-1}$) along the treatment flow path during the EW-BOFS demonstration-scale wastewater treatment experiment.

Date	Cell 1	Cell 2	Cell 3	Cell 4	DL ($\mu\text{g L}^{-1}$)
19-Feb-10	22	97	76	3.4	0.07
6-Apr-10	21	39	28	2.2	0.07
13-Apr-10	29	64	51	21	0.07
30-Apr-10	25	82	57	4.7	0.07
10-Dec-10	13	25	15	23	0.26
28-Jan-11	11	21	16	4.7	0.26

Table D 17: Concentrations of Mn ($\mu\text{g L}^{-1}$) along the treatment flow path during the EW-BOFS demonstration-scale wastewater treatment experiment.

Date	Cell 1	Cell 2	Cell 3	Cell 4	DL ($\mu\text{g L}^{-1}$)
19-Feb-10	4.9	11	89	0.15	0.04
6-Apr-10	16	25	102	0.04	0.04
13-Apr-10	17	39	140	2.1	0.04
30-Apr-10	36	75	89	0.84	0.04
10-Dec-10	4.0	25	31	3.8	0.03
28-Jan-11	24	15	30	23	0.03